MRI Investigation of a Model of Chronic Inflammation in the CNS

Kerry Anne Broom
Worcester College

MRC Biochemical and Clinical and Magnetic Resonance Unit,
Department of Biochemistry, University of Oxford

Submitted for the Degree of Doctor of Philosophy

Trinity 2003

RADCLIFFE SCIENCE LIBRARY OXFORD
6 MAY 2004

MRI Investigation of a Model of Chronic Inflammation in the CNS

Kerry Anne Broom
Worcester College
Doctor of Philosophy
Trinity 2003

Abstract

Magnetic resonance imaging (MRI) is an established clinical tool for diagnosing Multiple Sclerosis (MS), the archetypal CNS neuroinflammatory disease. The aim of this work was to develop and characterise a chronic demyelinating inflammatory lesion, like those in MS, using MRI, histology and immunocytochemistry, to identify MR-markers of disease activity and to correlate these with developing histopathology. The second aim of this work was to investigate the effect of a peripheral infection on a quiescent CNS lesion, since infections have been hypothesised to be important in the exacerbation of MS.

Prior to MRI, the DTH lesion was charcaterised histologically. An increase in macrophage and astrocyte numbers was the earliest histological event. Conventional MRI techniques, such as T_1- and T_2-weighted imaging were then used to characterise the lesion. The lesion was hypointense on T_1- and T_2-weighted images, and later, a hyperintense region was found to surround the hypointense core.

Contrast enhancement, diffusion and magnetisation transfer characteristics of the lesion were then investigated. Contrast enhancement occurred at the same time as T_2 hyperintensities. Increased ADC corresponded to areas of contrast enhancement and T_2 hyperintensity. Reactive astrocytes spatially mapped to these regions. Decreased ADC regions corresponded to regions of T_1 and T_2 hypointensity. The hypercellular lesion core, composed of T cells, macrophages and MHC class II expressing cells spatially mapped to the hypointense core on T_1- and T_2-weighted images and ADC maps. The MTR was reduced in the absence of demyelination and significant oedema.

Blood volume changes were also investigated, and focal increases in rCBV were found, and were associated with dilation of blood vessels and Laminin upregulation.

The final objective of this thesis was to investigate the effect of peripheral infection on the DTH lesion. The immune response was reactivated, and was observed by an increase in rCBV, T_1 relaxation time, and re-opening of the BBB six hours post-infectious challenge.

This work has successfully demonstrated that pathophysiological changes can be followed non-invasively with MRI throughout the evolution of the untreated DTH lesion.

This dissertation is the result of my own work and includes nothing that is the result of collaboration. The number of words in the main body of this thesis (not including figures, tables and appendices) is less than 50,000.

I would like to thank my supervisor Dr Niki Sibson, and Professor Peter Styles for giving me the opportunity to study for a DPhil. Being a supervisor must be hard, but supervising me must have required real patience, especially with the events that have happened during the course of my DPhil. Thank you so much, Niki.

I am indebted to Worcester College for providing me with accommodation, book grants, and funding for conference travel, and also the MRC for my studentship.

Thanks also goes to Professor Hugh Perry, and Dr Daniel Anthony for setting up and maintaining the collaboration that made all the experiments in this thesis possible. I would also like to thank all members of their respective labs for stimulating discussions, and making my frequent stays in Southampton more exciting. Special thanks goes to Sara Waters for sectioning all of my brains.

I have to thank Dr Andrew Blamire for creating the pulse sequences and image analysis packages that were used throughout this thesis and for being available to deal with many of my magnet related problems. Dr Graeme Waddington created filters for my data, created the cluster analysis programs, and an image analysis package. Thanks are also due to Mr Andre Thomas and Mr Philip Bradford, who were always 'on call' with ECG related problems, and filling the magnet so that I could actually do MRI experiments. Thanks to the BSU staff for looking after my constant supply of work for them.

All the members of Room 14 (when it existed) Room 26, and Room 31b deserve a mention. Especially Daniel Stuckey, who was on hand to help me, at almost every opportunity. Lowri Cochlin deserves a special thank-you because she has given me a constant supply of tea, and friendship over the last couple of years. Paul Cassidy too, out of everyone I know, he has the unique gift of always making me laugh, and he is very handy when it comes to building (and fixing!) the ECG boxes, ECG leads, coils, and probe bodies.

Finally, my grandparents, parents, and my sisters have given me continual support and encouragement throughout the course of my DPhil, to keep working hard, and not to give up. I have to say thanks to them for helping me to achieve great things, and for reminding me that...

'For I am convinced that neither death nor life, neither angels nor demons, neither the present nor the future, nor any powers, neither height nor depth, nor anything else in all creation, will be able to separate us from the love of God that is in Christ Jesus our Lord.' Romans 8 v38-39

Results from this Thesis presented to the Scientific Community

Oral Presentations

"Reactivation of the immune response by peripheral infection causes increased CBV". 11th Annual Scientific Meeting and Exhibition of the ISMRM, Toronto, Canada, 2003.

"A peripheral infection can reactivate a CNS lesion; Increased rCBV & T_1 and T_2 changes detected by MRI". 8th Annual Meeting of the British Chapter of the ISMRM, Sheffield, UK 2002.

"Characterisation of a Delayed Type Hypersensitivity lesion in the rat brain using MRI". 12th Annual NMR symposium, London, UK, 2002.

"Increased rCBV resulting from immune response activation in the DTH model of multiple sclerosis". 7th Annual Meeting of the British Chapter of the ISMRM, Cambridge, UK 2001.

"Magnetic Resonance Imaging investigation of a Delayed Type Hypersensitivity Lesion in the Rat Brain". 11th Annual NMR symposium, Nottingham, UK 2001.

Poster Presentations

"Does a reduction in MTR reflect a loss of myelin?" To be presented at 9th British Chapter of the ISMRM, London, UK, 2003.

"Reactivation of immune response by peripheral infection causes increased regional cerebral blood volume". 17th National Meeting of the British Neuroscience Association, 2003.

"Increased regional cerebral blood volume in the delayed type hypersensitivity lesion in the rat brain" Oxford Imaging Symposim, Oxford, UK 2002.

"MRI Investigation of a delayed type hypersensitivity lesion in the rat brain". 6th International Congress of Neuroimmunology, Edinburgh, UK 2001.

"Magnetic Resonance Imaging Investigation of a delayed type hypersensitivity in the rat brain". 9th Annual Scientific Meeting and Exhibition of the ISMRM, Glasgow, UK 2001.

"Magnetic Resonance Imaging Investigation of a Delayed Type Hypersensitivity Lesion it the rat brain". 14th International Congress of Neuropathology: Oxford Satellite, Oxford, UK 2000.

"Magnetic Resonance Imaging Investigation of a Delayed Type Hypersensitivity Lesion in the rat brain". 10th ARSEP Meeting; Molecules, Cells and Tissue imaging in Myelin Diseases, Paris, France 2000.

Contents

Chapter 1 *1*

Introduction *1*

1.1 Aims of this Thesis **3**

1.2 Overview of this thesis. **3**

Chapter 2 *6*

Background *6*

2.1 The Immune Response in the CNS **6**
2.1.1 The Cell Types 7
2.1.2 Blood Brain Barrier 8
2.1.3 Multiple Sclerosis 9
2.1.4 The Inflammatory Response in Multiple Sclerosis 10
2.1.5 MRI in MS 12
2.1.6 MRI and Histopathological Correlations 14
2.1.7 Animal Models of MS 15
2.1.8 MRI in EAE 19
2.1.9 Smart Contrast Agents in EAE 20
2.1.10 MRI Assessment of Targeted Therapies in EAE 21

2.2 MRI Theory **22**
2.2.1 Spin 22
2.2.2 Relaxation 23
2.2.3 Longitudinal Relaxation 23
2.2.4 Transverse Relaxation 24
2.2.5 T_2* Relaxation 25
2.2.6 Excitation 25

2.3 Image Contrast **26**
2.3.1 T_1 and T_2 Contrast 26
2.3.2 Gadolinium Enhancement 27
2.3.3 Diffusion-weighted Imaging 27
2.3.4 Magnetisation Transfer 28
2.3.5 Measurement of Tissue Perfusion 29

Chapter 3 *31*

Materials and methods *31*

3.1 Reagents **31**
3.1.1 Preparation of heat-killed BCG 31
3.1.2 LPS 31
3.1.3 TB 31

3.2 Animal Work **31**
3.2.1 Animals 32
3.2.2 Anaesthesia 32
3.2.3 Surgery 32

3.3 Magnetic Resonance Imaging Hardware **34**
3.3.1 MRI Probe 34
3.3.2 Physiological Monitoring during MRI 35

3.4 Tissue Preparation **36**
3.4.1 Fresh Tissue 36
3.4.2 PLP Fixed Tissue 36
3.4.3 Tissue for ELISA 36

3.5 Antibodies **37**
3.5.1 Immunohistochemistry 37
3.5.2 ELISA Antibodies 38

3.6 Histology Techniques **38**

3.6.1 Cresyl Violet 38
3.6.2 Acetycholinesterase 38
3.6.3 Immunohistochemistry 38
3.6.4 Counterstaining and Coverslipping 39
3.6.5 ELISA 39

3.7 Computing Hardware 41

3.8 Computing Software 41
3.8.1 Image Analysis 41
3.8.2 Data Analysis 42

Chapter 4 ***44***

The Histological Basis of the DTH Lesion ***44***

4.1 Introduction 44

4.2 Aims of this Chapter 46

4.3 Methods 46
4.3.1 Experimental Model 46
4.3.2 Histology and Immunohistochemistry 47
4.3.3 Data Analysis 48
4.3.4 Cell Counts 48
4.3.5 Quantitation of MHC Class II and Reactive Astrocytes 49
4.3.6 Levels of IgG 49
4.3.7 Statistical Analysis 49

4.4 Results 50
4.4.1 Refinement of Model 50

4.5 Qualitative Histology 51
4.5.1 Cresyl Violet 51
4.5.2 Acetylcholinesterase 52

4.6 Immunohistochemistry 53
4.6.1 BCG 53
4.6.2 Myelin 53
4.6.3 Reactive Astrocytes 54
4.6.4 Macrophage Recruitment 57
4.6.5 MHC Class II Expression 59
4.6.6 Recruitment of T and B lymphocytes 61
4.6.7 Blood Brain Barrier 63
4.6.8 Summary of Time-Course Results 65
4.6.9 Spatial Correlations 67
4.6.10 Histological Correlations 67

4.7 Discussion 69
4.7.1 Comparison of histopathological findings with previous studies of the DTH model 70
4.7.2 Comparison of DTH and MS Lesion Histopathology 72
4.7.3 Histological Correlations 73

Chapter 5 ***76***

T_1- and T_2-weighted Imaging ***76***

5.1 Introduction 76
5.1.1 T_1-weighted imaging 76
5.1.2 T_2-weighted Imaging 77

5.2 Aims of this Chapter 78

5.3 Materials and Methods 79
5.3.1 Experimental Model 79
5.3.2 Magnetic Resonance Imaging 79
5.3.3 Histology and Immunohistochemistry 80
5.3.4 Data Analysis 81
5.3.5 Cell Counts 82
5.3.6 Statistics 82

5.4 Results **83**
5.4.1 T_1 and T_2 Hypointensity 83
5.4.2 T_2 Hyperintensity 88
5.4.3 Correlation between T_2 Hypointensity and T_2 Hyperintensity 89
5.4.4 Total Area of Signal Change on T_2-weighted Images 90
5.4.5 Spatial Co-incidence of Histology and T_2 Hyperintensity 92
5.4.6 Quantitative Correlations with Histology 93

5.5 Discussion **99**
5.5.1 T_1 Hypointensities 99
5.5.2 T_2 Hypointensities 101
5.5.3 T_2 Hyperintensities 102
5.5.4 Conclusions 103

Chapter 6 ***104***

Contrast Enhancement, Diffusion and Magnetisation Transfer Imaging ***104***

6.1 Introduction **104**
6.1.1 Contrast Enhancement 104
6.1.2 Diffusion-Weighted Imaging 105
6.1.3 Magnetisation Transfer Imaging 107

6.2 Aims of this Chapter **109**

6.3 Materials and Methods **109**
6.3.1 Experimental Model 109
6.3.2 Magnetic Resonance Imaging 110
6.3.3 Histology and Immunohistochemistry 112
6.3.4 MRI Data Analysis 112
6.3.5 Immunohistochemical Data Analysis 113
6.3.6 Cell Counts 113
6.3.7 Statistics 114

6.4 Results **115**
6.4.1 BBB Breakdown. 115
6.4.2 Correlation Between Areas of BBB Breakdown and T_2 Signal Change 117
6.4.3 Spatial Co-incidence of Inflammatory Markers and Gadolinium Enhancement 119
6.4.4 Histological Correlations 121
6.4.5 ADC Hypointensity 123
6.4.6 ADC Hyperintensity 124
6.4.7 Total Change on ADC Trace Maps 126
6.4.8 Correlation Between ADC Hypointensity and ADC Hyperintensity 127
6.4.9 Spatial Co-incidence of Inflammatory Markers and ADC changes 128
6.4.10 Quantitative Correlations with Histology 129
6.4.11 Correlation of ADC changes with other MRI Changes 135
6.4.12 Diffusion Anisotropy 137
6.4.13 Magnetisation Transfer Ratios 138

6.5 Discussion **141**
6.5.1 Contrast Enhancement 141
6.5.2 ADC Changes 145
6.5.3 Diffusion Anisotropy 148
6.5.4 Magnetisation Transfer 149
6.5.5 Conclusions 150

Chapter 7 ***152***

Assessment Of Cerebral Blood Volume Changes ***152***

7.1 Introduction **152**

7.2 Aims of this Chapter **155**

7.3 Materials and Methods **156**
7.3.1 Surgery 156
7.3.2 MRI Techniques 156
7.3.3 Perfusion and Fixation 157

7.3.4 Data Analysis 158
7.3.5 Statistical Analysis 159

7.4 Results 160
7.4.1 Regional Cerebral Blood Volume (rCBV) 160
7.4.2 Quantification from Thresholded Maps 161
7.4.3 Laminin Expression 165
7.4.4 Cresyl Violet Blood Vessel Mapping 167
7.4.5 Correlations with other MRI Parameters 167
7.4.6 Correlations with other Histopathological Findings 168

7.5 Discussion 169
7.5.1 CBV changes 169
7.5.2 Blood Vessel Dilation 172
7.5.3 Summary 173

Chapter 8 ***174***

Reactivation of the DTH Lesion ***174***

8.1 Introduction 174
8.1.1 Overview 174
8.1.2 Clinical Studies of Exacerbation 175
8.1.3 The Infectious Hypothesis 176
8.1.4 Mechanisms behind Infection 177
8.1.5 Animal Studies 178

8.2 Aims of this Chapter 179

8.3 Methods 180
8.3.1 Experimental Model 180
8.3.2 Experimental Groups 180
8.3.3 Magnetic Resonance Imaging 181
8.3.4 Experimental Protocol 185
8.3.5 Enzyme Linked Immunosorbent Assay (ELISA) 185
8.3.6 Immunohistochemistry 186
8.3.7 MRI Data Analysis 186
8.3.8 Statistical Analysis 187

8.4 Results 188

8.5 Spontaneous DTH inflammatory Response 188
8.5.1 Cerebral Blood Volume 188
8.5.2 ELISA 190
8.5.3 Temporal Changes in T_1 Relaxation Time 192
8.5.4 Temporal Changes in T_2 Relaxation Time 194
8.5.5 T_2 Relaxation Times in the Lesion 196
8.5.6 Temporal Changes in T_2* Relaxation Time 198
8.5.7 Magnetisation Transfer Ratio 199
8.5.8 Temporal Changes in BBB Permeability 200
8.5.9 Temporal Changes in ADC 202
8.5.10 Temporal Changes in Diffusion Anisotropy 205

8.6 POST-LPS Challenge 207
8.6.1 Behavioural effects of LPS administration 207
8.6.2 Changes in rCBV Post-LPS Administration 207
8.6.3 Changes in T_1 Relaxation Time Post-LPS Challenge 209
8.6.4 Cortex 211
8.6.5 Changes in T_2 Relaxation Times post-LPS challenge 213
8.6.6 T_2* Striatum 215
8.6.7 Magnetisation Transfer 216
8.6.8 Re-opening of the Blood-Brain Barrier 217
8.6.9 ADC Changes 218
8.6.10 Diffusion Anisotropy 219
8.6.11 Immunohistochemistry 219

8.7 Discussion 221

8.7.1 Findings in this chapter 221
8.7.2 Acute Response 221
8.7.3 Post-LPS Inflammatory Response 226
8.7.4 Summary 232

Chapter 9 *233*

Conclusions and Future Work *233*

9.1 Conclusions 233
9.1.1 Evaluation of model 234
9.1.2 T_1- and T_2-weighted imaging 234
9.1.3 Contrast Enhancement, Diffusion and Magnetisation Transfer. 235
9.1.4 rCBV changes 236
9.1.5 MRI-Histology Correlations 237
9.1.6 LPS Reactivation of the Immune Response 238

9.2 Future Work 239
9.2.1 Investigation of Individual Cell Types 239
9.2.2 Investigation of MTR Changes 239
9.2.3 Mechanisms Behind Immune Response Reactivation 240
9.2.4 Magnetic Resonance Spectroscopy 241
9.2.5 Pharmacological Inhibition and Novel Contrast Agents 241

Appendix A *243*

A.1 Abbreviations 243

Appendix B *244*

B.1 Acetylcholinesterase method 244

Appendix C *245*

Histological Characteristics *245*

C.1 Macrophage and T & B Lymphocyte counts, GFAP and MHC Class II Expression in DTH animals 245

C.2 SAL PC 246

C.3 Correlation curves for Histological parameters 247

Appendix D *248*

T_1- and T_2-weighted imaging *248*

D.1 T_1 and T_2-Hypointensities 248
D.1.1 DTH 248
D.1.2 NPC 249
D.1.3 SAL PC 250

D.2 Total T_2 Signal Change and T_2 Hyperintensities 250
D.2.1 DTH 250
D.2.2 NPC 252
D.2.3 SAL PC 252

Appendix E *253*

Contrast Enhancement, Diffusion and Magnetisation Transfer *253*

E.1 Area and Intensity of BBB Breakdown 253
E.1.1 DTH 253

E.2 SAL PC 254

E.3 NPC 254

E.4 ADC Hypointensities and Hyperintensities 255
E.4.1 DTH 255
E.4.2 NPC 256
E.4.3 SAL PC 256

E.5 Total Area of ADC Change **257**
E.5.1 DTH 257
E.5.2 NPC 258
E.5.3 SAL PC 258

E.6 Diffusion Anisotropy **259**
E.6.1 DTH 259
E.6.2 NPC 260
E.6.3 SAL PC 260
E.6.4 PB IC 261

E.7 MTR **262**
E.7.1 DTH 262
E.7.2 NPC 263
E.7.3 SAL PC 263
E.7.4 PB IC 264

Appendix F ***265***

CBV data ***265***
F.1.1 DTH 265
F.1.2 NPC 266
F.1.3 SAL PC 267
F.1.4 PB IC 267

F.2 Correlations with Histological Parameters **268**

Appendix G ***269***

MRI Visible Exacerbation ***269***

G.1 CBV Changes **269**

G.2 IL-1β ELISA results **271**
G.2.1 24 hours 271
G.2.2 19 days 271

G.3 T_1 Relaxation Time **272**

G.4 T_2 Relaxation Time **273**

G.5 T_2 Relaxation time in lesion **274**

G.6 T_2* Relaxation Time **275**

G.7 BBB Permeability **276**

G.8 Diffusion Anisotropy **277**

G.9 ADC and MTR Values **278**

G.10 Post-LPS CBV Changes **279**

G.11 Post-LPS T_1 Relaxation Time **280**

G.12 Post-LPS T_2 Relaxation Time **281**

G.13 Post-LPS T_2* Relaxation Time **282**

G.14 Post-LPS MTR **283**

G.15 Post-LPS Diffusion Anisotropy **284**

G.16 Naïve T_1 and T_2 Relaxation Times **285**
G.16.1 T_1 Relaxation Time 285
G.16.2 T_2 Relaxation Time 285

List of Figures

Figure 2-1: *Migration across the BBB by activated T cells..... 9*
Figure 2-2: *Current understanding of pathology in MS.. ..... 11*
Figure 2-3: *Nuclei precess in the xy plane after being tilted by a 90° pulse,..... 23*
Figure 2-4: *The decay of magnetisation in the longitudinal direction. 24*
Figure 2-5: *The return of magnetisation in the transverse plane. 24*
Figure 3-1: *Injection coordinates in the horizontal and coronal planes of view..... 33*
Figure 3-2: *Photograph of coil and head holder with bite bar and nose restraint..... 35*
Figure 3-3: *Photograph showing temperature and heart-rate monitoring devices. 35*
Figure 4-1: *DTH lesion induced by different methods..... 51*
Figure 4-2: *Cresyl Violet characteristics of the DTH lesion. 52*
Figure 4-3: *Acetylcholinesterase activity in the core of the hypercellular DTH lesion..... 52*
Figure 4-4: *BCG antigens in and around the lesion site. 53*
Figure 4-5: *Myelin staining throughout brain parenchyma and DTH lesion..... 54*
Figure 4-6: *Area of reactive astrocyte staining around the DTH lesion.. ..... 56*
Figure 4-7: *ED1 positive macrophages in the DTH lesion..... 59*
Figure 4-8: *Areas of MHC class II expression over time in the DTH lesion.. ..... 61*
Figure 4-9: *Number of OX22 positive T & B lymphocytes throughout the lesion.. ..... 62*
Figure 4-10: *Score of BBB permeability in the DTH lesion.. ..... 64*
Figure 4-11: *Summary of time-course data for immunohistochemistry results. 66*
Figure 4-12: *Overlay of histochemical areas. 67*
Figure 4-13: *Relationships between different histological markers of inflammation. 68*
Figure 5-1: *Typical coronal and horizontal T_1 and T_2-weighted images..... 84*
Figure 5-2: *Areas of hypointensity observed on T_1-weighted images..... 85*
Figure 5-3: *Area of hypointensity observed on T_2-weighted images. 87*
Figure 5-4: *Relationship between the areas of T_1 and T_2 hypointensities.. ..... 87*
Figure 5-5: *Coronal T_2-weighted images showing hypointense core in the injected hemisphere. 88*
Figure 5-6: *Area of hyperintense region in DTH animals on T_2-weighted images over time. 89*
Figure 5-7: *Relationship between the areas of T_2 hypointensity and T_2 hyperintensity.. ..... 90*
Figure 5-8: *Area of total signal change observed on T_2-weighted images. 91*
Figure 5-9: *Spatial co-incidence of immunohistochemical markers and T_2-weighted change. 93*
Figure 5-10: *Relationship between T_1- and T_2-weighted change and macrophages. 95*
Figure 5-11: *Rrelationship between T_1- and T_2-weighted change and T & B lymphocytes..... 96*
Figure 5-12: *Relationship between T_1- and T_2-weighted change and reactive astrocytes..... 97*
Figure 5-13: *Relationship between T_1- and T_2-weighted change and MHC class II expression. 98*
Figure 6-1: *Post-contrast T_1-weighted images over time demonstrating BBB breakdown. 115*
Figure 6-2: *Area of gadolinium enhancement observed on post-contrast T_1-weighted images 116*
Figure 6-3: *Relationship between areas of BBB breakdown total signal change on T_2-weighted images. 118*
Figure 6-4: *Relationship between the areas of BBB breakdown and T_2-hyperintensity.. ..... 118*
Figure 6-5: *Relationship between the areas of BBB breakdown and the T_2 hypointensity..... 119*
Figure 6-6: *Spatial co-incidence of inflammatory markers and gadolinium enhancement. 120*
Figure 6-7: *Relationship between area of BBB breakdown and inflammatory markers. 122*
Figure 6-8: *ADC trace maps showing areas of hypointensity at the centre of a region of hyperintensity. 123*
Figure 6-9: *Area of hypointense region identified on ADC trace maps.. ..... 124*
Figure 6-10: *Area of hyperintensity observed on ADC trace maps..... 125*
Figure 6-11: *Area of total area of ADC change during the progression of the DTH lesion. 126*
Figure 6-12: *Relationship between areas of ADC hypointensity and hyperintensity.. ..... 127*
Figure 6-13: *Spatial co-incidence of inflammatory markers and ADC changes. 129*
Figure 6-14: *Relationship between the macrophages and areas of ADC change. 131*
Figure 6-15: *Relationship between T & B lymphocytes and ADC change. 132*
Figure 6-16: *Relationship between reactive astrocytes and ADC change..... 133*
Figure 6-17: *Relationship between MHC class II expression and area of ADC change..... 134*
Figure 6-18: *Relationship between areas of ADC and T_1- and T_2-weighted image signal change. 136*
Figure 6-19: *Relationship between areas of ADC and T_1- and T_2-weighted image hypointensities..... 137*
Figure 6-20: *Diffusion anisotropy map showing decreased anisotropy in the DTH lesion..... 138*
Figure 6-21: *MTR maps indicating region of reduced MTR in injected hemisphere. 139*
Figure 6-22: *L/R MTR during the DTH response. 139*
Figure 6-23: *Loss of myelin occurs within the hypercellular core only. 140*
Figure 7-1: *Effect of the gadolinium bolus on the signal intensity as it passes through the tissue..... 154*
Figure 7-2: *CBV map from DTH animals showing increased rCBV in injected hemisphere.. ..... 161*

Figure 7-3: *Post-contrast T_1-weighted image showing area of BBB breakdown.* *161*
Figure 7-4: *Unthresholded and thresholded CBV maps indicating increased rCBV.* *162*
Figure 7-5: *Left/right rCBV ratios obtained from CBV maps .* *163*
Figure 7-6: *Area of increased rCBV in the injected hemisphere..* *164*
Figure 7-7: *Area of increased rCBV in the contralateral hemisphere.* *164*
Figure 7-8: *Laminin expression throughout the brain and around the lesion site.* *165*
Figure 7-9: *Laminin expression on vessels in contact with the DTH lesion.* *166*
Figure 7-10: *Laminin expression on vessels at the interface of the DTH lesion .* *166*
Figure 7-11: *Dilated blood vessels can be spatially mapped onto areas of increased rCBV.* *167*
Figure 8-1: *Thresholded CBV maps from 1, 19 and 42 days after intracerebral injection of BCG* *189*
Figure 8-2: *Left/right hemispheric ratio of rCBV demonstrating large increases in rCBV* *189*
Figure 8-3: *Left/right hemispheric ratio of the areas of elevated rCBV* *190*
Figure 8-4: *Concentration of IL-1β in the cortex, striatum and injection site..* *191*
Figure 8-5: *T_1 maps from two extremes of animal showing hypointense lesion site.* *193*
Figure 8-6: *Striatal T_1 relaxation time after intracerebral injection of BCG.* *193*
Figure 8-7: *Cortical T_1 relaxation times after intracerebral injection of BCG.* *194*
Figure 8-8: *T_2 maps from two extremes of animal showing the hypointense lesion site* *195*
Figure 8-9: *Striatal T_2 relaxation time after intracerebral injection of BCG.* *196*
Figure 8-10: *Cortical T_2 relaxation times following intracerebral injection of BCG..* *198*
Figure 8-11: *T_2* maps showing a reduction in the T_2* relaxation time at the site of the lesion.* *198*
Figure 8-12: *MTR maps from two extremes of animal showing a central core of decreased MTR* *200*
Figure 8-13: *MTR of the lesion and analogous ROI in the contralateral hemisphere..* *200*
Figure 8-14: *Post-contrast T_1-weighted images showing increased BBB permeability..* *201*
Figure 8-15: *Area of BBB breakdown as identified by area of gadolinium enhancement* *202*
Figure 8-16: *ADC maps in two animals showing areas of increased and decreased ADC.* *203*
Figure 8-17: *ADC values in region of elevated ADC following intracerebral injection of BCG.* *204*
Figure 8-18: *Graph to show the area of increased ADC following intracerebral injection of BCG* *205*
Figure 8-19: *Diffusion anisotropy maps in two extremes of animal showing reduced anisotropy.* *206*
Figure 8-20: *Graph to show increased rCBV six hours post-LPS.* *208*
Figure 8-21: *Temporal changes in rCBV in LPS-challenged animals post-LPS administration..* *208*
Figure 8-22: *T_1 maps acquired pre-challenge and post-challenge* *209*
Figure 8-23: *Striatal T_1 relaxation times pre- and post-challenge..* *210*
Figure 8-24: *Cortical T_1 relaxation times pre- and post-challenge* *212*
Figure 8-25: *T_2 maps acquired pre- and post-LPS challenge.* *214*
Figure 8-26: *MTR maps obtained pre- and post-challenge showing reduced MTR of lesion.* *216*
Figure 8-27: *MTR ratio of lesion pre- and post-challenge.* *217*
Figure 8-28: *Post-contrast T_1-weighted images pre- and post-challenge showing BBB breakdown.* *217*
Figure 8-29: *Post-contrast T_1-weighted images showing delayed BBB reopening.* *218*
Figure 8-30: *ADC maps pre- and post-challenge showing decreased diffusion around lesion core* *218*
Figure 8-31: *Diffusion anisotropy maps, acquired pre- and post-challenge* *219*
Figure 8-32: *Immunohistochemical characteristics of the re-activated DTH lesion.* *220*
Figure 8-33: *Laminin expression on blood vessels around the lesion & throughout the striata..* *220*
Figure 8-34: *Areas of decreased ADC, T_1 , T_2 relaxation time, increased diffusion anisotropy and MTR spatially coincide. In addition, areas of increased ADC, T_1 and T_2 relaxation time, decreased diffusion anisotropy, MTR and BBB permeability, spatially correlate.* *226*

List of Tables

Table 3-1: *Primary antibodies used during immunohistochemistry.* *37*
Table 3-2: *Secondary antibodies used during immunohistochemistry.* *37*
Table 3-3: *Summary of computing hardware* *41*
Table 3-4: *Summary of computing software.* *41*
Table 4-1: *Summary of animals used* *47*
Table 4-2: *Unpaired t tests for areas of reactive astrocytes in DTH animals at each time-point* *55*
Table 4-3: *Unpaired tests for No. of macrophages in DTH animals at each time-point* *58*
Table 4-4: *Unpaired t tests for between group comparison of DTH and SAL PC at each time point* *58*
Table 4-5: *Unpaired t tests for areas of MHC class II expression in DTH animals at each time-point.* *60*
Table 4-6: *Unpaired t tests for No. of T & B lymphocytes in DTH animals at each time-point.* *62*
Table 4-7: *Unpaired t tests for IgG leakage within DTH animals at each time-point.* *63*
Table 4-8: *Correlation between T & B lymphocytes & macrophages, MHC class II & reactive astrocytes.* *68*
Table 5-1: *Parameters used for acquisition of scout images for positioning.* *80*
Table 5-2: *Parameters used for the acquisition of T_1- and T_2-weighted images.* *80*
Table 5-3: *Unpaired t tests for area T_1 hypointensity within the DTH group at each time-point.* *85*
Table 5-4: *Unpaired t tests for area of T_1 hypointensity between DTH and control groups* *85*
Table 5-5: *Unpaired t tests for comparisons between DTH and control groups* *87*
Table 5-6: *Correlation parameters for the relationship between T_1- and T_2-weighted hypointensity.* *88*
Table 5-7: *Unpaired t tests for T_2-weighted hyperintensity within the DTH group.* *89*
Table 5-8: *Correlation analysis of the relationship between areas of T_2 hypointensity and hyperintensity.* *90*
Table 5-9: *Unpaired t tests for area of total area of signal change within the DTH group* *92*
Table 5-10: *Unpaired t tests for total areas of signal change between DTH & control groups.* *92*
Table 5-11: *Correlation analysis between macrophages & T_1- and T_2-weighted change.* *95*
Table 5-12: *Correlation analysis between T & B lymphocytes & T_1- and T_2-weighted change.* *96*
Table 5-13: *Correlation analysis between reactive astrocytes & T_1- and T_2-weighted change.* *97*
Table 5-14: *Correlation analysis between MHC class II expression & T_1- and T_2-weighted change.* *98*
Table 6-1: *Parameters used for the acquisition of diffusion-weighted images.* *111*
Table 6-2: *Parameters used in the acquisition and creation of Magnetisation Transfer images* *112*
Table 6-3: *Unpaired t tests for area of BBB breakdown within the DTH group at each time-point* *117*
Table 6-4: *Unpaired t test results for area of gadolinium enhancement between DTH & control groups.* *117*
Table 6-5: *Correlation analysis between area of BBB breakdown & areas of T_2-weighted change.* *118*
Table 6-6: *Correlation analysis between the area of gadolinium enhancement & inflammatory markers.* *122*
Table 6-7: *Unpaired t tests for area of ADC hypointensity between DTH and control groups.* *124*
Table 6-8: *Unpaired t tests for area of ADC hyperintensity within the DTH group at each time-point.* *125*
Table 6-9: *Unpaired t tests for area of ADC hyperintensity between DTH & control groups* *126*
Table 6-10: *Unpaired t tests for total area of ADC change within the DTH group* *127*
Table 6-11: *Unpaired t tests for area of total ADC change between DTH & control groups.* *127*
Table 6-12: *Correlation analysis between areas of ADC hypointensity and ADC hyperintensity.* *128*
Table 6-13: *Correlation analysis between numbers of macrophages and areas of ADC change.* *131*
Table 6-14: *Correlation analysis between numbers of T & B lymphocytes and areas of ADC change.* *132*
Table 6-15: *Correlation analysis between areas of reactive astrocytes and area of ADC change* *133*
Table 6-16: *Correlation analysis between areas of MHC class II expression and area of ADC change.* *134*
Table 6-17: *Correlation analysis between ADC signal changes and other MRI parameters.* *136*
Table 6-18: *Correlation analysis between areas of ADC & T_1 and T_2 hypointensity* *137*
Table 6-19: *Magnetisation transfer ratio in DTH and control groups.* *140*
Table 7-1: *Parameters used for the acquisition and creation of rCBV maps.* *157*
Table 7-2: *Unpaired t test results for between group comparisons of rCBV at each time-point* *162*
Table 7-3: *Correlation analysis between increases in rCBV and other MRI parameters* *168*
Table 8-1: *Summary of different experimental groups used in this chapter.* *181*
Table 8-2: *Parameters used in the acquisition of T_1- and T_2-weighted images* *182*
Table 8-3: *Parameters used in the acquisition of images for the creation of T_1, T_2 and T_2* maps* *183*
Table 8-4: *Parameters used in the acquisition of diffusion-weighted images* *183*
Table 8-5: *Summary of parameters used in the acquisition of magnetisation transfer data* *184*
Table 8-6: *Summary of parameters used for the acquisition and creation of rCBV maps* *184*
Table 8-7: *T_2 relaxation times in the lesion and analogous area in contralateral striatum.* *197*
Table 8-8: *T_2* relaxation times in the striatum following intracerebral injection of BCG* *199*
Table 8-9: *Intensity ratio of signal enhancement on post-contrast T_1-weighted images* *201*
Table 8-10: *ADC values and area of elevated ADC.* *204*
Table 8-11: *Unpaired t tests between different time-points for ADC in region of ADC hyperintensity* *204*
Table 8-12: *Unpaired t tests between different time-points for area of ADC hyperintensity.* *205*

Table 8-13: *rCBV ratios pre-challenge and post-challenge.* *208*
Table 8-14: *Unpaired t tests between different time-points for striatal T_1 relaxation time of LPS-challenged animals.* *211*
Table 8-15: *Unpaired t tests between different time-points for striatal T_1 relaxation time in SAL PC controls.* *211*
Table 8-16: *Unpaired t-tests for cortical T_1 relaxation time in LPS-challenged animals between different time-points* *213*
Table 8-17: *T_2 relaxation time in both injected and contralateral striata pre- and post-challenge..* *214*
Table 8-18: *T_2 relaxation times in injected and contralateral cortices pre- and post-challenge.* *215*
Table 8-19: *T_2* relaxation time of striatum pre- and post-challenge.* *215*
Table 8-20: *Area of lesion on T_2* maps pre- and post challenge.* *215*

Chapter 1

Introduction

Multiple Sclerosis (MS) is one of most common inflammatory demyelinating diseases of the central nervous system, and is a major cause of disability in both the younger and older populations. The prevalence of MS varies according to geographical location, and is greatest in Europe, Australia and the USA. The disease is generally believed to be an immune mediated disorder occurring in genetically susceptible people, however the sequence of events triggering the disease remains unknown. The most common pathological features of the disease are focal areas of demyelination, immune mediated inflammation, and astrocytic gliosis. Lesions can occur at any site within the brain, although some affected regions give rise to greater clinical deficits. The disease usually presents in women during the third decade (mean age of onset is 31 years), and the prognosis can be variable depending on the type of MS. The form of MS present in the majority of patients has a relapsing remitting aetiology, which generally presents with visual disturbances. This type of MS is characterised by relapses of neurological dysfunction, which commonly arise sub-acutely over hours to days, plateau and then improve over days to weeks (Keegan 2002). The neurological symptoms depend on the location of the lesion within the brain, although many lesions may be clinically silent. Over the last decade tremendous progress has been made in elucidating the causes of MS and directing therapies towards improving patient outcomes, much work is still required.

Magnetic resonance imaging (MRI) is now one of the most powerful non-invasive diagnostic tools of many CNS disorders, including MS and Stroke. The phenomenon of

magnetic resonance was first described in 1945 by Bloch and Purcell, who were awarded the Nobel prize for Physics in 1952, but it was not until the early 1970's, that MRI was developed by Paul Lauterbauer. The last 10-15 years has seen many advances in MRI technology, such as the development of gradients, snapshot imaging techniques (such as Echo Planar Imaging) and higher field strength magnets, which has allowed various aspects of tissue structure and metabolism to be investigated.

Although the use of MRI to diagnose and study the progression of MS is common practice worldwide, very few correlations between the MRI-visible changes and underlying neuropathology have been carried out. This is mainly due to the inaccessibility of neurological correlates from autopsy material, and ethical considerations. Introduction of animal models have allowed these investigations to be carried out, and the major aim of the experiments described in this thesis is to determine the relationship between the histopathology of Multiple Sclerosis, disease processes occurring in MS, and MRI signal changes. Recent animal models of MS include experimental allergic encephalomyelitis (EAE) and Theiler's murine encephalomyelitis (TMEV), however a major problem with these models is that few of them adequately represent the pathology observed in the MS patient. In addition, the inflammatory lesions in these models appear spontaneously and occur at any site within the brain, making longitudinal studies difficult. The Delayed Type Hypersensitivity (DTH) model has recently been developed and yields an immune-mediated lesion within the brain parenchyma. This model confers a major advantage over previous models of MS, in that the site of the lesion is precisely dictated allowing for longitudinal study using MRI in association with histopathological correlation. The main differences between this model and other animal models of MS, is that it is not induced against self-antigens. Nevertheless, the ensuing lesion exhibits all the hallmarks of an MS lesion, therefore

owing to its advantages over typically used models of MS, the DTH model has been considered to be the model of choice for the studies reported in this thesis.

1.1 Aims of this Thesis

The aims of this thesis may be divided into the main areas listed below.

1. To use conventional histopathological techniques to qualitatively and quantitatively characterise and verify the DTH model as a valid model of Multiple Sclerosis, and to refine the model to allow MRI investigation.
2. To investigate DTH lesion progression using conventional T_1- and T_2-weighted imaging techniques, in order to compare with MS lesion progression on MRI and to correlate changes with underlying histopathology.
3. To assess the evolution of the DTH lesion using the more recently developed MRI techniques of contrast enhancement, diffusion-weighted and magnetisation transfer imaging and to correlate changes with underlying histopathology.
4. To make a quantitative assessment of regional cerebral blood volume changes, and again, to correlate any changes with ongoing histopathology.
5. To determine whether a peripheral infection can reactivate, or exacerbate a lesion within the CNS once the primary inflammatory response has resolved.

1.2 Overview of this thesis.

Chapter 2 covers the background of MS, including a brief discussion of the pathology, physiology and MRI characteristics of the disease. Animal models of MS will be compared and contrasted, and an introduction to the Delayed Type Hypersensitivity

(DTH) model will be given. That chapter also covers the various MRI contrast mechanisms that are used in this work, although an in-depth discussion of MR physics is not included.

Chapter 3, discusses in general terms of materials and methods used in order to carry out the experiments carried out throughout this thesis, greater detail is given in the individual chapters. Several sections exist in this chapter, describing immunohistochemical and MRI methods, details of surgical procedures and data analysis protocols.

Chapter 4 is the first of five experimental chapters. In this chapter the DTH model was presented and characterised extensively using histology and immunohistochemical techniques. Some refinement of the model was performed to obtain a consistently induced DTH lesion that could be studied using MRI. Quantitative counts of recruited immune cells and macrophages were obtained along with qualitative assessment of neuronal loss. Blood brain barrier permeability was also investigated.

Chapter 5 is the first MRI chapter, in which the DTH model was characterised using 'conventional' MRI techniques, i.e. T_1- and T_2-weighted imaging, since these are widely used in clinical practice to diagnose and assess development of the MS lesion. Part of the second aim of this thesis was to correlate any changes visible on these images with the histological characteristics identified in Chapter 4, therefore the second part of this Chapter investigated these histopathological correlates.

In chapter 6, contrast enhancement was used as a tool to investigate BBB permeability in the DTH lesion. Diffusion and magnetisation transfer properties of the DTH lesion and the surrounding tissue were also investigated. These latter techniques are relatively new

to the MS field, but are becoming more widely used in clinical practice. Underlying histopathology was correlated with the MRI changes.

Chapter 7 addresses the fourth aim of this thesis, primarily to investigate perfusion changes within the lesion and throughout the injected hemisphere. To date, there are very few studies studying perfusion and blood volume changes in MS patients or animal models of MS, and this chapter highlights the need for further investigation into this area. Again, in this chapter underlying histopathology was correlated with MRI changes.

Chapter 8 investigates the long-running hypothesis regarding peripheral infections, and their role in reactivation and relapse of neurological symptoms in MS patients. The first part of this chapter investigated the acute DTH inflammatory response further, by investigating additional MRI parameters, such as quantitative T_1, T_2 and T_2* mapping. The second part of this chapter addresses the fifth aim of this thesis; to investigate immune response reactivation in a previously quiescent DTH lesion by a peripheral infection. Reactivation was studied using conventional T_1- and T_2-weighted imaging, T_1-, T_2- and T_2*-mapping, diffusion-weighted, magnetisation transfer, and perfusion imaging.

In the final chapter, (Chapter 9) the major conclusions derived from the work described in this thesis are pulled together, and possible directions for future experiments were identified.

Chapter 2

Background

This Chapter is divided into 2 main parts: The first part of this Chapter will discuss the immunology and pathology of MS and animal models of MS, and how MRI is a crucial tool in relating visible changes with ongoing inflammatory processes. The second part of this chapter introduces the concept of contrast in MRI and covers the various contrast mechanisms that are central to this work. The physics of MRI, imaging sequences, and image formation are not covered here, as they are described in extensive detail in other sources.

2.1 The Immune Response in the CNS

The immune response is responsible for ensuring the integrity of the body when exposed to environmental and endogenous pathogens. In the brain, this response is controlled by the interaction between T and B cells, which are the primary immunoeffector cells within the CNS, and these must be delivered from the peripheral nervous system, to the site of injury or infection by the local blood supply. In the brain, recruitment of T and B lymphocytes to the brain parenchyma is controlled by the blood brain barrier (BBB). Resident glial cell populations, such as microglia and astrocytes, become rapidly activated as part of an intrinsic immune defence of the brain, whilst peripheral monocytes and polymorphonuclear neutrophils may be recruited to the brain parenchyma.

2.1.1 The Cell Types

There are three main types of cell present in the CNS that are important in regulation of the immune response. Astrocytes are the most abundant cells, and are the main component of the BBB, and are also responsible for antigen presentation. Following activation, the so-called reactive astrocytes are also capable of secreting cytokines, although activation of astrocytes tends to occur later than microglia (Gehrmann 1995).

Microglia are the resident macrophages of the CNS, and as the main effector cells of the CNS, their functions include production and release of cytokines, antigen presentation and phagocytosis. In addition, they also produce and release complement components, glutamate, oxidative free radicals and nitric oxide. Macrophages are also responsible for myelin opsonisation, which facilitates myelin uptake (Gehrmann 1995). In addition, perivascular microglia are an important component of the BBB.

T lymphocytes, which can be found throughout the peripheral and central nervous systems following an inflammatory response, may be specifically activated by astrocytes and macrophages in the CNS. They express Major Histocompatibility Complex (MHC) class II on their surface, enabling their activation and migration across the BBB where antigens are recognised. T lymphocytes play a key-role in initiating and perpetuating the disruptive inflammatory response in autoimmune conditions, such as MS. They too secrete cytokines, which in turn are able to activate more T lymphocytes and initiate the inflammatory cascade. B lymphocytes in contrast, have a role in the humoral immune response, by antibody production, but they have a less important role in acute inflammatory CNS lesions. Polymorphonuclear cells, such as neutrophils are important cells involved in very acute inflammatory responses, for example, following trauma.

2.1.2 Blood Brain Barrier

The BBB normally restricts entry of macromolecules and circulating cells, and it consists mainly of endothelial cells and perivascular microglia, and exhibits special tight junctions that restrict cell entry.

After disease or injury within the brain parenchyma, one of the earliest events in the inflammatory response is expression of adhesion molecules (e.g. selectins and integrins) by the vascular endothelial cells. The presence of these molecules at the luminal side of the cerebral vessels aids binding to, and translocation across, the BBB of other inflammatory cells such as macrophages, neutrophils and T & B lymphocytes.

The CNS was once thought to be an immune privileged site, because of the lack of lymphatic drainage and the presence of the brain endothelium, the BBB. However, it is now clear that activated T cells and monocytes can enter the CNS parenchyma, independent of specificity. Nevertheless, a delay occurs in the CNS inflammatory response, because there are very few lymphocytes in the normal brain (Hickey 1988). After initiation of a T cell response, activated T cells can readily cross the BBB, invade the CNS, and initiate disease pathogenesis. After an encounter with specific antigen presented by local antigen presenting cells (APC's), e.g. the perivascular macrophages, T cells undergo clonal expansion and change from having a naïve, to an effector phenotype, and up-regulating co-stimulatory and adhesion proteins. Some T cells can recognise antigens presented at the BBB. In this scenario, T cells bind to the BBB, facilitated by selectin and integrin expression at the endothelial surface. Firm attachment of activated T cells must occur before migration takes place, which occurs with the aid of cytokines, chemo-attractants and complement.

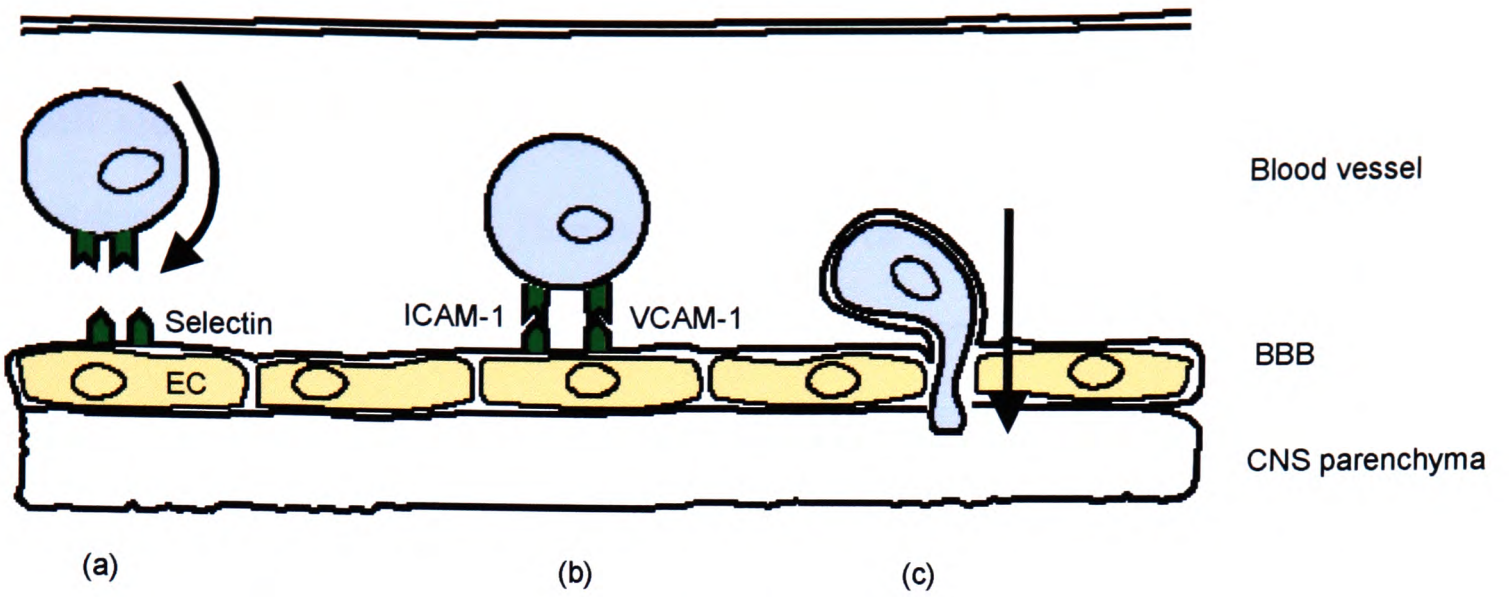


Figure 2-1: Migration across the BBB by activated T cells, the first stage (a) is capture and rolling, followed by (b) activation and adhesion, and ultimately (c) migration between endothelial cells (EC) making up the basement membrane.

After migration across the BBB (Figure 2-1), activated T cells interact with microglia (resident macrophages), which can release chemokines and cytokines. These chemicals upregulate the inflammatory cascade, by allowing activation and recruitment of other inflammatory cells, such as astrocytes, dendritic cells, and monocytes.

2.1.3 Multiple Sclerosis

MS is one of the commonest disabling neurological diseases. It is a chronic inflammatory disease of the white matter in the CNS, and affects both the young and older populations in the western hemisphere. Currently there are 85,000 patients with MS in the United Kingdom alone (Multiple Sclerosis Society). The disease usually presents in women, although can be seen in men, during early adulthood. Among the first of the clinical symptoms are sensory disturbances, limb weakness, and clumsiness. The patient may become completely wheelchair-bound as the disease progresses. The presentation and course of MS depends on the type of disease; of which there are three main forms. The first is relapsing-remitting MS (RR MS), which occurs in 85% MS patients, and may last for 8-15 years (Trapp 1999), and is subsequently followed by a course of secondary

progressive MS (SP MS), where there is progressive neurological degeneration. In a small group of patients (5%), symptoms get progressively worse resulting in primary progressive MS (PP MS). However, irrespective of aetiology, each type of disease pattern results in the same neuropathology at post-mortem (McDonald 1999).

2.1.4 The Inflammatory Response in Multiple Sclerosis

In MS, the inflammatory response is thought to be brought about by the action of T cells and macrophages on autoantigens, which results in a demyelinating plaque, the development of which is directly related to clinical symptoms. Lesions may occur throughout the brain and spinal cord, but more specifically, the periventricular white matter, brain stem, cerebellum and spinal cord white matter are sites that lead to functional damage (Noseworthy 2000). The pathology of the MS lesion is caused by many factors, including cell-mediated toxicity, antibody- and complement mediated lysis, and the toxic effects of cytokines (e.g. IL-1β, TNF-α), oxygen radicals and nitric oxide. The current understanding of MS pathology is summarised in Figure 2-2. The MS lesion is a hypercellular area in which axonal damage, gliosis and atrophy (tissue loss) occurs. In addition, up-regulation of cellular adhesion molecules, such as the selectins and ICAMs has been demonstrated. In acute MS, perivascular cuffing occurs with parenchymal infiltration of macrophages and lymphocytes, visible on electron microscopy. Oligodendrocyte damage also occurs early in plaque development resulting in demyelination and alteration of axonal conduction, significantly contributing to neurologic dysfunction. Sub-acute lesions show varying stages of remyelination, whereas chronic plaques have no acute inflammation and are completely demyelinated with marked gliosis and a variable axonal loss (Miller 1999). Demyelination may be brought about by numerous mechanisms, including direct toxicity of T cells, cytokine secretion,

antibody-mediated toxicity, complement and macrophage activation, these mechanisms are reviewed in the literature by Brosnan et al. (Brosnan 1996). The variability in these processes, which may occur separately or in association with each other, may explain the heterogeneity of clinical presentation and pathology encountered.

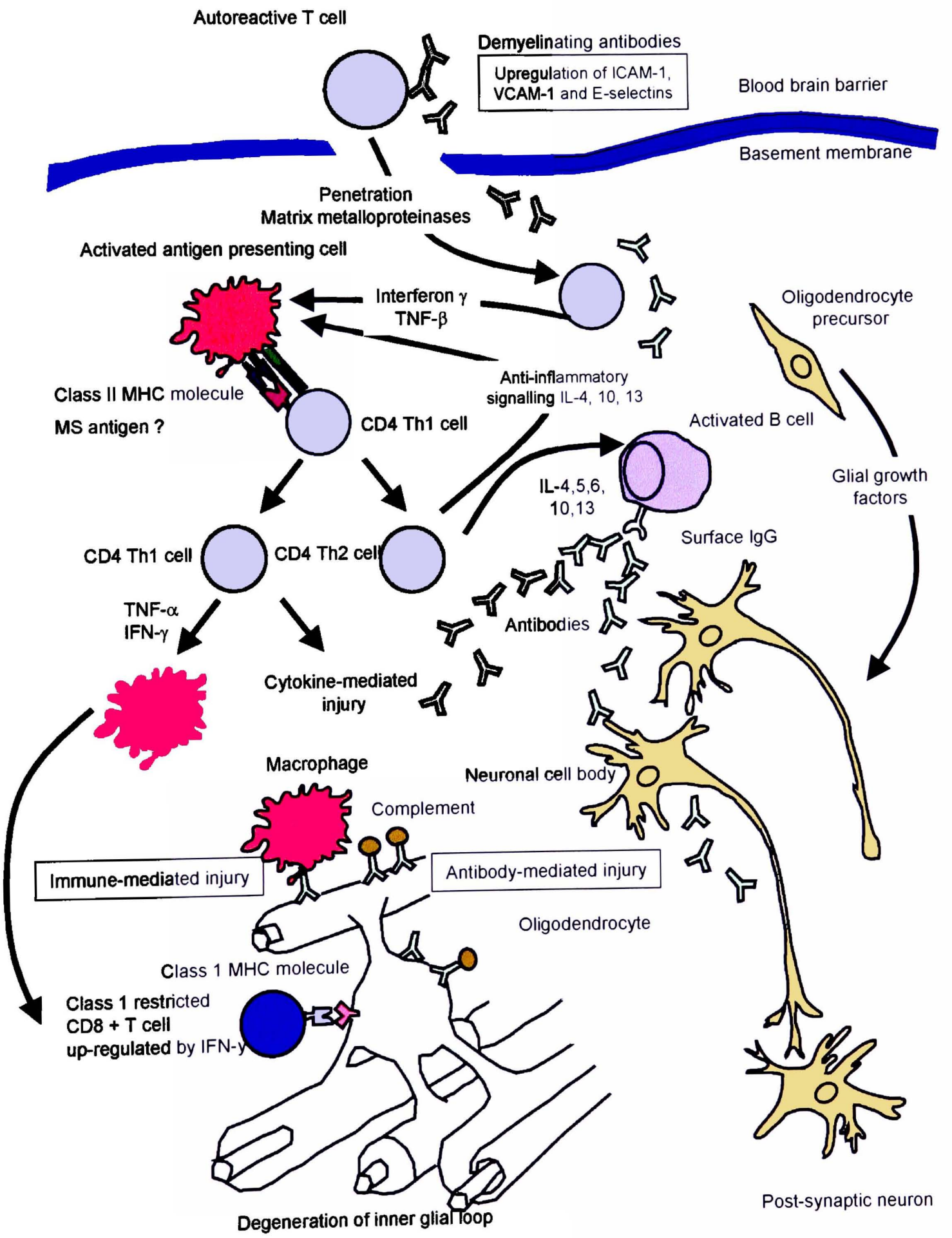


Figure 2-2: Current understanding of pathology in MS. Based on a diagram from Multiple Sclerosis, Noseworthy et al. (Noseworthy 2000).

2.1.5 MRI in MS

Various MRI studies have been performed on MS patients since MRI was first used as an investigative tool in the early 1980's (Young 1981). MS lesions were often confused with other neurological disorders such as Systemic Lupus Erythematosus, although as the number of patient studies increased and the technology advanced, MRI became the prime diagnostic tool for MS. Different MRI sequences detect various aspects of the disease process. Typical MR sequences include T_1-weighted, with and without contrast enhancement, and T_2-weighted, these are described in context of image contrast in Section 2.3.1. The first recognised characteristic of MS lesions on MRI, were hypointensities on T_1-weighted images (Uhlenbrock 1989). In time, it was found that these hypointensities correlated with tissue alteration resulting from demyelination and axonal loss (van Waesberghe 1999), (Bitsch 2001).

Clinicians now currently use the observation of gadolinium enhancement on post-contrast T_1-weighted images to evaluate development of new lesions (Fazekas 1999), although not all new lesions may be contrast enhancing. BBB breakdown is the first characteristic of MS lesions detected using MRI (Kermode 1990). Acute lesions appear highly enhancing, and generally enhance for as long as the inflammatory response occurs. Lesions may exhibit different patterns of enhancement as they evolve, for example, when the lesion moves from being acute to chronic, ring-like enhancement is observed, whilst no enhancement is seen in fully chronic lesions despite the lesion being highly active at the histopathological level (Petrella 1996).

In some cases, T_2-weighted imaging is the favoured MRI modality to use when identifying MS lesions, since a great deal of information is obtainable from tissue structure. MS lesions appear hyperintense on T_2-weighted images (van Waesberghe

1997), (van Walderveen 1998), (Simon 1999), (Miki 1999), and lesions can be identified in regions of the brain that appear entirely normal on T_1-weighted images (Fazekas 1999). The primary features of MS lesion pathology, such as demyelination, oedema, gliosis, inflammation and axonal loss all increase water content and therefore are likely to contribute to signal changes on T_2-weighted images, although oedema and demyelination are the most likely candidates for the MRI visible changes. Furthermore, T_2-weighted imaging does not give any information about the age of the lesion since both enhancing and non-enhancing lesions appear hyperintense on T_2-weighted images (Fazekas 1999).

The advent of more advanced MRI techniques, such as diffusion-weighted imaging and magnetisation transfer (MT) imaging has broadened the scope of clinical MRI for diagnosis and monitoring of MS. Diffusion-weighted imaging revealed that MS lesions have an increased Apparent Diffusion Coefficient (ADC) (Larsson 1992), (Christiansen 1993), (Horsfield 1996), (Droogan 1999), (Tievsky 1999), (Werring 2000), (Wilson 2001), (Caramia 2002). The increased ADC is thought to result from an increased intracellular space resulting from demyelination. Interestingly, it is not just the lesion that shows water diffusion changes. The ADC in normal appearing white matter (NAWM) has been shown to increase prior to lesion enhancement on post-contrast T_1-weighted images, indicating that structural changes occur before lesion appearance. After the first appearance of lesions on post-contrast T_1-weighted images the ADC decreases again, reflecting either repair of the BBB, remyelination or gliosis (Werring 2000).

MT imaging is another method whereby subtle changes in tissue structure can be identified. This technique was first utilised by Balaban et al. in 1989, but owing to the complex nature of magnetisation transfer, the technique is not fully understood. Similar to diffusion-weighted imaging, MT imaging is also able to detect changes in the NAWM away from the lesion (Pike 2000). Generally, MS lesions that are apparent on T_2-

weighted images and post-contrast T_1-weighted images have been shown to have a reduced magnetisation transfer ratio (MTR) (Hiehle 1995), (van Buchem 1996), (Campi 1996), (Rovaris 1999). A low MTR indicates a reduced capacity of the molecules of the brain tissue matrix to exchange magnetisation with surrounding water molecules.

In MS, it is generally thought that a low MTR is brought about by a reduction in the integrity of the macromolecular matrix, reflecting myelin loss or axonal damage. In support of this concept, lesions exhibiting substantial myelin loss have a lower MTR than those with less demyelination (Hiehle 1995). Alternatively, it has also been suggested that a low MTR may arise through dilution of the macromolecular pool resulting from oedema, although it has been reported that lesions that have a large oedema component, only a mild reduction in MTR is observed (Hiehle 1995). Furthermore, a positive correlation has been shown between MTR and T_1 hypointensity (Hiehle 1995), (Loevner 1995).

2.1.6 MRI and Histopathological Correlations

Several attempts have been made to correlate MRI visible changes and clinical signs, disease duration, or disability, to attempt to understand the underlying neuropathology of MS. To date, it has been found that ADC changes correlate with disability, disease duration and cerebral atrophy, whilst T_2 lesion volume correlated with disability only (Wilson 2001). In other studies, reduced MTR and T_1 hypointensity have also been shown to correlate (Loevner 1995), (Hiehle 1995), and MTR correlates with demyelination (van Waesberghe 1998) and axonal density (van Waesberghe 1999). Thus, it follows that T_1 contrast ratio correlates with axonal density (van Waesberghe 1999). Since a great deal of confounding information regarding the underlying effects of MS

currently exist, development of models of disease processes occurring in MS lesions have vast potential.

2.1.7 Animal Models of MS

Animal models of human diseases provide unique insights into the development of disease progression. As mentioned in the previous section, there is little conclusive information concerning neurological correlates of MRI changes observed in the MS patient. A primary goal of animal studies is to determine the relationship between disease histopathology and MRI signal changes. Different animal models of MS have been developed to investigate the inflammatory processes occurring within the CNS, these primarily are Experimental allergic encephalomyelitis (EAE) model (in rodents and primates) and Theiler's Murine Encephalomyelitis Virus Model (TMEV).

2.1.7.1 Experimental Allergic Encephalomyelitis (EAE) Model

MS and EAE are autoimmune disorders that share many radiological, clinical and immunopathological characteristics. EAE can be induced actively in different species by peripheral immunisation with either CNS components or purified components of myelin, e.g. myelin basic protein (MBP), proteolipid protein, or myelin oligodendrocyte glycoprotein (MOG). The ensuing disease can take a variety of forms, including acute, chronic progressive, or relapsing-remitting, which has features in common with RR MS. An alternative model is that known as adoptive transfer EAE, involving transfer of specific sensitised T cells, such as MHC class II-restricted CD4+ Th1 cells that are reactive with peptides (e.g. MOG) in the target animal. This type of EAE runs a more synchronous course than MOG-induced EAE (Gold 2000). In rats, EAE usually manifests as an inflammatory rather than a demyelinating disease, confined to the brain

stem and spinal cord (Jordan 1999). Lewis rats are commonly used, in which maximum disease expression is usually reached 2-4 days after disease onset. Recovery from the monophasic disease, is associated with increased apoptosis of T cells in the lesion (Gold 2000). Clinical symptoms occur 10-12 days after EAE induction, and these include weight loss, paralysis, incontinence and muscle wasting, and eventually death ensues. EAE lesions in rats can show demyelination, and remyelination is also observed (Bubis 1964). In addition, EAE lesions exhibit similar inflammatory infiltrates to the MS lesion, composed of macrophages, T and B lymphocytes, and neutrophils, which form perivascular cuffs. Oedema surrounds the lesion and extends beyond the cellular infiltrates (Bubis 1964), which may be found in the white matter, meninges and perivascular regions (Ahrens 1998). However, the EAE model has a number of limitations, in that it is induced with a known auto-antigen in genetically susceptible animals, whereas MS occurs spontaneously in a heterogeneous population with some degree of genetic susceptibility. In addition, the inflammatory infiltrate differs between EAE and MS, such that in EAE lesions, granulocytes are visible, which are not seen in the MS lesion (Gijbels 2000). EAE affected animals may on occasion exhibit meningeal inflammation and a haemorrhagic component, both of which are absent in MS patients (Karlik 1989). It has also been shown that chronic EAE lesions exhibit more remyelination than MS lesions (Prineas 1969). In RR MS, patients relapse and their symptoms worsen, however EAE animals do not spontaneously relapse and remit (Gold 2000).

In mice, however, EAE can have a chronic relapsing disease course and also shows evidence of demyelination and remyelination (Ahrens 1998). Mouse models have the advantage that genetic engineering can be used to manipulate genes controlling

susceptibility, disease course and remyelination. But there is variability in disease course and susceptibility with different mice strains.

More recently, EAE has been studied in non-human primates, and the general principles underlying demyelination and inflammation observed in rodent models of EAE have been confirmed in the primate models. These models are more advantageous over rodent models for potential pharmacological intervention of disease progression. A further advantage is that in primates, EAE causes a neurological deficit after each disease phase (Kornek 2000), yielding a disease course more similar to that observed in MS patients.

2.1.7.2 Theiler's Murine Encephalomyelitis Virus (TMEV)

Theiler's Murine Encephalomyelitis Virus (TMEV) is induced in mice by an infection in the CNS with the virus. TMEV is an endogenous mouse pathogen that normally establishes a lifelong persistent CNS infection leading to a progressive T cell mediated demyelinating disease similar to MS. Mice infected with the virus normally develop the disease 30-35 days post-infection. The infection has two stages, of which the second mimics MS pathology. In the first stage of the disease, the virus affects neurons, whereas in the second phase, white matter glial cells are affected. Widespread demyelination occurs around 50-60 days post-injection (Olson 2001). The spinal cord is also affected by chronic inflammation and demyelination (Brahic 2002). Axonal damage does occur during the later stages of the persistent infection, and cytokine production has been observed (Stohlman 2001). This is a useful model for the investigation of a molecular mimicry mechanism behind the pathogenesis of MS, and since this is a mouse model, there is potential for investigation of various gene epitopes for myelin proteins. However, like EAE, it does not reproduce all the features of a typical MS lesion.

2.1.7.3 Delayed Type Hypersensitivity (DTH) Model

A more recently developed animal model exhibiting an MS-like lesion is the Delayed Type Hypersensitivity (DTH) model, which confers several advantages over EAE. DTH reactions occur following the re-exposure of an individual to an antigen to which it has previously been sensitised. In the DTH model, a lesion is induced when heat-killed Bacillus Calmette-Guerin (BCG), is sequestered behind the BBB, and is later targeted by a DTH response following an intradermal challenge of Tuberculosis (TB) (Matyszak 1995). In this model, a focal lesion is induced, which is characterised by macrophage and T lymphocyte infiltration, BBB breakdown and tissue damage including myelin loss. DTH lesions are pathologically similar to those found in both MS and EAE, however DTH lesions are more chronic than EAE lesions (Matyszak 1997). In addition dendritic cells are found in greater numbers in DTH lesions than acute EAE lesions, and may persist for months. Cytotoxic T cells with high affinity for heat shock proteins are also found in vast numbers in both DTH and MS, whilst they are much less common in EAE (Matyszak 1996). Extensive tissue damage is seen in MS, involving demyelination and axonal damage, which is mimicked by DTH lesions (Matyszak 1995), but not EAE lesions (Lassman 1983). Another important factor is that EAE lesions do not appear to change in size; MS lesions increase in size with time (Lassman 1983), and the DTH lesion also alters in size with time (see Chapters 5, 6, and 8). DTH lesions can be shown to exacerbate or worsen, with relative ease, as discussed later in Chapter 8. EAE lesions occur spontaneously at any site in the CNS, whilst in the DTH model, the exact site of the lesion and time of induction are known, thus facilitating temporal studies throughout lesion development. This also enables correlative studies of immunological and MRI abnormalities that may occur before lesion development. Finally, it has been hypothesised that an environmental trigger brings about MS. In this respect, the DTH

model may more closely represent MS aetiology than EAE, since it is induced by an environmental trigger, in this case a bacterium (BCG).

2.1.8 MRI in EAE

Most of the MRI investigations that have been carried out in EAE studies mimic the findings observed in MRI studies of MS patients. Early investigations of EAE using MRI identified that lesions appear as hypointense regions on T_1 weighted images (Karlik 1990), (Barnes 1991), (Seeldrayers 1993) with older, more gliotic lesions having a greater increased T_1 relaxation time (Stewart 1991). During acute EAE, the lesions also appear as regions of increased signal intensity on T_2-weighted images (Barnes 1987), (Grossman 1987), (Namer 1992), (Namer 1998), (Hart 1998), (Karlik 1999). These regions have been correlated with a variety of histological parameters, including oedema, inflammatory cell infiltration, demyelination, and perivascular cuffing (Grossman 1987), (Namer 1992), (Namer 1993), (Duckers 1997), (Jordan 1999). BBB breakdown is observed on post-contrast T_1-weighted images (Hawkins 1991), (Namer 1992), (Namer 1993), (Seeldrayers 1993), (Hart 1998), (Namer 1998), (Karlik 1999), and a correlation exists between BBB breakdown and the onset of clinical signs (Namer 1992), (Jordan 1999). In addition, a correlation has been demonstrated between increased T_2 signal intensity, and both BBB permeability (Namer 1992), with signal changes on proton density weighted images (Jordan 1999).

The observation that MRI changes occur before the onset of clinical signs was first seen in the EAE model (Stewart 1985), and it was in EAE that the first *in vivo* MTI experiment of the brain was carried out (Dousset 1992). Mild MTR reductions are observed during acute EAE (Dousset 1992), whilst greater reductions are found during the chronic phases (Gareau 2000). Furthermore, MTR imaging has demonstrated abnormalities that parallel the onset of clinical signs and that are not visible on other MRI modalities (Gareau 2000).

Diffusion-weighted imaging has also been performed in EAE studies. Increases in water diffusion have been observed in both acute and chronic EAE (Heide 1993), (Richards 1995), (Verhoye 1996). There is also evidence that diffusion-weighted imaging is able to detect changes in water diffusion before lesion onset (Heide 1993). Increased ADC correlates with worsening of clinical signs (Verhoye 1996), as well as with histopathological evidence of demyelination, inflammation, haemorrhage and necrosis (Richards 1995).

2.1.9 Smart Contrast Agents in EAE

Although gadolinium has many advantages as a contrast agent in assessing acute MS lesions, the presence of specific cell types cannot be investigated. Very recently, new contrast agents that are targeted to distinct molecules of pathology, for example mononuclear phagocytes, have been introduced. Ultrasmall particles of iron oxide (USPIO) are dextran coated nanoparticles of iron oxide that will be phagocytosed by, and hence accumulate in the cytoplasm of mononuclear phagocytic cells. In a magnetic field these particles give rise to decreased signal intensity on T_2 and T_2*-weighted images, and several hours after administration they can be found in macrophages in the lymph nodes of animals with EAE (Dousset 1999), (Dousset 1999), (Dousset 1999). In another study, the use of monocrystalline iron oxide nanoparticles (MION) in mice, allowed the visualisation of EAE lesions (Xu 1998). These methods have been verified using histological techniques and may provide further information about the inflammatory processes occurring in the DTH lesion, particularly regarding temporal macrophage recruitment. Another molecule targeted specifically for visualisation, is the adhesion molecule ICAM-1. A contrast agent is linked to Gadolinium, with monoclonal antibodies to ICAM-1, which is up-regulated during EAE and MS (Sipkins 2000).

2.1.10 MRI Assessment of Targeted Therapies in EAE

Inhibition of various elements involved in inflammation, have been targeted to identify ways of reducing inflammation in EAE as determined by MRI. In the EAE model, MRI visible BBB breakdown, can be prevented by TNF-α inhibitors (Genain 1995). Similarly, inhibition of matrix metalloproteinases reduces the amount of BBB breakdown and T cell recruitment (Matyszak 1996). An antibody specific to α-integrin has been shown to prevent infiltration of inflammatory cells into the CNS, and to reduce MRI visible oedema and BBB breakdown (Kent 1995), (Gareau 2000). Antibodies to ICAM-1 reduce T_1 relaxation times, prior to BBB breakdown (Morrissey 1996). Finally, treatment with analogues of neurotropic peptides, such as ACTH have been shown to reduce the size of lesions on T_2-weighted images, which reduces the functional and morphological manifestations of EAE (Duckers 1997).

2.2 MRI Theory

For a detailed discussion of nuclear magnetic resonance (NMR) theory the reader is referred to more comprehensive sources (Gadian, 2nd Edition 1995). A brief review of contrast mechanisms only will be given here, as these aspects of MRI are central to the work in this thesis.

2.2.1 Spin

MRI depends on the quantum property of certain nuclei (such as ^1H) known as spin. Because the nuclei have an electric charge, they also have magnetic properties. If this spinning nucleus is placed in a static magnetic field, it has an interaction with the field, owing to the angular momentum of the spinning nucleus. Thus, it will precess in the magnetic field with an angular frequency, which is directly proportional to the static magnetic field. This frequency is known as the Larmor frequency, and is proportional to the strength of the magnetic field. The frequency is given by:

$$\omega = \gamma B_0$$

where B_0 is the magnetic field, and γ is the gyromagnetic ratio of the nucleus.

In reality, in MRI, many populations of spinning nuclei are investigated, and all of these nuclei precess about the direction of the magnetic field (the z direction) to give a net magnetisation in line with the static magnetic field. To detect the magnetisation, the precessing nuclei are tilted into the xy (transverse) plane by application of a 90° radiofrequency (RF) pulse (B_1). After the magnetisation has been tilted the nuclei then precess in the xy plane (Figure 2-3) inducing a signal that can be detected and decays exponentially.

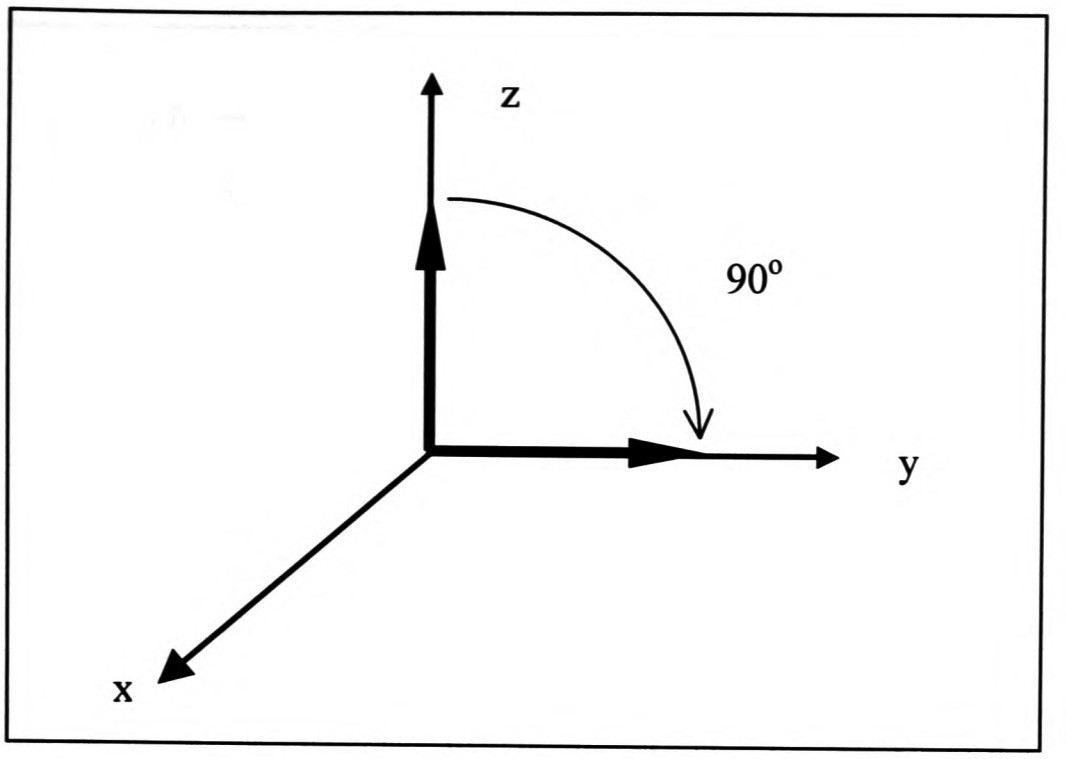


Figure 2-3: Nuclei precess in the xy plane after being tilted by a 90° pulse,

This is known as the free induction decay (FID), which is the observable signal in nuclear magnetic resonance (NMR).

2.2.2 Relaxation

Following excitation by application of an RF pulse, the energy of protons decay in an exponential manner, which is defined by two relaxation processes, having their own time constants, T_1 and T_2.

2.2.3 Longitudinal Relaxation

The first, T_1, is the spin-lattice relaxation, which is associated with the return of the magnetisation to the equilibrium state aligned in the direction of B_0. Protons that have been excited to a higher energy level dissipate their energy to molecules of the surrounding structure (or lattice). The characteristic pattern of decay for longitudinal spin relaxation following a 180° (inversion) pulse is shown in Figure 2-4.

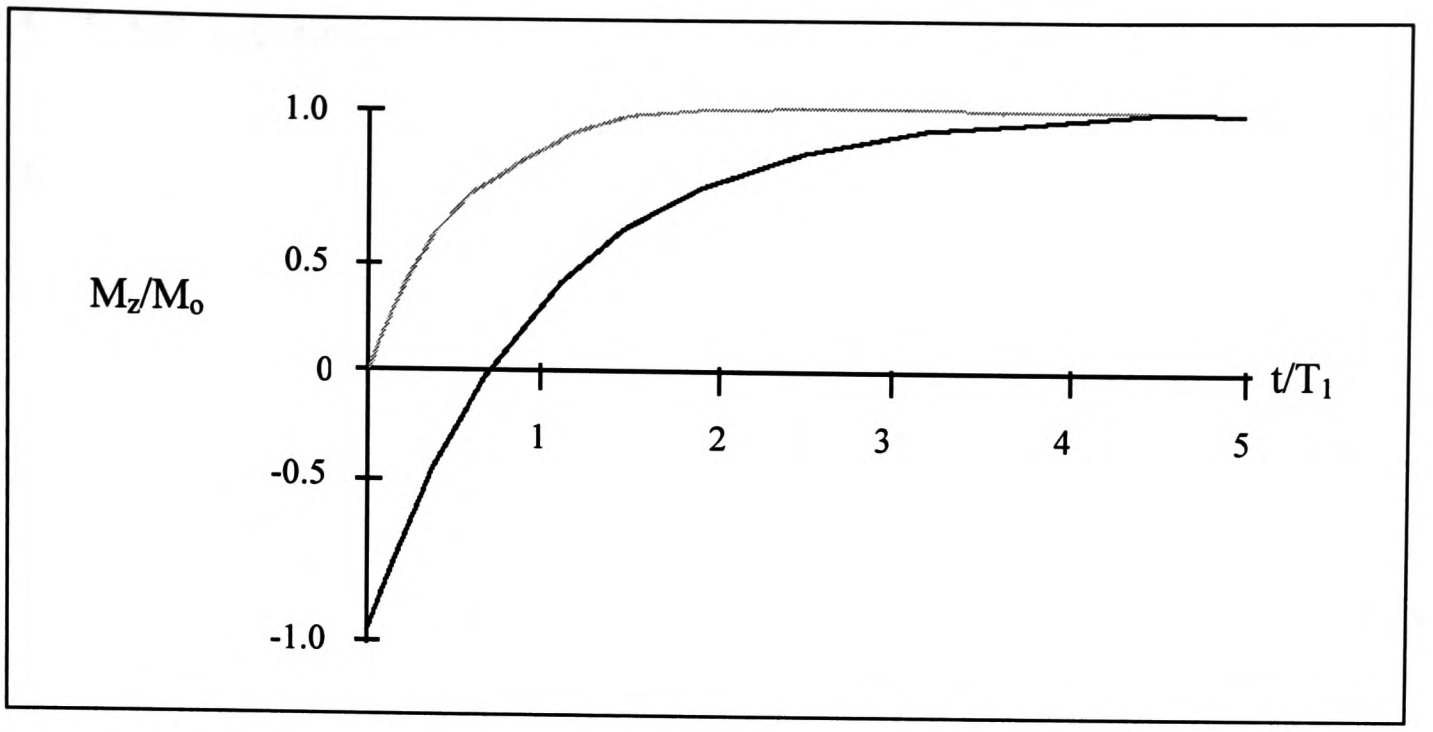


Figure 2-4: The decay of magnetisation in the longitudinal direction. The black line represents the decay of magnetisation following a 180° pulse, and the grey line represents the decay following a 90° pulse.

2.2.4 Transverse Relaxation

T_2, the spin-spin relaxation, is the decay of magnetisation in the plane perpendicular to B_0 (xy plane) causing reduction of the FID amplitude. This relaxation constant measures the exchange of energy between nuclei. The greater the energy transfer, the faster the loss of coherence, causing the overall magnetisation in the xy plane to decrease (Figure 2-5). In pure solutions $T_1=T_2$, but *in vivo*, the T_2 relaxation time is less than T_1, resulting in disappearance of the observed signal before the magnetisation has returned to equilibrium.

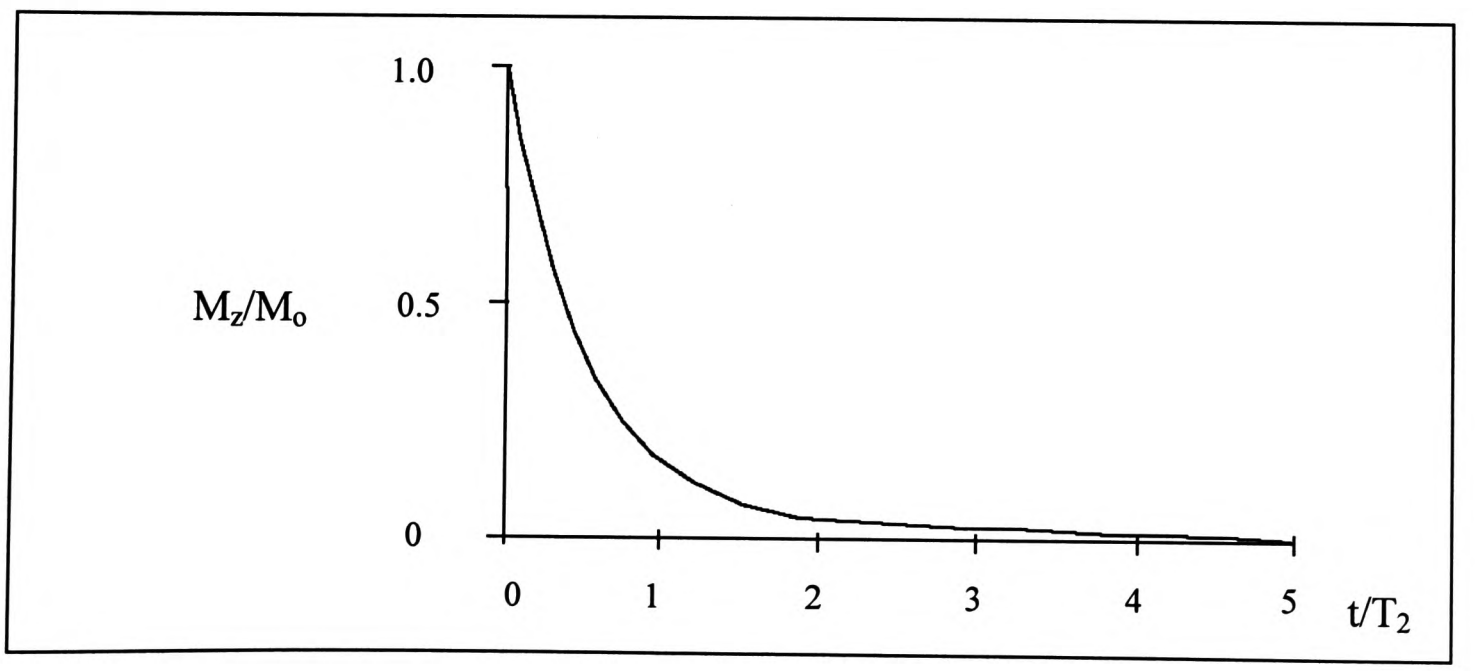


Figure 2-5: The return of magnetisation in the transverse plane.

2.2.5 T_2* Relaxation

If the applied magnetic field is non-uniform, due to an imperfect field generated by the magnet or local susceptibility differences in the sample itself, then spin dephasing will also occur. Nuclei will be precessing at different rates as determined by the Larmor frequency for the particular field strength at their location, and will therefore lose coherence, allowing less net transverse magnetisation. The loss of magnetisation due to field inhomogeneity is faster than natural T_2 signal delay. This leads to a further relaxation time, T_2*, which is the effective decay rate of the signal, allowing for any field inhomogeneities.

2.2.6 Excitation

If an RF pulse oscillating at the Larmor frequency of the nuclei under investigation is applied perpendicular to the z axis (along the y axis), it induces a B_1 field perpendicular to the B_0 field (along the y axis). This B_1 field rotates the equilibrium magnetisation away from the static B_0 field. The angle through which the magnetisation moves way from its equilibrium position along the z axis depends on the amplitude (B_1) and duration of the applied RF pulse.

$$\theta = \gamma B_1 t$$

where the oscillating B_1 field has been applied for time t, and θ is the flip angle of the pulse.

The strength of the detected signal is proportional to the net transverse magnetisation i.e., the component of the vector sum of all the nuclear spins that are not aligned with B_0, which is proportional to sin θ, and is maximal for a 90° pulse.

2.3 Image Contrast

This characteristic is based on differences in signal intensity brought about by differences in tissue structure or composition. The resulting NMR signal is therefore brought about by the interaction of proton density, T_1 and T_2 relaxation times, magnetic susceptibility and also the applied RF pulse characteristics. The contribution of these characteristics may be controlled by altering pulse sequence parameters, such as the repetition time (TR) defined as the time between 90° pulses, or the echo time (TE), the time between the 90° pulse excitation pulse and the centre of the echo.

2.3.1 T_1 and T_2 Contrast

Manipulation of the T_1 and T_2 relaxation time enables images to be generated where the intensity of the signals depends strongly on T_1 and T_2 values rather than proton density of the tissue. Relaxation times of different tissues vary widely, and values of T_1 and T_2 vary according to the local environment in which protons exist. Image contrast can be enhanced, by weighting of the image sequence for either T_1, or T_2 effects, enabling discrimination of different tissues. Pathological conditions affect these relaxation times, thus T_1 and T_2 values in diseased tissue are often significantly different to normal tissue, for example, addition of water, such as in oedema lengthens both T_1 and T_2 relaxation times.

If the TR of the imaging sequence is long compared to the T_1 of the tissue imaged, then image contrast is independent of T_1. If however the TR is less than or equal to T_1, then regions of the image corresponding to tissue with a long T_1, will be dark compared to those with a short T_1. Therefore decreasing the TR results in greater T_1 contrast in the image. Lengthening the TE, allowing time for spin dephasing, which is highly dependent

on the local environment, enhances T_2 contrast. To obtain T_1-weighted images, the TE is kept short to minimise T_2 contrast, and the TR is made short, whereas in order to obtain T_2-weighted images, the TE is lengthened and TR is long, in order to allow full T_1 relaxation and minimise T_1 contrast.

2.3.2 Gadolinium Enhancement

The diagnostic sensitivity of MRI can be improved with paramagnetic substances as contrast media. Ions and molecules that contain unpaired electrons demonstrate paramagnetic behaviour when they are placed in an external magnetic field. Gadolinium, is from the lanthanide series of rare earth elements and contains seven unpaired electrons, providing gadolinium with strong magnetic properties, thus it is widely used as a paramagnetic contrast agent for MRI. A stable complex is formed when gadolinium is chelated to diethylaminetriaminepentaacetic acid (Gd-DTPA). It shortens the T_1 relaxation rate of the tissue, increasing signal intensity on T_1-weighted images. After intravenous application it distributes in the extracellular space and quickly passes into the interstitial space if there is permeability in the membrane. In the brain, it is unable to cross the intact BBB, therefore gadolinium enhancement is a good indicator of BBB breakdown.

2.3.3 Diffusion-weighted Imaging

Diffusion-weighted imaging is based upon the random diffusion of spins through the sample due to Brownian motion, and is determined by the kinetic energy of the molecules and viscosity. Movement of molecules in a gradient field generates random phase dispersion of spins, leading to an exponential decay of magnetisation. *In vivo*, microscopic water movement within the intra- and extracellular space is hindered by

cellular structures that affect the signal observed on diffusion-weighted images. Diffusion of water molecules becomes anisotropic; it is dependent on orientation. Exchange of water across membranes also occurs in the natural system, creating microenvironments with different diffusion characteristics. Diffusion-weighting may be achieved by placing special gradient pulses around the 180° pulse in a spin-echo experiment, which attenuates the signal coming from spins diffusing in the presence of these gradient pulses. In a diffusion image, structures with fast diffusion appear dark due to greater signal attenuation, whereas structures with slow diffusion are bright. Varying the time and amplitude of the applied gradient pulses enables the calculation of the quantitative maps of the apparent diffusion coefficient (ADC). Here, fast diffusion appears bright (the reverse of the diffusion-weighted image). Diffusion-weighted imaging is more sensitive to motion artefacts during acquisition, where bulk movement leads to a net motion of all magnetisation and therefore changes the phase of all spins at once, by the same amount. This does not cause dephasing and signal loss, which happens with random diffusion. To reduce these motion artefacts, navigator echoes may be employed to record an extra non-phase-encoded echo that is then used to correct the phase of other echoes recorded. Pathological processes that modify the size, spacing or integrity of CNS structures may produce abnormal diffusion characteristics; meaning that diffusion weighted imaging may be valuable in determining disease processes.

2.3.4 Magnetisation Transfer

Magnetisation Transfer is based upon the cross-relaxation of immobile protons on macromolecules and mobile protons in free water. Application of an RF pulse away from the water frequency, but within the frequency range of macromolecular protons results in saturation of the macromolecular proton resonance. Exchange of this saturated

magnetisation with free water decreases the signal intensity following an off resonance pulse. Saturation of the macromolecular protons results in a disturbance of the steady state magnetisation of the free water protons brought about by magnetisation transfer between the two spin systems (Wolff 1989). Thus, changes in the population of bound protons results in regions exhibiting different MT contrast than that found in normal tissue. During MT imaging, an RF pulse or pulse-train is applied, designed to selectively saturate the broad resonance peak of the macromolecular protons. As the macromolecular pool approaches and reaches a stable condition of partial saturation, the saturation is transferred to the free pool so that the free pool also reaches a stable condition of partial saturation resulting in lower signal intensity on the MR image. The higher the rate of magnetisation transfer, the greater the level of signal suppression, assuming that other factors which may have an influence on the signal intensity are equal. The MT ratio reflects the difference in signal intensity between images with and without saturation.

2.3.5 Measurement of Tissue Perfusion

Measurement of tissue perfusion requires an assessment of the blood flowing at low velocities through capillaries that are too small to visualise directly. A paramagnetic agent such as gadolinium can be administered intravenously, and its passage can be tracked as a decrease in signal intensity observed in a series of rapid images (such as T_2*) susceptible to the dephasing effects of the paramagnetic agent. During the first pass transit through the cerebrovascular bed (which lasts 5 to 15 seconds), gadolinium is restricted to the intravascular space. The restricted intravascular presence of highly paramagnetic contrast molecules (gadolinium) creates microscopic field gradients around the cerebral microvasculature, resulting in shortening of T_2* relaxation and signal loss occurs. If blood supply to a region of interest is decreased, the change in signal on T_2* images may be either attenuated or delayed. In contrast, if perfusion to a region is

increased, then a greater signal change will be observed, since the gadolinium cannot pass through the intact BBB, it stays inside the vasculature. Using standard kinetic tracer analysis the time series of images can be converted into a map of cerebral blood volume (CBV); in which increased regional CBV (rCBV) appears as increased intensity, and decreased rCBV as decreased intensity.

Chapter 3

Materials and methods

3.1 Reagents

3.1.1 Preparation of heat-killed BCG

Live Bacillus Calmette-Guerin (BCG) organisms, strain 1173 P2 (5×10^8 organisms/ml; a gift from the Pasteur Institute, France) were killed by boiling for 10 minutes and then diluted to a concentration of 10^8 organisms/ml using sterile 0.1M phosphate buffer.

3.1.2 LPS

Escherichia coli lipopolysaccharide strain CO111:B4 (Sigma) in sterile pyrogen free saline was used at a dose of 100μg/kg.

3.1.3 TB

100mg *Mycobacterium tuberculosis* (TB) (Difco) was mixed with 6.7ml Complete Freunds Adjuvant (CFA) (Sigma). This solution was then diluted 1:1 with sterile saline and was well homogenised for 1 hour before use.

3.2 Animal Work

All of the experiments carried out in this thesis were carried out in concordance with UK home office guidelines and regulations.

3.2.1 Animals

Male Lewis rats were used for all experiments, and were obtained from Charles River. The animals were maintained on a 12 hour light and dark cycle and had free access to food and water at all times.

3.2.2 Anaesthesia

All surgical procedures were performed using a closed circuit ventilation system using halothane or isoflurane. Halothane was used at 0.8-1.5% halothane in 70% N_2O/30% O_2. Isoflurane was used at 2.0% at a flow rate of 0.8 l/min oxygen and 1.0 l/min Nitrous oxide (BOC). The compressed gas sources were connected via high-pressure tubing to the vaporiser. The vaporiser was connected via further tubing to a clear Perspex anaesthetising chamber with removable perforated floor, for the induction of anaesthesia with an additional outlet to the scavenging system. The anaesthetic entered the chamber through an inlet below the level of the perforated floor. At the opposite end of the chamber was an outlet that allowed vortex creation, to enable the gas to percolate through the floor and leave via the outlet. Whilst MRI was being performed anaesthesia was achieved using halothane or isoflurane. Halothane was used at 0.8-1.5% halothane in 70% N_2O/30% O_2. Isoflurane was used at 0.7-1.5% at a flow rate of 0.8 l/min oxygen and 1.0 l/min Nitrous oxide. Excess gaseous anaesthesia was scavenged using a Fluovac system consisting of fluosorber canisters (International Market Supply, UK) containing charcoal for the absorption of excess halothane or isoflurane.

3.2.3 Surgery

Once animals had been fully anaesthetised, rats were placed onto a stereotaxic frame (Kopf instruments). Instruments were sterilised using 70% ethanol prior to surgery.

Surgery was performed under an operating microscope (WILD M650). The fur on the animal's head was removed and a longitudinal incision was made into the scalp to reveal the underlying skull, where tissue was scraped off. A burr hole was drilled at the following co-ordinates (Bregma +1mm, lateral 3mm) (Figure 3-1) using a dentist's drill so that the surface of the brain was revealed. A pulled glass micropipette was used to deliver 1μl of the BCG. The tip of the pipette was placed on the surface of the brain and was then slowly advanced to the depth required (details are given in individual chapters). Injections were performed using a 10ml syringe attached to the end of the micropipette, over a period of 5 minutes to avoid damage to the brain, and to prevent reflux of the BCG up the injection tract. The micropipette was then removed and the skin closed using suture. Animals were then carefully monitored post-surgery.

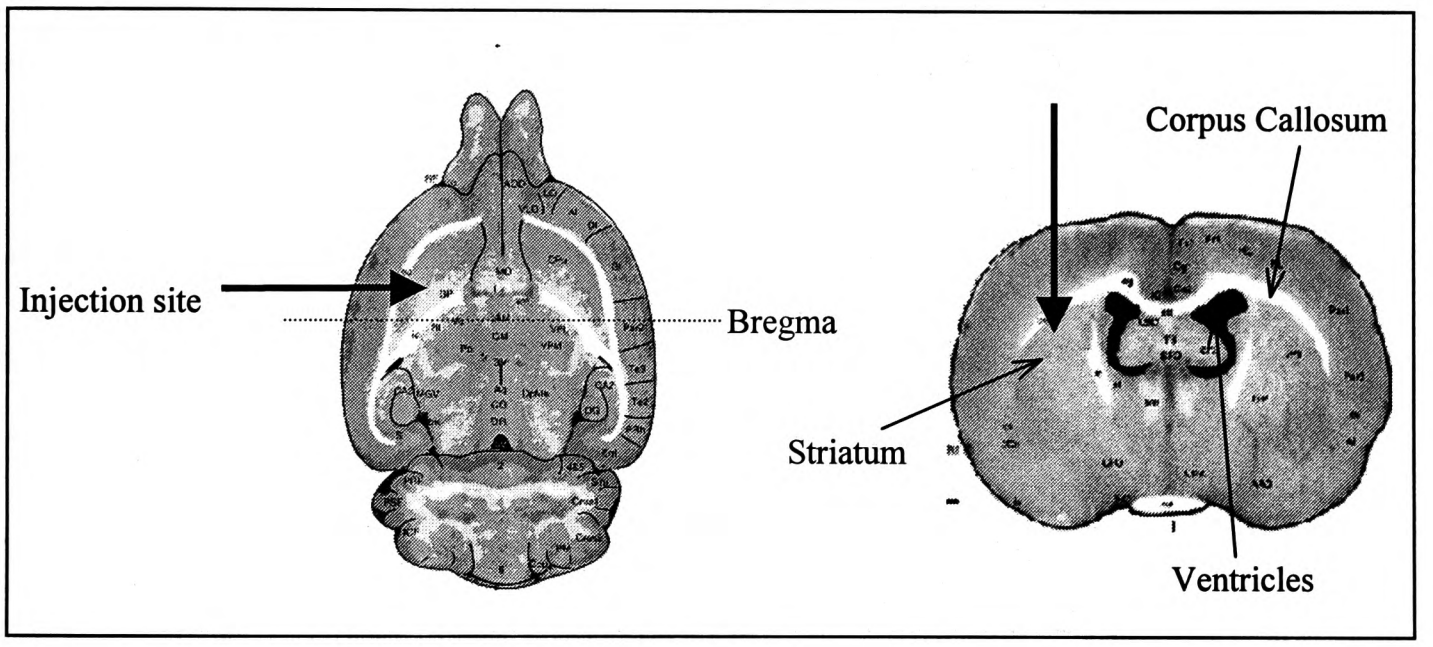


Figure 3-1: Injection coordinates in the horizontal planes of view, and depth of injection on coronal field of view.

3.3 Magnetic Resonance Imaging Hardware

Initial magnetic resonance measurements were made using a 7 Tesla (300 MHz) vertical bore spectrometer, and later studies were performed on a 300 MHz horizontal bore spectrometer. All data was acquired using a Varian Inova console (Varian, Palo Alto, CA, USA).

3.3.1 MRI Probe

A 34mm diameter Alderman-Grant resonator (42mm in length) was fitted in a home-built cylindrical Perspex probe body (34cm length; aluminium base plate: 21cm in length). The internal dimensions of the coil closely matched the head size of the rats, thereby minimising noise acquisition and enabling good signal induction. A copper shield was placed around the coil to earth the probe, preventing coupling between the probe and the gradients. Two variable capacitors were attached to the coil to allow independent tuning and matching. The animals head was placed in a home-built head-holder with bite bar and nose restraint (Figure 3-2) at a fixed placement from within the coil to minimise motion artefacts and ensuring reproducible animal positioning relative to the coil. The animal was placed supine within the probe body. To account for the difference between the bore sizes of the horizontal and vertical bore magnets a Perspex holder was made to fit over the probe body to allow positioning of the coil at the magnet iso-centre. The probe was fitted with a circulating warm water system to allow heating of the animal during experiments.

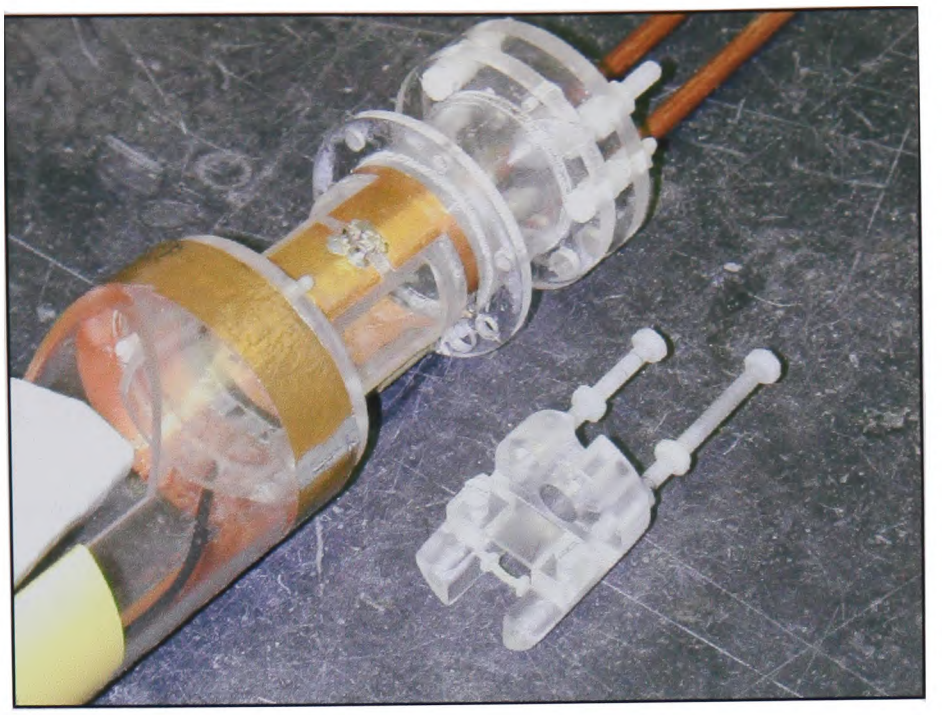


Figure 3-2: Photograph of coil and head holder with bite bar and nose restraint.

3.3.2 Physiological Monitoring during MRI

Heart rate was assessed by using a custom-built cardiac monitoring system (designed by Dr Paul Cassidy, Department of Physiology, University of Oxford) (Figure 3-3), and core body temperature was monitored via a rectal probe and homeothermic control system (Figure 3-3).

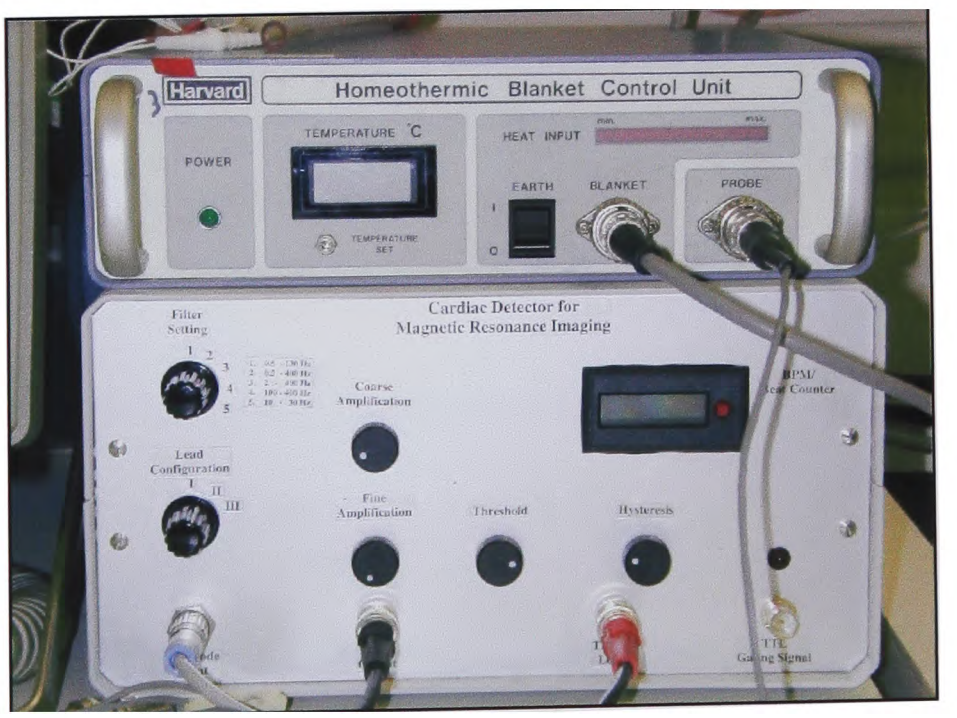


Figure 3-3: Photograph showing temperature and heart-rate monitoring devices.

3.4 Tissue Preparation

3.4.1 Fresh Tissue

Rats were terminally anaesthetised with 1ml sodium pentobarbitone. Brain tissue intended for ELISA, was transcardially perfused with 0.9% heparinsed saline. The thoracic cavity was opened to reveal the heart, and a 21 gauge needle was inserted into the left ventricle, the right atrium snipped and saline was used to perfuse the animal until all blood was washed out. The brains were then removed and striatal, cortical and injection site regions of interest for ELISA were punched out with a sterile pipette tip from a 2mm coronal section rostral and caudal from the injection site. Tissue was snap frozen in liquid nitrogen, and were stored at -80°C prior to assay.

3.4.2 PLP Fixed Tissue

For tissue intended for immunohistochemistry, transcardial perfusions were performed as described above, with heparinised 0.9% saline solution followed by 2% paraformaldehyde-lysine-periodate fixative (PLP) (McLean 1974). After dissection, the brains were post-fixed for 4-6 hours in PLP and then immersed in 30% sucrose buffer for 24 hours to cryoprotect. The tissue was then embedded in Tissue Tek Optimal Cutting compound (OCT) (Miles Inc, Elkhart, USA) and frozen in isopentane cooled to -40°C over liquid N_2. Subsequently the blocks were sectioned to either 10μm or 50μm using a cryostat. All frozen brain tissue was kept at -20°C.

3.4.3 Tissue for ELISA

Tissue samples were homogenised in phosphate buffer containing a cocktail of enzyme inhibitors using a motor-driven disposable plastic pestle. The enzyme inhibitor cocktail

comprised AEBSF (20uM), benzamidine (0.5mM), and ε amino-caproic-n-acid (10mM). Homogenates were centrifuged at 14,0000 rpm for 10 minutes, the supernatants were then ultracentrifuged at 430000g for 1 hour at 4°C, and stored at -80°C prior to assay

3.5 Antibodies

3.5.1 Immunohistochemistry

The primary antibodies that were used for immunohistochemistry are summarised in Table 3-1, and the secondary antibodies are summarised in Table 3-2.

Antibody	Primary Antibody	Concentration	Indicates	Supplier
ED1	Mouse monoclonal ED1	1:200	Macrophages Monocytes	Serotec
GFAP	Rabbit αGFAP	1:2000	Reactive astrocytes	Dako, Ltd. UK
IgG	N/A	N/A	BBB breakdown	Vector Laboratories
Laminin	Rabbit αLaminin	1:500	Upregulation of Laminin	Sigma
OX6	Mouse monoclonal OX6	1:100	MHC class II expression	Serotec
OX22	Mouse monoclonal OX22	1:1	T and B cells	In-house
MBP	Rabbit αMBP	1:1000	Demyelination	Biogenesis
BCG	Rabbit αBCG	1:2000	Presence of BCG antigens	Dako

Table 3-1: Primary antibodies used during immunohistochemistry, their concentration, specificity and manufacturer.

Primary Antibody Type	Secondary Antibody	Concentration	Manufacturer
Mouse monoclonal	Biotinylated horse α mouse	1:100	Vector Laboratories
Rabbit polyclonal	Biotinylated goat α rabbit	1:200	Vector Laboratories
IgG	Biotinylated rabbit α rat (mouse adsorbed)	1:100	Vector Laboratories

Table 3-2: Secondary antibodies used during immunohistochemistry, their concentration and manufacturer.

3.5.2 ELISA Antibodies

For ELISA, the primary antibody used was goat anti-rat IL-1β (at a concentration of 144μg/ml), and the secondary antibody was biotinylated goat anti-rat IL1β (at a concentration of 63μg/ml).

3.6 Histology Techniques

3.6.1 Cresyl Violet

Cresyl Violet-stained sections (50μm) were examined for histological signs of neuronal damage.

3.6.2 Acetycholinesterase

Cholinesterase chemistry (using acetylcholinesterase as a substrate) was used to assess neuronal loss. Frozen sections (10μm) on slides were thawed and washed twice in distilled water. They were then left overnight in incubating medium on the rotating table. After another two washes in distilled water, slides were placed in sodium sulphide solution for two minutes in a fume hood. Details of media components are detailed in Appendix B.

3.6.3 Immunohistochemistry

Sections were air-dried and incubations were carried out at room temperature. Frozen, serial sections (10μm thick) were cut from the paraformaldehyde-fixed tissue and mounted on gelatin-coated glass slides. After slides had been allowed to air dry, a ring was drawn around each section using an ImmEdge pen (Vector Laboratories Inc). The

tissue sections were incubated in alcoholic 0.3% hydrogen peroxide to quench endogenous peroxide activity, they were then washed in phosphate buffered saline (PBS), with 0.1% Tween 20. Subsequently, the sections were incubated for 30 minutes in 10% serum to block non-specific binding. Excess serum was drained from the sections, which were then incubated for 1-1.5 hrs with the appropriate primary antibody. Negative control sections were incubated in the absence of the primary antibody. Sections were washed with PBS containing 0.1% Tween 20 and the secondary antibody was added. In the case of IgG staining, the biotinylated anti-rat IgG antibody was used as a secondary antibody without using a primary antibody. After incubation with the secondary antibody for 45 minutes, the sections were washed with PBS containing 0.1% Tween 20, and then incubated with an avidin-biotin-peroxidase complex (Vectastain elite ABC, Vector Laboratories) for 45 minutes. The peroxidase was visualised using 0.05% diaminobenzidine hydrochloride (DAB; Sigma) and 0.05% hydrogen peroxide.

3.6.4 Counterstaining and Coverslipping

All of the slides were counterstained with 0.5% Cresyl Violet, dehydrated with alcohols (water/acetic acid, 70% ethanol, 80% ethanol, 90% ethanol, absolute ethanol, xylene), and subsequently permanently embedded in Depex mounting medium (Sigma) coverslipped, and allowed to air dry in a fume hood before examination using light microscopy.

3.6.5 ELISA

The concentration of IL-1β in brain tissue was determined by ELISA. The plates were prepared overnight prior to assay. Goat anti-rat IL-1β antibody in PBS was used to coat the plate. The wells were then washed with wash buffer three times. After washing, the plates were blocked by sucrose in PBS, and washed a further three times. The plates were

then ready for assay. Samples were diluted in reagent diluent and 100µl were added to the wells for two hours at room temperature. The plate was then washed three times. Subsequently, 100µl biotinylated goat anti-rat IL-1β was added to each well for a further two hours. Streptavidin-HRP was then added to each well. The plate was kept dark for 20 minutes. The wash step was repeated, and subsequently 100µl of the substrate solution was added and incubated for 20 minutes in the dark. 50µl of the stop solution was added to each well to stop the colour reaction taking place. The plate was tapped to ensure thorough mixing. The optical density of the wells was then determined immediately at 450nm. Protein concentration was determined using the Biorad protein assay based on the Bradford dye-binding procedure where bovine serum albumin was used as the standard.

3.7 Computing Hardware

All the work carried out in this thesis was used with the computing hardware described in Table 3-3.

Item	Description	Manufacturer
UNIX Workstations	SPARC station 5	Sun Microsystems Inc., Mountain View, CA, U.S.A
Personal computers	Desk-top computer Notebook	Dell Computer Corp, U.S.A Tiny Computers Ltd
Network	Ethernet linked	
Transfer from Spectrometers	Ethernet Linked	
Data Storage	Hard disk CD-ROM	Various Various

Table 3-3: Summary of computing hardware.

3.8 Computing Software

3.8.1 Image Analysis

Viewing and quantitation of images were carried out using Image Browser (Varian), and a custom-designed image display package written by Dr Andrew Blamire. Cluster analysis was performed using a custom-designed automated program written by Dr Graeme Waddington, (Waddington 1998), which is described in Section 3.8.2. Other computer software utilised during this thesis is described in Table 3-4.

Item	Description	Manufacturer
Spectrometer Software	Varian vnmr image visualisation package	Varian Medical Systems, CA, U.S.A
MRI Image Analysis	Varian Image Browser	Varian Medical Systems, CA, U.S.A
Histology Image Analysis	Leica Qwin	Leica, Milton Keynes, UK
Statistical Analysis Software	Instat (v 3.05) statistical Analysis program	Graph Pad Software Inc, CA, U.S.A
Ancillary Software (word processing, & spreadsheets)	Office 2000 Professional Office XP	Microsoft Corporation, U.S.A

Table 3-4: Summary of computing software.

3.8.2 Data Analysis

3.8.2.1 Cluster Analysis

Cluster analysis, was performed on many of the MRI images. This method of analysis forms a dataset consisting of voxel intensities at the same localisation in different images, where points representing the same tissue type cluster together, regardless of their spatial positioning within the images. In agglomerative hierarchical clustering methods, clusters are identified using an algorithm that starts with (n) clusters of one object each, where (n) is the total number of objects present in the dataset. The algorithm proceeds by merging into a single cluster that pairs existing clusters that are most similar. Thus, at each merger stage, the number of clusters present is reduced by one, and a hierarchy of clusters is produced by a series of successful mergers. In this method, clusters to be merged are chosen on the basis of minimum variance criterion (sum of squares).

The original MRI images are masked to restrict the dataset to voxels representing only those tissues under study to construct a region of interest (ROI), which is applied to each of the images used in the analysis. Ward's cluster analysis of the data set is then carried out, by using programs which extract information from the binary output file from the cluster program and produces images. Images are produced with pixel intensities set to the cluster number to which the pixel belongs in the cluster hierarchy. These images gave rise to regions of interest that could be quantitatively analysed.

3.8.2.2 Thresholding

To determine regions of hypointensity and hyperintensity, MRI images that were thresholded by eye to determine regions of interest. It was found that cluster analysis was

not able to determine hypointense and hyperintense regions as two distinct regions of interest, therefore all images were set at the same threshold level in Image Browser (Varian), in order for drawing around regions of interest by hand. The data was analysed in an un-blinded fashion, and owing to the large number of animals used at each time-point, it was not feasible to have an independent person verifying the data.

3.8.2.3 Immunohistochemistry

Quantitation of levels of MHC class II and reactive astrocytes was achieved using the Leica Qwin software. To quantitate MHC class II positive staining the x40 objective was used, and the x4 objective was employed to quantitate reactive astrocytes. Fields of the highest cell density were chosen by eye for MHC class II positive staining, and fields of view covering the whole lesion were used for the GFAP staining. A threshold of staining of normal tissue was arbitrarily set at a level consistent with the level of staining on all sections, so that only immunohistochemical positive areas were selected for analysis. The intensities of staining within the lesion were subsequently measured.

Chapter 4

The Histological Basis of the DTH Lesion

4.1 Introduction

Over the last 20 years, Experimental Allergic Encephalomyelitis (EAE) has been the most widely used animal model of MS, for investigating the pathological mechanisms underlying this disease. However, a full understanding of these processes has not yet been achieved, owing in part to the very complex nature of the MS lesion, and in part due to the limitations of the EAE model, (described and discussed in Chapter 2). Development of other animal models that exhibit the hallmarks of an MS lesion would provide further information on the inflammatory events taking place throughout MS lesion progression. One such model is the Delayed Type Hypersensitivity (DTH) in the rat that has recently been developed and was first described by Matyszak et al. in 1995 (Matyszak 1995).

The DTH model recently described in the literature is an extension of experiments carried out in 1975 by Wisniewski et al. (Wisniewski 1975) where it was demonstrated that DTH responses to non-CNS antigens in guinea pigs can lead to extensive immune-mediated tissue responses, including myelin loss. In the DTH model, non-CNS antigens (heat-killed Bacillus Calmette-Guerin (BCG)) are injected into the brain parenchyma, and remain sequestered behind the BBB long after the initial acute response to the foreign antigens has resolved. The immune system remains immunologically naïve to the BCG antigens in the brain, until it is activated by a peripheral subcutaneous challenge with TB or BCG several weeks later. Following peripheral challenge, a chronic lesion develops at

the site of the original BCG deposit, leading to extensive tissue damage. The ensuing lesion bears many of the pathological hallmarks of an MS lesion, which include infiltration of inflammatory cells, loss of myelin, and breakdown of the BBB. Previous studies of the DTH model have detailed various aspects of the chronic inflammatory response. In the first study of the DTH model, the persistence of non-CNS antigens in the brain was investigated, and changes in the permeability of the BBB and activation of microglia were reported (Matyszak 1995). The studies that followed, investigated the differences in inflammatory response in different CNS compartments to the same antigens and demonstrated that the CNS does have a significant degree of immune privilege (Matyszak 1996), (Matyszak 1998). The recruitment and presence of dendritic cells, and their role as antigen presenting cells in DTH lesions have also been studied, since these cells are not resident in the normal CNS parenchyma (Matyszak 1996). Later studies focussed more on mechanisms underlying the tissue destruction, such as the role of metalloproteinases, and axonal injury (Matyszak 1996), (Anthony 1998), (Newman 2001).

The DTH model of chronic inflammation confers several advantages over previous animal models used to study aspects of MS pathology, such as EAE; these are discussed in detail in Section 2.1.8, and will be summarised here. The principal drawback of the EAE model is that lesions can occur at any site within the CNS parenchyma, spinal cord and brainstem, and at any time. Furthermore, the different lesions may exhibit different evolution profiles, making longitudinal Magnetic Resonance Imaging (MRI) studies of the EAE brain over extended time courses difficult. In contrast, the primary advantage of the DTH model is that the site of the lesion is dictated by the location of the intracerebral injection of BCG. In addition, the DTH lesion is temporally and spatially consistent, and highly reproducible in comparison to EAE. These features facilitate study of the DTH

model using MRI, since the exact time of lesion induction and location are known. Thus, investigation of changes at the lesion site, which may occur before or after lesion enhancement, is readily possible. In MS studies, MRI is used conventionally as a non-invasive method of diagnosis and monitoring the progression of the MS lesion, but direct histopathological correlations with MRI changes is extremely difficult. The combination of the rodent DTH model and together with the use of MRI, enables investigation of these correlations between MRI changes and histopathological changes. It is hoped therefore, that this approach may enhance the use of MRI in clinical diagnosis and monitoring MS, by elucidating the causes of MRI detectable changes.

4.2 Aims of this Chapter

The primary objective of the work described in this chapter was to set up the Delayed Type Hypersensitivity (DTH) model within the laboratory and ensure that it provided a valid model in terms of the histopathology for the subsequent MRI studies in the Chapters that follow. The histopathology of the DTH lesion was compared with previous work in this model and with that reported from human MS studies. In addition, further characterisation of the DTH lesion was carried out using the acetylcholinesterase method to investigate neuronal loss, and correlations between the different pathological features of the lesion was investigated.

4.3 Methods

4.3.1 Experimental Model

Four groups of three-week-old male Lewis rats (Charles River) were studied. In the first group, heat-killed BCG ($5x10^5$ organisms in 1µl 0.1M sterile phosphate buffer) was

injected stereotaxically into the left striatum, as previously described in Chapter 3, to initiate a DTH lesion. Four weeks later, 100µl of 7.45mg TB in 1ml complete Freund's adjuvant (CFA) solution was given into each of the hind-limbs as a peripheral challenge. Both surgery and the peripheral challenge was performed under halothane-induced anaesthesia (0.8–1.5% halothane in 70% N_2O/30%O_2). In addition, three control groups were investigated (as summarised in Table 4-1). (a) Intracerebral injection of BCG alone i.e. no peripheral challenge (NPC), (b) intracerebral injection of vehicle solution (0.1M sterile phosphate buffered saline (PBS)), and peripheral challenge with TB four weeks later (PB IC), and (c) intracerebral injection of BCG and saline peripheral challenge four weeks later (SAL PC).

Experimental Group	Intracerebral Challenge	Peripheral Challenge	Histological Analysis
DTH	BCG	TB (36)	Yes
Controls NPC	BCG	N/A (4)	No
Controls SAL PC	BCG	Saline (4)	Yes
Controls PB IC	Phosphate buffered saline	TB (4)	Yes

Table 4-1: Summary of animals used in this chapter, () total number of animals in studied, and histological analysis performed.

4.3.2 Histology and Immunohistochemistry

At specific time-points post-peripheral challenge, (0, 5, 8, 12, 19 and 31 days post-peripheral challenge) rats were terminally anaesthetised with sodium pentobarbitone and transcardially perfused with heparinised 0.9% NaCl solution followed by 2% paraformaldehyde-lysine-periodate fixative (PLP) (McLean 1974). Control animals, without peripheral challenge (NPC) were sacrificed 31 days after peripheral challenge. After dissection, the brains were post-fixed for 4-6 hours in the PLP and then immersed in 30% sucrose buffer for 24 hours to cryoprotect. The tissue was then embedded in Tissue Tek (Miles Inc, Elkhart, USA) and frozen in isopentane at -80°C. Subsequently the

blocks were sectioned using a cryostat to enable histology and immunohistochemistry to be carried out. Cresyl Violet-stained sections (50μm) were examined for histological signs of neuronal damage. Cholinesterase histochemistry, (using acetylcholinesterase as a substrate) was used to assess neuronal loss as described in Section 3.6.2. Areas of neuronal loss were assessed using light microscopy.

Immunohistochemistry was used to confirm the presence and distribution of specific cell populations and was performed as described in Section 3.6.3, using primary antibodes listed in Table 3-1 and secondary antibodies in Table 3-2.

4.3.3 Data Analysis

Histological sections were observed under a light microscope to qualitatively evaluate the distribution of staining in each lesion. Fields were selected to cover the whole lesion. Areas occupied by specific populations of inflammatory cells (macrophages, T cells and activated microglia) were drawn using a camera lucida. Drawings of the lesions were then scanned as regions of interest (ROI's) and stored as electronic images (jpegs) suitable for analysis in image software (described in Table 3-4).

4.3.4 Cell Counts

Fields of the highest cell density in each DTH lesion were chosen by eye for counts of T lymphocytes and macrophages. The cells were then counted in these fields under the x40 objective in an area of $0.084mm^2$. In sections where lesions covered two or more fields of view, areas were counted in each field of view, however in sections where lesions covered one field of view only, just one area was counted. The mean ± S.D values were calculated for each time point.

4.3.5 Quantitation of MHC Class II and Reactive Astrocytes

Quantitation of levels of MHC class II and reactive astrocytes was achieved as described earlier in Section 3.8.2.3 using the Leica Qwin software. To quantitate MHC class II positive staining the x40 objective was used, since the staining was observed within the hyperintense cellular lesion only. The x4 objective was employed to quantitate reactive astrocytes since cells were found beyond the hypercellular area. The area of the hypercellular lesion on the same sections was also determined, by drawing around the hypercellular regions to allow the areas of MHC class II positive cells and reactive astrocytes to be expressed as area of staining per mm^2 lesion area.

4.3.6 Levels of IgG

Changes in BBB permeability were assessed by IgG staining. The intensity and spread of IgG staining within the brain parenchyma was assessed on sections running through the middle of lesions stained with anti-rat IgG antibody. Levels of IgG in the injected hemisphere were assessed semi-quantitatively. The lesion from each animal was given a score from 1-3, where a score of 3 corresponded to the maximal area and intensity of staining observed in all animals studied.

4.3.7 Statistical Analysis

Differences between the areas of interest at the different time-points were tested by analysis of variance (ANOVA). All correlations were tested using linear regression analysis, and the significance was tested using a student's t-test. An unpaired students t test with welch correction was used to determine any differences between regions of interest at different time-points, and also between DTH and control groups. All data are presented as the mean ± S.D for n animals.

4.4 Results

Following recovery from anaesthesia, none of the animals showed any physical effects or any signs of distress as a result of intracerebral injections. Animals were monitored on a day-to-day basis for 7 days after the intracerebral injection, and then once a week until the day of peripheral challenge. Similarly there were no signs of pain or distress following the peripheral challenge, and the animals were monitored as for the intracerebral injection.

4.4.1 Refinement of Model

Preliminary experiments were carried out using the previously described DTH model, and refining it for MRI study. Initial experiments showed that lesions induced using the dose described in the literature (1×10^5 BCG organisms in 1µl) were too small to be consistently visible with MRI. The dose was subsequently increased to 5×10^5 BCG organisms in 1µl. It was also noted that use of the 27 G 10µl Hamilton syringe (used in the literature to initiate the DTH lesion), occasionally gave rise to a spontaneous DTH response (Figure 4-1a), likely to have been brought about by activation of T & B lymphocytes outside of the BBB. A finely drawn glass canula was then used instead, to assess tissue damage compared to when the Hamilton syringe was used. It was found that the glass canula caused minimal damage to the brain parenchyma from the injection *per se* (Figure 4-1b), therefore the glass canula was used for all experiments.

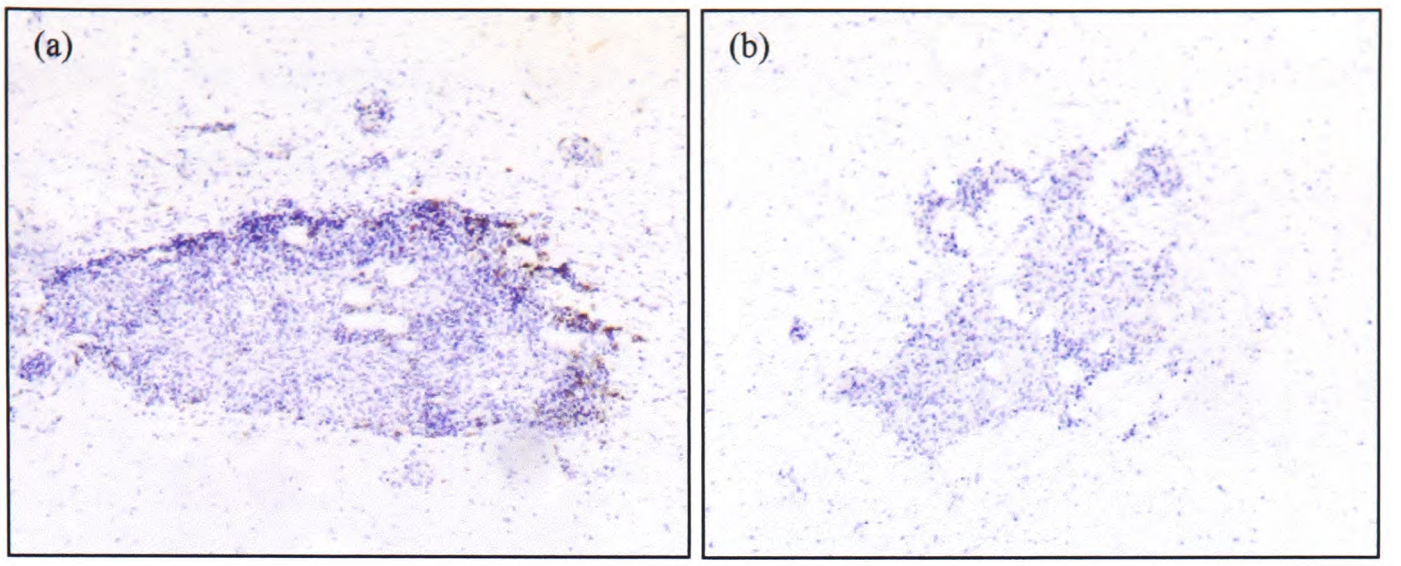


Figure 4-1: (a) DTH lesion at day 0 (the day of peripheral challenge) induced with a Hamilton syringe showing the presence of a large number of T & B lymphocytes brought about by a spontaneous DTH reaction (x4).

(b) DTH lesion at day 0 induced with a finely drawn glass canula showing minimal tissue damage, and minimal T & B lymphocyte recruitment (x4).

4.5 Qualitative Histology

4.5.1 Cresyl Violet

Cresyl Violet staining allowed the gross morphology of the DTH lesion to be established. Lesions were identified as areas of hypercellularity, which appeared as an increase in the intensity of staining (Figure 4-2a) and infiltration of inflammatory cells. This hypercellularity appeared to be maximal at day 19, and after this time point decreased in size. Maximum cell staining was found at the centre of the lesion; the inflammatory core. The lesion is granulomatous in nature (Figure 4-2b), i.e. it is composed of several layers, including macrophages and lymphocytes. Away from the inflammatory core, perivascular cuffs were found, in which local blood vessels were surrounded by inflammatory cells. Further away from the lesion, there were no other signs of tissue damage, and no changes in cell morphology or cell activation were found in the non-injected hemisphere. In controls that received intracerebral challenge of BCG (SAL PC and NPC) an area of hypercellularity was also observed throughout the time-course. The area of hypercellularity appeared to be slightly larger at days 12 and 19, although there

appeared to be less variation than in DTH animals. No area of hypercellularity was observed in PB IC controls.

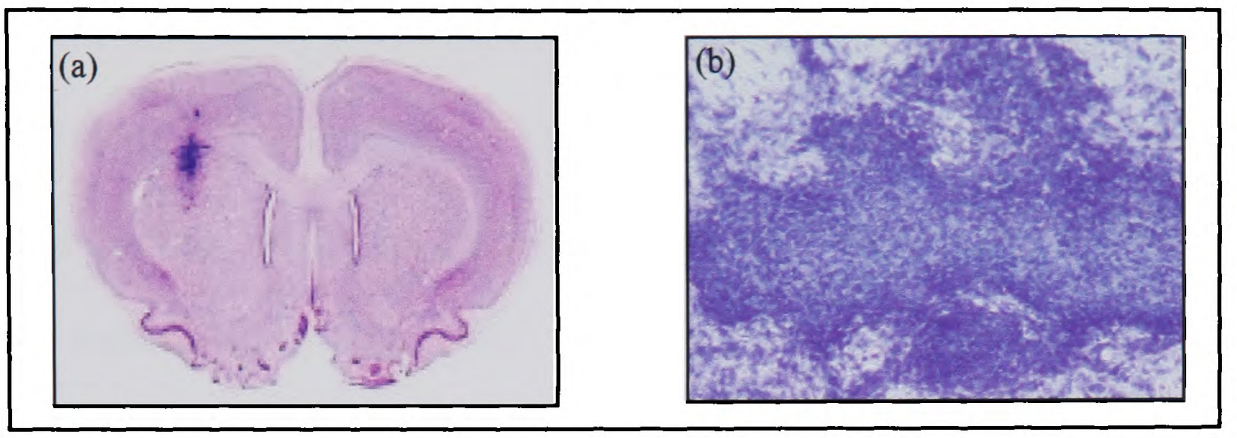


Figure 4-2: (a) Cresyl Violet stained section of whole brain at day 19 demonstrating the spatial extent and hypercellular nature of the DTH lesion in the left hemisphere.

(b) Magnified view of a Cresyl stained section (50 μm thick) in which the granulomatous nature of DTH lesion at day 19 can be seen (x25).

4.5.2 Acetylcholinesterase

Decreased activity of acetylcholinesterase was found in the DTH lesion area indicating loss of neurones and the neuropil (Figure 4-3). Qualitatively, there appeared to be no relationship between the age of lesion and the amount of neuronal loss, i.e. the same amount of neuronal loss was observed at each time-point investigated. Areas of neuronal loss as indicated by loss of acetylcholinesterase activity, was restricted to the area of hypercellularity only, therefore control animals with no area of hypercellularity (PB IC) showed no loss of acetylcholinesterase activity.

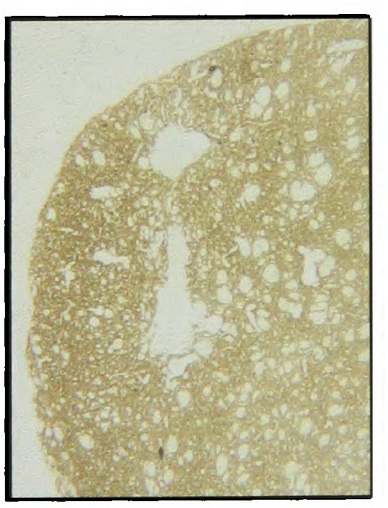


Figure 4-3: Low power photomicrograph of injected hemisphere showing a decrease in acetylcholinesterase activity in the core of the hypercellular DTH lesion (day 19), which indicates loss of neurones and neuronal processes in the neuropil (x4).

4.6 Immunohistochemistry

4.6.1 BCG

The BCG antigens persisted until at least day 19 after the peripheral challenge. Brown staining indicating BCG antigens was observed around the lesion site and along the injection track (Figure 4-4). BCG antigens were also observed in control animals receiving an intracerebral injection of BCG, and were again observed until at least day 19. No staining was observed in the contralateral hemisphere. As expected, no BCG antigens were observed in PB IC controls.



Figure 4-4: Photomicrograph of whole brain section indicating purple hypercellular lesion surrounded by BCG antigens, (stained brown) which were present both in and around the lesion site, and also throughout the striatum of the injected hemisphere until at least 19 days after the initiation of the DTH lesion.

4.6.2 Myelin

In DTH animals, areas of myelin loss were observed throughout the hypercellular lesion. In particular, in cases where the lesion crossed the corpus callosum there was extensive loss of myelin. The myelin loss appeared to be progressive throughout the DTH phase. The early DTH lesions (Figure 4-5a) showed far less disruption of the myelin bundles that surround axons traversing the brain from anterior to posterior, than lesions that had been allowed to progress further (Figure 4-5b). In addition, older lesions showed disruption of some myelin bundles outside the hypercellular area (Figure 4-5b). Myelin bundles in PB IC control animals were completely intact and showed no loss of myelin, whereas control

animals receiving BCG intracerebrally (NPC and SAL PC) showed a mild degree of myelin loss in the hypercellular region, but not to the same extent as in the DTH lesions.

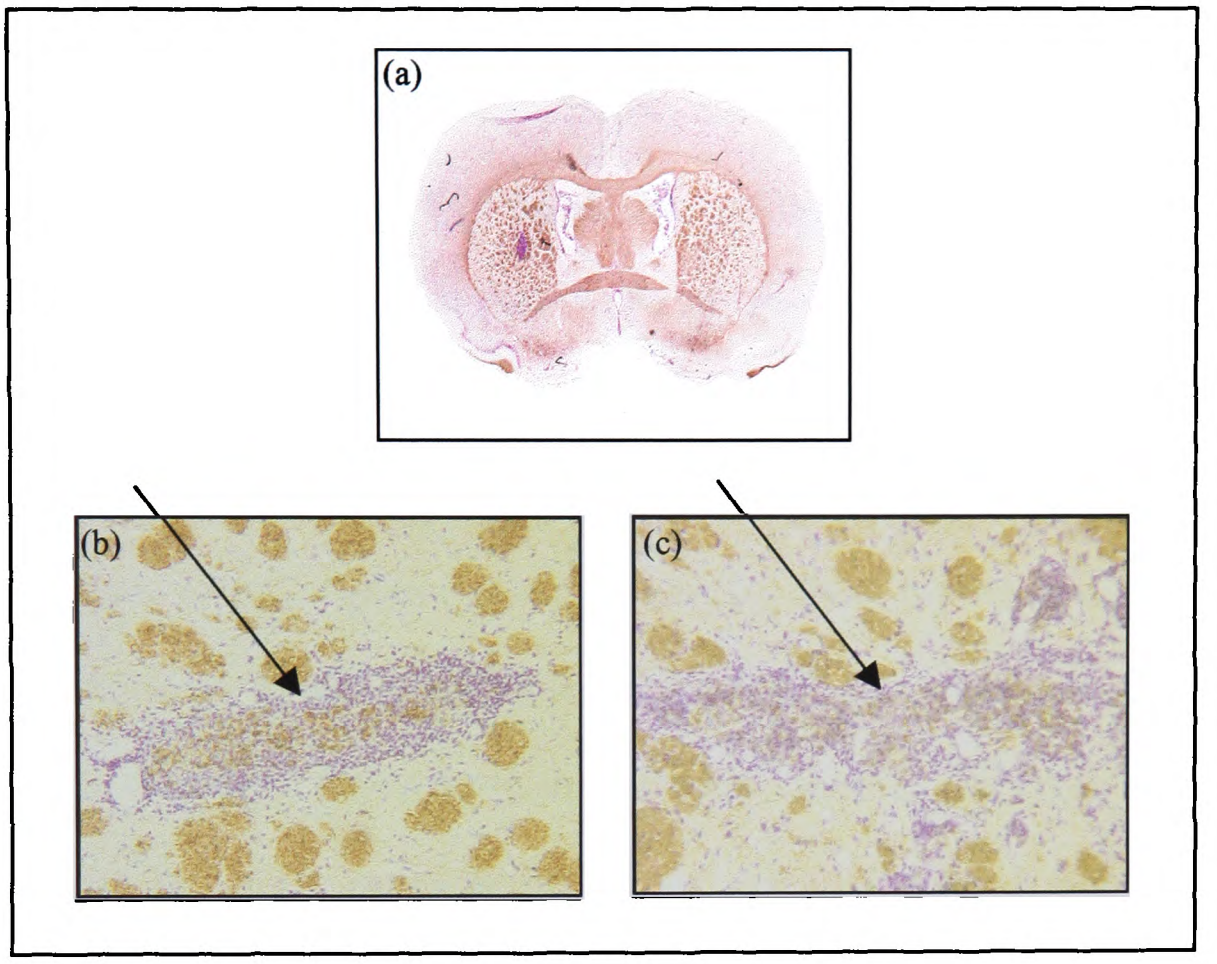


Figure 4-5: (a) Photomicrograph of whole brain section showing myelin staining of myelin bundles (brown) throughout the brain parenchyma, also showing hypercellular DTH lesion (stained purple) in the left hemisphere disrupting the myelin bundles at day 12.

(b) Disruption of brown circular myelin bundles within the hypercellular lesion at 5 days (x10).

(c) Loss of myelin throughout hypercellular area, and disruption of bundles as indicated by arrows surrounding DTH lesion at 12 days (x10).

4.6.3 Reactive Astrocytes

Astrocyte activation was determined from the expression of glial fibrillary acidic protein (GFAP). In DTH animals, small numbers of GFAP positive cells (reactive astrocytes) were found within the DTH lesion as early as day 0 (the day of peripheral challenge), and were present throughout the time-course (Figure 4-6a). These cells are most likely to be residual from a particularly potent acute inflammatory response resulting from intracerebral injection. Maximal GFAP staining was observed around the edge of the hypercellular lesion, which decreased with increased distance from the hypercellular lesion (Figure 4-6b). Reactive astrocytes had extended astrocytic processes (Figure 4-6c)

and the ends of the processes tended to be in contact with the hypercellular area of the lesion (Figure 4-6d). Over time, the area of staining occupied by reactive astrocytes increased, and analysis of variance demonstrated that this change was significant ($p<0.01$). The area of staining appeared to be maximal at day 19, and at this time-point, was significantly greater than day 0 (unpaired t test, $p<0.05$). The area of staining occupied by reactive astrocytes at days 5 and 12 were also significantly greater ($p<0.02$ and $p<0.05$ respectively) than that observed at day 0 (Table 4-2). Some reactive astrocytes were found scattered throughout in the contralateral hemisphere in DTH animals (Figure 4-6e). Control animals receiving BCG into the brain, (both with a peripheral challenge of saline and those which received no peripheral challenge) had activation of astrocytes following a similar time-course to the DTH animals, though activation was not to the same degree (Figure 4-6f). Individual results are given in Appendix C.1 and C.2. In control animals receiving an intracerebral challenge of phosphate buffered saline, no evidence of reactive astrocytes was found at the site of injection.

DTH						
Time-Point (Day)	**0**	**5**	**8**	**12**	**19**	**31**
0	-	$p<0.02$	/	$p<0.05$	$p<0.05$	$p=0.0571$
5	-	-	/	/	/	/
8	-	-	-	/	/	/
12	-	-	-	-	/	/
19	-	-	-	-	-	/
31	-	-	-	-	-	-

Table 4-2: Summary of p values for (unpaired t tests) within group comparisons for areas of reactive astrocytes in DTH animals at each time-point. (values for comparisons that did not quite reach significance are also included, "/" denotes difference not significant).

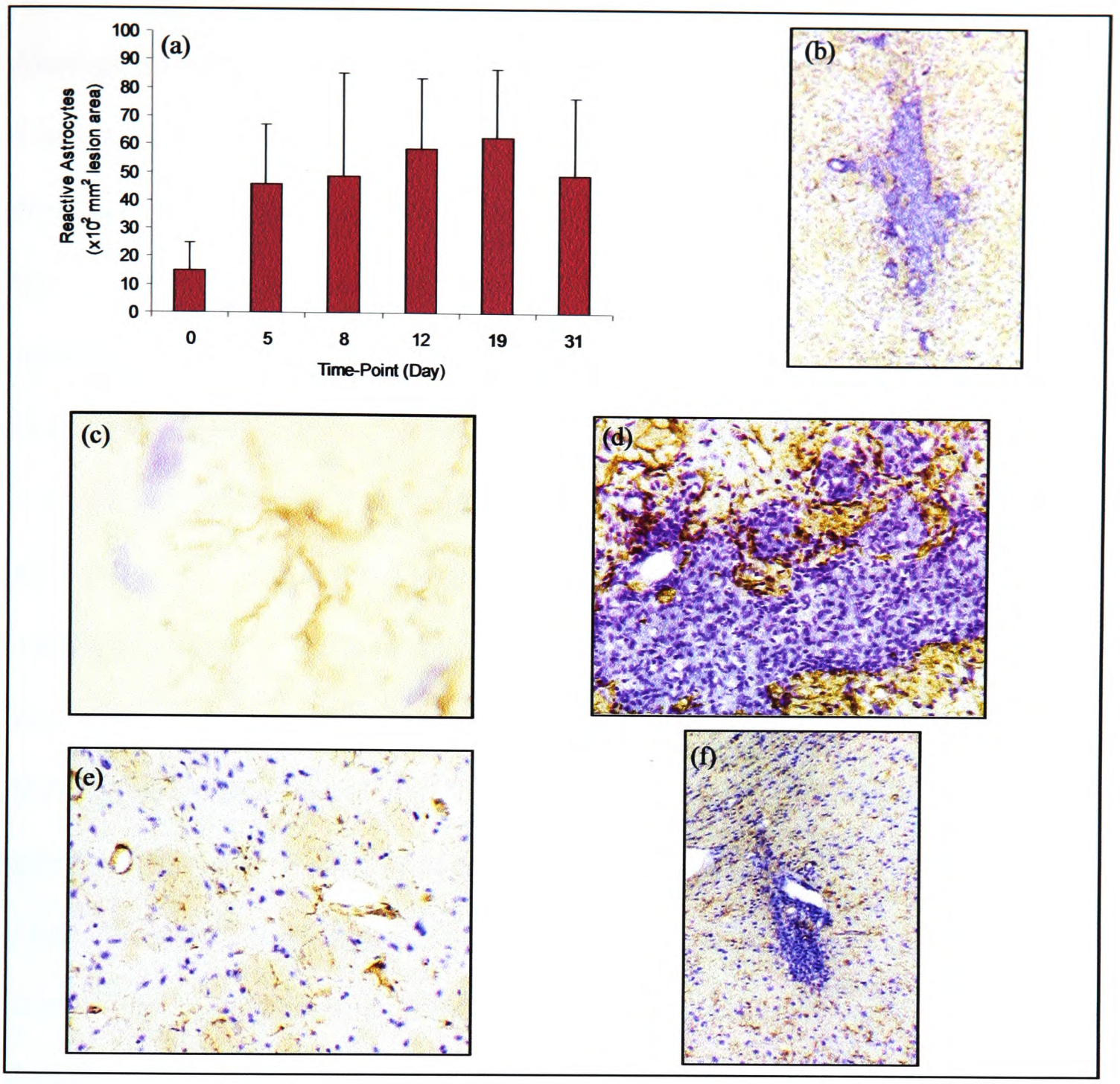


Figure 4-6: (a) Graph to show the area of reactive astrocyte staining around the DTH lesion during lesion progression. Values expressed as the mean ± S.D. ANOVA demonstrated a significant ($p<0.01$) change over time.

(b) Low power (x4) micrograph of GFAP positive astrocytes. Staining extended for some distance beyond the DTH lesion.

(c) High power photomicrograph of an activated astrocyte in the brain parenchyma in close proximity to the DTH lesion, showing extended processes as a result of activation (x100).

(d) Photomicrograph (x25) of densely stained (brown) reactive astrocyte end feet around the perimeter of the purple hypercellular DTH lesion at day 19. No staining was observed in the lesion *per se*.

(e) Reactive astrocytes were also found in the opposite hemisphere at day 19 in DTH animals, but were no activated as indicated by the lack morphology change that occurs as upon activation.

(f) Low power photomicrograph of SAL PC control animal showing considerably less astrocyte activation around the hypercellular lesion (stained purple).

4.6.4 Macrophage Recruitment

Macrophage recruitment was assessed using the mouse monoclonal antibody ED1, which binds to a cytoplasmic antigen in monocytes and activated macrophages/microglia (Dijkstra 1985). Low levels of macrophage recruitment were seen as early as day 0 (the day of peripheral challenge) in both DTH and control animals that received a saline peripheral challenge (SAL PC) (Figure 4-7a). Positive staining continued throughout the time course, until day 31. However in the SAL PC control group, the number of macrophages either stayed constant or decreased (Figure 4-7a) while in the DTH group the number increased to reach maximal levels at day 8. Analysis of variance revealed a significant change ($p<0.05$) in the number of recruited macrophages in the DTH animals over time. Post-hoc unpaired t tests revealed that numbers of T & B lymphocytes were significantly greater in DTH than SAL PC animals at day 5 ($p<0.05$) and 12 ($p<0.01$), as given in Table 4-4. In DTH animals, day 0 was significantly reduced when compared to other time-points these results are summarised in Table 4-3. Individual results are summarised in Appendix C.1 and C.2. Macrophages were usually found scattered throughout the lesion and were components of the perivascular cuffs. Macrophages were also found slightly further away from the core hypercellular region (Figure 4-7b). No macrophage recruitment to the site of injection was observed in control animals that received an intracerebral injection of phosphate buffered saline (PB IC).

No. of Macrophages (per 0.1mm^2 lesion area) in DTH						
Time-Point (Day)	**0**	**5**	**8**	**12**	**19**	**31**
0	-	$p<0.005$	$p<0.01$	$p<0.005$	$p<0.005$	$p<0.02$
5	-	-	/	/	/	/
8	-	-	-	/	/	$p<0.05$
12	-	-	-	-	/	/
19	-	-	-	-	-	$p=0.0792$
31	-	-	-	-	-	-

Table 4-3: Summary of p values for within group comparisons (unpaired t tests) for No. of macrophages in DTH animals at each time-point. ("/" denotes difference not significant, values for comparisons that did not quite reach significance are also included). No significant differences were observed for the same tests carried out in SAL PC controls.

Number of Macrophages per 0.1 mm^2 in DTH						
Time-Point (Day)	**0**	**5**	**8**	**12**	**19**	**31**
SAL PC	/	$p<0.05$	/	$p<0.01$	/	$p=0.0614$

Table 4-4: Summary of unpaired t test results for between group comparison of DTH and SAL PC at each time point. ("/" denotes difference not significant, values for comparisons that did not quite reach significance are also included).

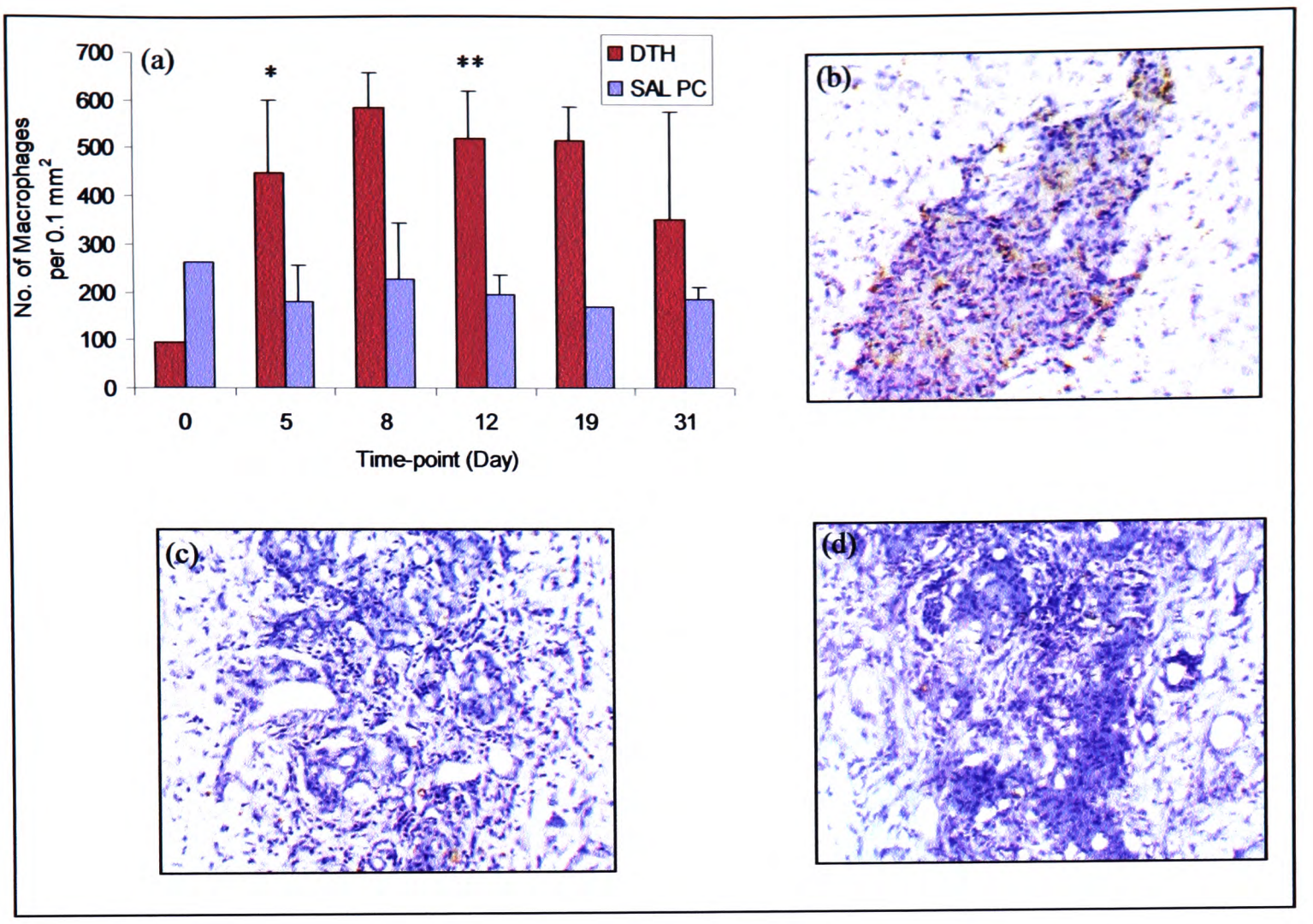


Figure 4-7: (a) Graph to show number of ED1 positive macrophages in the DTH lesion throughout the progression of the DTH lesion. Values are expressed as the mean ± S.D. ANOVA demonstrated a significant ($p<0.05$) change over time in the DTH animals, significant differences were found between DTH and SAL PC controls at days 5 and 12, (unpaired t tests $^{**}p<0.01$, $^{*}p<0.05$)

(b) Photomicrograph of ED1 positive macrophages (stained brown) scattered randomly throughout hypercellular lesion (stained purple) at day 8 (x20).

(c) In contrast to the DTH animal in (b) a SAL PC control animal at day 8, shows less macrophage recruitment to the lesion (x20).

(d) NPC control animal at day 31, showing relatively few macrophages present in the hypercellular lesion (x20).

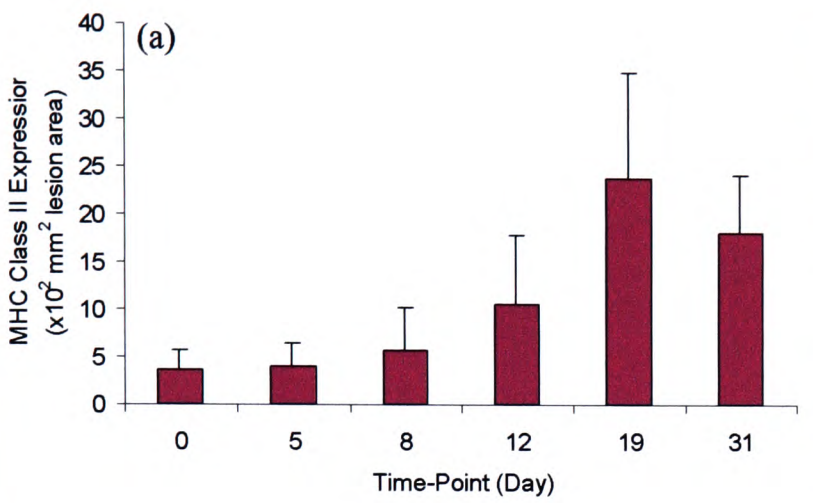
4.6.5 MHC Class II Expression

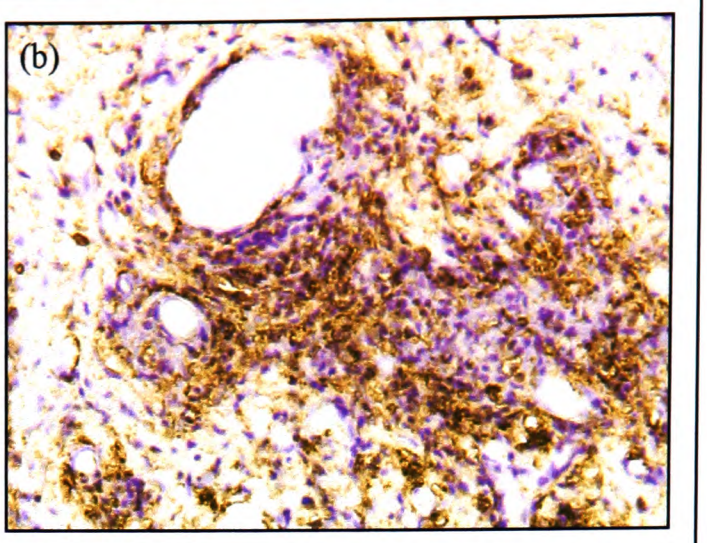
The use of the mouse monoclonal antibody OX6 enabled assessment of MHC class II expression in and around the DTH lesion. Low levels of positive staining were observed from day 0 (the day of peripheral challenge) in DTH animals (Figure 4-8a) however maximum MHC class II expression appeared to occur at day 19. Analysis of variance demonstrated a highly significant change over time ($p<0.0005$). Unpaired t tests revealed that the area of MHC class II expression was significantly greater at day 19 than day 0

($p<0.01$); day 5 ($p<0.05$); and day 8 ($p<0.05$). The expression of MHC class II expression at day 31 was also significantly greater than day 0 ($p<0.01$), day 5 ($p<0.005$), and day 8 ($p<0.05$) as shown in Table 4-5. As with the macrophage staining, MHC class II was expressed by cells scattered throughout the hyperintense cellular lesion, but predominately at the edges of the lesion. MHC class II expressing cells were also a major component of the perivascular cuffs (Figure 4-8b), SAL PC control animals had a small amount of MHC class II expression, but levels were considerably less than DTH animals, however in PB IC controls, no expression of MHC class II was observed. Individual results are given in Appendix C.1 and C.2.

Area of MHC Class II Expression						
Time-Point (Day)	**0**	**5**	**8**	**12**	**19**	**31**
0	-	/	/	/	p<0.01	p<0.01
5	-	-	/	/	p<0.05	p<0.005
8	-	-	-	/	p<0.05	p<0.05
12	-	-	-	-	/	/
19	-	-	-	-	-	/
31	-	-	-	-	-	-

Table 4-5: Summary of p values for within group comparisons (unpaired t tests) for areas of MHC class II expression in DTH animals at each time-point. ("/" denotes difference not significant).





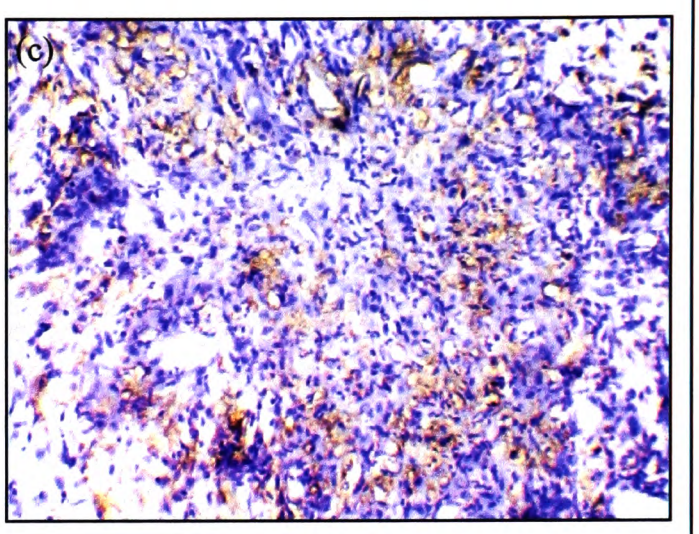


Figure 4-8: (a) Graph to show areas of MHC class II expression over time in the DTH lesion. Values are expressed as mean ± S.D. ANOVA demonstrated a highly significant ($p<0.0005$) change over time.

(b) MHC class II expression (stained brown) by macrophages throughout hypercellular area (stained purple) and surrounding perivascular cuffs (x25)

(c) SAL PC control animal showing considerably less MHC class II expression throughout the hypercellular lesion at day 19 (x20).

4.6.6 Recruitment of T and B lymphocytes

The recruitment of T and B lymphocytes to the DTH lesion was assessed using the mouse-monoclonal antibody OX22. OX22 positive cells were found predominately at the edges of DTH lesions, but were also components of the perivascular cuffs. A small number of these cells were first present at day 0 (the day of peripheral challenge), and were seen throughout the study (Figure 4-9). A significant (ANOVA $p<0.01$) change in the number of T & B lymphocytes was found in the lesion over time. Post-hoc unpaired t tests indicated that the number of T & B lymphocytes present at day 12 was significantly

greater than at day 0 ($p<0.01$), and day 19 ($p<0.05$) as observed in Table 4-6. T & B lymphocytes were notably absent from the striata of PB IC controls. Individual results are given in Appendix C.1 and C.2.

Time-Point (Day)	No. of T & B lymphocytes				
	0	5	12	19	31
0	-	p=0.0806	p<0.02	/	p<0.05
5	-	-	p=0.0825	/	/
12	-	-	-	p<0.05	/
19	-	-	-	-	/
31	-	-	-	-	-

Table 4-6: Summary of p values for within group comparisons (unpaired t tests) for No. of T & B lymphocytes in DTH animals at each time-point. ("/" denotes difference not significant, values for comparisons that did not quite reach significance are also included).

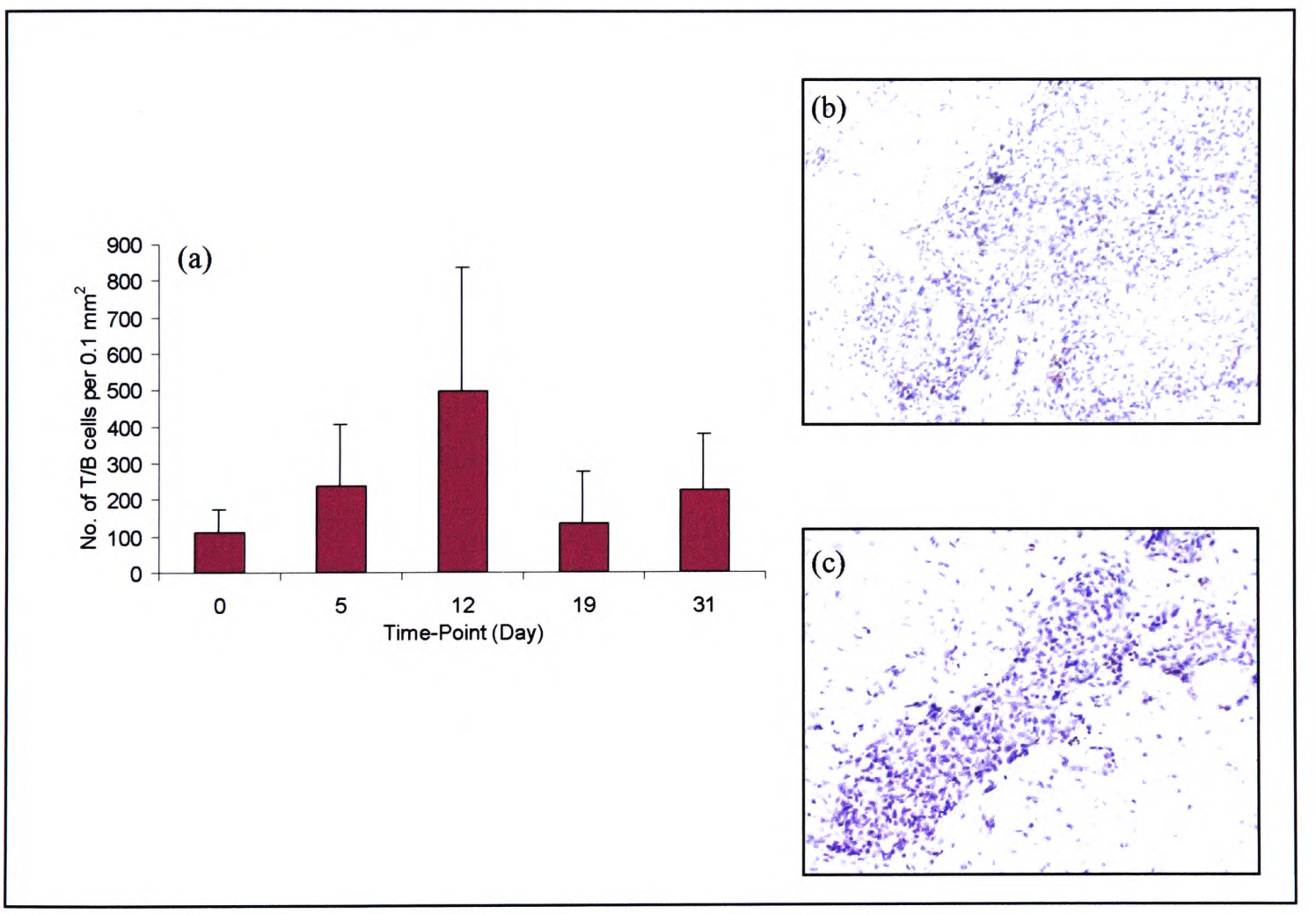


Figure 4-9: (a) Number of OX22 positive T & B lymphocytes throughout the lesion area increased over time to reach a maximum at day 12 in the DTH lesion. Values are expressed as mean ± S.D. ANOVA demonstrated a significant ($p<0.01$) change over time.

(b) T and B lymphocytes (stained brown) were mainly found towards the edges of the hypercellular lesion (x20), and were maximal in the lesion at day 12.

(c) T and B lymphocytes were less prevalent in the lesion at day 31, although were still located at the lesion perimeter (x20).

4.6.7 Blood Brain Barrier

Changes in the permeability of the BBB were assessed by immunohistochemistry with biotinylated anti-rat IgG antibody. A small amount of BBB breakdown was observed from day 0 (the day of peripheral challenge) onwards (Figure 4-10a). The level of staining was relatively constant up to day 12, but increased thereafter. By day 31, most of the animals had maximal positive staining (Figure 4-10a). Analysis of variance demonstrated a significant ($p<0.001$) change in the levels of IgG staining over time. Post-hoc pair-wise t tests revealed that the level of IgG staining at day 31 was significantly greater than days 0, 5, 12, and 19 as observed in Table 4-7. Staining was only observed in the injected hemisphere, and was detected over a large area of the striatum, cortex and corpus callosum (Figure 4-10b). Some SAL PC control animals that were injected intracerebrally with BCG exhibited mild leakage of IgG into the brain parenchyma, however no leakage was observed in PB IC controls. Individual results are given in Appendix C.1.

Time-Point (Day)	IgG Leakage				
	0	5	12	19	31
0	-	/	/	p=0.0776	p<0.0005
5	-	-	/	/	p<0.05
12	-	-	-	/	p<0.001
19	-	-	-	-	p<0.05
31	-	-	-	-	-

Table 4-7: Summary of unpaired t tests for IgG leakage within DTH animals at each time-point. ('/' denotes difference not significant, values for comparisons that did not quite reach significance are also included).

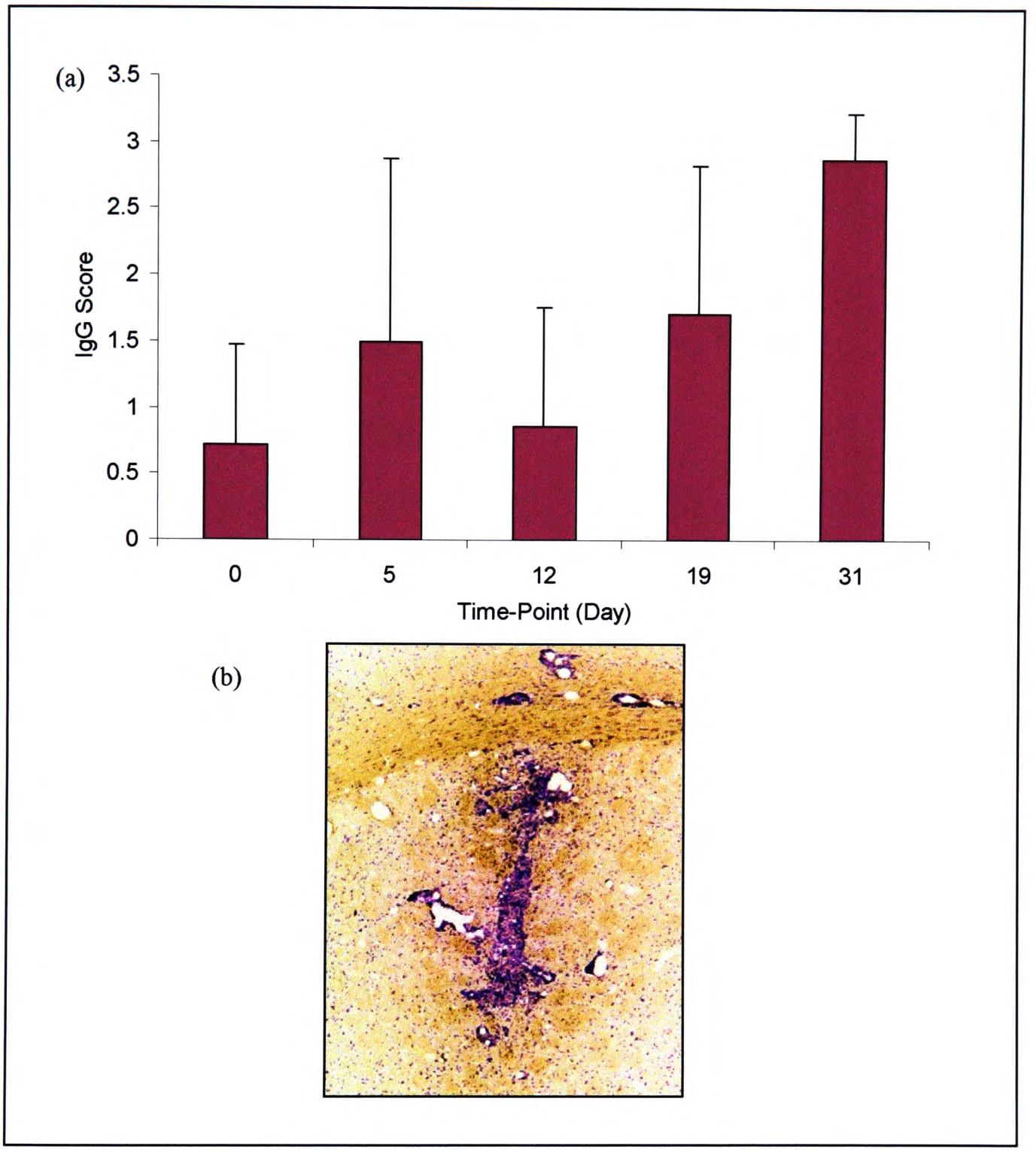


Figure 4-10: (a) Graph to show score of BBB permeability in the DTH lesion. The maximal staining was observed at day 31. Values are expressed as the mean ± S.D.

(b) Brown staining indicating IgG leakage suggesting BBB breakdown was observed around the lesion site and for some distance throughout the injected hemisphere at day19.

4.6.8 Summary of Time-Course Results

From Figure 4-11, it can be noted that many of the histological time-course profiles are similar. Macrophage recruitment to the lesion appears to be the first histological event, peaking at day 8, although numbers remain high throughout the time-course (Figure 4-11a). Some activation of astrocytes occurs at the beginning of the time-course, but activation increases over time to reach a maximum around day 19 (Figure 4-11b). Overt expression of MHC class II occurs later in the time-course, again peaking at day 19 (Figure 4-11c). Numbers of T and B cells also appear to be an early event in the DTH lesion, their numbers appear to peak at day 12, prior to maximal MHC expression activation of astrocytes (Figure 4-11d).

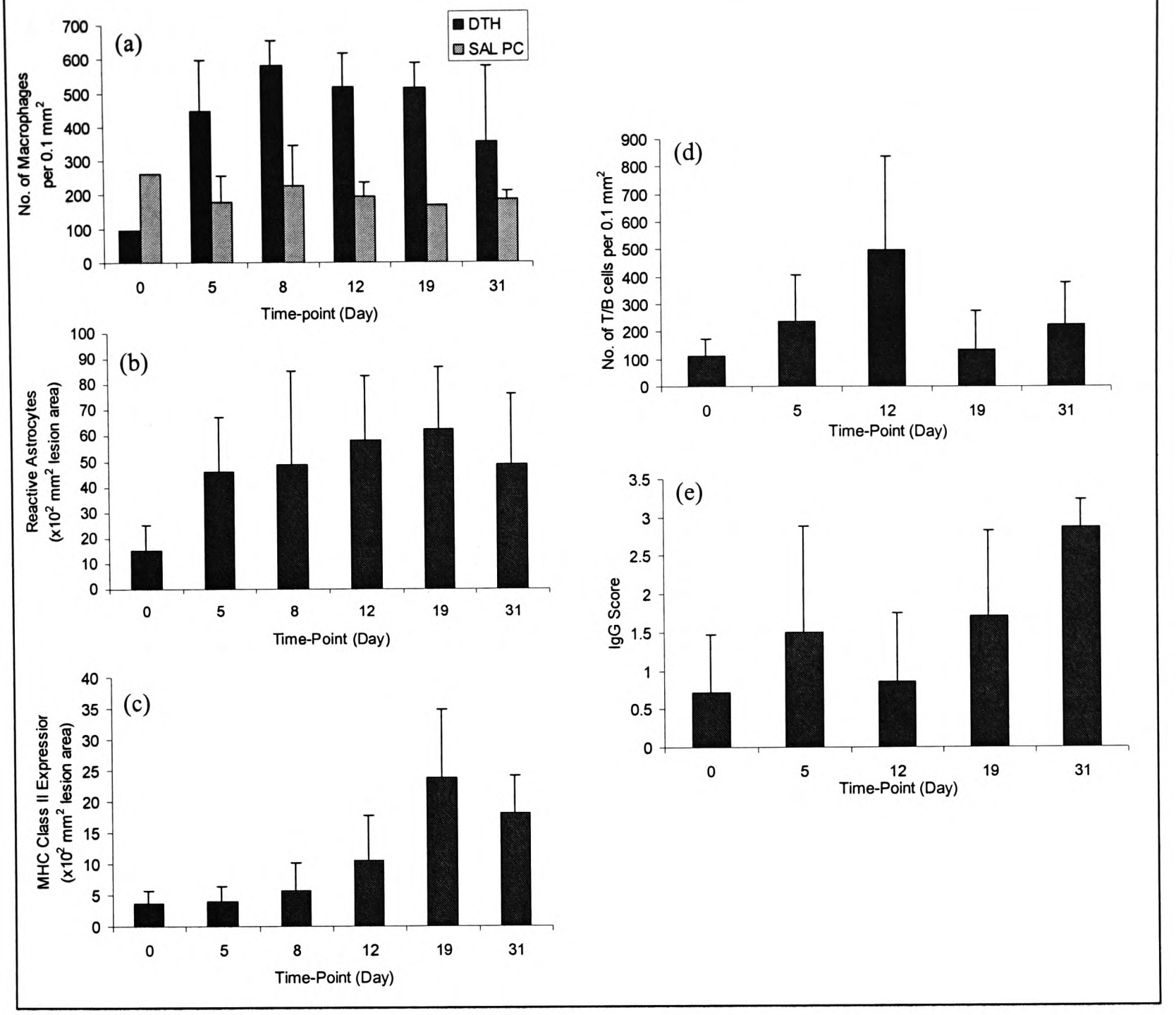


Figure 4-11: Summary of time-course data for immunohistochemistry results indicating similar profiles of inflammatory activity.

(a) Number of macrophages per 0.1mm^2 lesion area over the time-course.

(b) Reactive Astrocytes (x10^2 mm^2 lesion area).

(c) Expression of MHC class II (x10^2 mm^2 lesion area).

(d) Number of T and B cells per 0.1mm^2 lesion area.

(e) IgG staining score.

4.6.9 Spatial Correlations

When areas of immunohistochemical parameters were drawn around using the camera lucida and mapped onto each other, it was observed that the areas occupied by reactive astrocytes (in blue), BCG antigens (in orange), and IgG leakage (in purple) were all spatially co-incident with each other, although the area of IgG leakage extended further than the area of BCG antigens and reactive astrocytes (Figure 4-11). All of these areas extended beyond the area of hypercellularity, identified from the Cresyl Violet histology, shown in black (Figure 4-11).

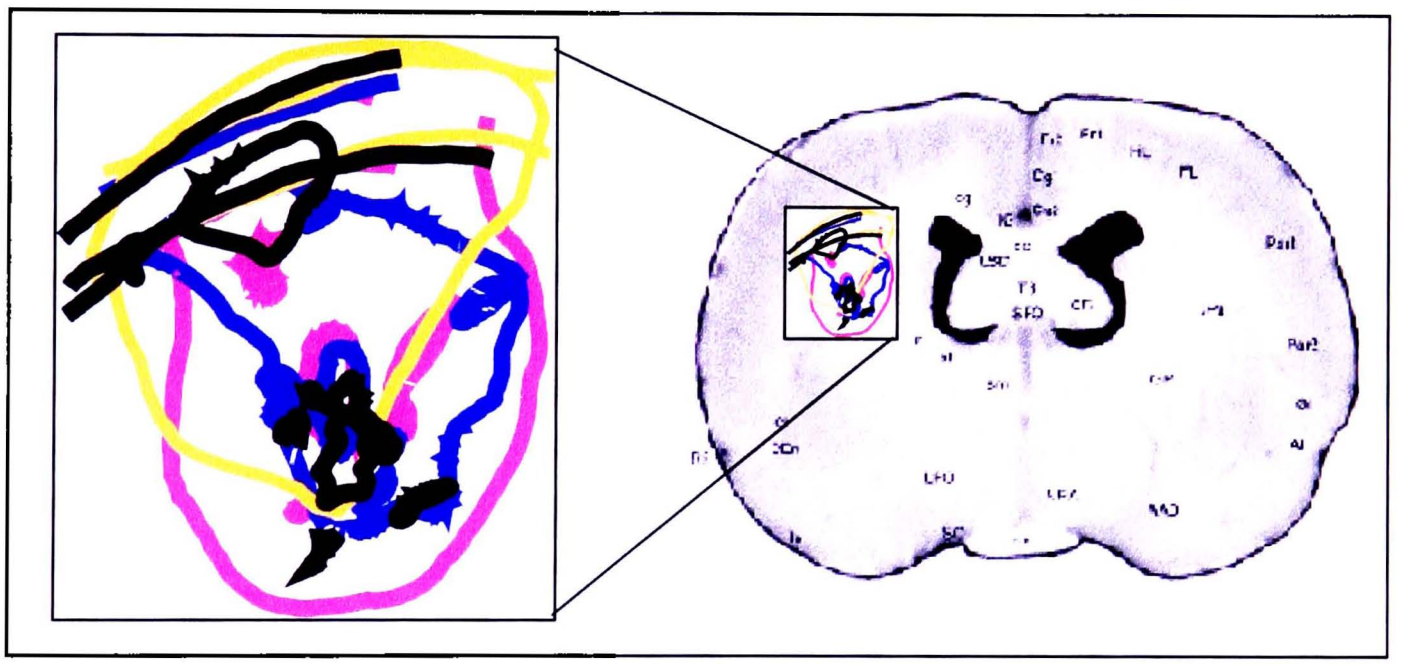


Figure 4-12: Overlay of histochemical areas as identified by light microscopy, onto a diagram of the rat brain to demonstrate the position of the lesion relative to the rest of the brain. The black line indicates the area of hypercellularity as identified by Cresyl Violet, the blue line represents the area of reactive astrocytes, the orange line represents the area occupied by BCG antigens, and the purple line indicates the extent of IgG leakage into the parenchyma.

4.6.10 Histological Correlations

In order to assess whether specific staining areas were coincident with each other, correlations were determined between inflammatory cell recruitment, astrocyte activation and MHC class II expression. A trend towards a significant correlation was found between numbers of macrophages and numbers of T & B lymphocytes ($p=0.074$) (Table 4-8 and Figure 4-12a). Areas of reactive astrocyte staining showed a trend towards

correlation with MHC class II expression but this again, did not reach significance (p=0.074) (Table 4-8 and Figure 4-12b). Other correlations between immunohistochemical parameters that did not reach significance are shown graphically in Appendix C.3.

Correlation Between ...	Correlation Parameters	
	r	p
T & B Lymphocytes and Macrophages	0.389	p=0.0745
MHC class II expression and Reactive Astrocytes	0.388	p=0.0736

Table 4-8: Summary of results from correlation analysis between T & B lymphocytes and macrophages, and also between MHC class II expression and reactive astrocytes.

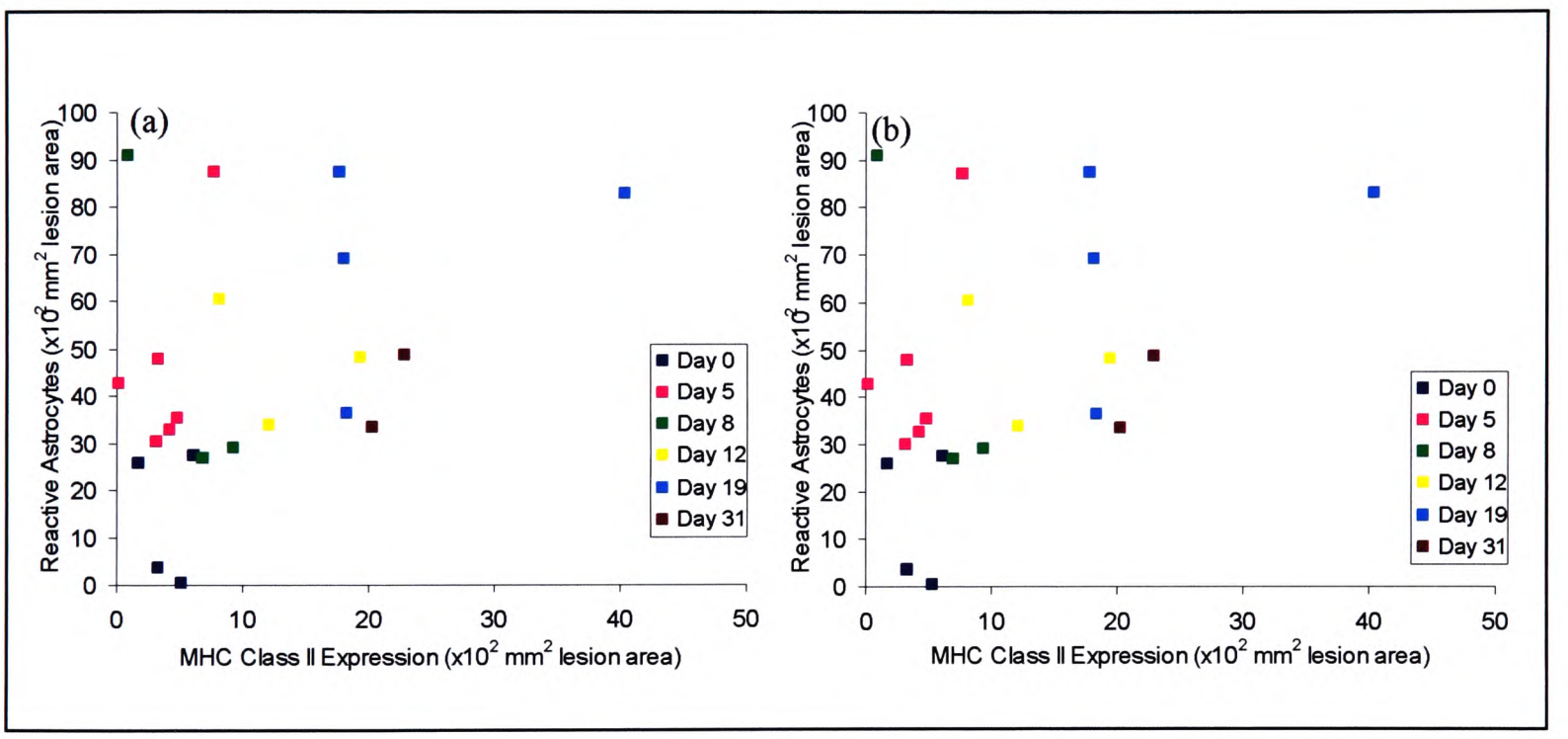


Figure 4-13: Graphs to show the relationships between different histological markers of inflammation.

(a) Trend towards a positive correlation (p=0.074) between numbers of T & B lymphocytes and macrophages.

(b) Trend towards a positive correlation (p=0.074) between areas of reactive astrocytes and MHC class II expression.

4.7 Discussion

BCG injected intracerebrally remained sequestered behind the BBB in the CNS for at least one month despite an initial acute inflammatory response. Following sensitisation of the immune system to the BCG antigens by peripheral injection of TB, a chronic inflammatory response to the non-CNS BCG antigens ensued - the Delayed Type Hypersensitivity (DTH) response. The DTH response resulted in a macrophage-dominated cellular infiltrate, together with T and B lymphocyte recruitment. The lesions were granulomatous and extremely hypercellular, with macrophages and reactive astrocytes strongly present at the edges of the lesions. It is likely that these cells are involved in myelin damage and phagocytosis as myelin loss was also observed throughout the lesion. This myelin loss increased over time and eventually spread outside the main area of the lesion to the areas of perivascular cuffs. However, loss of acetylcholinesterase, an indicator of neuronal loss, occurred at the centre of the lesion. Perivascular cuffs involving macrophages and T lymphocytes were frequently observed. Reactive astrocytes were found most densely around the edges of the DTH lesion, although they were also found throughout the injected hemisphere. Widespread MHC class II expression by macrophages and mononuclear phagocytes in the DTH lesion was a consistent feature of all lesions. Correlations were identified between recruitment of T & B lymphocytes and macrophages, and also between activation of astrocytes and expression of MHC class II. Finally, progressive breakdown of the BBB was also observed as indicated by increased permeability of IgG throughout the DTH time-course. The histological profile of the DTH lesion is in close agreement with previously published data using this model (Matyszak 1996), however the histological correlations and the acetylcholinesterase findings are in addition to those published observations; each of these findings will be considered in more detail.

4.7.1 Comparison of histopathological findings with previous studies of the DTH model

Progressive breakdown of the BBB was observed throughout the DTH time-course. Alterations in permeability of the BBB have previously been reported in this model (Matyszak 1995), (Newman 2001), but these alterations have not been reported in terms of the time-course of IgG leakage. When the BBB is damaged, IgG accumulates in the brain parenchyma, so if the BBB is permeable for a long time, it is expected that IgG accumulation will appear to occur at the terminal time point studied in these experiments. If the time-course were allowed to progress further, then it would become apparent when maximal BBB breakdown would occur. Some control animals, especially those that had BCG injected intracerebrally, exhibited mild leakage of IgG into the brain parenchyma; this is probably due to the inflammatory response brought about by the initial intracerebral injection of BCG. DTH lesions have previously been shown to produce a large amount of BBB breakdown, both in the lesion and for some area extending it and throughout the injected hemisphere (Matyszak 1995), (Matyszak 1996). The same pattern of BBB breakdown was observed in this study, although the responses appeared to be less overt than that published previously in the DTH model. This may be due to the use of a glass canulae for lesion induction, rather than a Hamilton syringe as used in the published work.

In agreement with previous work BCG antigens were found to persist in the DTH lesion and in the surrounding CNS parenchyma for up to 6 weeks after their introduction to the brain parenchyma (Matyszak 1995), (Matyszak 1997). Large numbers of macrophages and T lymphocytes were present in the DTH lesion, and were also present around blood vessels, forming perivascular cuffs. Within these cuffs, the most prominent cell types were activated macrophages, microglia and T lymphocytes. These same characteristics

were observed previously by Matyszak and colleagues (Matyszak 1995), (Matyszak 1996). In the centre of the lesion, microglia were the most prominent cell type, and had the typical appearance of activated cells; i.e. rounded with short processes. Neutrophils were absent from the DTH lesion, which is in good agreement with published data (Matyszak 1995), (Anthony 1998). Leukocyte recruitment to the CNS has previously been reported to occur 5 days after the subcutaneous challenge (Matyszak 1996). However, in the current study, small numbers of T & B lymphocytes were present at day 0. The presence of these cells at this time-point in this study, may reflect low level priming of the peripheral nervous system as a result of BCG spilt on the surface of the brain at the time of the original intracerebral injection. Consequently, a mild DTH-like response may have occurred prior to the peripheral challenge. Alternatively, the inflammatory cells present at the earliest time-point (day 0) may remain from the initial acute inflammatory response that had not fully resolved.

DTH lesions have previously been shown to be accompanied by pronounced astrogliosis (Matyszak 1997). The results presented in this chapter are in agreement with this, and it was found that the level of astrogliosis increased over time, to peak at day 19 and subsequently decreased slightly. The myelin loss described here, was generally restricted to the area of hypercellularity. Even in control animals with BCG in the brain, there was a limited amount of myelin loss. In contrast, the DTH lesions have previously shown areas of demyelination throughout the corpus callosum and surrounding grey matter (Matyszak 1996). The differences in these results may simply be explained by the method of BCG injection into the brain parenchyma. In previously published work, the DTH lesions were induced by using a Hamilton syringe, with a much larger diameter than the finely drawn glass canulae used throughout this study. This allows the more direct deposition of BCG at a single site in the parenchyma, resulting in a considerably more

focal lesion, where demyelination would only occur in that region. The Hamilton syringe on the other hand may produce several deposits along the needle tract that has to pass through the corpus callosum. As a consequence, the BCG organisms may spread further, thus increasing the area of myelin loss. With the larger needle, it is also likely that there is reflux of BCG organisms back up the needle track when the needle is being removed, again adding to the spread of BCG.

The finding that there is a loss of acetylcholinesterase activity suggesting neuronal loss in the centre of the hypercellular lesion has not been shown before, however this finding is in accord with previous observations of reduced Cresyl Violet staining within the DTH lesion that is indicative of neuronal loss (Matyszak 1995).

4.7.2 Comparison of DTH and MS Lesion Histopathology

The perivascular cuffs observed in the DTH model are similar to those reported in MS lesions, composed predominately of T lymphocytes and macrophages. B lymphocytes may also be found in the perivascular cuffs. In this work, OX22 positive cells, a marker of both T and B lymphocytes, were found in the perivascular cuffs; it is difficult to determine whether the cells were T or B lymphocytes without using specific antibodies. Macrophages and activated microglia are predominately found at the edge of MS lesions, bordering on NAWM. Widespread MHC class II expression by inflammatory cells in MS lesions and perivascular cuffs have also been reported (Cuzner 1988). Both of these characteristics were observed in the DTH lesion in the current study. When the levels of T cells and macrophages returned to normal levels in the DTH lesion, reactive astrocytes still appear to be present. Once again, this finding is also in agreement with clinical studies, where reactive astrocytes are present in chronic MS lesions (van Walderveen 1998), whilst T and B lymphocytes are less likely to be present in these chronic MS

lesions. The loss of myelin data observed here agrees with that reported by Bruck et al. (Bruck 1997). In that study, it was found that the maximal level of macrophage infiltration occurred in early active MS lesions. At that time-point most of the macrophages were found at the lesion border, whereas in late active lesions macrophages were found scattered through the lesion, which did not change as the lesion exhibited demyelination and remyelination. In contrast, DTH lesions showed a scattered macrophage distribution throughout the time-course of study, including throughout the acute and chronic phases of lesion progression.

4.7.3 Histological Correlations

A correlation was found between numbers of T & B lymphocytes and numbers of macrophages. Both of these cell types are primarily found in the hypercellular core of the DTH lesion, so the areas that they occupy overlap. T lymphocytes are activated by the BCG antigens, these cells then drive the recruitment of macrophages to the DTH lesion, by synthesis and production of chemokines. Macrophages themselves are also responsible for recruitment of other macrophages, again, by synthesis and production of chemokines, which explains why the number of macrophages is greater than the numbers of T and B cells. PB IC control animals exhibited a minor amount of inflammatory cell recruitment to the lesion. Those cells were probably recruited at the time of the intracerebral injection, and a residual inflammatory response may have been present at the time the animal was killed. A correlation was also found between the area of reactive astrocytes and MHC class II expression. MHC class II is expressed by primarily by T and B lymphocytes, but also by macrophages. T and B lymphocytes are recruited during the early acute inflammatory response, when astrocytes also begin to become activated (Matyszak 1998). Over time, both the number of T and B lymphocytes and the level of astrocyte activation increase to reach maximal levels at day 12 and 19, respectively. It is

perhaps not surprising, that the numbers of macrophages and reactive astrocytes correlate since macrophages actively produce potent cytokines, such as Interferon-γ, which will activate astrocytes. However it should be noted, that although recruitment of macrophages and activation of astrocytes appear to be correlated, they do not peak at the same time-point. Thus, although recruitment peaks earlier at day 12, astrocyte activation by the released cytokines persists to reach maximal levels at day 19.

The method that was used to quantify the area of reactive astrocytes and MHC class II expression was based upon thresholding the amount of positive staining on each section. This method may not be the most reliable method since much of the immunohistochemistry experiments were carried out at different time-points, meaning that the levels of staining may vary. Antibody binding to the tissue is also dependent on tissue fixation, and incomplete transcardial perfusion-fixation of animals results in poor antibody binding. Occasionally, it was impossible to avoid these problems and this may have contributed to variability in levels of staining, leading to false or misleading results, sections from animals where this was obviously the case, were not included in the analysis.

Spatial co-incidence of BBB breakdown as indicated by permeability of IgG with areas of BCG antigens and reactive astrocytes, suggests that reactive astrocytes play an important role in the breakdown of the BBB. The areas of reactive astrocytes overlap the area of BCG antigens suggesting that the persistence of the BCG antigens may be driving the continual presence of reactive astrocytes, which in turn affects BBB permeability.

In summary, the results presented here using the DTH model are comparable with the previously published DTH studies. In addition, the DTH lesion exhibits many of the histopathological hallmarks of an MS lesion: expression of MHC class II throughout the

lesion; recruitment of inflammatory T and B lymphocytes as well as macrophages; activation of astrocytes, BBB breakdown; neuronal and myelin loss. New findings from this work are the relationships between T & B lymphocytes and macrophages, loss of acetylcholinesterase activity and the temporal characteristics of the DTH lesion. In conclusion, the DTH model is a valid model for investigating MRI characteristics and correlating these with histopathological changes.

Chapter 5

T_1- and T_2-weighted Imaging

5.1 Introduction

T_1- and T_2-weighted imaging are the traditional methods used by clinicians worldwide, to support diagnosis of brain pathology and to monitor disease progression in the brain. Using these conventional MRI techniques, contrast is determined by the properties of the protons giving rise to the NMR signal; the transverse and longitudinal relaxation rates as well as the proton density, as discussed in Chapter 3. T_1- and T_2-weighted imaging methods were solely used by clinicians for a number of years since they provided an excellent means of distinguishing between normal appearing and abnormal tissue in numerous brain disorders, such as stroke, and MS. Indeed, MRI has become the single most important tool for understanding the dynamic pathology of MS (Miller 1994).

5.1.1 T_1-weighted imaging

Uhlenbrock and Stehlen first identified the presence of T_1-weighted hypointense regions in the MS brain in 1989 (Uhlenbrock 1989). These regions usually represent chronic MS lesions, in which there is irreversible damage to the surrounding tissue matrix, but it has also been shown that some acute lesions may also appear hypointense prior to gadolinium enhancement (van Waesberghe 1998). The irreversible tissue damage that occurs is a loss of neuropil density, which occurs following demyelination (van Walderveen 1998). In addition, there may be loss of astrocytes and concomitant destruction of oligodendrocytes in lesions showing axonal loss. This loss of oligodendrocytes probably reflects a failure

of the repair mechanisms in the MS affected brain (van Waesberghe 1998). T_1 hypointense lesions, which appear as regions of low signal intensity when compared with the surrounding brain tissue, generally demonstrate increased signal intensity on T_2-weighted images (van Walderveen 1998). Despite the fact that T_2 hyperintense regions represent 'active' lesions associated with oedema resulting from increased tissue water content, T_1 hypointense lesions, are a more specific marker of tissue destruction than T_2 hyperintense lesions, since these regions have been shown to correlate more strongly with disability, than with T_2 hyperintense lesions visible in MS patients (van Walderveen 1995), (Truyen 1996). In rodent models of MS, such as EAE, an increased T_1 relaxation time has been shown to occur (Karlik 1990), (Stewart 1991), (Namer 1992), (Morrissey 1996), although the presence of T_1 hypointensities have not been reported in non-primate models.

5.1.2 T_2-weighted Imaging

In MS patients, abnormalities occur on T_1- and T_2-weighted images during the acute phase of lesion development, and may often persist into the chronic phase. To date, T_2-weighted imaging has provided the most accurate MRI modality for assessment of lesion size, which is related to disease activity (Miki 1999), (see (Filippi 2002) for review). Furthermore, T_2-weighted imaging provided the first MRI measurement that demonstrated positive effects in a clinical treatment trial (see (Filippi 2002) for review). Some clinical studies have shown a moderate correlation between T_2-weighted image abnormalities and disability (Mammi 1996), (van Walderveen 1998), (Schreiber 2001), while other studies have shown no correlation at all (Miki 1999), (Miki 1999). However, correlations between T_2-weighted imaging changes and disability appear to be affected by the type of MS studied (RR MS, SP MS or PP MS) with SP MS showing the strongest positive correlations. Both acute and chronic MS lesions appear as regions of

hyperintensity on T_2-weighted images (Fazekas 1999). These regions are generally taken to reflect regions of increased water content, i.e. oedema, (either vasogenic or cytotoxic) which may occur as a result of BBB breakdown. However, areas of increased signal on T_2-weighted images may be brought about by a wide variety of pathological processes from demyelination and gliosis to axonal loss and inflammation, as indicated by EAE studies. Increases in T_2 signal intensity have been shown to correspond to demyelination (Duckers 1997), regions of macrophage recruitment, oedema (Grossman 1987), (Duckers 1997), and gliosis (Jordan 1999) in different models of EAE adding to the confusion regarding the pathology behind T_2 hyperintensities. Hypointense regions have also been observed on T_2-weighted images in MS patients. These regions, which are found in the grey matter (especially in the thalamus) often away from the MS lesions (Bakshi 2001), (Bakshi 2002) are thought to reflect increased iron deposition. They correlate with both disease duration, and neurological disability.

In order to investigate the contribution of demyelination, axonal loss and inflammatory cell recruitment to the T_1 and T_2 hypointensity, and T_2 hyperintensity observed in MS patients, animal models, such as the Delayed Type Hypersensitivity (DTH) model (described in Chapter 4), are invaluable, since full correlations with underlying histopathology can be made.

5.2 Aims of this Chapter

In this chapter, T_1- and T_2-weighted imaging techniques were used to investigate the progression of oedema and hypointense regions during the progression of the DTH lesion. The relationship between T_1- and T_2-weighted imaging was investigated, and the MRI visible effects were correlated with underlying histopathology in order to understand

more fully, the mechanisms behind oedema and tissue damage in a demyelinating CNS lesion.

5.3 Materials and Methods

5.3.1 Experimental Model

Heat-killed BCG ($5x10^5$ organisms) in 1μl was injected stereotaxically into the left striatum of 3-week-old male Lewis rats, as described in Section 3.2.3. Four weeks after the intracerebral injection, a peripheral challenge of TB in CFA was given into each of the hind limbs to initiate a DTH lesion. Both surgery and peripheral challenge were performed under halothane-induced anaesthesia (0.8–1.5% halothane in 70% N_2O/30% O_2). The temperature of the animals was monitored throughout surgery via a rectal probe and homeothermic heating system (Harvard Apparatus, Ltd, UK). In addition, three control groups were investigated, as summarised in Table 4-1. Animals were studied specific time-points following peripheral challenge (days 0 (n=14), 5 (n=13), 8 (n=9), 12 (n=11), 19 (n=11), and 31 (n=11)). Some animals were killed and processed for immunohistochemistry and histology after the MRI protocol, thus giving different sample sizes at each time-point. The day on which the animals received the peripheral challenge was day 0.

5.3.2 Magnetic Resonance Imaging

Animals were anaesthetised with 2-3% halothane and were then positioned in the probe described in Section 3.4.1. Anaesthesia was maintained in the magnet using 0.8–1.5% halothane in 70% N_2O/30% O_2. The temperature of the animals was maintained at 37°C using a circulating warm water system and heart rate was monitored throughout. Once

the animals were in the magnet, a scout image was acquired, using the parameters summarised in Table 5-1 to determine the position of the animal.

Parameter	Value
Repetition time	0.05 sec
Echo time	0.005 sec
Field of view	3 x 3 cm^2
Slice Thickness	1 mm
Number of Averages	2
Total acquisition time	6 sec

Table 5-1: Summary of parameters used for acquisition of scout images for positioning.

From this scout, a horizontal T_2-weighted image using the parameters summarised in Table 5-2, was positioned and acquired through the injection site 3.5mm below the surface of the brain. The injection site was visible as a small hypointense area. A single coronal slice centred on the injection site was selected for the full imaging protocol. All MRI was acquired by 2DFT.

T_1- and T_2-weighted images were acquired using the parameters given in Table 5-2. In most cases following MRI, the animals were perfusion fixed for histological comparisons.

Parameter	T_1-weighted	T_2-weighted	
Slice Orientation	**Coronal**	**Horizontal**	**Coronal**
Repetition time	0.5 sec	3.0 sec	3.0 sec
Echo time	0.02 sec	0.07 sec	0.07 sec
Field of view	3 x 3 cm^2	3 x 3 cm^2	3 x 3 cm^2
Slice Thickness	1 mm	2 mm	1 mm
Number of Averages	8	2	4
Total acquisition time	8 min 44 sec	1 min 48 sec	3 min 36 sec

Table 5-2: Summary of parameters used for the acquisition of T_1- and T_2-weighted images in the coronal and horizontal planes.

5.3.3 Histology and Immunohistochemistry

At specific time-points during the DTH response, (0, 5, 8, 12, 19 and 31 days post peripheral challenge) some animals were terminally anaesthetised and transcardially

perfused with 0.9% NaCl solution as described in Section 3.4.2, to enable histology and immunohistochemistry to be carried out as described in Section 3.6.3.

5.3.4 Data Analysis

5.3.4.1 MRI

Regions of interest (ROI's) were drawn around hypointense and hyperintense areas appearing on T_1- and T_2-weighted images. The mean (± standard deviation) of signal intensity within the ROI's was then quantitated and compared with values obtained from analogous ROI's in the non-injected hemisphere. In addition, the area of each ROI was also measured. Subsequently, the T_2-weighted images were subjected to an in-house cluster analysis program (created by Dr Graeme Waddington (Waddington 1998) and described in Section 3.8.2) to segment regions of total signal change. The area and intensity of these regions were then quantified using a custom-designed image display package, (created by Dr Andrew Blamire). Regions of hypointensity and hyperintensity on T_2-weighted images were also subjected to objective quantification by setting the threshold of image intensity so that all levels of hypo/hyperintensity could be observed.

5.3.4.2 Immunohistochemical Data Analysis

Drawings of histological sections were carried out as described in Section 4.3.3. These were subsequently scanned and stored as electronic images. The scanned drawings were then overlaid on to the MRI images using anatomical markers, such as the corpus callosum, and in some cases, the ventricles, to enable them to be scaled appropriately. In this manner, spatial correlations between histological and MRI-detectable changes could be determined.

5.3.5 Cell Counts

Cell counts were carried out as described previously in Section 4.3.4.

5.3.6 Statistics

Differences between the areas of interest at the different time-points were tested by analysis of variance (ANOVA). Linear regression analysis was performed when an independent variable (or causative factor) could be identified in a relationship. Where this was not the case, correlation analysis was performed. The significance of both linear regression and correlation analysis was tested using a student's t test. An unpaired student's t test with welch correction was used to determine any differences between regions of interest between different time-points, and also between DTH and control groups. All data are presented as the mean ± S.D for n animals.

5.4 Results

DTH animals were imaged throughout the evolution of the DTH lesion (days 0, 5, 8, 12, 19 and 31 post-peripheral challenge) and were killed at selected time-points to correlate T_1 and T_2 changes with the developing histopathology. Control animals were studied at the same time-points.

5.4.1 T_1 and T_2 Hypointensity

Regions of decreased signal intensity (hypointensity) were observed at the site of the original intracerebral injection on both T_1- and T_2-weighted images throughout the time-course. These regions were visible in both transverse and coronal planes as shown in Figure 5-1a and b, and were spatially co-incident on T_1- and T_2-weighted images (as shown in red on Figure 5-1d and e). These regions were observed in both DTH animals and control animals that were injected intracerebrally with BCG (NPC and SAL PC), but not in the control injected intracerebrally with sterile phosphate buffer (PB IC). The hypointense regions on T_1-weighted images were quantified in terms of area over time (Figure 5-2). The area of T_1 hypointensity appeared to be largely constant in all groups from day 0 until day 12, but in DTH animals, the area increased considerably at day 19. This change over time was significant (ANOVA $p<0.05$), and post-hoc pairwise tests showed that day 12 was significantly different to days 0 ($p<0.01$) and 8 ($p<0.02$) (Table 5-3). At days 0, 5 and 8, the area of the T_1 hypointense region in DTH animals was significantly ($p<0.02$ at day 0, $p<0.05$ at days 5 and 8) greater than that observed in NPC controls (Table 5-4). However, due to the large variation at day 19, no significant differences were found between DTH and control experimental groups at this time-point, although this increase appears to be a DTH-specific change (Figure 5-2). No significant

changes in T_1 signal intensity within the hypointense regions were found in any group, and no differences between the control and DTH groups were observed. These data are given in Appendix D.1.

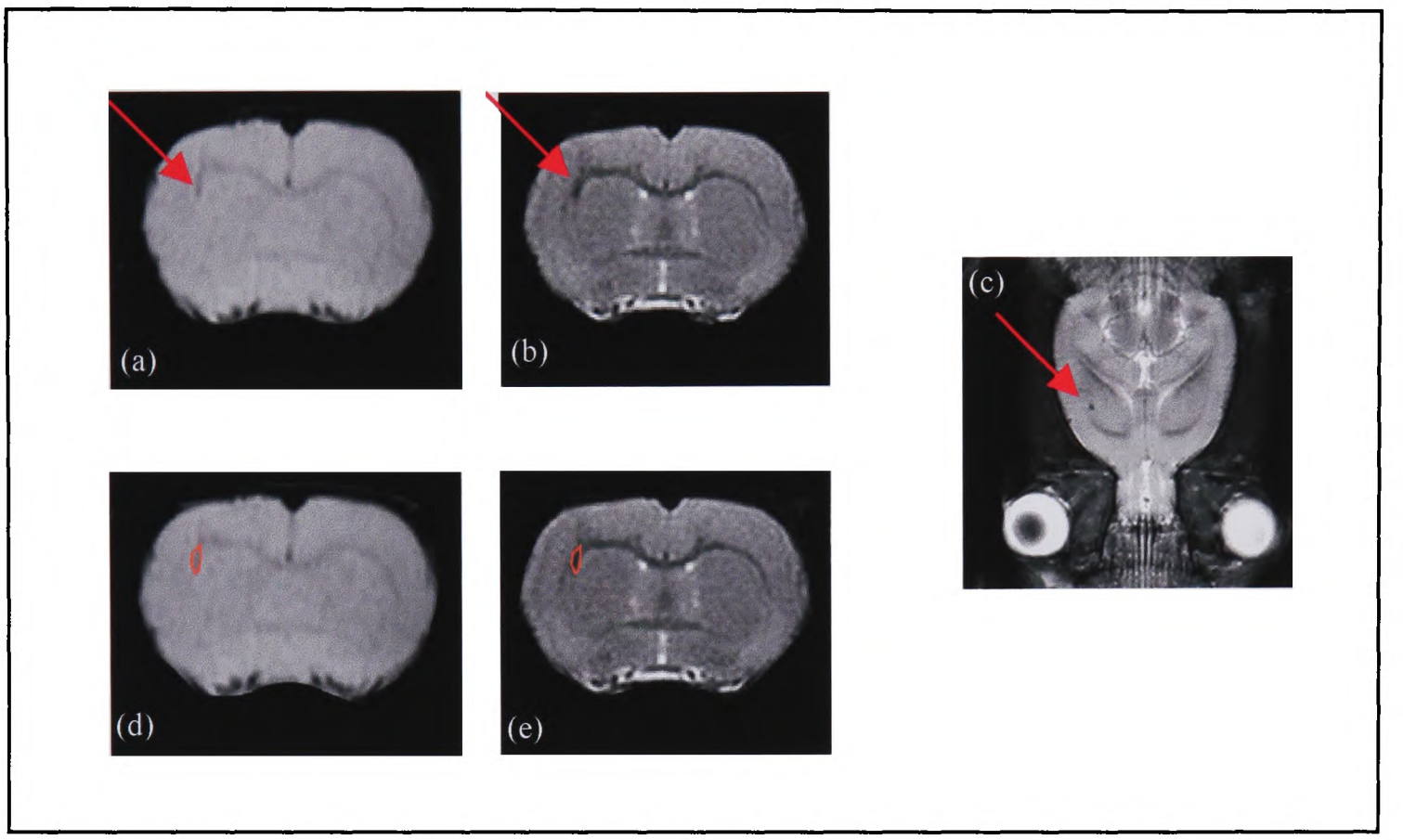


Figure 5-1: (a) Typical coronal T_1-weighted image (b) coronal T_2-weighted image and (c) Horizontal T_2-weighted image, through the site of the intracerebral BCG injection. Regions of hypointensity are visible at the site of original intracerebral injection of BCG in the left hemisphere (indicated by arrows). The hypointense region observed on the T_1-weighted image (d) mapped spatially onto the hypointense region in the T_2-weighted image (e) as indicated here by the red ROI.

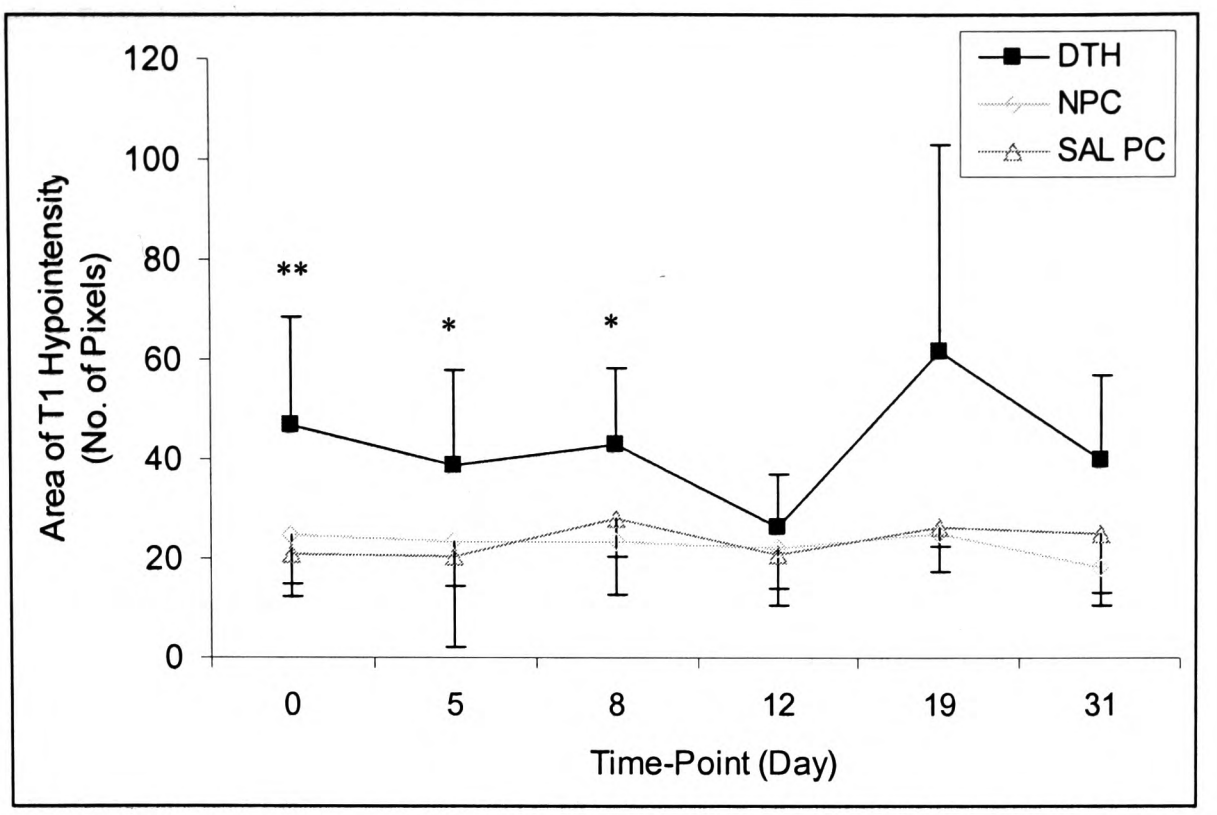


Figure 5-2: Graph to show areas of hypointensity observed on T_1-weighted images throughout the progression of the DTH lesion, indicating maximal area at day 19 in DTH animals. Values are expressed as the mean ± S.D. (NPC; no peripheral challenge, SAL PC; saline peripheral challenge). A significant difference over time was observed in DTH animals (ANOVA $p<0.05$). A significant difference between DTH and NPC controls was found at days 0, 5, and 8 (unpaired t test $^{**}p<0.02$, $^{*}p<0.05$).

DTH Area of T_1 Hypointensity						
Time-Point (Day)	**0**	**5**	**8**	**12**	**19**	**31**
0	-	/	/	$p<0.01$	/	/
5	-	-	/	$p=0.0714$	/	/
8	-	-	-	$p<0.02$	/	/
12	-	-	-	-	$p=0.0914$	$p<0.05$
19	-	-	-	-	-	/
31	-	-	-	-	-	-

Table 5-3: Summary of unpaired t test results for comparison of the area T_1 hypointensity within the DTH group at each time-point. ('/' denotes difference is not significant, values for comparisons that did not quite reach significance are also included).

DTH Area of T_1 Hypointensity						
Time-Point (Day)	**0**	**5**	**8**	**12**	**19**	**31**
NPC	$p<0.02$	$p<0.05$	$p<0.05$	/	$p=0.0803$	$p=0.0657$
SAL PC	$p=0.0583$	/	$p=0.0636$	/	/	/

Table 5-4: Summary of unpaired t test results between DTH and control groups ('/' denotes difference is not significant, values for comparisons that did not quite reach significance are also included NPC; no peripheral challenge, SAL PC; saline peripheral challenge).

Hypointense regions observed on T_2-weighted images were also quantified and are shown in Figure 5-3. The maximal area again appeared to be at day 19, although there was a

great deal of variation in this group contributing to lack of statistical significance at this time-point. At days 8, 12, 19, and 31 however, significant differences were found between DTH and SAL PC animals (unpaired t tests $p<0.05$, $p<0.005$, $p<0.02$, and $p<0.0001$ respectively) (Table 5-5). In addition, it is clear from Figure 5-3 that in both control groups, the area of hypointensity steadily decreases with time, whilst in the DTH group this area increases gradually from day 0 until day 19, after which point it decreases. Individual results are summarised in Appendix D.1. When the relationship between the areas of T_1 and T_2 hypointensity was investigated no significant correlation was found (Figure 5-4 and Table 5-6), despite the areas being spatially co-incident (Figure 5-1d and e). This is probably due to the data being very bunched as a result of the relatively small area measurements.

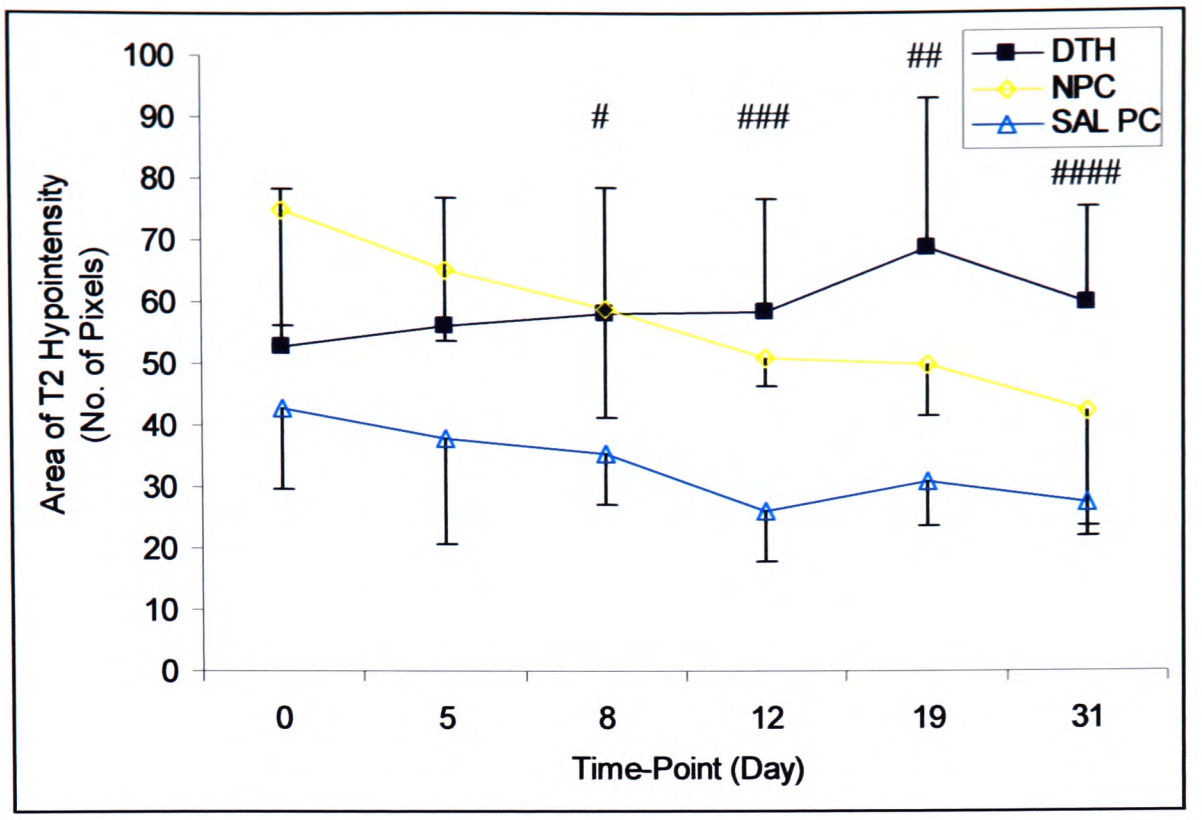


Figure 5-3: Area of hypointensity observed on T_2-weighted images throughout the progression of the DTH lesion. The maximal area of hypointensity appeared to be at day 19. Values are expressed as the mean ± S.D. (NPC; no peripheral challenge, SAL PC; saline peripheral challenge). Significant differences between DTH and SAL PC controls were found at days 8, 12, 19 and 31 (unpaired t tests ####$p<0.0001$, ###$p<0.005$, ##$p<0.02$, #$p<0.05$).

DTH Area of T_2 Hypointensity						
Time-Point (Day)	**0**	**5**	**8**	**12**	**19**	**31**
NPC		/	/	/	/	/
SAL PC	/	/	$p<0.05$	$p<0.005$	$p<0.02$	$p<0.0001$

Table 5-5: Summary of unpaired t test results for comparisons between DTH and control groups ('/' denotes difference is not significant, values for comparisons that did not quite reach significance are also included, NPC; no peripheral challenge, SAL PC; saline peripheral challenge).

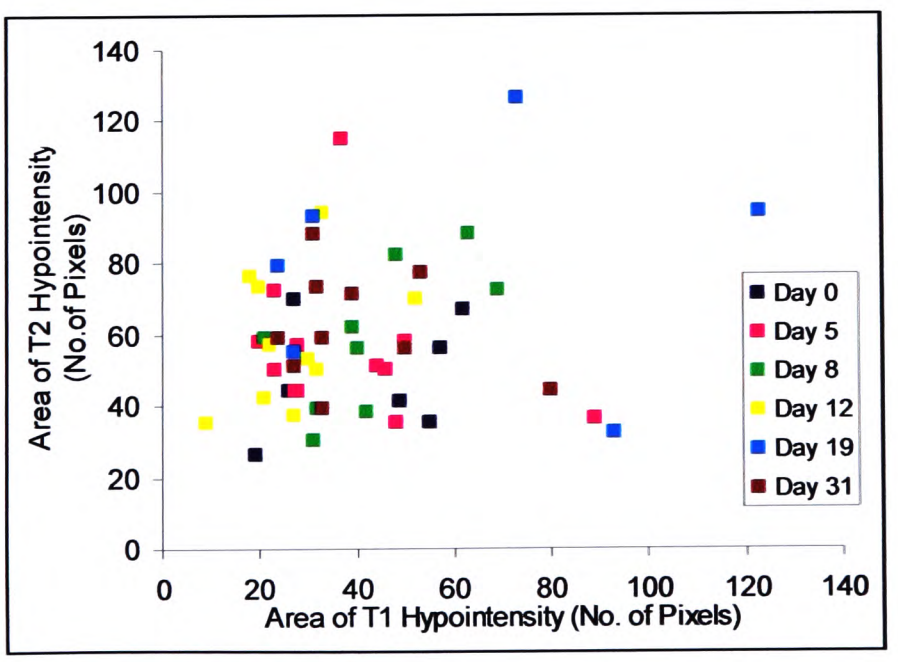


Figure 5-4: Graph to demonstrate the relationship between the areas of T_1 and T_2 hypointensities. No correlation was found, probably due to the very closely grouped data.

Correlation Between Areas of...	Correlation Parameters	
	r	p
T_1 hypointensity and T_2 hypointensity	0.16	0.23

Table 5-6: Summary of correlation parameters for the relationship between the areas of hypointensity observed on T_1- and T_2-weighted images.

5.4.2 T_2 Hyperintensity

A region of hyperintensity, which appeared to surround the core of hypointensity, was visible at all time-points in most DTH animals on T_2-weighted images in the coronal plane. Representative images of a typical animal are shown in Figure 5-5. At days 0 and 5, where present, the hyperintense region was usually restricted to a bright rim of a few pixels around the hypointense core. The extent of the hyperintense region varied over time (ANOVA $p<0.005$). At day 19, the extent of this region was significantly greater than days 0 and 31 (unpaired t test compared with day 0, $p<0.02$ and $p<0.05$ respectively). Days 5, 8, 12, and 19 were all significantly greater than day 0 ($p<0.02$ in all cases) as observed in Table 5-7. After day 19, the hyperintensity decreased in size again (Figure 5-6). No hyperintensity was observed in any of the control groups, despite the presence of the hypointense region at all time-points. In terms of left/right signal intensity ratio (ROI's were restricted to the hyperintense area and flipped vertically onto the contralateral hemisphere), no significant changes were observed over time. Individual results for intensity data are detailed in Appendix D.1.

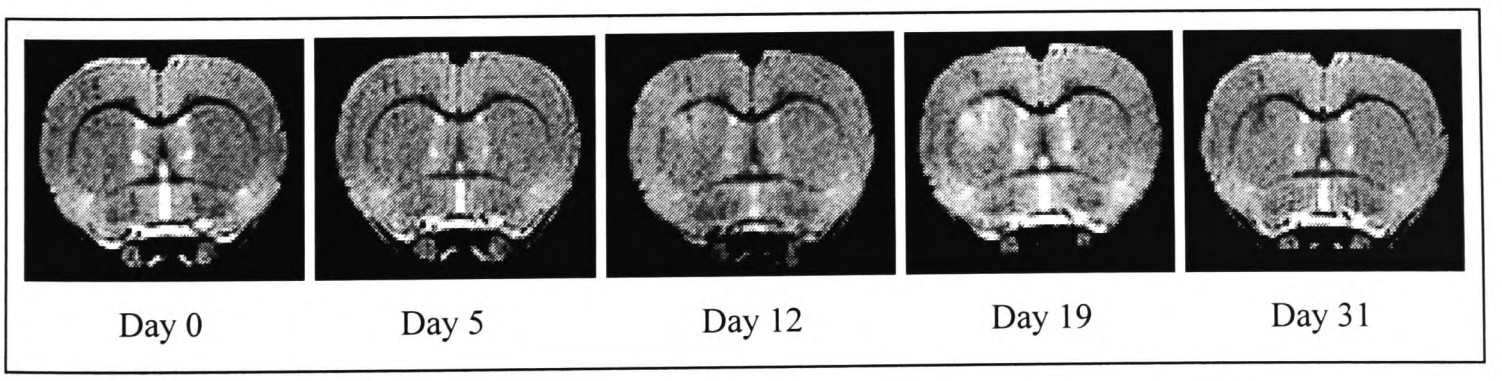


Figure 5-5: Coronal T_2-weighted images throughout the progression of a DTH lesion, showing hyperintense region surrounding the hypointense core in the injected (left) hemisphere.

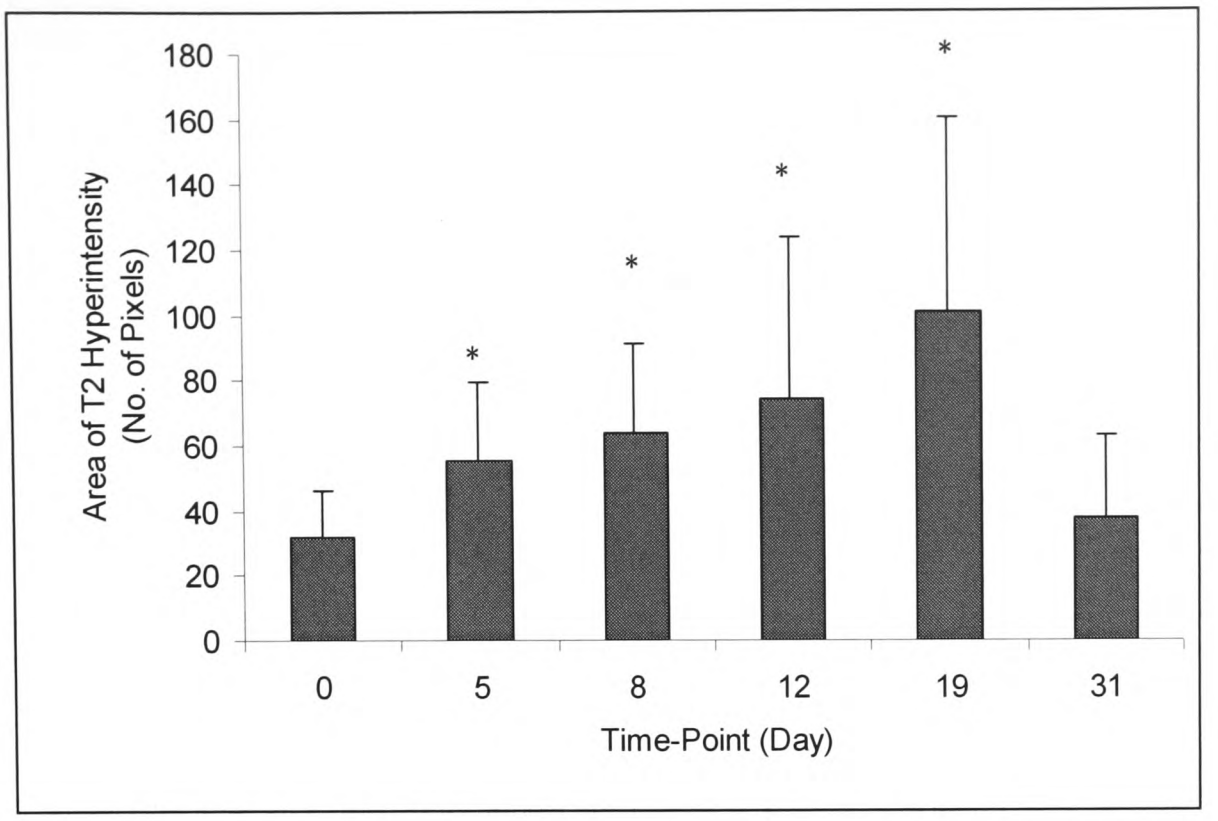


Figure 5-6: Graph to show area of hyperintense region in DTH animals on T_2-weighted images over time. Values are expressed as the mean ± S.D. A significant change over time was observed (ANOVA $p<0.005$, unpaired t test *$p<0.02$ when compared with day 0).

DTH T_2 Hyperintensity						
Time-Point (Day)	**0**	**5**	**8**	**12**	**19**	**31**
0	-	$p<0.02$	$p<0.02$	$p<0.02$	$p<0.02$	/
5	-	-	/	/	$p=0.0737$	/
8	-	-	-	/	/	$p=0.0569$
12	-	-	-	-	/	$p<0.05$
19	-	-	-	-	-	$p<0.05$
31	-	-	-	-	-	-

Table 5-7: Summary of unpaired t test results for comparison of the hyperintensity on T_2-weighted images, within the DTH group at each time-point ('/' denotes difference is not significant, values for comparisons that did not quite reach significance are also included).

5.4.3 Correlation between T_2 Hypointensity and T_2 Hyperintensity

Areas of hypointensity and hyperintensity were identified in the same animal on T_2-weighted images. A highly significant ($p<0.005$) correlation was found between areas of T_2 hypointensity and T_2 hyperintensity (Figure 5-7 and Table 5-8).

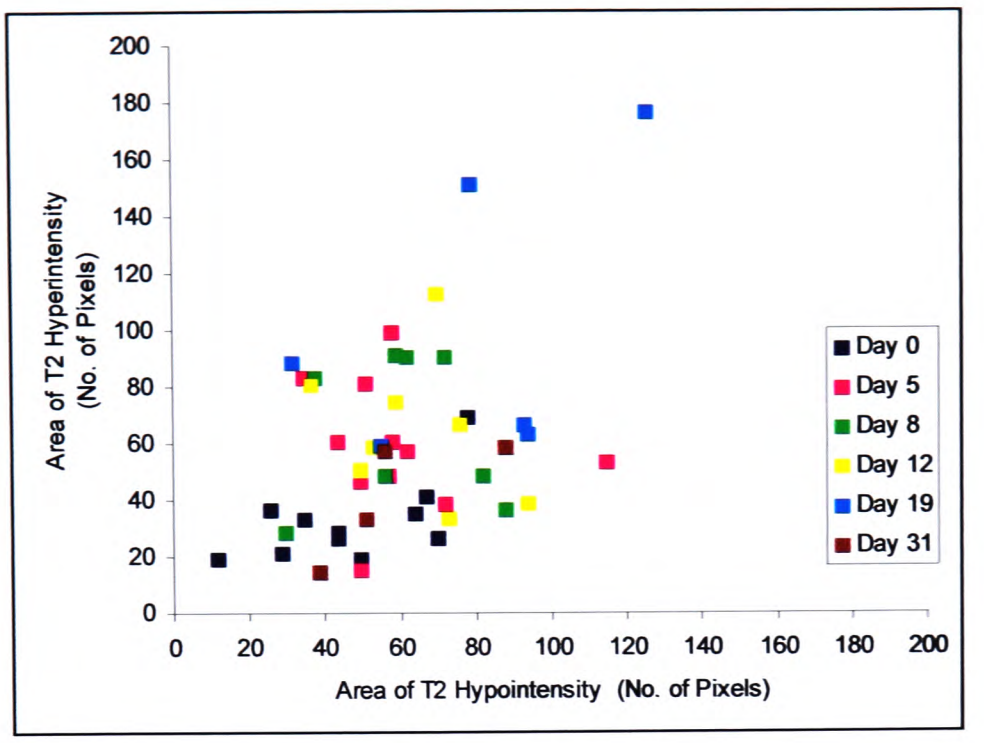


Figure 5-7: Graph to show relationship between the areas of T_2 hypointensity and T_2 hyperintensity. A highly significant ($p<0.005$) correlation was found.

Correlation Between Areas of...	Correlation Parameters	
	r	p
T_2 hypointensity and T_2 hyperintensity	0.39	$p<0.005$

Table 5-8: Summary of the results of the correlation analysis of the relationship between areas of T_2 hypointensity and areas of T_2 hyperintensity.

5.4.4 Total Area of Signal Change on T_2-weighted Images

Throughout the MS literature, lesion load on T_2-weighted images is calculated from the total area of signal change observed on T_2-weighted images. Therefore, areas of total signal change (encompassing both the hypointense and hyperintense regions) on T_2-weighted images were segmented via cluster analysis (described in Section 3.8.2). In addition, the previous measurements of hypointense and hyperintense areas observed on T_2-weighted images were carried out subjectively by eye, and consequently were open to operator bias. Performing one dimensional cluster analysis on T_2-weighted images, enables a non-subjective quantitation of the total area of signal change. These

measurements would, therefore allow an objective validation of visual measurements and findings.

In general the area of total T_2 signal change (Figure 5-8) was far greater in DTH animals than that observed in either control group, and a significant change over time was found (ANOVA $p<0.05$). At days 8, 12 and 19, DTH animals were significantly different from NPC controls (Table 5-10) and at days 5, 8, 12, 19, and 31, DTH animals were significantly different from SAL PC controls (Table 5-10). The area of total T_2 signal change was significantly greater than day 0 at each time-point (Table 5-9). The maximal area of total signal change appeared to occur at day 5, and after this time-point the area of total signal change decreased gradually.

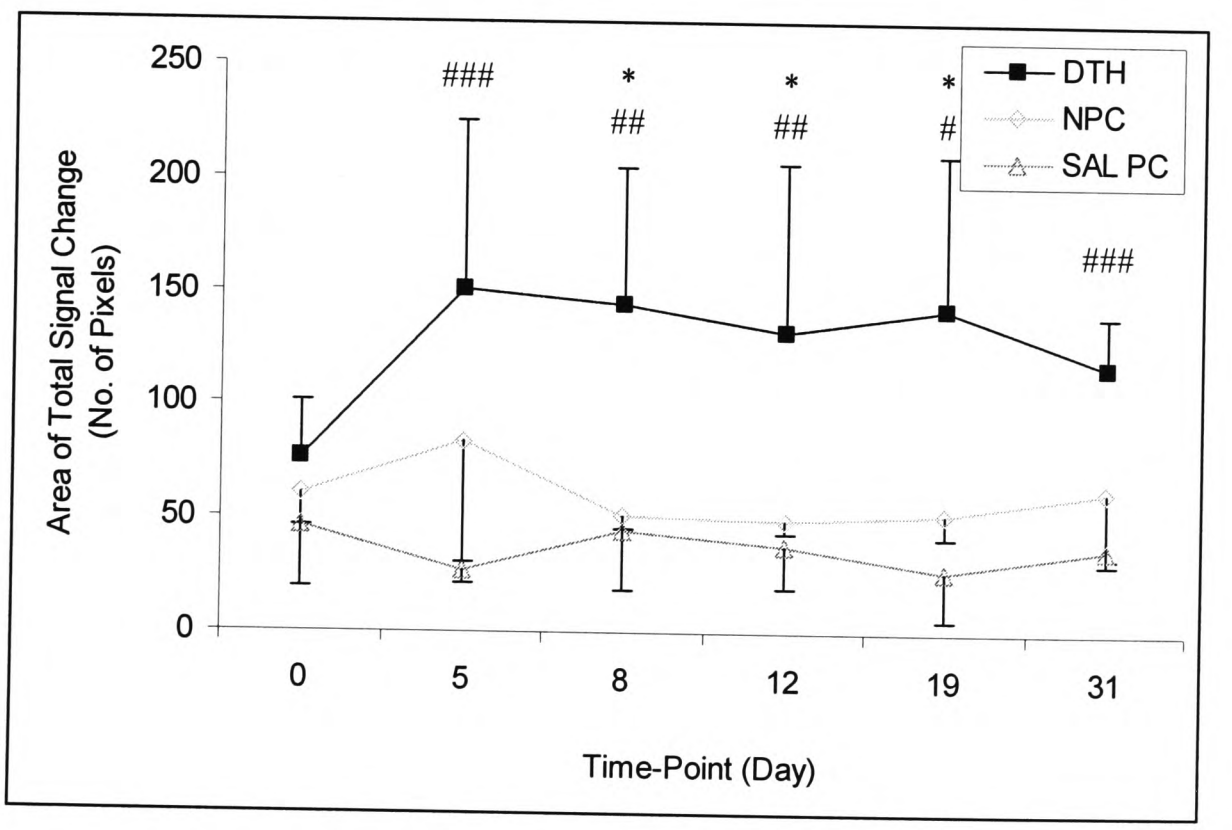


Figure 5-8: Graph to show area of total signal change observed on T_2-weighted images throughout the progression of the lesion in DTH and control groups. All values are expressed as the mean ± S.D. (NPC; no peripheral challenge, SAL PC; saline peripheral challenge). A significant difference over time in DTH animals was detected ANOVA $p<0.05$. Significant differences were found between DTH and control groups at days 5, 8, 12, 19, and 31 (unpaired t tests ###$p<0.0001$, ##$p<0.005$, #$p<0.01$, *$p<0.005$, where * versus NPC and # versus SAL PC controls).

DTH Total T_2 Signal Change						
Time-Point (Day)	**0**	**5**	**8**	**12**	**19**	**31**
0	-	p<0.005	p<0.02	p<0.05	p<0.05	p<0.001
5	-	-	/	/	/	/
8	-	-	-	/	/	/
12	-	-	-	-	/	/
19	-	-	-	-	-	/
31	-	-	-	-	-	-

Table 5-9: Summary of unpaired t test results for comparison of the area of the total area of signal change within the DTH group at each time-point. ('/' denotes difference is not significant).

DTH Total T_2 Signal Change						
Time-Point (Day)	**0**	**5**	**8**	**12**	**19**	**31**
NPC	/	p=0.0547	p<0.05	p<0.005	p<0.005	/
SAL PC	/	p<0.0001	p<0.005	p<0.005	p<0.01	p<0.0001

Table 5-10: Summary of unpaired t test results for comparison of total areas of signal change between DTH and control groups at each time-point ('/' denotes difference is not significant, values for comparisons that did not quite reach significance are also included, NPC; no peripheral challenge, SAL PC; saline peripheral challenge).

5.4.5 Spatial Co-incidence of Histology and T_2 Hyperintensity

BCG antigens (in orange on Figure 5-9a) were found for some distance surrounding the hypercellular area, but did not appear to spatially coincide with any T_2 weighted image characteristics. Areas of reactive astrocytes (in blue) appeared to most closely map spatially to the regions of T_2 hyperintensity (Figure 5-9b). Areas of IgG staining, indicating BBB breakdown, also mapped fairly closely to the T_2 hyperintensity (Figure 5-9c) although tended to be slightly larger. These spatial co-incidences were found to exist with the different inflammatory markers at all time-points when the T_2 hyperintensity was overt. In contrast, areas of macrophage and T & B lymphocyte recruitment in green (Figure 5-9d), areas of MHC class II expressing cells (in yellow) (Figure 5-9e), and areas of neuronal loss in red (Figure 5-9f), mapped spatially to the hypercellular region. This region, in turn appeared to map to the hypointense area on T_2-weighted images at day 19

when it was maximal spatially (Figure 5-3). Areas of demyelination were almost always restricted to the hypercellular area, (data not shown).

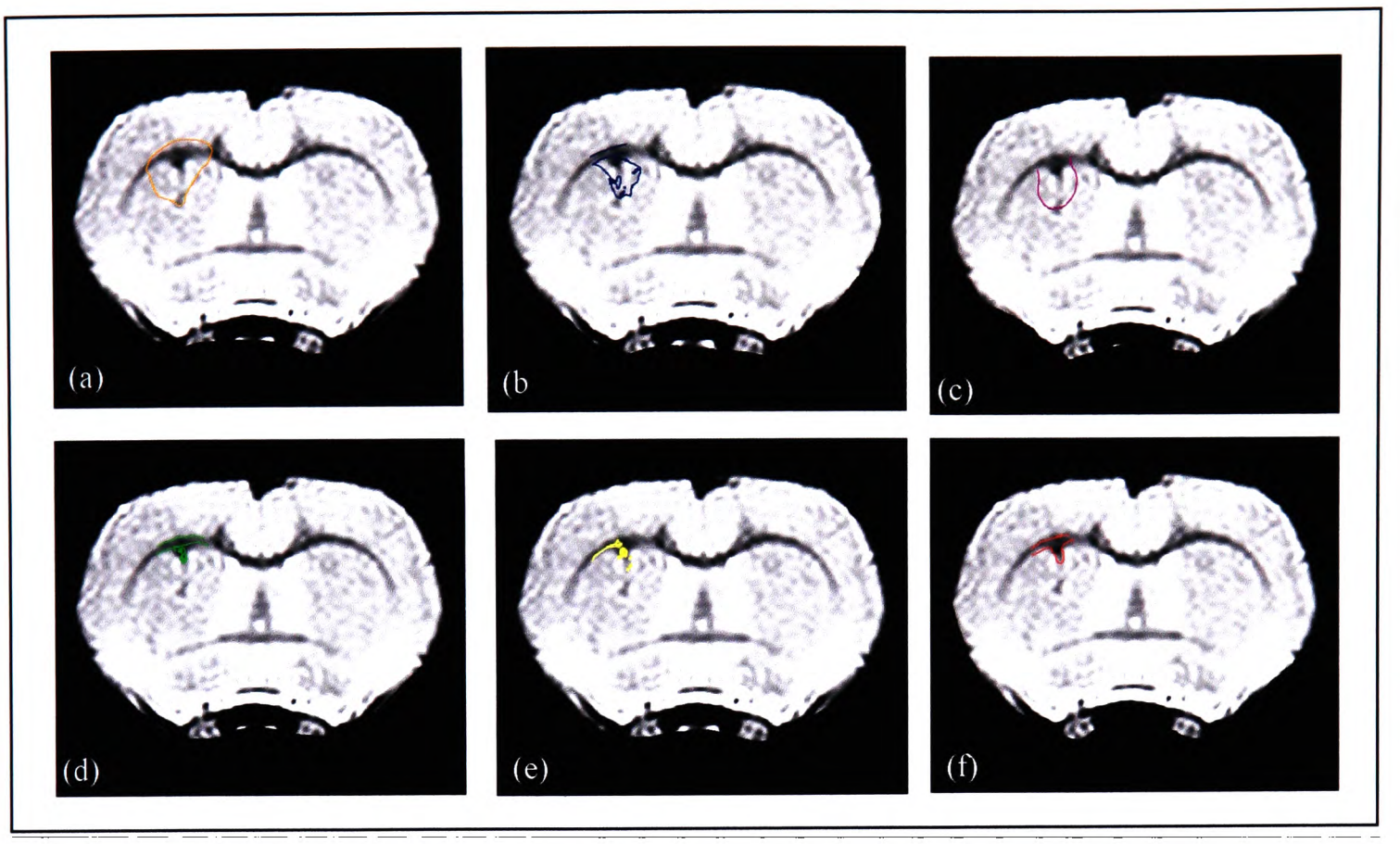


Figure 5-9: (a) The area of BCG antigens, (shown in green), overlaps, but extends beyond the area of change on T_2-weighted images.

(b) The area of staining occupied by reactive astrocytes (in blue) maps fairly closely to the area of T_2-hyperintensity at day 12.

(c) In purple, the area of IgG indicating BBB breakdown tended to be similar to, but slightly larger than the area of hyperintensity on T_2-weighted images.

(d) The area of staining occupied by macrophages and T & B lymphocytes is restricted to the hypercellular area, which is observed as a hypointense region on T_2-weighted images.

(e) In yellow, areas occupied by MHC class II expressing cells also spatially coincide with the area of hypointensity on T_2-weighted images.

(f) In red, the area of neuronal loss again, only occurs in area of hypercellularity, which maps spatially to the region of hypointensity on T_2-weighted images.

5.4.6 Quantitative Correlations with Histology

The different MRI parameters identified on T_1- and T_2-weighted images were correlated with immunohistochemical data obtained in Chapter 4 at all time-points investigated. Many spatial relationships were inferred from Section 5.4.5, therefore linear regression analysis was performed for the correlations. No significant correlations were found between macrophage numbers and areas of T_1 hypointensity, or T_2 hyperintensity,

however significant correlations were found with the area of T_2 hypointensity ($p<0.001$), as indicated by their spatial coincidence, and with the total area of T_2-weighted image signal change ($p<0.001$) (Figure 5-10 and Table 5-11).

No significant correlation was found between numbers of T & B lymphocytes, and either T_1 hypointensity or T_2 hyperintensity, however a trend towards a significant correlation was found between numbers of T & B lymphocytes and areas of T_2 hypointensity ($p=0.067$) and a significant correlation was found with the total area of T_2 signal change ($p<0.01$) (Figure 5-11 and Table 5-12).

In terms of areas of astrocyte activation, both the area of T_2 hypointensity, and total area of T_2 signal change exhibited a trend towards significance with the area of astrocyte activation ($p=0.068$ and $p=0.07$ respectively) however, the area of T_2 hyperintensity exhibited a significant correlation ($p<0.005$) with the areas of astrocyte activation, as indicated by their spatial coindence. In contrast, areas of T_1 hypointensity did not correlate with areas of astrocytes (Figure 5-12 and Table 5-13).

Lastly, the area of T_2 hyperintensity was found to significantly correlate with the area of MHC class II expression ($p<0.01$), however the areas of T_1 hypointensity, T_2 hypointensity, and total T_2 signal change did not correlate with areas of MHC class II expression (Figure 5-13 and Table 5-14).

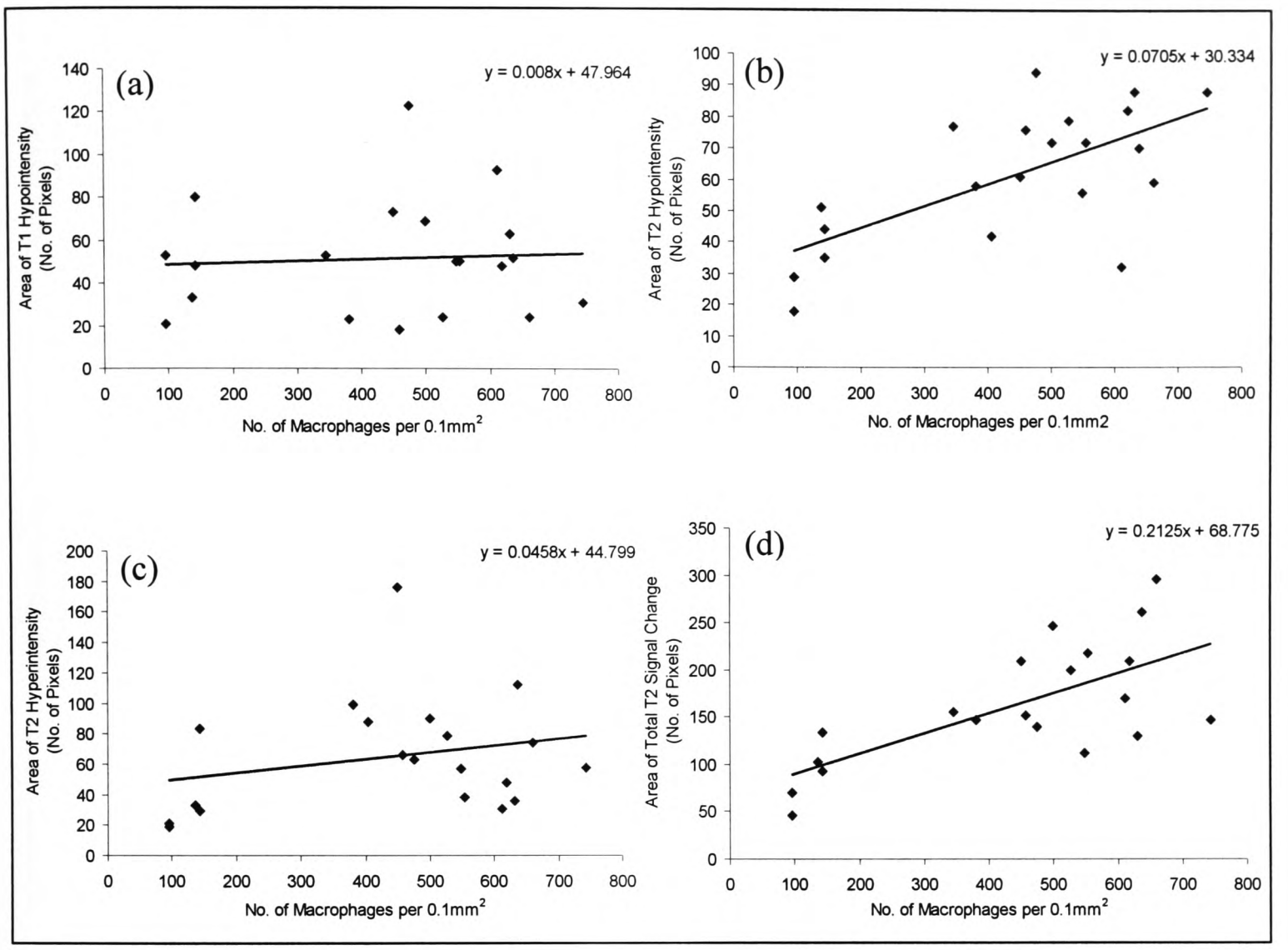


Figure 5-10: Graphs to demonstrate relationship between areas of T_1- and T_2-weighted image signal change and presence of macrophages.

(a) No significant correlation was found with the area of T_1-weighted hypointensity,

(b) A highly significant ($p<0.001$) correlation was found with the area of T_2 hypointensity.

(c) No correlation was found with the area of T_2 hyperintensity,

(d) A highly significant ($p<0.001$) correlation was found with total area of T_2 signal change.

Correlation between Macrophages and area of...	Correlation Parameters			
	r	p	Slope	Y intercept
T_1 Hypointensity	0.06	0.79	0.01	47.96
T_2 Hypointensity	0.67	$p<0.001$	0.07	30.33
T_2 Hyperintensity	0.25	0.28	0.05	44.80
Total area of T_2 signal change	0.69	$p<0.001$	0.21	68.78

Table 5-11: Summary of correlation analysis between macrophages per $0.1mm^2$ lesion area and T_1- and T_2-weighted image measurements.

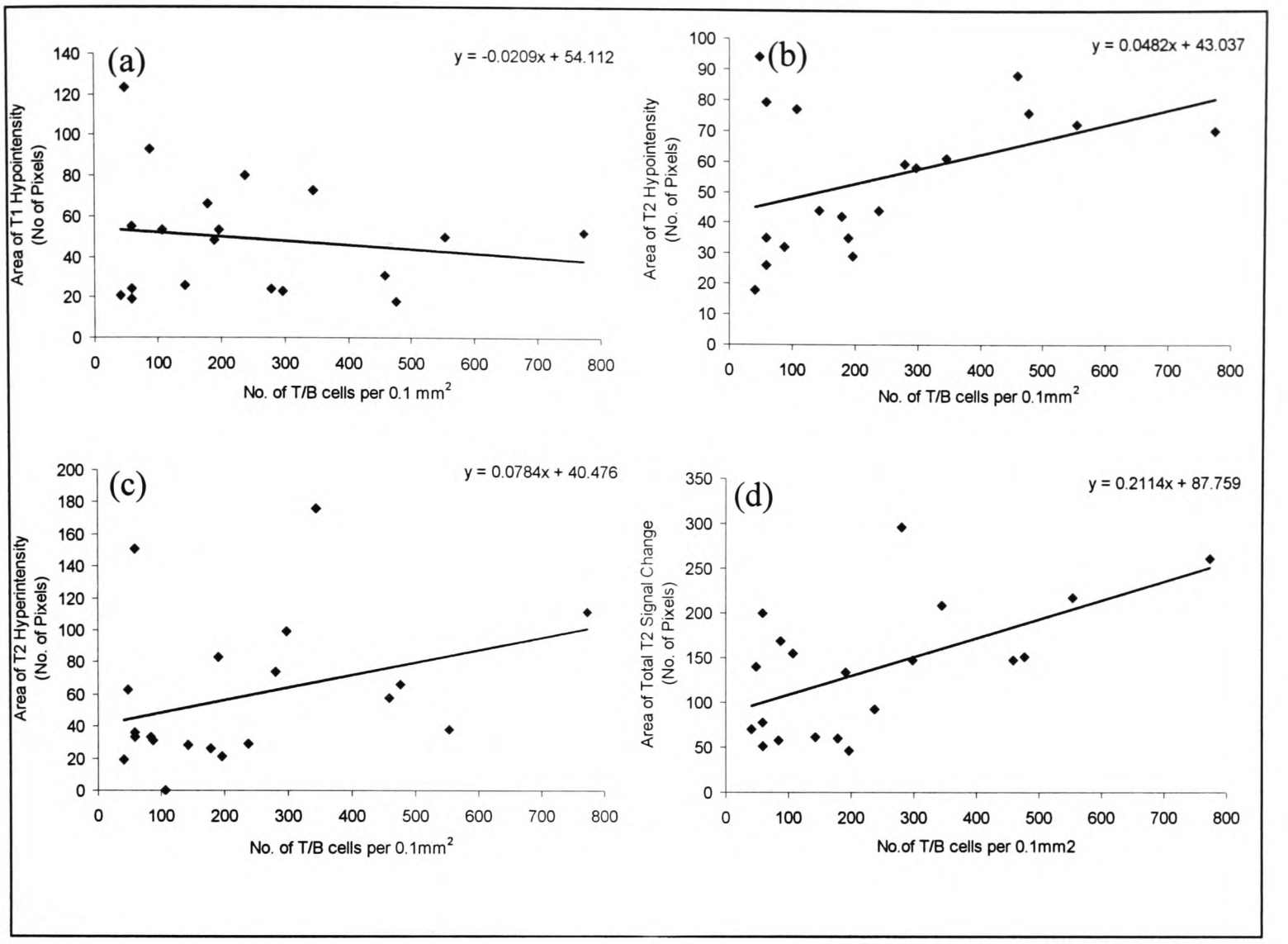


Figure 5-11: Graphs to demonstrate relationship between areas of T_1- and T_2-weighted image signal change and presence of T & B lymphocytes in the DTH lesion.

(a) No significant correlation was found with the area of T_1-weighted hypointensity.

(b) A trend towards a significant ($p=0.067$) correlation was found with the area of T_2 hypointensity.

(c) No correlation was found with the area of T_2 hyperintensity.

(d) A highly significant ($p<0.01$) correlation was found with the total area of T_2 signal change.

Correlation between T & B Lymphocytes and area of ...	Correlation Parameters			
	r	p	Slope	Y intercept
T_1 Hypointensity	-0.15	0.55	-0.02	54.11
T_2 Hypointensity	0.43	p=0.067	0.05	43.03
T_2 Hyperintensity	0.34	0.14	0.08	40.48
Total area of T_2 signal Change	0.58	p<0.01	0.21	87.76

Table 5-12: Summary of correlation analysis between T & B lymphocytes per $0.1mm^2$ lesion area and T_1- and T_2-weighted image measurements.

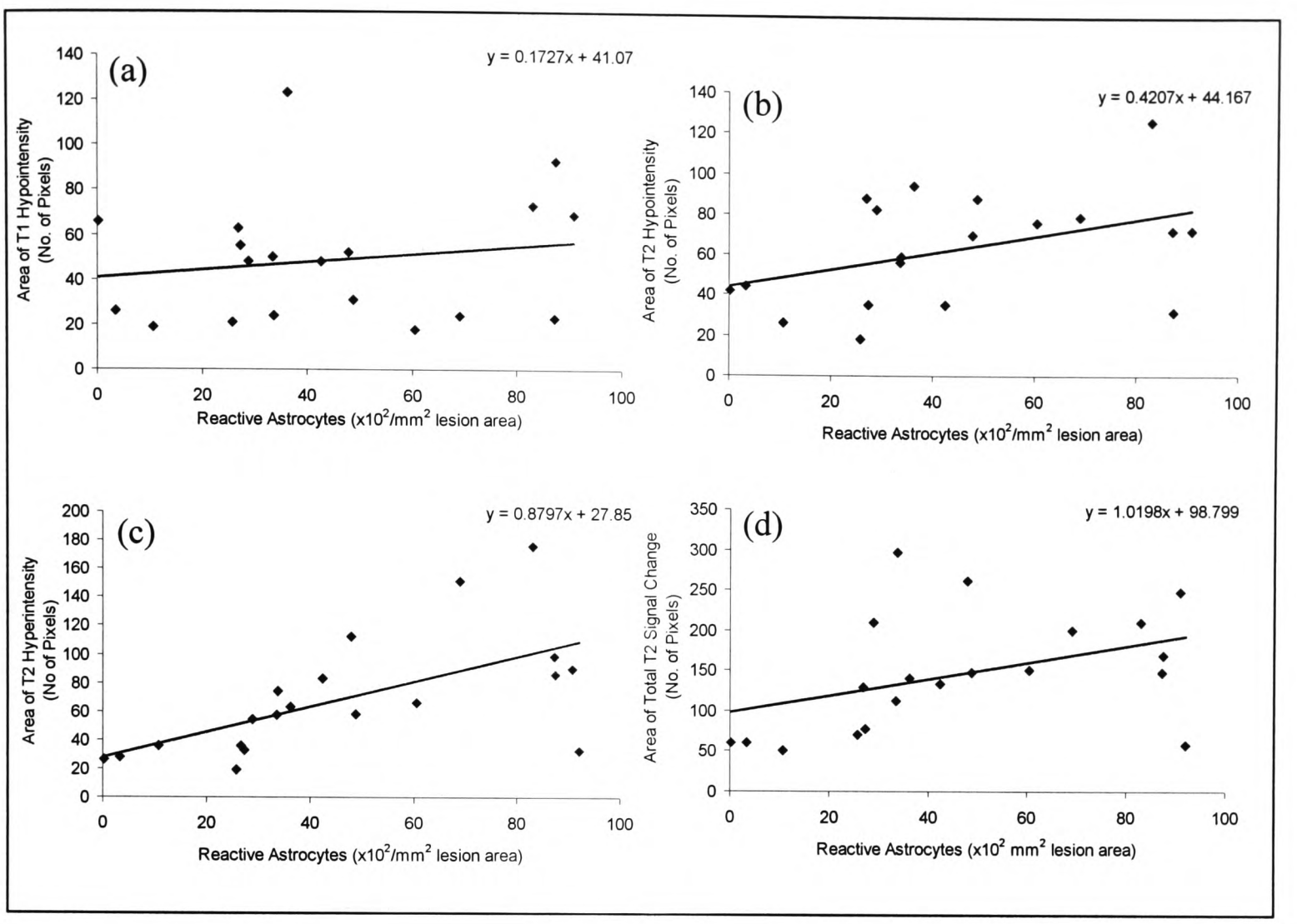


Figure 5-12: Graphs to demonstrate relationship between areas of T_1- and T_2-weighted image signal change and areas of reactive astrocytes.

(a) No correlation was found with the area of T_1-weighted hypointensity.

(b) A trend towards a significant ($p=0.068$) correlation was found with the area of T_2-hypointensity.

(c) A highly significant ($p<0.005$) correlation was found with the area of T_2-hyperintensity.

(d) A trend towards a significant ($p=0.07$) correlation was found with the total area of T_2 signal change.

Correlation between reactive astrocytes and area of ...	Correlation Parameters			
	r	p	Slope	Y intercept
T_1 Hypointensity	0.17	0.48	0.17	41.07
T_2 Hypointensity	0.43	$p=0.068$	0.42	44.17
T_2 Hyperintensity	0.62	$p<0.005$	0.88	27.85
Total area of T_2 signal Change	0.41	$p=0.07$	1.02	98.80

Table 5-13: Summary of correlation analysis between the area of reactive astrocytes and T_1- and T_2-weighted image measurements.

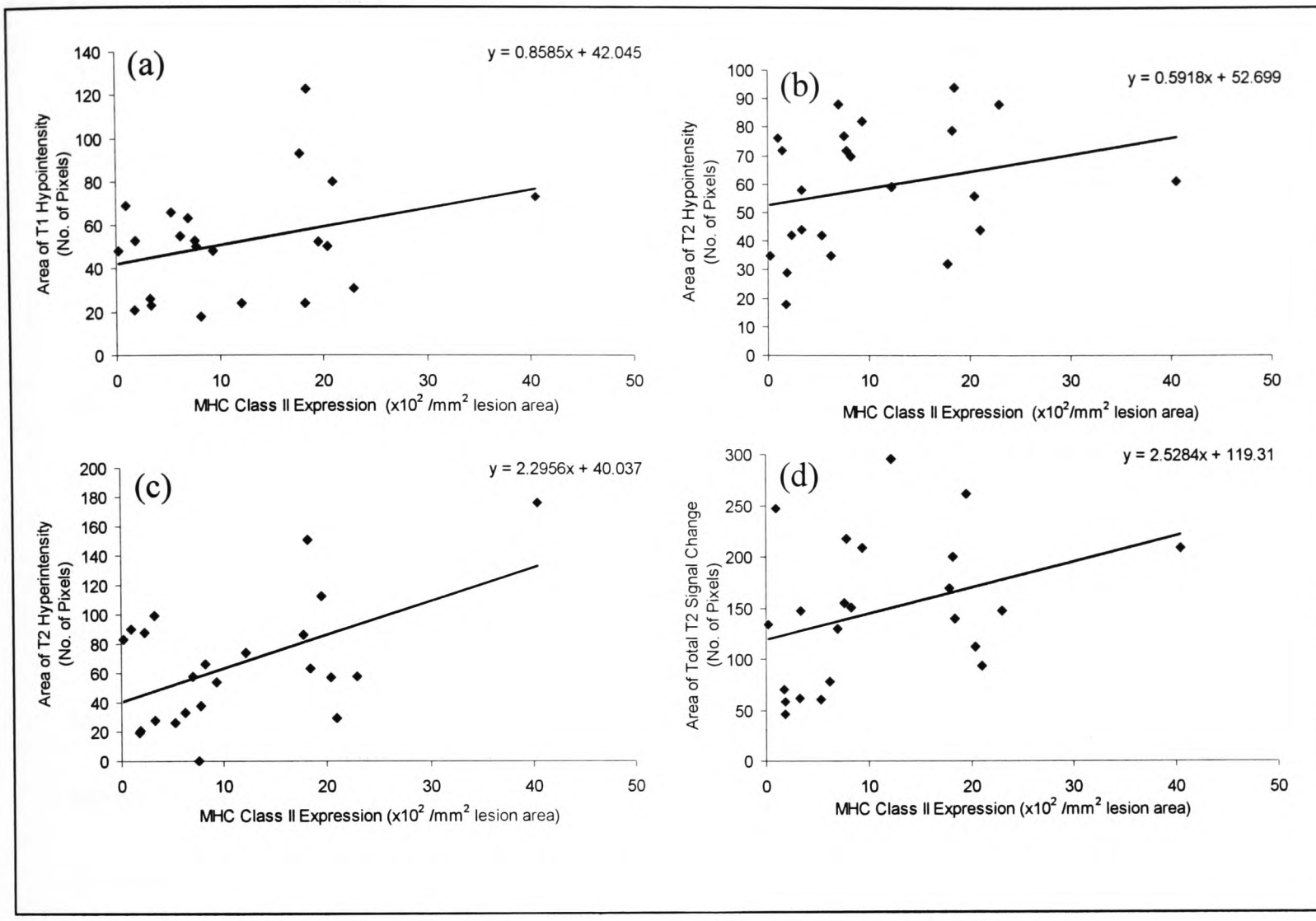


Figure 5-13: Graphs to demonstrate relationship between areas of T_1- and T_2-weighted image signal change and areas of MHC class II expression.

(a) No correlation was found with the area of T_1-weighted hypointensity.

(b) No correlation was found with the area of T_2 hypointensity.

(c) A highly significant ($p<0.01$) correlation was found with the area of T_2 hyperintensity,

(d) No correlation was found with the total area of T_2 signal change.

Correlation between MHC class II expression and area of ...	Correlation Parameters			
	r	p	Slope	Y intercept
T_1 Hypointensity	0.32	0.14	0.86	42.05
T_2 Hypointensity	0.27	0.22	0.59	52.70
T_2 Hyperintensity	0.53	$p<0.01$	2.30	40.04
Total area of T_2 signal Change	0.35	0.10	2.53	119.31

Table 5-14: Summary of correlation analysis between MHC class II expression and T_1- and T_2-weighted image measurements.

5.5 Discussion

This study demonstrates that the DTH lesion gives rise to the same conventional MRI characteristics that are used clinically in the diagnosis and monitoring of MS. The hallmark MRI characteristics of the MS lesion, are hypointense regions on T_1- and T_2-weighted images and hyperintensity on T_2-weighted images. Areas of T_1 and T_2 hypointensity, and T_2 hyperintensity were consistently observed in DTH animals and were found to change with time. Most of these MRI detectable changes appeared to occur maximally at day 19, considered to be the peak of the DTH response. A significant correlation was found between areas of T_2 hypointensity and T_2 hyperintensity, however the intensity of hypointense and hyperintense regions on T_1- and T_2-weighted images did not appear to change with time. SAL PC and NPC control animals exhibited T_1 hypointensities throughout the time-course, but these areas did not alter in size, in contrast to the DTH group, which changed temporally. PB IC controls did not show these hypointensities. In addition, development of a hyperintense region was not observed in any of the control groups.

5.5.1 T_1 Hypointensities

T_1 hypointensities are commonly observed in MS, and have been linked to axonal loss (van Walderveen 1998). In the DTH model, similar axonal loss has previously been shown to occur (Newman 2001), and this is consistent with observations in rat and marmoset EAE (Kornek 2000), (Mancardi 2001). The primary reason for axonal loss is thought to be via matrix metalloproteinases (MMP's) action, which have also been detected in DTH lesions (Anthony 1997). In MS, axon damage occurs during the acute inflammatory stage (Kuhlmann 2002), whilst in the DTH model, axonal damage is ongoing throughout the acute and chronic inflammatory phases (Newman 2001). In the

current work, hypointense regions were visible on T_1-weighted images and were present throughout the study, therefore, it is possible that these changes reflect ongoing axonal damage in the DTH lesion. Furthermore, areas of neuronal loss, as identified by acetylcholinesterase staining in chapter 4, correlated spatially with the hypointensities suggesting that indeed neuronal/axonal loss may be an underlying cause of these MRI changes. However, T_1 hypointense regions have also been shown to reflect expansion of the extracellular space, probably resulting from myelin loss (Barnes 1987). In support of this suggestion, in this work, myelin loss only occurred within the hypointense regions. Histologically, in the DTH model these regions represent the presence of macrophages, T & B lymphocytes, fibrillary gliosis and neuronal loss. Similarly, in MS, T_1 hypointense regions have been shown to reflect these histological characteristics, as well as an absence of central myelinated axons (van Walderveen 1996), (van Walderveen 1997). Thus, several possible explanations for the underlying cause behind T_1 and T_2 hypointensities exist, including loss of neurones, axons, and myelin. In this study, the T_1 hypointense area appeared to increase substantially at day 19, and after this time-point, the area decreased once more. If the area of hypointensity was stable over time, then this would be an indication that axonal loss occurred at an early stage, but the increase at day 19 suggests that either a further loss of axons occurred, or other factors responsible for the appearance of T_1 hypointensity may be involved, such as MHC class II expression. The maximal expression of MHC class II expression also occurred at day 19 (Section 4.6.5). Because no single histological factor (macrophages, T & B lymphocytes, reactive astrocytes, or MHC class II expression) appeared to correlate with the areas of T_1 hypointensity, this suggests that either a combination of these factors cause these MRI changes, or factors such as myelin or axonal loss may correlate, since these were not quantitatively correlated with T_1 hypointense areas. The results represented in this work are in good agreement with that of van Walderveen et al. (van Walderveen 1998) who

showed that there was no correlation between T_1 hypointensity and reactive astrocytes. Interestingly, no change in the intensity of the hypointense region was found in this study, which is contrary to the findings in MS where variations in intensity have been shown; lesions became more hypointense over time, and gained signal intensity to become less hypointense as the lesion began to remyelinate (Bitsch 2001).

5.5.2 T_2 Hypointensities

Although T_2 hypointense regions have been reported in the MS literature, the T_2 hypointensities observed in this study are in different regions of the brain to those published. In the literature, the T_2 hypointensities are reported to occur in the grey matter at a distance from the lesions. It has been suggested that these occur as a consequence of abnormal iron deposition, resulting from tissue destruction, since these regions correlate with cerebral atrophy. Iron deposits have previously been found in MS and EAE (LeVine 1997), (Forge 1998).

In contrast to the literature, in this study, the hypointense regions were found at the centre of the lesion. However, it is possible that in this case, these changes also occur as a result of iron mediated tissue damage, owing to the high presence of macrophages in the core of the lesion. Iron contributes to oxidative damage by catalysing the formation of the hydroxyl radical and by causing lipid peroxidation. Macrophages and astrocytes are partly responsible for the production of free radicals, leading to demyelination. Owing to the large numbers of macrophages in the core of the lesion, and the fact that the number of macrophages correlates with the area of this hypointensity observed on T_2-weighted images, it is possible that there is a high concentration of iron deposit also at the core of the hypercellular lesion. The area of T_2 hypointensity appears to be maximal at day 19, which is at the same time as high levels of macrophage recruitment to the DTH lesion (as

observed in Section 4.6.4). In addition, iron deposits could come from plasma proteins, which entered the CNS through the permeable BBB. The BBB would have been transiently permeable following the initial intracerebral injection, allowing entry of these iron rich plasma proteins. The decrease in the area of the T_2 hypointensity at day 31, once the BBB has closed up supports this hypothesis. Investigation of iron by histochemical techniques, such as Prussian Blue staining would allow localisation of any non-haem iron deposits in the DTH lesion. The hypointense regions that were observed on the T_2-weighted images in this study, spatially mapped onto the hypointense areas on T_1-weighted images. Despite this, these areas did not quantitatively correlate, due to the nature of the bunched data. A strong correlation was found between the areas of T_2 hypointensity and T_2 hyperintensity, which is interesting because they mapped to distinct histological processes, although, perhaps not surprising since both these MRI characteristics reflect progression of the same DTH lesion.

5.5.3 T_2 Hyperintensities

T_2-weighted hyperintensities are commonly observed during the acute phase of MS lesions and were consistently observed in animals with a DTH lesion. EAE lesions have also been shown to appear hyperintense on T_2-weighted images (Namer 1994), (Karlik 1999), (Jordan 1999). Vasogenic oedema, demyelination, axonal loss as well as 'inflammation' all provide similar increases in signal intensity on T_2-weighted images, but in the case of MS lesions, the T_2 hyperintensities appear to most closely reflect the extent of demyelination in the spinal cord (Nijeholt 2001). However, in this study, the histological parameters that most closely correlate spatially with the areas of T_2 hyperintensity were reactive astrocytes and IgG staining (indicating BBB breakdown), thus, it seems likely that reactive astrocytes play a vital role in the induction and

maintenance of vasogenic oedema, which probably underlie the increase in T_2 hyperintensity. In this study, the area of T_2 hyperintensity in DTH animals was found to increase over time to become maximal at day 19. Once the DTH lesion had passed the peak of the inflammatory response at day 19, the area of hyperintensity subsequently decreased.

5.5.4 Conclusions

In conclusion, this chapter has investigated the appearance of the DTH lesion using MRI techniques that are routinely used in MS diagnosis and monitoring of lesion progression. The data suggest that the DTH lesion yields similar MRI pathology to that of MS lesions, and thus provides a useful model of an MS-like lesion. Hypointense regions found on both T_1- and T_2-weighted images correlate spatially with macrophages, T & B lymphocytes, neuronal loss, and MHC class II expression, suggesting that these factors may be the underlying cause of the MRI changes.

T_2 hyperintensities were found to correlate with reactive astrocytes, MHC class II expression and IgG staining (BBB breakdown) suggesting that astrocytes play a vital role in the induction and/or maintenance of BBB breakdown and subsequent oedema formation.

Chapter 6

Contrast Enhancement, Diffusion and Magnetisation Transfer Imaging

6.1 Introduction

Although T_1- and T_2-weighted imaging have been conventionally used clinically in MS, a fundamental problem with this approach, is that many different types of tissue pathology, including demyelination, oedema and inflammation present as similar signal changes observed on T_1- and T_2-weighted images. Consequently there is a need to improve the specificity of the imaging paradigms to obtain pathology specific information. This problem has led to the development of a number of 'specialised' imaging approaches, including the development of contrast agents, sequences weighted towards the diffusion of tissue water, and magnetisation transfer imaging.

6.1.1 Contrast Enhancement

Contrast agents, such as gadolinium, increase the contrast between tissues by shortening the T_1 relaxation rate of tissues that take up the agent. The use of gadolinium chelates, such as gadolinium-DTPA in combination with T_1-weighted imaging allows assessment of regional alterations in blood brain barrier (BBB) permeability. In the normal brain, the BBB is impermeable to gadolinium. If, however, there is a transient increase in permeability the gadolinium can pass through the BBB and enter the tissue, which alters the contrast in that region on T_1-weighted images. Contrast enhanced imaging has led to

the improved detection of new lesions in MS patients, such that up to twice as many lesions can be identified using contrast enhanced MRI rather than conventional T_2-weighted imaging (Miller 1993).

The use of gadolinium contrast enhancement has led to the now widely accepted view, that one of the earliest detectable events in the inflammatory process of the acute MS lesion is a regional increase in BBB permeability. Thus, contrast enhancement is generally taken to be a marker of acute MS lesions. This opening of the BBB is rapidly followed by alterations on T_2-weighted images, as discussed previously. However, it has also been shown that contrast enhancement can indicate the presence of reactivation of lesions that already exist. A significant correlation has been shown to exist between the number of enhancing lesions in MS and the occurrence of clinical relapse (Thompson 1992). Although BBB breakdown has also been shown to precede clinical symptoms in some MS patients (Kermode 1990).

Animal models of MS, such as EAE also exhibit gadolinium enhancement which has been found to correlate with the number of inflammatory cells within the lesion and has been suggested to represent macrophage activation (Seeldrayers 1993),(Namer 1994), (Morrissey 1996).

6.1.2 Diffusion-Weighted Imaging

Although conventional T_1- and T_2-weighted imaging together with gadolinium-enhanced MRI have been shown to be reasonably sensitive for the detection of MS lesions, these imaging techniques do not provide quantitative measures of the damage within and outside of macroscopic lesions. Further advancement of more specialised clinical MRI techniques has led to the development of diffusion-weighted and magnetisation transfer

(MT) imaging, as tools for diagnosis and monitoring of MS. Both of these modalities have the potential to provide quantitative information, and have been used to provide estimates of the severity of tissue damage in both T_2-visible lesions and in the normal-appearing surrounding brain tissue.

Diffusion-weighted imaging is based upon the microvascular water environment and is sensitive to the translational motion (diffusion) of water molecules over short distances in tissue. Subtle tissue damage destroys the tissue architecture, affecting the permeable or impermeable tissue barriers to diffusion of water. With fewer barriers in the tissue, diffusion of water molecules in the tissue would increase. Quantitation of water diffusion may be carried out by the application of magnetic field gradients of varying degrees of diffusion sensitisation, allowing the apparent diffusion coefficient (ADC) to be calculated.

Larsson et al. carried out the first diffusion-weighted imaging study in MS patients in 1992 (Larsson 1992). This study was the first to observe an increased ADC in MS lesions, which was taken to reflect increases in the extracellular space occurring as a result of demyelination. As the phagocytosed myelin is replaced by water, the usually restricted diffusion becomes less restricted. Since then, numerous studies of diffusion in MS lesions have been reported, (Larsson 1992), (Christiansen 1993), (Horsfield 1996), (Tievsky 1999), (Droogan 1999), (Werring 2000), (Cercignani 2000), (Wilson 2001), (Caramia 2002). These studies have consistently shown an increase in water diffusion in the MS lesion, however latter studies failed to find a correlation between an increased ADC and either clinical symptoms or disability. The first diffusion study in EAE was carried out a year after the first study of diffusion in MS, and that too showed increases in diffusion, both in lesions that were hyperintense on T_2-weighted images, and also prior to the appearance of hyperintensities (Heide 1993). Other studies of diffusion-weighted

imaging in EAE have suggested that directional changes in diffusion may differentiate between acute and chronic lesions (Richards 1995). In acute lesions, diffusion increases in all three orthogonal directions, most likely as a result of oedema associated with BBB breakdown. By contrast, in chronic lesions, diffusion only increases in the direction perpendicular to the main fibre tracts, and this is suggested to reflect demyelination. In addition, in one case, correlations have been found between increased diffusion and increased severity of clinical signs of EAE (Verhoye 1996). However, to date, no histopathological correlate has conclusively been found for increased diffusion.

In a homogenous medium, diffusion of water is isotropic, however in the brain the diffusional motion of water is influenced by the presence of cell membranes and myelin fibres. Anisotropy is a measure of deviation from isotropy and reflects both the degree of alignment of cellular structures within fibre tracts as well as their structural integrity. Diffusion parallel to the myelin fibres will be higher than in directions perpendicular to the fibres, which leads to anisotropy (van Gelderen 1994). If the tissue is disrupted by removal of barriers to water, this will result in a decrease in diffusion anisotropy and an increase in tissue water diffusion in that region. MS lesions have a reduced diffusion anisotropy compared to that of the surrounding tissue, and the anisotropy index has been shown to be lower in MS patients when compared to controls (Droogan 1999). Similarly decreased diffusion anisotropy has been reported in EAE affected animals (Heide 1993).

6.1.3 Magnetisation Transfer Imaging

Magnetisation transfer (MT) imaging is a relatively new method of MR imaging, first described as a technique in 1992, by Dousett et al. (Dousset 1992), and it provides many advantages over conventionally used T_1- and T_2-weighted imaging. Greater levels of morphological and pathological information about tissue damage, with higher specificity,

are provided. Consequently, this method is often used by clinicians to make a diagnosis between MS and other immune-mediated disorders affecting the human brain. Secondly, it has been found that the 'invisible' disease burden in brain tissue, which does not show macroscopic abnormalities on T_1- and T_2-weighted imaging, can be assessed with the more sensitive MT imaging. MT imaging can pick up subtle abnormalities in the white matter of MS patients, which are thought to be the greatest contributors to disease burden. To obtain magnetisation transfer weighted data, pairs of images are acquired with and without the application of saturation pulse, which saturates magnetisation within the pool of bound or restricted protons. Tissues with a large number of restricted protons will show a large decrease in signal intensity when the saturation pulse is applied, in contrast to tissues with few or no restricted protons, which have a small MT effect.

In MS patients, MTR imaging is not routinely used, however the MTR is consistently reported to be decreased in both the lesion and the surrounding normal appearing tissue, (Campi 1996), (Filippi 1999), (Rovaris 2000), (for review see Filippi 2000). The low MTR observed in MS patients reflects the reduced capacity of the molecules in the brain tissue matrix to exchange magnetisation transfer with the surrounding 'free' water molecules that are visible by MRI. This has historically been attributed to a reduction in the integrity of the macromolecular matrix in MS, as a consequence of myelin loss or damage to the axonal membrane. However, a more recent suggestion is that these changes may also reflect the dilution of macromolecules brought about by inflammatory oedema (for review see Filippi 2000). The reductions in the MTR of the surrounding tissue are relatively small when compared to the reductions within the lesion itself. This was thought to be due to varying degrees of myelin degradation in the lesion (Vavasour 1998), (Brochet 1999), but on some occasions this has been shown not to be the case (Gass 1994), (Campi 1996). Studies in EAE have shown that the MTR is reduced with

oedema, but the reduction is greater with axonal loss and demyelination (Dousset 1992). Furthermore, in EAE, mild reductions in MTR have been associated with reversible inflammatory events that accompany myelin degradation rather than demyelination *per se* (Brochet 1999), (Gareau 2000). This conflicting information between the MT studies of EAE and MS patients suggests that magnetisation transfer may not accurately reflect loss of myelin, as has been the long-standing view. Other animal models of MS, such as the Delayed Type Hypersensitivity (DTH) model (described in Chapter 4), may shed further light on this conflict. Using the DTH model, the contribution of demyelination, axonal loss and inflammatory cell recruitment to the increased water diffusion and reduction in MTR observed in MS patients can be investigated.

6.2 Aims of this Chapter

The initial aim of this chapter was to use contrast enhanced T_1-weighted imaging, diffusion-weighted and magnetisation transfer imaging to determine the characteristics of the DTH lesion with respect to these modalities, and to establish whether the DTH lesion exhibits the same properties as the MS lesion. A further aim was to correlate these changes with the underlying histopathology in the same animal in order to understand more fully, the mechanisms behind contrast enhancement, increased water diffusion, decreased anisotropy and a reduced MTR in a demyelinating CNS lesion.

6.3 Materials and Methods

6.3.1 Experimental Model

As described in Chapter 3, heat-killed BCG was injected stereotaxically into the striatum of three-week-old male Lewis rats, to initiate a DTH lesion. Four weeks after the

intracerebral injection, a peripheral challenge of TB in CFA was given into each of the hind limbs. Both the surgery and peripheral challenge was performed under halothane-induced anaesthesia. The temperature of the animals was monitored throughout surgery via a rectal probe and homeothermic heating system (Harvard apparatus, Ltd, UK). In addition, three control groups were investigated, as summarised in Table 4-1. MRI was performed on all animals at the following time-points after peripheral challenge: 0 (n=12), 5 (n=10), 8 (n=8), 12 (n=11), 19 (n=9) and 31 (n=10) days. Some animals were killed and processed for immunohistochemistry and histology after the MRI protocol, thus giving different sample sizes at each time-point.

6.3.2 Magnetic Resonance Imaging

Animals were anaesthetised with 2-3% halothane and a canula was inserted into the tail vein. The animals were then positioned in the probe described in Section 3.4.1. Anaesthesia was maintained in the magnet using 0.8-1.5% halothane in 70% N_2O/30% O_2. The temperature of the animals was maintained at 37°C using a circulating warm water system and heart rate was monitored throughout. Once the animals were in the magnet, a scout image was acquired, using the parameters summarised in Table 5-1 to determine the position of the animal.

From this scout, a horizontal T_2-weighted image using the parameters in Table 5-2, was positioned and acquired through the injection site 3.5mm below the surface of the brain. The injection site was visible as a small hypointense area. A single coronal slice centred on the injection site was selected for the full imaging protocol.

6.3.2.1 Diffusion-weighted Imaging

Diffusion-weighted images were then acquired using a pulsed-gradient spin-echo sequence using the parameters shown in Table 6-1. Diffusion weighting was achieved by using 3 diffusion weighting ("b") values defined by $b = (\gamma G\delta)^2[\Delta - \delta/3]$, where G is the diffusion gradient strength, Δ is the diffusion time, and δ is the diffusion gradient duration. Images were acquired with the diffusion gradients applied on each of the three orthogonal axes sequentially, and "trace" apparent diffusion coefficient maps were created.

Parameter	Values
Gradient b Values	125, 750, 1500 s mm^{-2}
Diffusion Gradient Duration (δ)	0.012 sec
Diffusion gradient Separation (Δ)	0.022 sec
Repetition time (TR)	2 sec
Echo time (TE)	0.041 sec
Field of view	3 x 3 cm^2
Slice Thickness	1 mm
Number of Averages	1
Total acquisition time	12 min 51 sec

Table 6-1: Summary of parameters used for the acquisition of diffusion-weighted images, which are used for the creation of apparent diffusion coefficient (ADC) maps.

6.3.2.2 Magnetisation Transfer Imaging

Magnetisation transfer ratio images were acquired with the parameters given in Table 6-2. MT saturation was achieved with a train of twelve 32ms Gaussian RF pulses, 1.5KHz off resonance. MT ratio (MTR) maps were created as described in Section 6.3.4 from the images acquired with, and without saturation.

Parameter	Values
MT Pulse Length	32 msec
No of MT Pulses	12
Repetition time (TR)	1.5 sec
Echo time (TE)	0.02 sec
Field of view	3 x 3 cm^2
Slice Thickness	1 mm
Number of Averages	1
Total acquisition time	6 min 28 sec

Table 6-2: Parameters used in the acquisition of images used for the creation of Magnetisation Transfer images, one image was acquired with the MT pulse on, and one acquired without this pulse.

6.3.2.3 Assessment of BBB Permeability

Following the acquisition of MT images, 100µl of a gadolinium-based contrast agent (Gadodiamide, Omniscan, Nycomed) was injected via a tail vein canula. A T_1-weighted image was acquired 10 minutes after this injection to look for image enhancement owing to increased BBB permeability.

6.3.3 Histology and Immunohistochemistry

At specific time-points during the DTH response, (0, 5, 8, 12, 19 and 31 days post peripheral challenge) some animals were killed and transcardially perfused with 0.9% NaCl solution as described in Section 3.4.2, to enable histology and immunohistochemistry to be carried out as described in Section 3.6.3.

6.3.4 MRI Data Analysis

Maps of the apparent diffusion coefficient (ADC) were generated on a pixel by-pixel basis from the diffusion-weighted images (Basser 1994). An anisotropy index was estimated from the measurements of diffusion using the standard deviation index given by van Gelderen et al. (van Gelderen 1994). ADC trace maps were subjected to an custom-

designed cluster analysis program (created by Dr Graeme Waddington (Waddington 1998) and described in Section 3.8.2) to segment regions of signal change. The area and intensity of these regions were then quantified. Regions of interest (ROI) were drawn around each hemisphere in the anisotropy maps, and the mean intensity of each ROI was quantified.

Post-gadolinium T_1-weighted images were also subjected to cluster analysis to segment regions of BBB breakdown. The area and intensity of these regions were then quantified using a custom-designed image display package, (created by Dr Andrew Blamire).

Magnetisation Transfer Ratio (MTR) maps were created on a pixel-by-pixel basis, by subtracting the pre-saturation scan from the reference scan and then dividing by the pre-saturation scan (i.e. by using the equation given by Dousset et al. (Dousset 1992), (Mo-Ms)/Mo x 100%, where Ms is the magnitude of signal when the saturation pulse is applied, and Mo is the magnitude of signal without the pulse).

6.3.5 Immunohistochemical Data Analysis

Drawings of histological sections were carried out as described in Section 4.3.3. These were subsequently scanned and stored as electronic images. The scanned drawings were then overlaid on to the MRI images, as described in Section 5.3.4.2 to determine spatial correlations between histological and MRI-detectable changes.

6.3.6 Cell Counts

Cell counts were carried out as previously described in Section 4.3.4.

6.3.7 Statistics

Differences between the areas of interest at the different time-points were tested by analysis of variance (ANOVA). Linear regression analysis was performed when an independent

Chapter 6. Contrast Enhancement, Diffusion & Magnetisation Transfer

ip. Where this was not the case, correlation analysis was performed. The significance of both linear regression and correlation analysis was tested using a student's t test. An unpaired student's t test with welch correction was used to determine differences between regions of interest between different time-points, and also between DTH and control groups. All data are presented as the mean ± S.D for n animals.

6.4 Results

6.4.1 BBB Breakdown.

BBB breakdown as identified by gadolinium enhancement, was clearly visible on post contrast T_1-weighted images in the coronal plane at days 12 and 19 post-peripheral challenge in DTH animals. In some animals gadolinium enhancement was observed as early as day 5, although typically, this enhancement was only just detectable. In addition, in some DTH animals gadolinium enhancement persisted until at least day 31 (Figure 6-1).

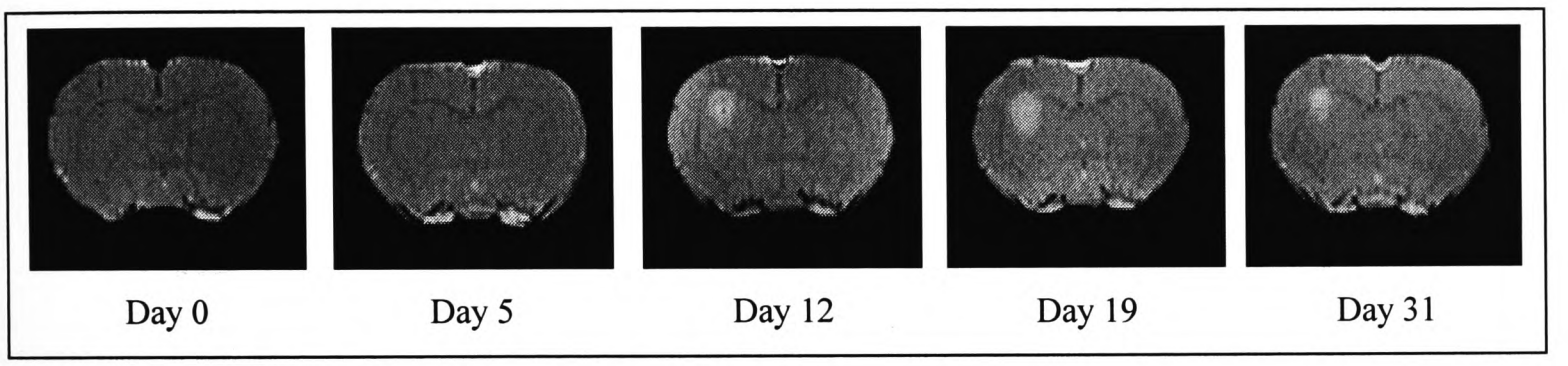


Figure 6-1: Post-contrast T_1-weighted images over time demonstrating BBB breakdown in and around the DTH lesion as detected by gadolinium enhancement from day 12 to day 31.

Areas of signal enhancement were quantified from the ROI's that were identified by cluster analysis. A significant (ANOVA $p<0.0001$) change in the extent of the BBB breakdown was found over time in the DTH animals. The intensity of BBB breakdown in DTH animals appeared to be greatest at day 12, although this did not reach significance, (this data is shown in Appendix E.1). No gadolinium enhancement was observed in PB IC controls, and only very small amounts was observed occasionally in NPC and SAL PC controls (Figure 6-2). Furthermore, when enhancement did occur in NPC and SAL PC animals, the area of BBB breakdown was considerably smaller than that observed in DTH animals, and did not change in extent over time. Moreover, at days 12 and 19 when the areas of enhancement increased dramatically in DTH animals, large differences were

found between DTH and control groups. At day 5, the DTH group showed significantly larger areas of enhancement when compared to NPC and SAL PC control groups (unpaired t test $p<0.05$ and $p<0.001$). However, at day 8 the difference between DTH and NPC animals did not quite reach significance ($p=0.056$), but the difference between DTH and SAL PC was significant ($p<0.05$). At day 12, unpaired t tests between DTH and NPC, and between DTH and SAL PC, yielded p values of <0.001 and <0.0001 respectively. Similarly, at day 19, the p value for an unpaired t test between DTH and NPC was $p<0.005$, (the difference between DTH and SAL PC was not significant (Table 6-4). Between group comparisons are shown in Table 6-3.

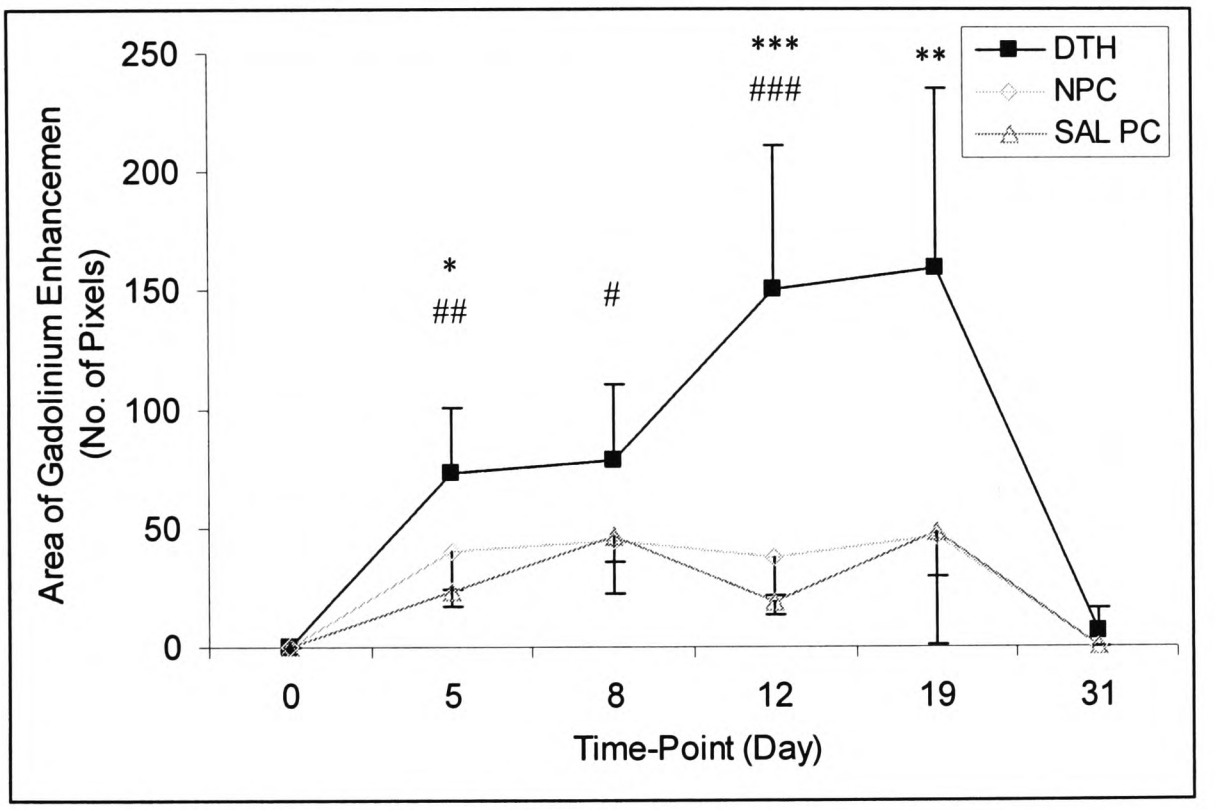


Figure 6-2: Graph to show area of gadolinium enhancement observed on post-contrast T_1-weighted images as identified by one dimensional cluster analysis. A significant (ANOVA $p<0.0001$) change over time in DTH animals was found. Values are expressed as the mean ± S.D. (NPC; no peripheral challenge, SAL PC; saline peripheral challenge). Significant differences were found between DTH and control groups at days 5, 8, 12 and 19 (unpaired t tests ###$p<0.0001$, ***$p<0.001$, ##$p<0.001$, **$p<0.005$, *$p<0.05$, #$p<0.05$, where * versus NPC and # versus SAL PC controls).

DTH Area of Gadolinium Enhancement						
Time-Point (Day)	**0**	**5**	**8**	**12**	**19**	**31**
0	-	$p<0.0001$	$p<0.0001$	$p<0.0001$	$p<0.0001$	/
5	-	-	/	$p<0.005$	$p<0.02$	$p<0.0001$
8	-	-	-	$p<0.01$	$p<0.02$	$p<0.0001$
12	-	-	-	-	/	$p<0.0001$
19	-	-	-	-	-	$p<0.001$
31	-	-	-	-	-	-

Table 6-3: Summary of unpaired t test results for comparison of the area of gadolinium enhancement within the DTH group at each time-point ('/' denotes difference is not significant).

DTH Area of Gadolinium Enhancement						
Time-Point (Day)	**0**	**5**	**8**	**12**	**19**	**31**
NPC	/	$p<0.05$	$p=0.0559$	$p<0.001$	$p<0.005$	/
SAL PC	/	$p<0.001$	$p<0.05$	$p<0.0001$	/	/

Table 6-4: Summary of unpaired t test results for comparison of the area of gadolinium enhancement between DTH and control groups ('/' denotes difference is not significant, values for comparisons that did not quite reach significance are also included, NPC; no peripheral challenge, SAL PC; saline peripheral challenge).

6.4.2 Correlation Between Areas of BBB Breakdown and T_2 Signal Change

A highly significant correlation ($p<0.01$) was found to exist between the area of gadolinium enhancement and the total area of signal change on T_2-weighted images (taken from chapter 5), in the same animals (Figure 6-3 and Table 6-5). This area encompassed both the hypointense and hyperintense regions on T_2-weighted images at all time-points investigated. At day 0, this largely reflects the hypointensity observed on T_2-weighted images, while at later time-points the spatial extent of T_2-weighted signal change is mainly determined by the hyperintense region, which surrounds the hypointense core. In order to determine which aspect of the T_2-weighted image signal change specifically correlates with signal enhancement, the relationships between T_2 hypointensity, T_2 hyperintensity and gadolinium enhancement were investigated. When the relationship between the area of gadolinium enhancement and the T_2 hyperintense area was investigated (Figure 6-4 and Table 6-5), a more significant relationship was found ($p<0.005$). However, a highly significant ($p<0.05$) correlation between the area of

T_2 hypointensity and gadolinium enhancement was found (Figure 6-5). Areas of gadolinium enhancement and T_2 hyperintensity were quantitatively correlated ($p<0.005$), as were the total areas of T_2 signal change and areas of gadolinium enhancement ($p<0.01$), as can be seen from Figure 6-3 and Table 6-5. The areas of contrast enhancement were consistently greater than the areas of T_2-weighted signal change.

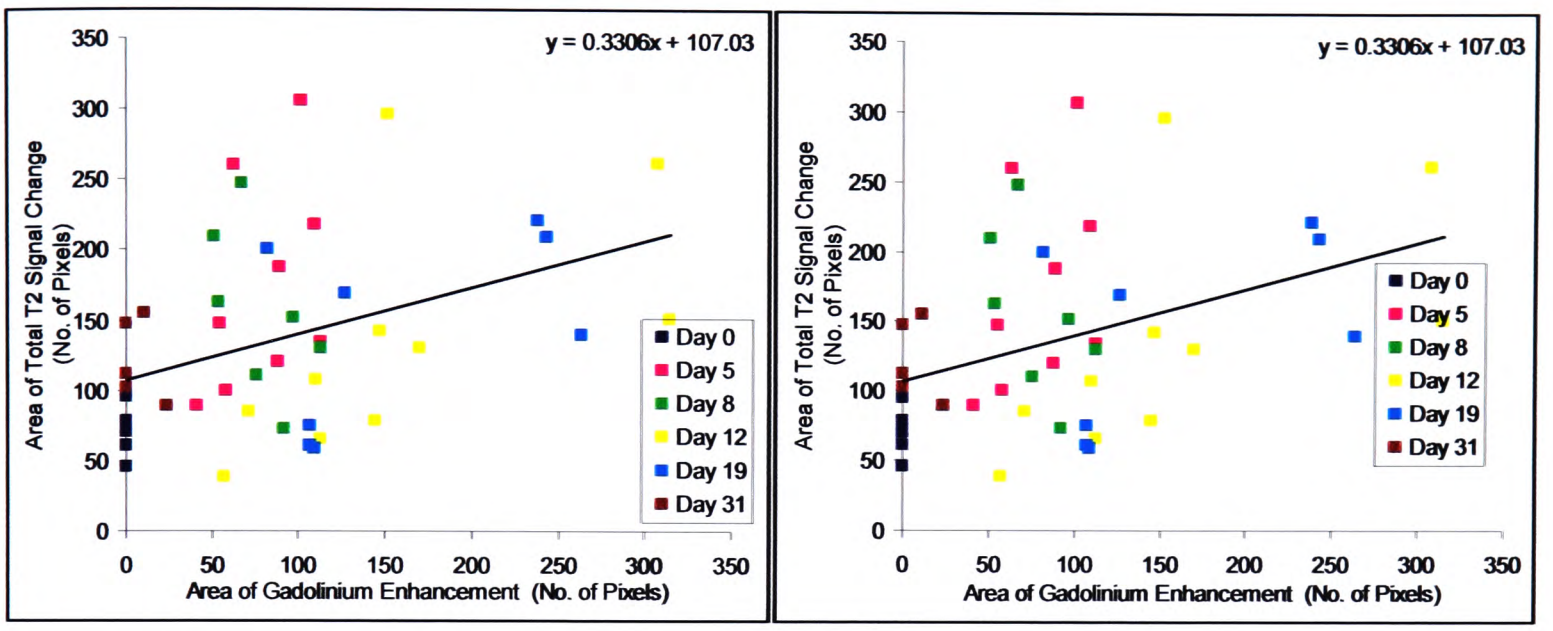


Figure 6-3: Graph to show relationship between areas of BBB breakdown as identified by gadolinium enhancement and total signal change on T_2-weighted images. A positive correlation was found ($p<0.01$).

Figure 6-4: Graph to show the relationship between the areas of BBB breakdown and T_2-hyperintensity. A positive correlation was found ($p<0.005$).

Correlation Between Gadolinium Enhancement and ...	Correlation Parameters			
	r	p	Slope	Y intercept
Total area of T_2 signal change	0.39	$p<0.01$	0.33	107.03
Area of T_2 hyperintensity	0.56	$p<0.005$	0.31	34.70

Table 6-5: Summary of results from correlation analysis between area of BBB breakdown and areas of signal change on T_2-weighted images.

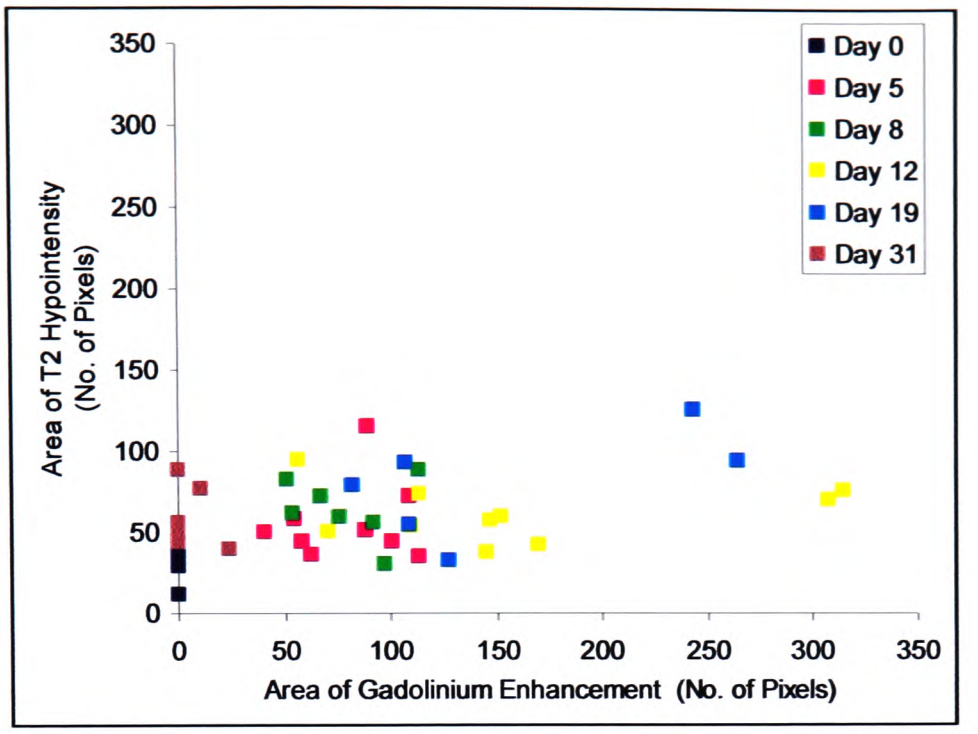


Figure 6-5: Graph to show the relationship between the areas of BBB breakdown and the T_2 hypointensity. A positive correlation was found ($p<0.05$). The Pearson product moment was 0.38.

6.4.3 Spatial Co-incidence of Inflammatory Markers and Gadolinium Enhancement

Areas of staining occupied by different inflammatory cells were drawn using the camera lucida. These areas were then stored as electronic images and overlaid onto the post-contrast T_1-weighted images obtained from the same animal at the same time-point. At day 19, a time-point when gadolinium enhancement was maximal in most animals (Figure 6-2), areas of staining occupied by reactive astrocytes (Figure 6-6a), appeared to match most closely with areas of BBB breakdown. Areas occupied by BCG antigens also appeared to be co-incident with the area of gadolinium enhancement (Figure 6-6b), as did the area of IgG staining (Figure 6-6c). Areas of macrophage staining (Figure 6-6e), MHC class II expressing cells (Figure 6-6d), and neuronal loss (Figure 6-6f) did not appear to spatially map to changes visible on post-contrast T_1-weighted images. Neither did areas of myelin loss, which were almost consistently restricted to the hypercellular area (data not shown). Similar results were seen with data obtained at day 12, also when BBB breakdown was overt.

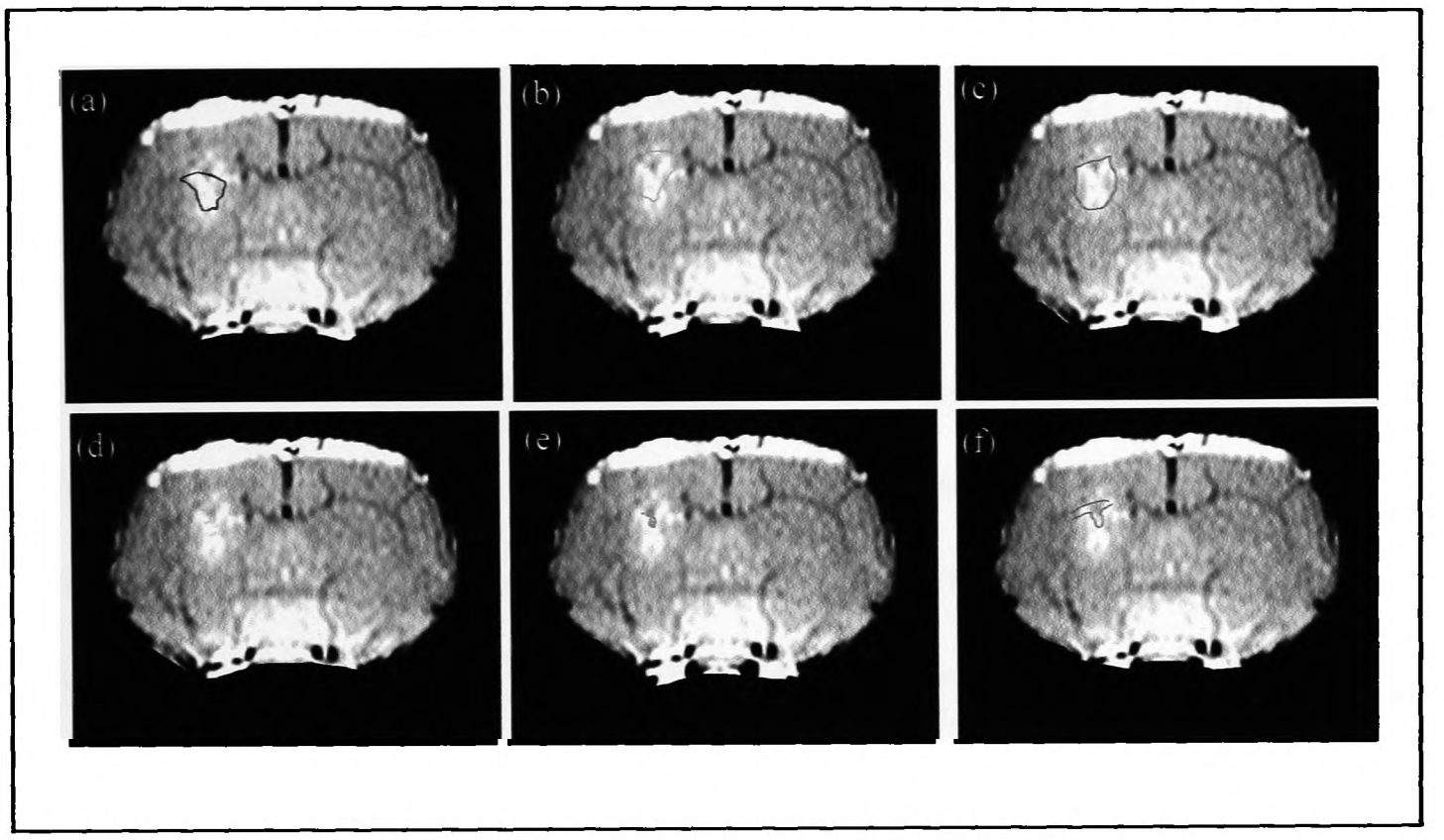


Figure 6-6: Spatial co-incidence of inflammatory markers and gadolinium enhancement on post-contrast T_1-weighted images.

(a) In blue, the area of staining occupied by reactive astrocytes coincides with the area of gadolinium enhancement.

(b) In orange, the area occupied by BCG antigens closely matches the area of gadolinium enhancement.

(c) In purple, the area of IgG staining is co-incident with the area of gadolinium enhancement.

(d) In yellow, the areas occupied by MHC class II expressing cells did not spatially coincide with the area of gadolinium enhancement.

(e) In green, the area of staining occupied by macrophages (and also T & B lymphocytes) is restricted to the hypercellular area, which does not fully overlap area of gadolinium enhancement.

(f) In red, the area of neuronal loss also only occurs within the area of hypercellularity, which does not appear to map to the region of gadolinium enhancement.

6.4.4 Histological Correlations

The relationships between the area of gadolinium enhancement (indicating the extent of BBB breakdown), and histological markers of inflammation were investigated (Figure 6-7). Many spatial relationships were inferred from Section 6.4.3, therefore linear regression analysis was performed for the correlations. Although not quite statistically significant ($p=0.078$), the areas of reactive astrocytes did appear to correlate with the area of BBB breakdown, as indicated by their spatial coincidence (Figure 6-7a and Table 6-6). No significant correlation was found between area of BBB breakdown and the number of macrophages, or with the area of MHC class II expression (Figures 6-7b,c and Table 6-6). However, a significant ($p<0.02$) correlation was found between the areas of BBB breakdown and the number of T & B lymphocytes (Figure 6-7d and Table 6-6).

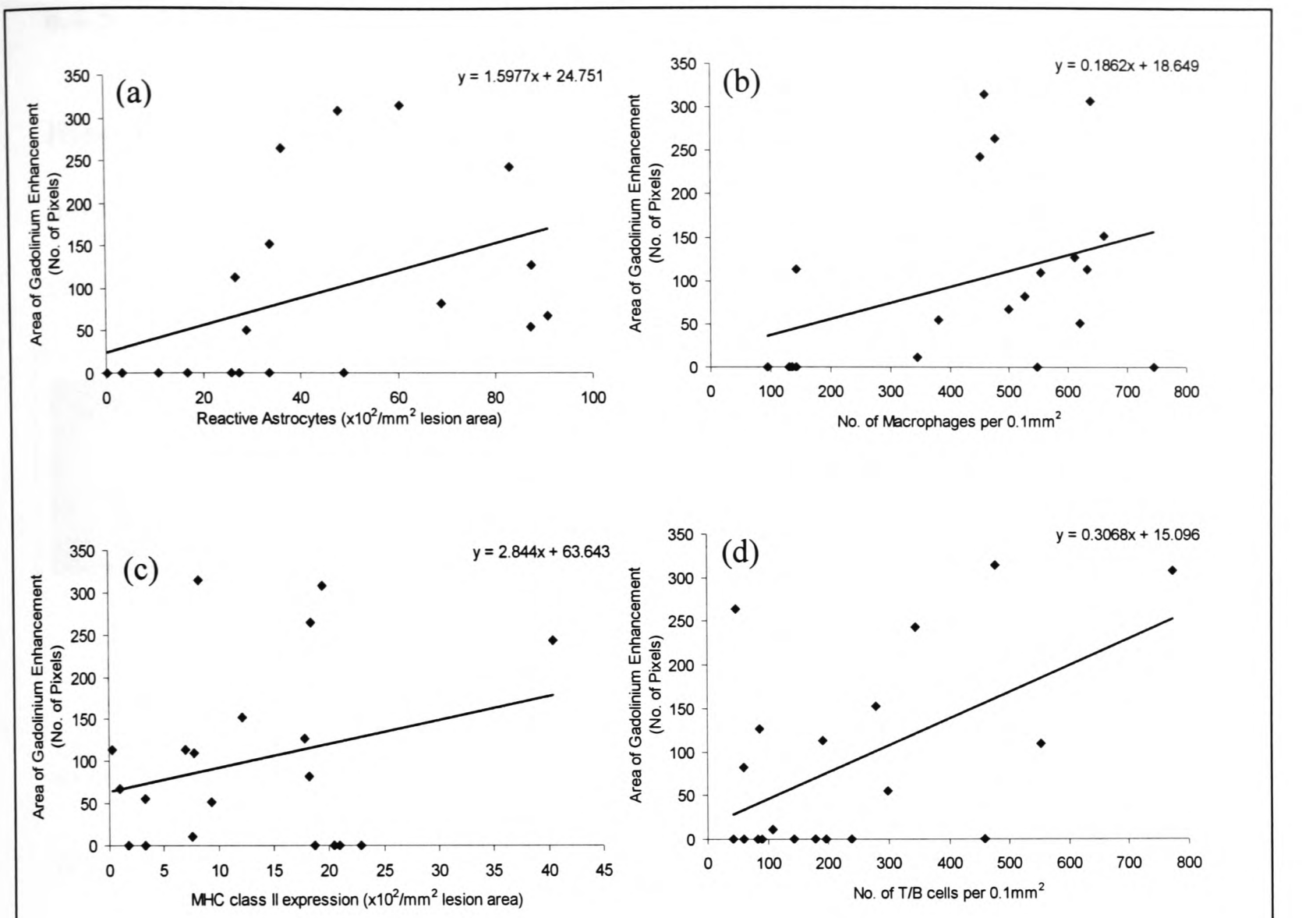


Figure 6-7: Graphs to demonstrate relationship between area of BBB breakdown and inflammatory markers.

(a) Although not statistically significant ($p=0.078$) a trend towards a correlation was found between the areas of BBB breakdown and reactive astrocytes per mm^2 lesion area.

(b) No correlation was found between the area of gadolinium enhancement, and number of macrophages per $0.1mm^2$ lesion area.

(c) No correlation found between the areas of BBB breakdown and MHC class II expression per mm^2 lesion area.

(d) A significant ($p<0.02$) correlation was found between the area of BBB breakdown and number of T & B lymphocytes per $0.1mm^2$ lesion area.

Correlation Between Gadolinium Enhancement and ...	Correlation Parameters			
	r	p	Slope	Y intercept
Reactive Astrocytes	0.42	p=0.078	1.60	24.75
Macrophages	0.36	0.12	0.19	18.65
MHC Class II Expression	0.26	0.26	2.84	63.64
T & B Lymphocytes	0.55	p<0.02	0.31	15.09

Table 6-6: Summary of results of the correlation analysis between the area of gadolinium enhancement and inflammatory markers.

6.4.5 ADC Hypointensity

Hypointense regions (decreased ADC) were observed at the site of the original intracerebral BCG injection on ADC trace maps in all DTH animals throughout the time-course (Figure 6-8).

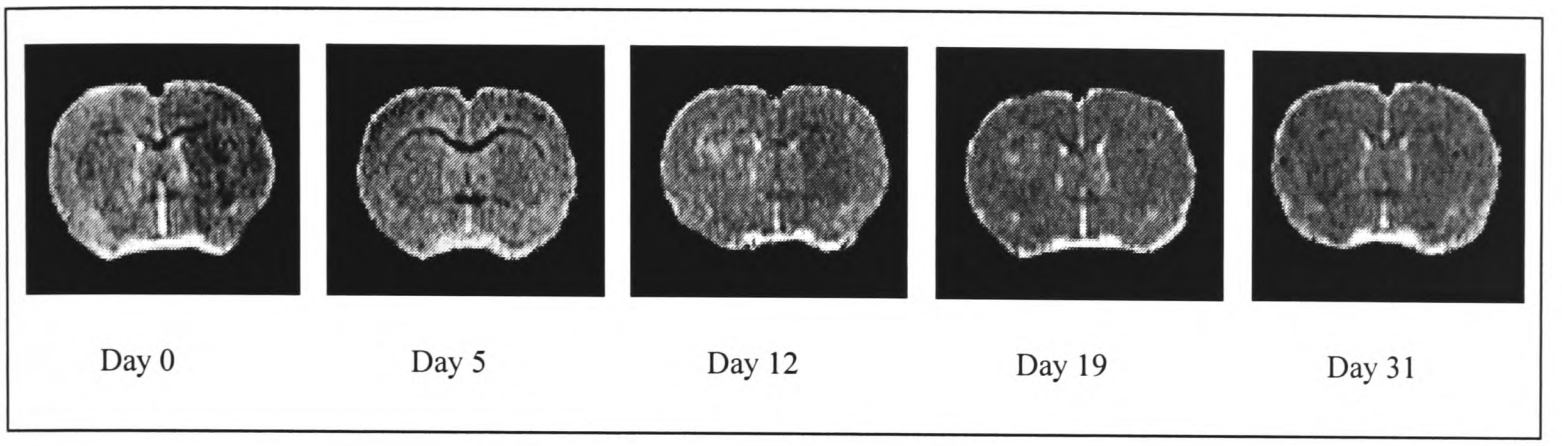


Figure 6-8: ADC trace maps throughout lesion progression showing areas of hypointensity at the centre of a region of hyperintensity.

Both NPC and SAL PC controls also showed this hypointense region throughout the time-course, however there were no significant changes in intensity of this region with time. Individual results are given in Appendix E.4. PB IC controls showed no changes on ADC trace maps. Regions of interest were drawn around the hypointense regions and it was found that at day 0, the extent of the hypointense area was not significantly different from the control groups. In DTH animals, the hypointense area increased in size over time (ANOVA $p<0.05$) and appeared to reach a maximum around day 19 (Figure 6.9). In contrast the hypointense area in control animals remained largely constant over time, and were of similar extent in both groups. At day 12, the area of ADC hypointensity in DTH animals was significantly ($p<0.05$) greater than SAL PC controls. At day 19, the difference between DTH and NPC was significant ($p<0.05$), but no difference was found between the DTH and SAL PC animals (Table 6-7), probably due to the temporal variation amongst the DTH animals at those time-points, and the small sample size in the control groups. A significant difference was also found at day 31 between DTH and SAL PC controls ($p<0.005$).

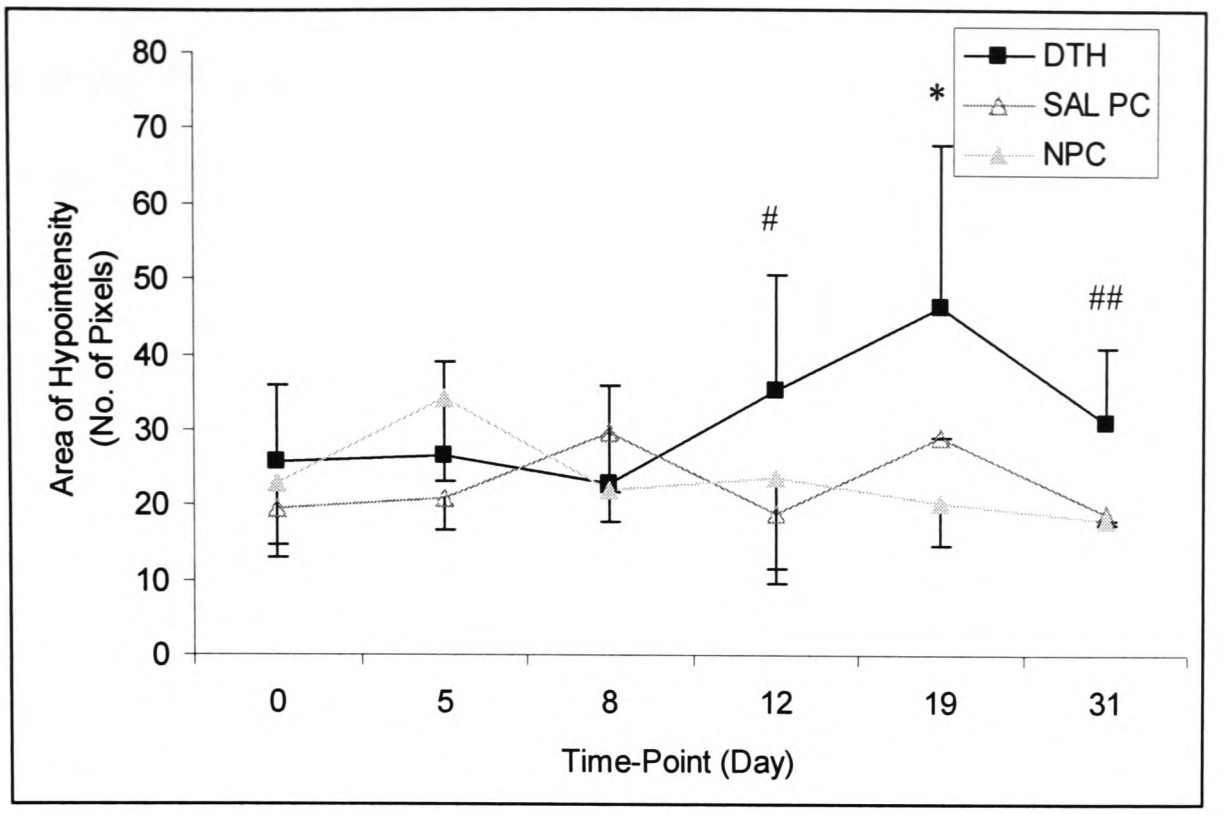


Figure 6-9: Graph to show area of hypointense region identified on ADC trace maps. Values are expressed as the mean ± S.D. (NPC; no peripheral challenge, SAL PC; saline peripheral challenge). A significant change in DTH animals was found over time (ANOVA $p<0.05$). A significant difference was found at days 12, 19, and 31 between DTH and controls (unpaired t test ##$p<0.005$, #$p<0.05$, *$p<0.05$, where * versus NPC and # versus SAL PC controls).

DTH Area of ADC Hypointensity						
Time-Point (Day)	**0**	**5**	**8**	**12**	**19**	**31**
NPC	/	/	/	/	$p<0.05$	/
SAL PC	/	/	/	$p<0.05$	/	$p<0.005$

Table 6-7: Summary of unpaired t test results for comparison of area of ADC hypointensity between DTH and control groups at each time-point ("/" denotes difference is not significant, NPC; no peripheral challenge, SAL PC; saline peripheral challenge).

6.4.6 ADC Hyperintensity

A region of hyperintensity, which appeared to surround the core of hypointensity (Figure 6-8), was visible on ADC trace maps in DTH animals. Both SAL PC and NPC controls exhibited similar regions of raised ADC, although the spatial extent of these regions was considerably less than those observed in DTH animals (Figure 6-10). Furthermore, areas of elevated ADC in both groups remained largely constant over time. In contrast, the areas of ADC hyperintensity altered significantly over time in DTH animals (ANOVA $p<0.02$). More specifically, the area of ADC hyperintensity increased as the inflammatory response progressed in the DTH animals (Figure 6-10), and appeared to be

maximal at day 19 (unpaired t test when compared to day 0, $p<0.02$) (Table 6-8). After this time-point, the area of elevated ADC decreased in size. DTH animals had a significantly larger area of ADC hyperintensity than NPC controls at day 5 ($p<0.05$), day 8 ($p<0.05$), day 12 ($p<0.02$), day 19 ($p<0.05$) and day 31 ($p<0.05$). Similarly, the area of ADC hyperintensity in DTH animals was significantly larger than SAL PC controls at day 5 ($p<0.005$), day 8 ($p<0.05$), day 12 ($p<0.005$), day 19 ($p<0.01$), and day 31 ($p<0.05$). PB IC controls showed no visible ADC hyperintensity at any time-point.

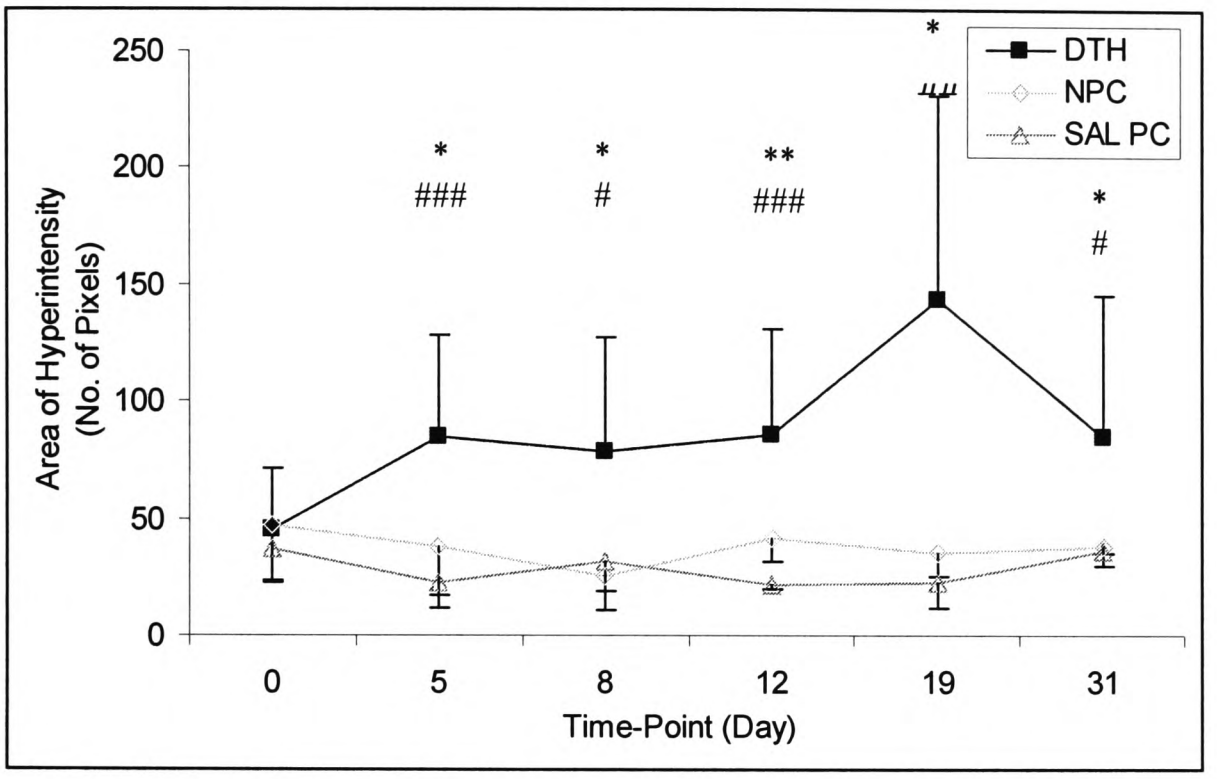


Figure 6-10: Graph to show the area of hyperintensity observed on ADC trace maps. Values are expressed as the mean ± S.D. (NPC; no peripheral challenge, SAL PC; saline peripheral challenge). A significant change over time was found in DTH animals (ANOVA $p<0.02$). Significant differences were found between DTH and controls at days 5, 8, 12 and 19 (unpaired t test ###$p<0.005$, **$p<0.02$, ##$p<0.01$, *$p<0.05$, #$p<0.05$, where * versus NPC and # versus SAL PC controls).

DTH Area of ADC Hyperintensity						
Time-Point (Day)	**0**	**5**	**8**	**12**	**19**	**31**
0	-	$p<0.05$	/	$p<0.05$	$p<0.02$	$p=0.0755$
5	-	-	/	/	/	/
8	-	-	-	/	$p=0.0917$	/
12	-	-	-	-	/	/
19	-	-	-	-	-	/
31	-	-	-	-	-	-

Table 6-8: Summary of unpaired t test results for comparison of the area of ADC hyperintensity within the DTH group at each time-point. ('/' denotes difference is not significant, values for comparisons that did not quite reach significance are also included).

DTH Area of ADC Hyperintensity						
Time-Point (Day)	**0**	**5**	**8**	**12**	**19**	**31**
NPC	/	$p<0.05$	$p<0.05$	$p<0.02$	$p<0.05$	$p<0.05$
SAL PC	/	$p<0.005$	$p<0.05$	$p<0.005$	$p<0.01$	$p<0.05$

Table 6-9: Summary of unpaired t test results for comparison of area of ADC hyperintensity between DTH and control groups at each time-point ('/' denotes difference is not significant, NPC; no peripheral challenge, SAL PC; saline peripheral challenge).

6.4.7 Total Change on ADC Trace Maps.

The area of total ADC change in DTH animals was shown to significantly (ANOVA $p<0.005$) vary with time, and no change was observed in control animals (Figure 6-11). Post-hoc unpaired t tests revealed that the area of total ADC change at day 0 was significantly lower than subsequent time-points (Table 6-10). The area of total ADC change was far greater in DTH animals than that observed in either control group throughout the time-course, and was significantly greater than both NPC and SAL PC controls at all time-points, with the exception of NPC controls at day 0 (Table 6-11).

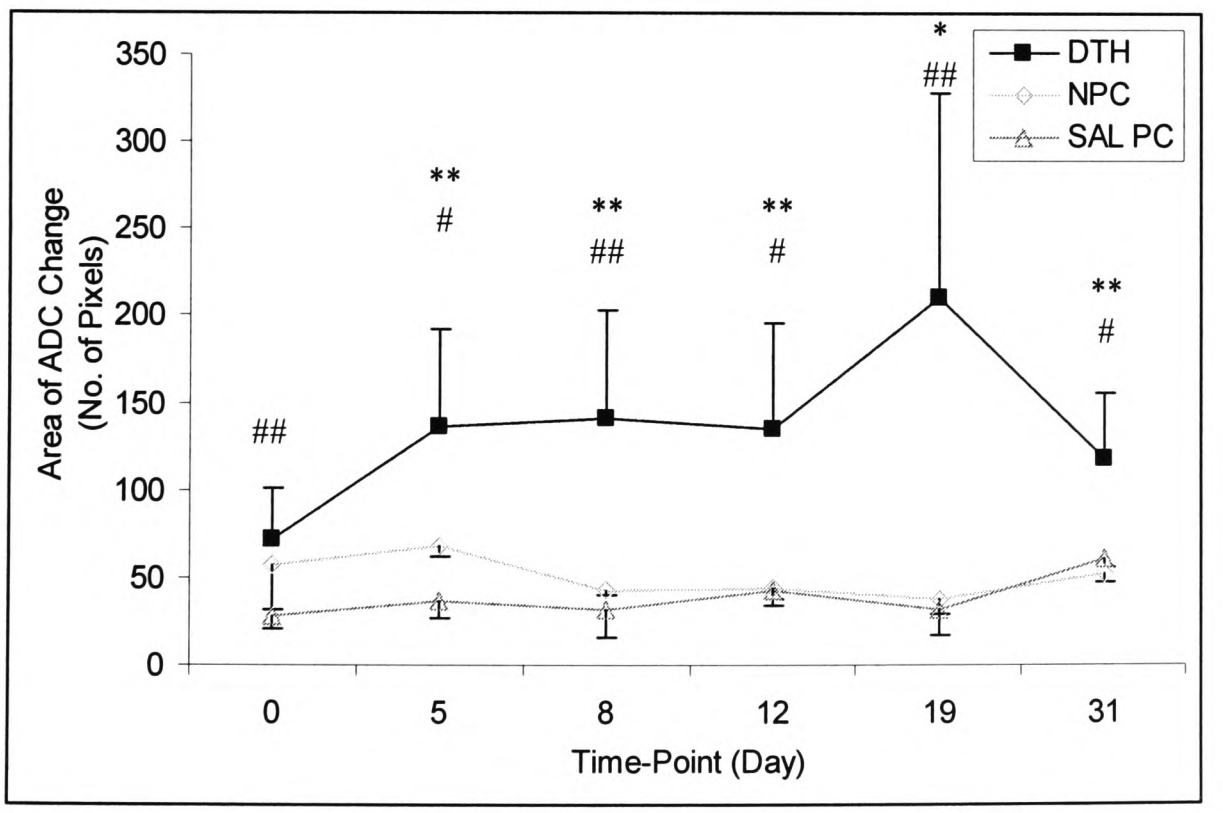


Figure 6-11: Graph to show the area of total area of ADC change during the progression of the DTH lesion. Values are expressed as the mean ± S.D. (NPC; no peripheral challenge, SAL PC; saline peripheral challenge). A significant change in DTH animals was found over time (ANOVA $p<0.005$), significant differences were found between DTH and control groups at days 5,8,12,19 and 31 (unpaired t test ##$p<0.005$, #$p<0.001$, **$p<0.005$, *$p<0.01$, where * versus NPC and # versus SAL PC controls).

DTH Area of Total ADC Change						
Time-Point (Day)	**0**	**5**	**8**	**12**	**19**	**31**
0	-	p<0.01	p<0.02	p<0.02	p<0.02	p<0.01
5	-	-	/	/	/	/
8	-		-	/	/	/
12	-	-	-	-	/	/
19	-	-	-	-	-	p=0.0654
31	-	-	-	-	-	-

Table 6-10: Summary of unpaired t tests for comparison of the total area of ADC change within the DTH group at each time-point. ('/' denotes difference is not significant, values for comparisons that did not quite reach significance are also included NPC; no peripheral challenge, SAL PC; saline peripheral challenge).

DTH Area of Total Area of ADC Change						
Time-Point (Day)	**0**	**5**	**8**	**12**	**19**	**31**
NPC	/	p<0.005	p<0.005	p<0.005	p<0.01	p<0.005
SAL PC	p<0.005	p<0.001	p<0.005	p<0.001	p<0.005	p<0.001

Table 6-11: Summary of unpaired t tests for comparison of area of total ADC change between DTH and control groups at each time-point. ('/' denotes difference is not significant, NPC; no peripheral challenge, SAL PC; saline peripheral challenge).

6.4.8 Correlation Between ADC Hypointensity and ADC Hyperintensity

Areas of decreased ADC and areas of increased ADC were identified in the same animal at all time-points. An extremely significant correlation ($p<0.005$) was found between areas of decreased ADC and areas of increased ADC (Figure 6-12 and Table 6-12).

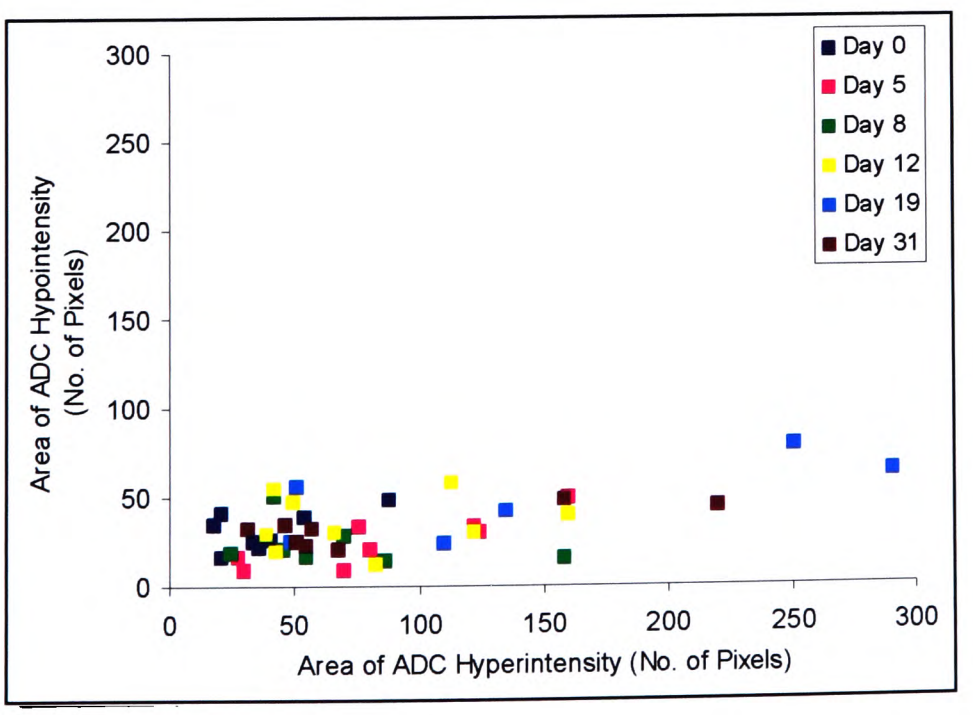


Figure 6-12: Graph to show the relationship between area of hypointensity and area of hyperintensity observed on ADC trace maps. An extremely significant ($p<0.005$) correlation was found.

Correlation Between Area of...	Correlation Parameters	
	r	p
ADC Hypointensity and ADC Hyperintensity	0.53	$p<0.005$

Table 6-12: Summary of the results of correlation analysis between areas of ADC hypointensity and areas of ADC hyperintensity. An extremely significant correlation was found ($p<0.005$).

6.4.9 Spatial Co-incidence of Inflammatory Markers and ADC changes

Areas of immunohistochemical change did not appear to map to the ADC changes in the same way as they did to changes on post-contrast T_1-weighted images (Figure 6-13). The broad region of increased ADC was greater in extent than areas occupied by reactive astrocytes (Figure 6-13a), BCG antigens (Figure 6-13b), and IgG permeability (Figure 6-13c). However, the areas of decreased ADC appeared to spatially correspond to areas of MHC class II expression (Figure 6-13d), macrophage cell recruitment (Figure 6-13e) and areas of neuronal loss (Figure 6-13f).

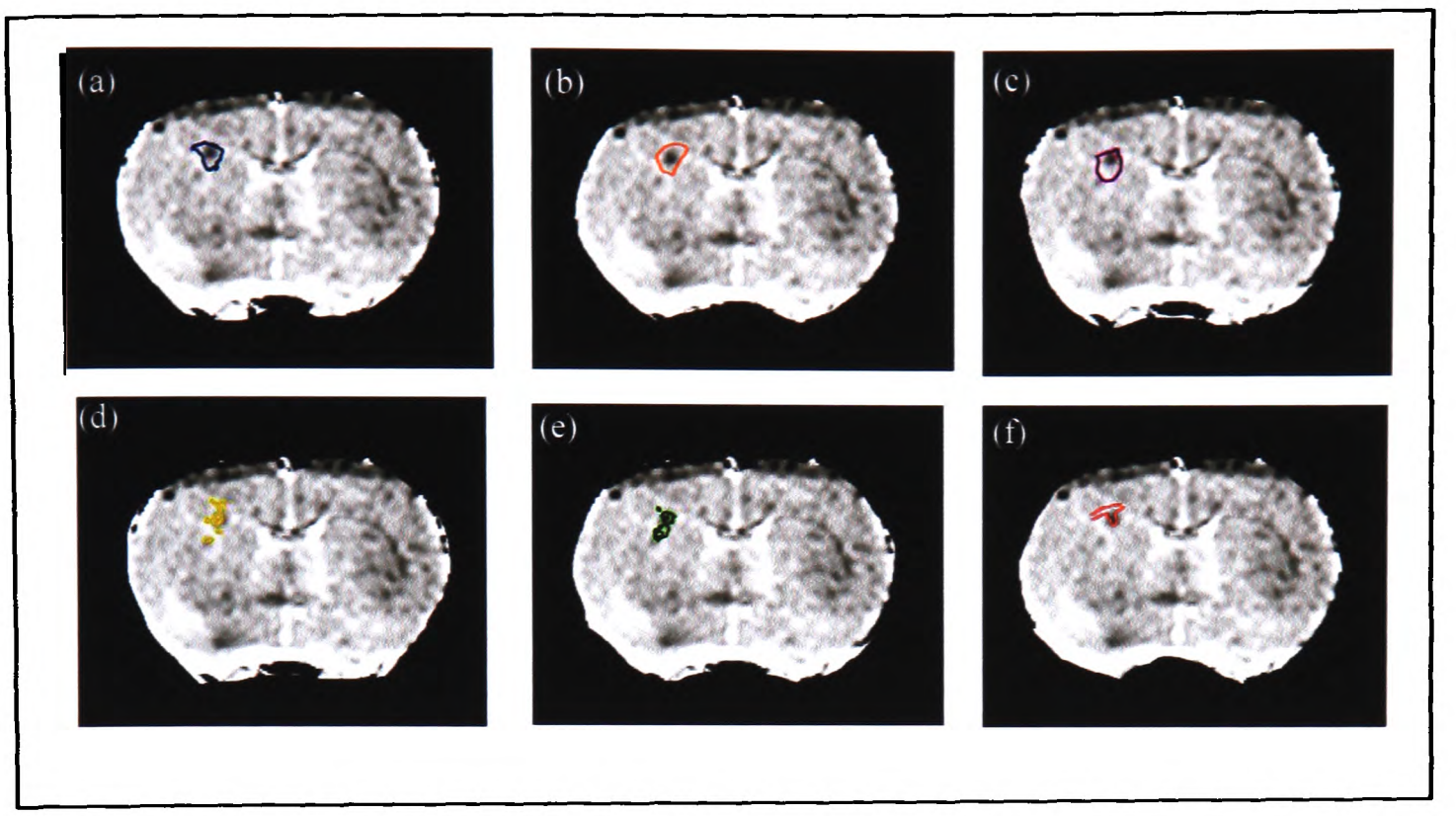


Figure 6-13: Spatial co-incidence of inflammatory markers and ADC changes.

(a) In blue, the area of staining occupied by reactive astrocytes is slightly greater than the area of decreased ADC on ADC trace maps and extends slightly into the hyperintense region.

(b) In orange, the area occupied by BCG antigens closely encompasses the area of decreased ADC enhancement on ADC trace maps and extends slightly into the hyperintense region.

c) In purple, the area of IgG staining is greater than the area of decreased ADC but also part of the area of increased ADC on ADC trace maps and extends slightly into the hypercellular region.

(d) In yellow, areas occupied by MHC class II expressing cells also spatially coincide with the area of hypointensity on ADC trace maps.

(e) In green, the area of staining occupied by macrophages is restricted to the hypercellular area, which spatially coincides with the area of decreased ADC on ADC trace maps.

(f) In red, the area of neuronal loss is also only found in the area of hypercellularity, and again appears to map to the region of decreased ADC on ADC trace maps.

6.4.10 Quantitative Correlations with Histology

The areas of change identified on the ADC trace maps were quantitatively correlated with immunohistochemical data obtained in Chapter 4 at all time-points investigated. Numbers of macrophages showed no correlation with the area of ADC hypointensity (Figure 6-14a and Table 6-13). However, significant correlations were found with the areas of ADC hyperintensity ($p<0.05$), and total ADC change ($p<0.05$) (Figure 6-14b,c and Table 6-13).

Numbers of T & B lymphocytes did not appear to correlate with the areas of ADC hypointensity, or total ADC change (Figure 6-15a,c and Table 6-14). However, a significant ($p<0.05$) correlation was found with ADC hyperintensity (Figure 6-15b and Table 6-14).

No correlation was found between areas of reactive astrocytes and the area of ADC hypointensity (Figure 6-16a and Table 6-15). However a trend towards a significant correlation was found with the area of ADC hyperintensity ($p=0.093$) (Figure 6-16b). A significant correlation ($p<0.02$) was also found with the total area of ADC change (Figure 6-16c and Table 6-15).

MHC class II expression showed an extremely significant correlation with the area of ADC hypointensity ($p<0.001$), as indicated by their spatial coincidence in Section 6.4.9 (Figure 6-17a and Table 6-16), the area of ADC hyperintensity ($p<0.0001$) (Figure 6-17b). A less significant correlation was found the area of total ADC change ($p<0.05$) (Figure 6-17c and Table 6-16).

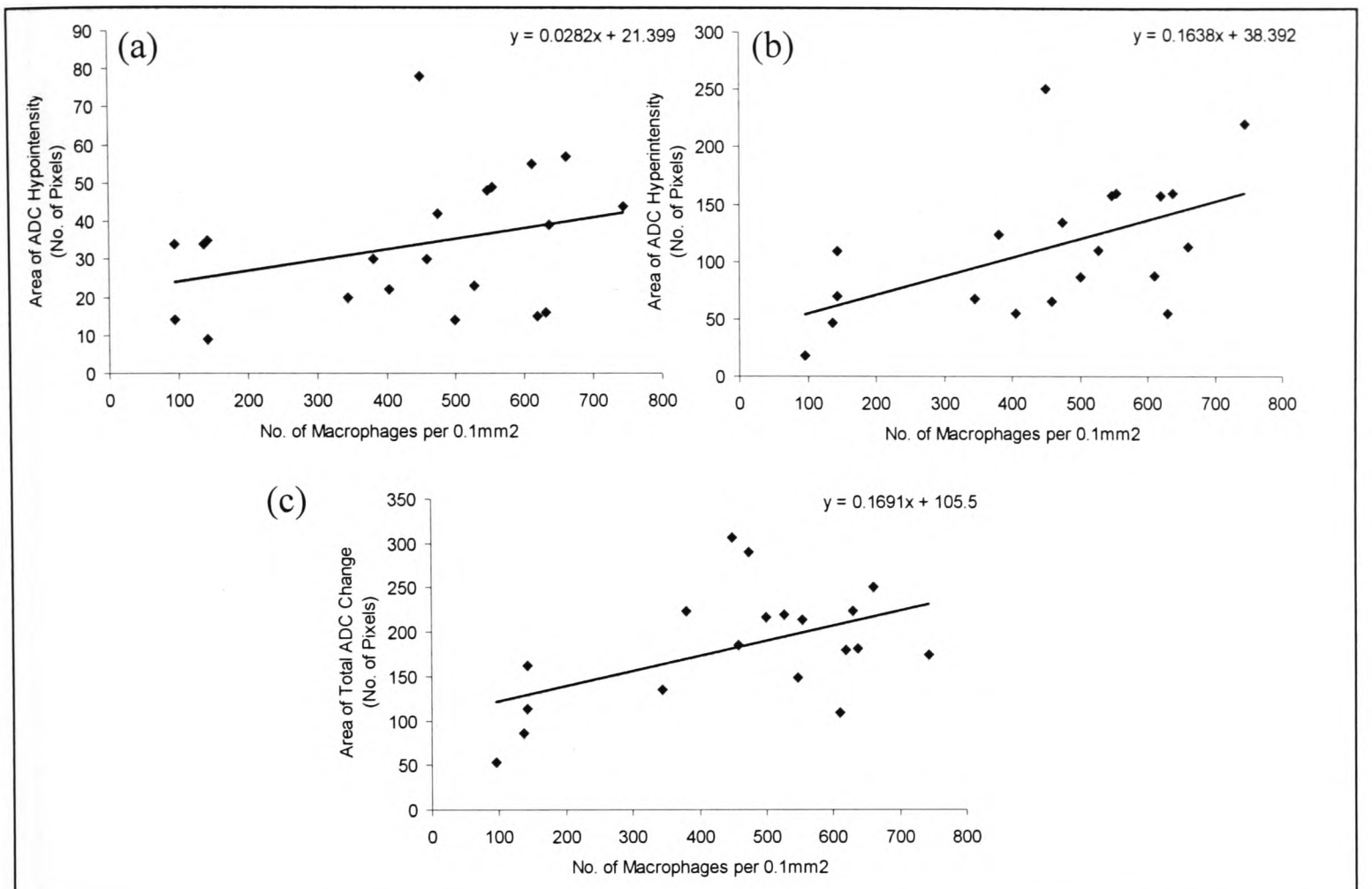


Figure 6-14: Graphs to show the relationship between the macrophages and areas of ADC change.

(a) No correlation was found between macrophages and the area of ADC hypointensity.

(b) A positive correlation ($p<0.05$) was found between macrophages and the area of ADC hyperintensity.

(c) A positive correlation ($p<0.05$) was found between macrophages and the area of total ADC change.

Correlation Between Macrophages and area of...	Correlation Parameters			
	r	p	Slope	Y intercept
ADC Hypointensity	0.33	0.14	0.03	21.40
ADC Hyperintensity	0.53	$p<0.05$	0.16	38.39
Total ADC change	0.51	$p<0.05$	0.17	105.50

Table 6-13: Summary of correlation analysis between numbers of macrophages and areas of ADC change.

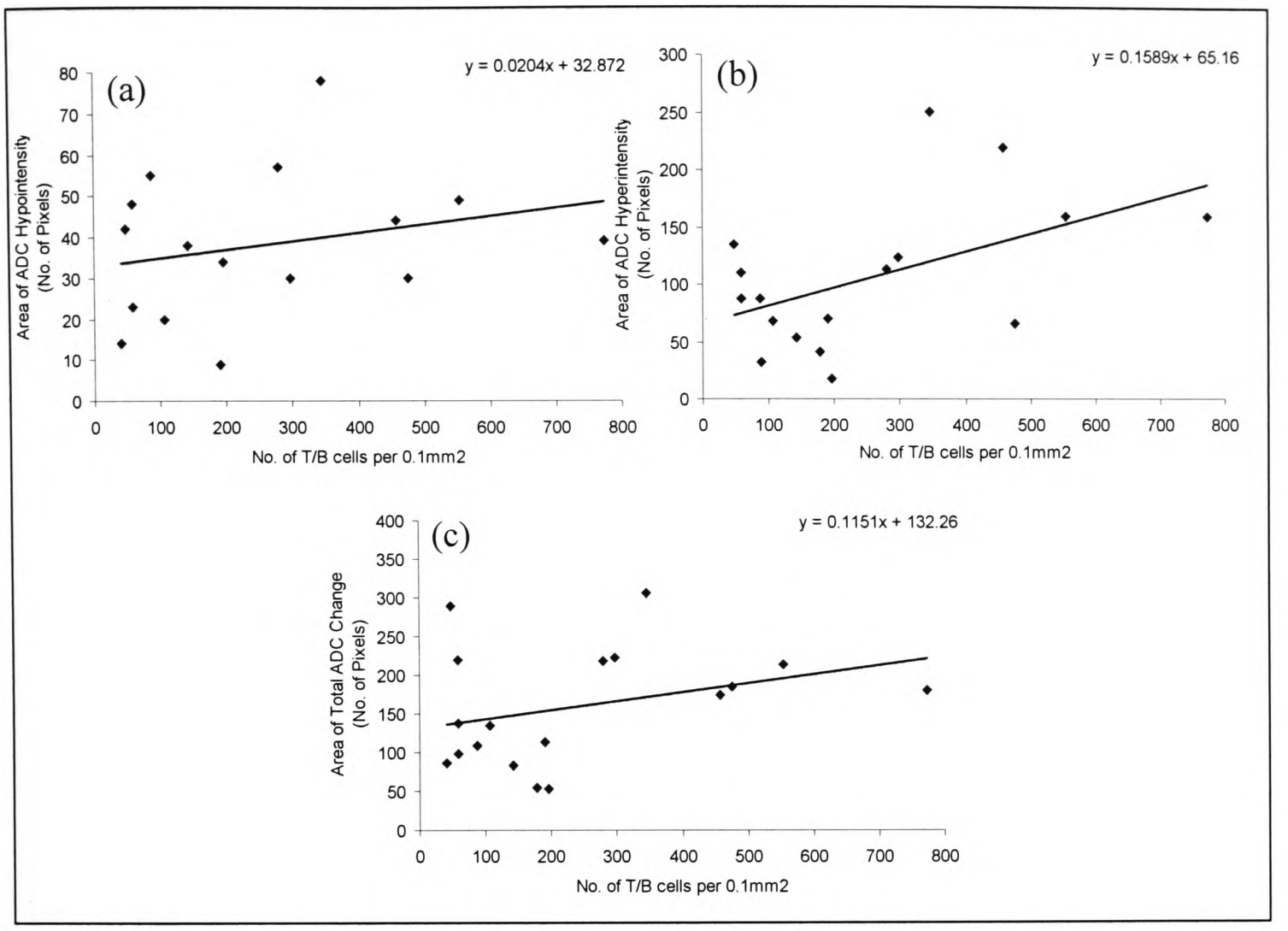


Figure 6-15: Graphs to show the relationship between T & B lymphocytes and ADC change.

(a) No correlation was found between T & B lymphocytes and the area of ADC hypointensity.

(b) A positive ($p<0.05$) correlation was found between T & B lymphocytes and the area of ADC hyperintensity.

(c) No correlation was found between T & B lymphocytes and the area of total ADC change.

Correlation Between T & B Lymphocytes and area of...	Correlation Parameters			
	r	p	Slope	Y intercept
ADC Hypointensity	0.25	0.35	0.02	32.87
ADC Hyperintensity	0.51	$p<0.05$	0.16	65.16
Total ADC change	0.32	0.20	0.12	132.26

Table 6-14: Summary of correlation analysis between numbers of T & B lymphocytes and areas of ADC change.

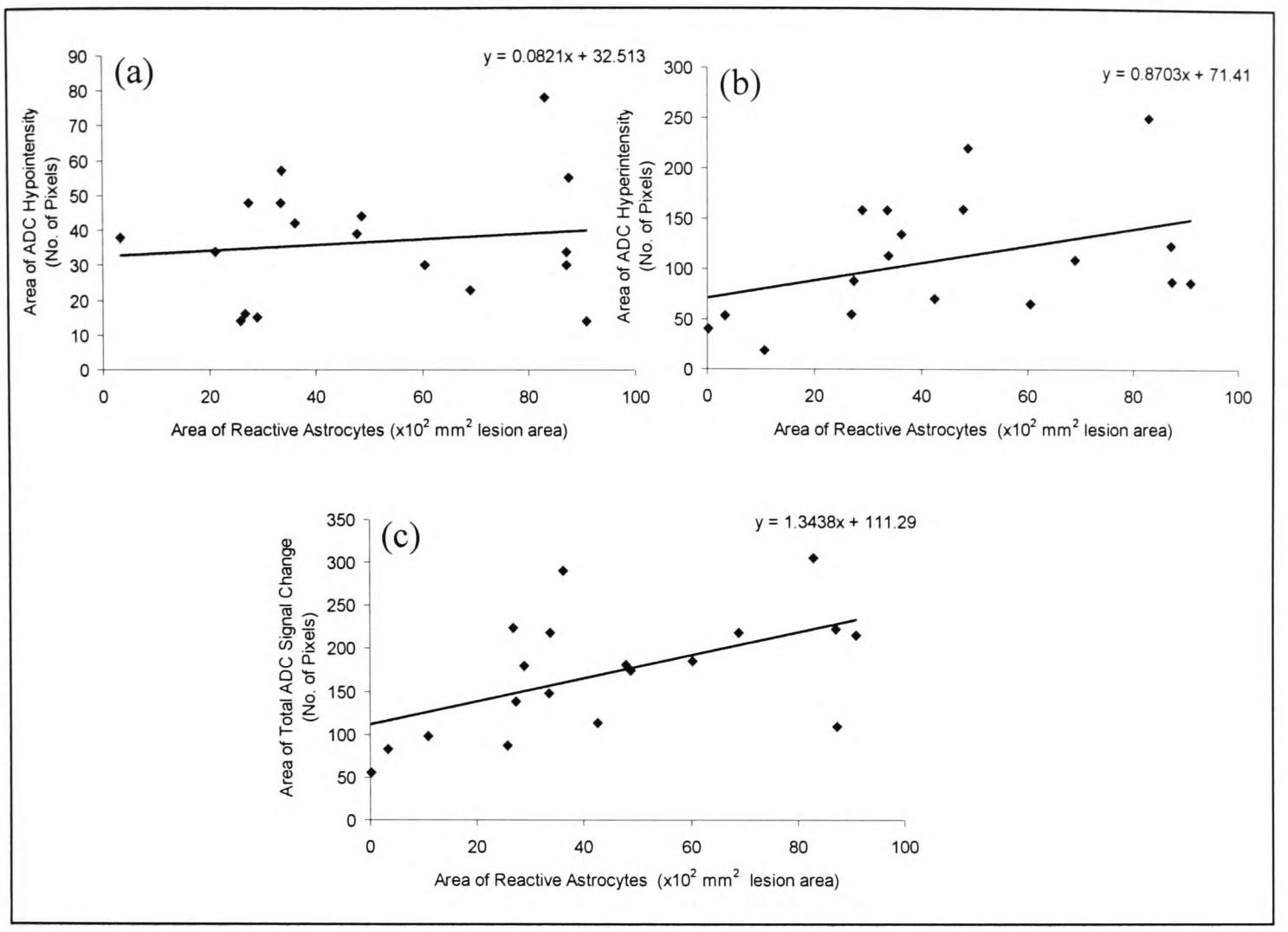


Figure 6-16: Graphs to show the relationship between reactive astrocytes and ADC change

(a) No correlation was found between reactive astrocytes and the area of ADC hypointensity.

(b) Although not statistically significant ($p=0.093$), a trend towards a correlation was found between reactive astrocytes and the area of ADC hyperintensity.

(c) A significant ($p<0.02$) correlation was found between reactive astrocytes and the area of total ADC change.

Correlation Between Reactive Astrocytes and area of...	Correlation Parameters			
	r	p	Slope	Y intercept
ADC Hypointensity	0.13	0.60	0.08	32.51
ADC Hyperintensity	0.41	p=0.093	0.87	71.41
Total ADC change	0.55	p<0.02	1.34	111.29

Table 6-15: Summary of correlation analysis between areas of reactive astrocytes and area of ADC change.

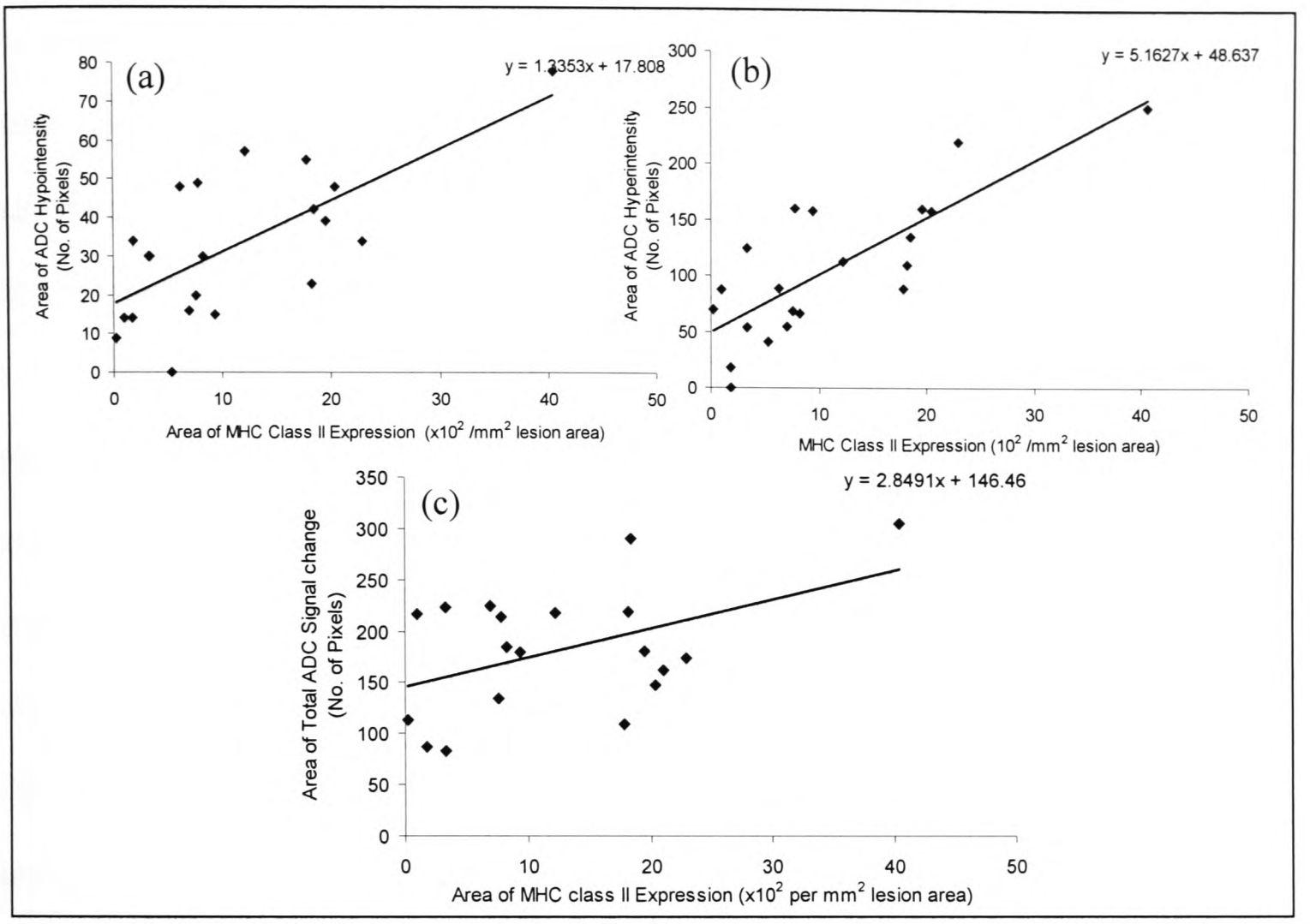


Figure 6-17: Graphs to show the relationship between MHC class II expression and area of ADC change.

(a) An extremely significant ($p<0.001$) correlation was found between MHC class II expression and the area of ADC hypointensity.

(b) An extremely significant ($p<0.0001$) correlation was found between MHC class II expression and the area of ADC hyperintensity.

(c) A significant ($p<0.05$) correlation was found between MHC class II expression and the area of total ADC change.

Correlation Between MHC Class II Expression and Area of...	Correlation Parameters			
	r	p	Slope	Y intercept
ADC Hypointensity	0.69	$p<0.001$	1.33	17.81
ADC Hyperintensity	0.80	$p<0.0001$	5.16	48.64
Total ADC change	0.47	$p<0.05$	2.84	146.45

Table 6-16: Summary of correlation analysis between areas of MHC class II expression and area of ADC change.

6.4.11 Correlation of ADC changes with other MRI Changes

The areas of signal change on ADC trace maps were correlated with areas of signal change on T_1- and T_2-weighted images (obtained from Chapter 5), as well as areas of change on post-contrast T_1-weighted images (Figure 6-18 and Table 6-17). It was found that the ADC hyperintense area correlated both spatially and qualitatively with the areas of T_2 hyperintensity ($p<0.0001$) and gadolinium enhancement ($p<0.01$) observed in the same animals (Figure 6-18a and Table 6-17). Although it appeared that the areas of increased ADC extended further than either the areas of T_2 hyperintensity or gadolinium enhancement. The total area of ADC change, that is both increased and decreased ADC areas, correlated significantly ($p<0.001$) with the area of gadolinium enhancement and with the area of total T_2 signal change ($p<0.0001$) (Figure 6-18c,d and Table 6-17). Surprisingly, the ADC hypointense area did not significantly correlate with the areas of hypointensity observed on T_1- and T_2-weighted images (Figure 6-19a,b and Table 6-18). However, this is most likely, to be due to the data points being very bunched. Spatially, the areas of T_2-weighted image and ADC hypointense regions were very closely matched, although in some cases the areas of decreased ADC were slightly larger than on T_2-weighted images. The area of gadolinium enhancement generally overlapped the area of ADC hyperintensity.

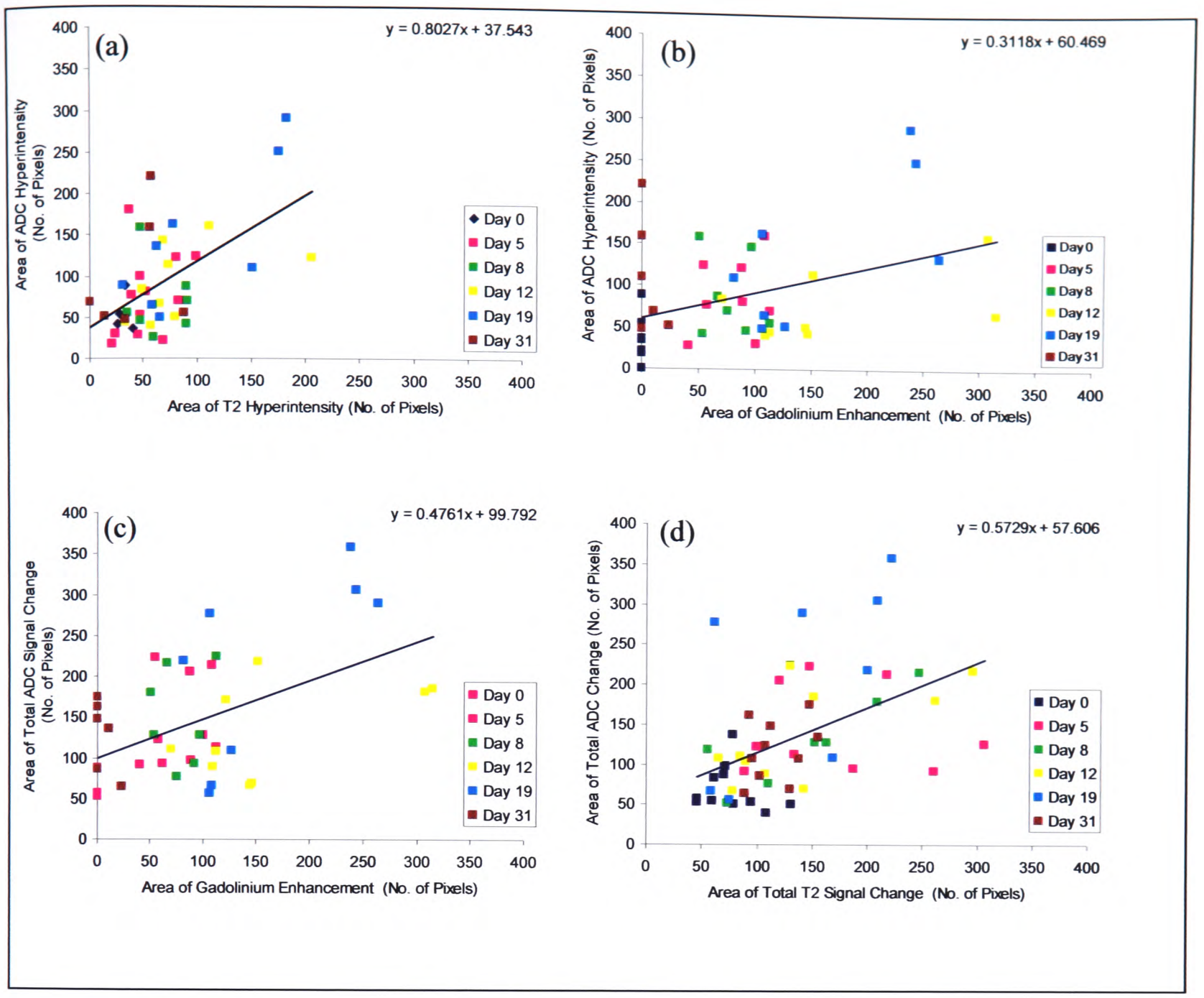


Figure 6-18: Graphs to show the relationship between areas of ADC signal changes and areas of signal changes observed on T_1- and T_2-weighted images.

(a) An extremely significant ($p<0.0001$) correlation was found between area of ADC hyperintensity and the areas of T_2 hyperintensity.

(b) A significant ($p<0.01$) correlation was also found between the area of ADC hyperintensity and the area of BBB breakdown (gadolinium enhancement).

(c) A highly significant ($p<0.001$) correlation was also found between the total area of change on ADC trace maps and the area of gadolinium enhancement on post-contrast T_1-weighted images.

(d) The total area of change on both ADC trace maps and T_2-weighted images were found to extremely significantly ($p<0.0001$) correlate.

Correlation of ADC changes with other MRI parameters	Correlation Parameters			
	r	p	Slope	Y intercept
ADC hyperintensity v T_2 hyperintensity	0.56	$p<0.0001$	0.80	37.54
ADC hyperintensity v BBB breakdown	0.41	$p<0.01$	0.31	60.47
Total ADC v BBB breakdown	0.51	$p<0.001$	0.47	99.79
Total ADC v total T_2 change	0.50	$p<0.0001$	0.57	57.61

Table 6-17: Summary of correlation analysis between ADC signal changes and other MRI parameters obtained from Chapter 5 (T_2 hyperintensity, BBB breakdown and total T_2 signal change).

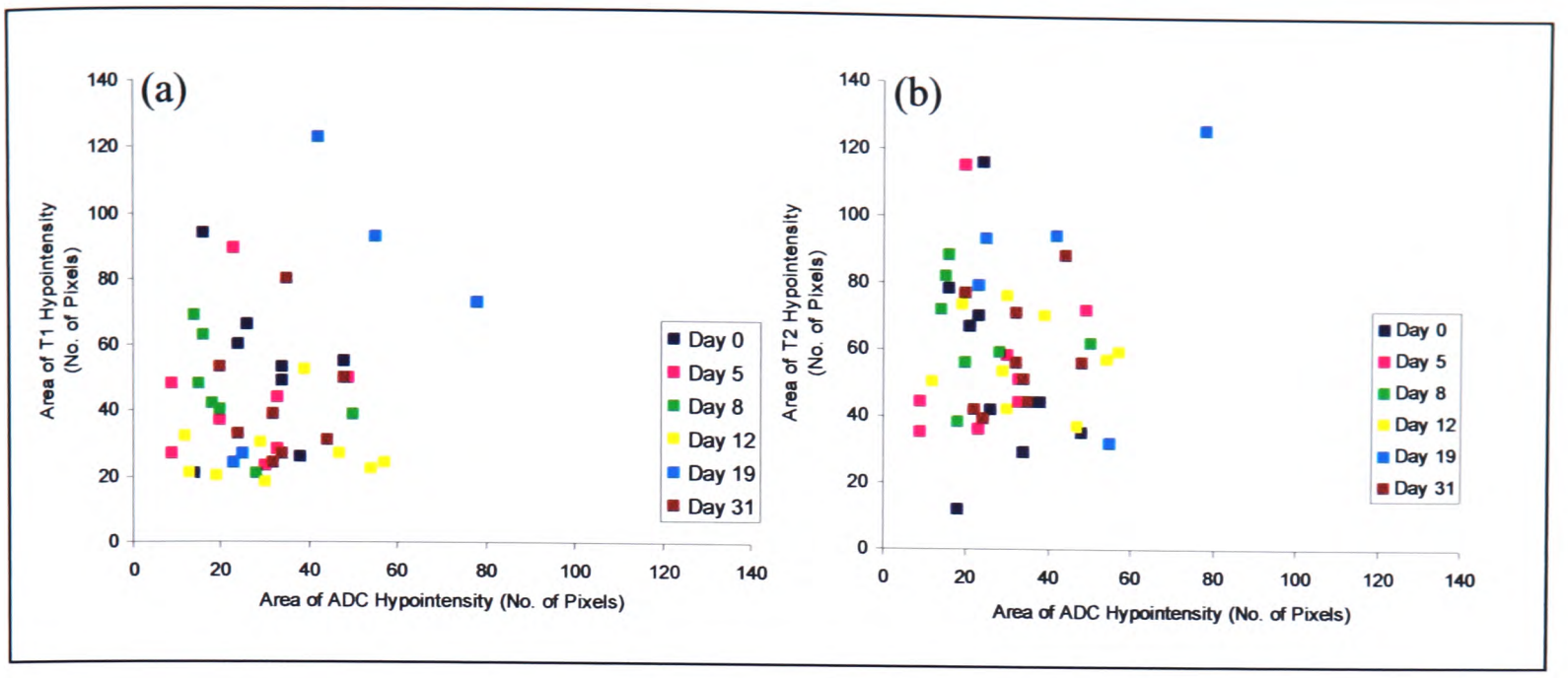


Figure 6-19: Graphs to show relationship between areas of ADC hypointensity and areas of hypointensity observed on T_1-weighted images (a) and T_2-weighted images (b). No significant correlations were found, probably due to the lack of spread of the data.

Correlation between area of ADC hypointensity and ...	Correlation Parameters	
	r	p
Area of T_1 hypointensity	0.15	0.34
Area of T_2 hypointensity	0.11	0.45

Table 6-18: Summary of correlation analysis between areas of ADC hypointensity and areas of T_1 and T_2 hypointensity (taken from chapter 5). In both cases, no significant correlation was found.

6.4.12 Diffusion Anisotropy

Diffusion anisotropy was investigated by using the van Gelderen approach as described in section 6.3.4. In most animals that were injected with BCG into the brain (both DTH and control groups), a region of decreased anisotropy was observed at the injection site (Figure 6-20a). This decreased anisotropy was spatially coincident with the area in which myelin and neuronal loss occurred, i.e. the hypercellular region (Figure 6-20b). This specific region was not quantitatively analysed owing to levels of noise on the anisotropy maps, which occasionally made it difficult to identify the lesion. Some preliminary data are included in Appendix E.6.

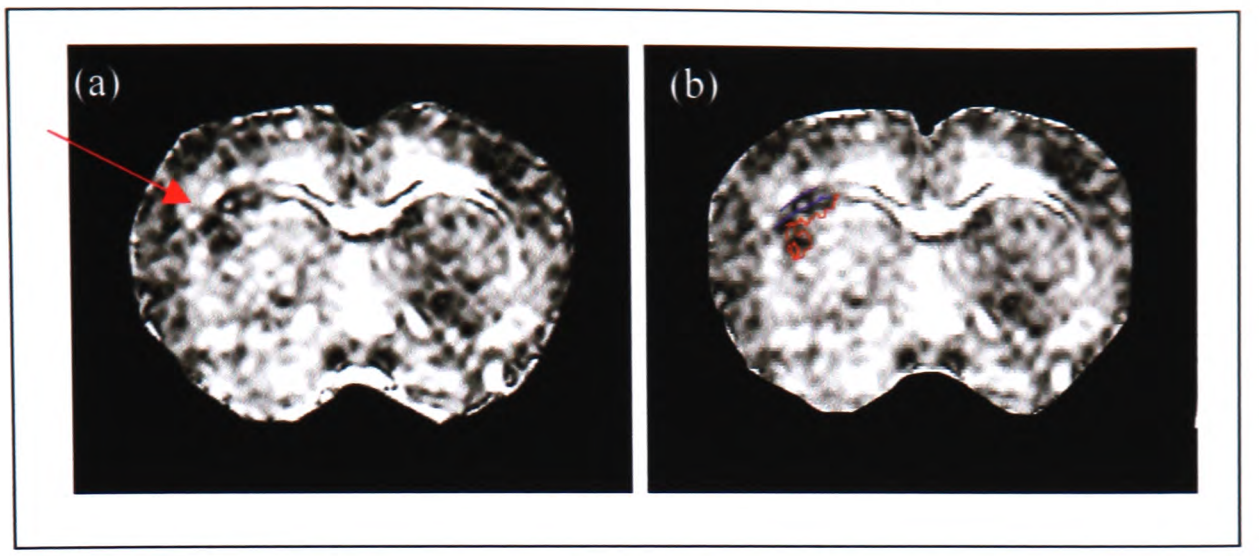


Figure 6-20: (a) Diffusion anisotropy map showing decreased anisotropy in the DTH lesion at day 19. (b) Area of myelin and neuronal loss overlaid onto the same anisotropy map to indicate spatial co-incidence of loss of anisotropy with loss of myelin and neurones in hypercellular region.

6.4.13 Magnetisation Transfer Ratios

Magnetisation transfer maps were created from the magnetisation transfer images as described in section 6.3.4. ROI's were drawn around the striatum encompassing the lesion, and similarly in the contralateral (right) hemisphere. In DTH animals, small areas of reduced MTR were apparent in the core (hypercellular area) of the lesion (Figure 6-21a), therefore ROI's encompassing the striatum were chosen. Although the overall MTR appeared reduced in DTH animals (Figure 6-22), the difference over time was not quite significant (ANOVA $p=0.0663$). In addition, there was no significant change in the MTR within the striatum of control groups over time. Nonetheless, significant differences were found between DTH and NPC controls. At day 5, the MTR was significantly lower in DTH animals than NPC controls (unpaired t test $p<0.02$), day 8 $p<0.005$, and day 12 ($p<0.02$). Individual data is included in Appendix E.7.

In addition to the small regions of MTR loss, there appeared to be an a further reduction in MTR in the corpus callosum in the injected hemisphere during the DTH inflammatory response (Table 6-19). Although there appeared to be some thinning of the corpus callosum, the obvious loss of the corpus callosum was not observed in NPC and SAL PC controls, and no apparent loss in the MTR was observed in PB IC controls (Figure 6-21b

and c). Where decreases in MTR were observed in the hypercellular lesion, it was found that the small area of MTR loss spatially corresponded to areas of myelin and neuronal loss (Figure 6-21d). However, in contrast, on closer examination of immunohistochemistry, it was found that the corpus callosum was intact, and that there was no demyelination corresponding to the loss of MTR in this region (Figure 6-23).

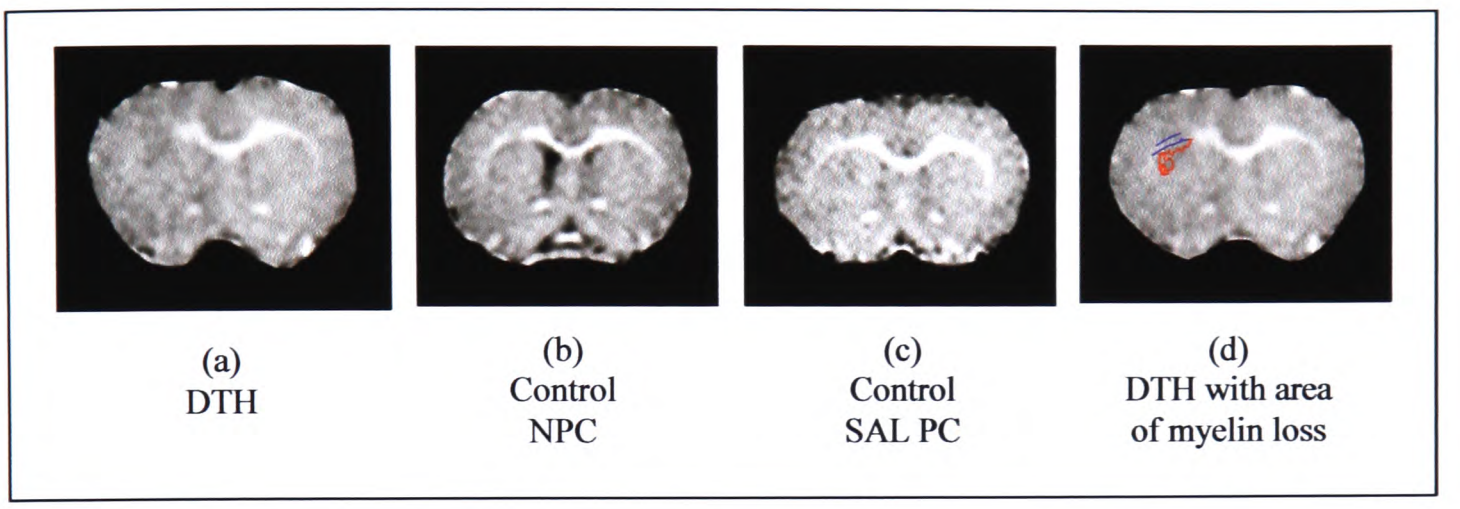


Figure 6-21: MTR maps from day 19 indicating region of reduced MTR in injected hemisphere, and apparent loss of corpus callosum in the DTH animals (a). This loss was not observed in control animals with no peripheral challenge (b) or control animals with a saline peripheral challenge (c). The core area of MTR loss appears to spatially coincide with the area of myelin loss (d).

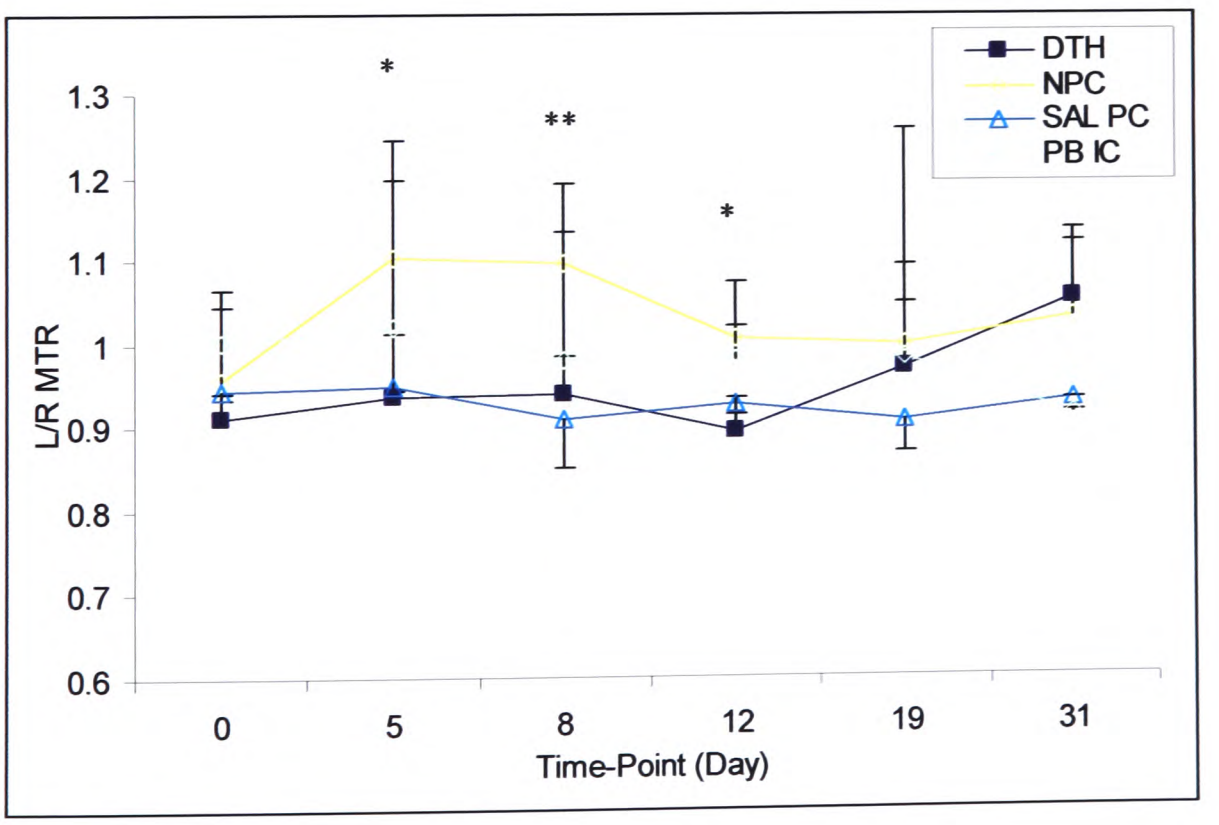


Figure 6-22: Graph to show change in L/R MTR during the DTH response. Values are expressed as L/R mean ± S.D. (NPC; no peripheral challenge, SAL PC; saline peripheral challenge, PB IC; saline intracerebral challenge). Significant differences were found between DTH and NPC animals at days 5, 8 and 12 (unpaired t test **$p<0.005$, *$p<0.05$).

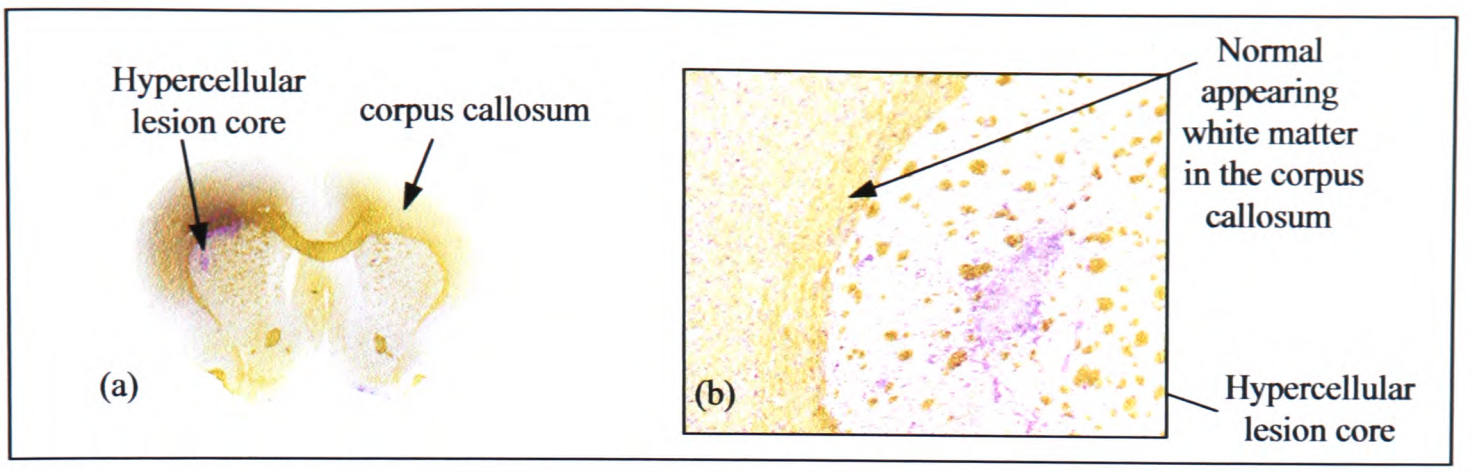


Figure 6-23: (a) Immunohistochemistry reveals that the corpus callosum is intact. (b) Loss of myelin occurs within the hypercellular core only.

Time-Point (Day)	MTR of Corpus Callosum (L/R)
0	0.88 ± 0.10 (10)
5	0.90 ± 0.10 (6)
8	0.88 ± 0.03 (9)
12	0.88 ± 0.05 (7)
19	0.89 ± 0.09 (4)
31	0.99 ± 0.12 (7)

Table 6-19: Magnetisation transfer ratio (MTR) expressed as left/right hemispheric ratios in DTH and control groups over time. Values expressed as mean ± S.D for (n) animals.

6.5 Discussion

In this chapter it has been demonstrated that the DTH lesion exhibits a contrast enhancing profile similar to that observed in MS and EAE lesions. Contrast enhancement occurred in some DTH animals from day 5, but maximal enhancement appeared to occur at day 19. The DTH lesion also exhibits ADC changes; throughout the study the lesion appeared hypointense on ADC trace maps, surrounded by an area of increased ADC at later time-points. Maximal changes in ADC also appeared to occur at day 19; the time-point at which maximal contrast-enhancement was observed. Contrast enhancement, and areas of increased ADC spatially (and quantitatively in the case of ADC) correlated with reactive astrocytes. The area of decreased ADC correlated quantitatively and spatially with MHC class II expression, areas of macrophages, T & B lymphocytes and neuronal loss. Diffusion anisotropy was reduced which spatially correlated with the area of hypercellularity. In addition, a decreased MTR was also observed in a large region of the injected hemisphere, which did not appear to be associated with myelin loss, or the hypercellular region; this reduction increased temporally to appear to be maximal at day 19.

6.5.1 Contrast Enhancement

BBB breakdown was consistently observed in the DTH lesion. BBB permeability is a characteristic of acute MS and EAE lesions, that is visible on contrast enhanced MRI. MS lesions may exhibit two patterns of gadolinium enhancement; homogenous and ring-like. The ring like enhancement, where there is a central, non-enhancing region surrounded by a peripheral enhancing rim, reflects inflammation surrounding a central area of complete demyelination (Nesbit 1991), (Petrella 1996). This ring enhancement is

usually observed during the acute phase of MS lesion development. In contrast, homogenous enhancement is primarily observed during the latter stages of the inflammatory response in MS patients. In this study, the enhancement was mainly homogenous, however, in some cases mild rim enhancement was observed, although this generally occurred towards the end of the time-course, rather than during the acute phase. In the MS brain, contrast-enhancing lesions are demyelinated and filled with macrophages when examined at post-mortem (Bruck 1997). The number of enhancing lesions correlates with severity and frequency of MS relapses; see Barkhof et al. for review (Barkhof 1999). In enhancing lesions, it has been suggested that vasogenic oedema resulting from BBB breakdown may have a direct effect on nerve conduction by altering the axonal environment (Kermode 1990). Alternatively, it may cause compression of local blood vessels in regions where the axons are tightly packed. In the current study, the correlation between T_2 hyperintensity and BBB breakdown showed almost showed a 1:1 relationship, implying that the changes occurred at the same rate. In addition, a strong correlation was found between BBB breakdown and the area of T_2 hypointensity in the current study. This is in accordance with a study by Miki et al. (Miki 1999), where it was shown that a correlation exists between the area of gadolinium enhancement and the area of lesion on T_2-weighted image. However, since these areas differed markedly in spatial extent this correlation suggests that the two events are related, but not directly linked as for the case with gadolinium enhancement and T_2 hyperintensity.

In MS studies, BBB breakdown has been shown to correlate with macrophages (Nesbit 1991), (Katz 1993). In addition, in EAE, similar correlations between BBB breakdown and macrophage recruitment have been found (Hawkins 1990), (Morrissey 1996). In contrast to the literature, in the current study, no correlation was found between

macrophage recruitment and BBB breakdown. In particular, the regions demonstrating the presence of recruited macrophages and BBB breakdown were not spatially co-incident. This finding suggests that despite the quantitative correlations found between macrophage numbers and BBB breakdown in MS and EAE, macrophage recruitment is not the underlying cause of BBB breakdown. If that were the case, then spatial coincidence would be expected. Thus, it is more likely that BBB breakdown facilitates macrophage recruitment, resulting in the correlations previously reported. However, increasing the sample size in the current work, might also yield a significant correlation.

The numbers of contrast enhancing lesions have also been shown to correlate with the level of myelin basic protein in the cerebrospinal fluid, which is a marker of myelin destruction (Barkhof 1999). This concept would fit with the observation in the current work that myelin degradation worsens when the lesion becomes more gadolinium enhancing, even though the areas of myelin loss did not spatially match the areas of BBB breakdown, making it unlikely, that myelin loss alone is a direct cause of BBB breakdown.

In one clinical study, lesions that showed gadolinium enhancement also showed a prominent astroglial response at post-mortem (Nesbit 1991), which suggests that the BBB breakdown is dependent not on the astroglial response, but on inflammatory cell recruitment. However, in this work, a quantitative and spatial correlation was found between BBB breakdown and astrocyte activation, suggesting that reactive astrocytes may be directly or partly responsible for contrast enhancement. In contrast, no correlation was found between BBB breakdown and macrophage recruitment in DTH lesions, disagreeing with a study in MS patients post mortem (Nesbit 1991). That work suggested that macrophages are the most likely to play an important role in the breakdown of the BBB. Interestingly, numbers of inflammatory cells in the CSF of MS patients have been

shown to correlate with the number of gadolinium enhancing lesions (Wang 2002). In the current study, the number of T & B lymphocytes also quantitatively correlated with the area of contrast enhancement. Peak T & B lymphocyte recruitment occurred before the peak astrocytic response (See Section 4.6.6 and 4.6.3), it is possible that T & B lymphocytes caused some degree of BBB breakdown, but additional astrocytic activation may have caused the area of BBB breakdown to increase. Peak T & B lymphocyte recruitment also occurred prior to BBB permeability changes; this also suggests that these lymphocytes play a role in BBB breakdown, however, since these cells are not spatially localised to the area of gadolinium enhancement, they are unlikely to be a direct cause of BBB breakdown.

The area of gadolinium enhancement was spatially co-incident with the area of IgG permeability, which is expected to be the case, since both are markers of BBB permeability. However, gadolinium enhancement confers a significant advantage over IgG, since it may be used to determine BBB permeability at each specific time-point *in vivo*. In contrast, IgG continues to be present in the brain at all times after the BBB has been open, irrespective of whether the BBB has closed or not. Areas occupied by BCG antigens also appeared to match the areas of contrast enhancement fairly closely, indicating that the extent of the BCG deposit largely determines the extent of the resulting lesion.

It is likely that the control animals that exhibited some degree of gadolinium enhancement may have had an ongoing inflammatory response that had not resolved following the initial injection of BCG into the brain. It is also possible that a small amount of BCG antigens may have leaked onto the cortical surface during the initial intracerebral injection. As a result, a low level sensitisation of the immune system to the BCG antigens may have occurred, giving rise to minor DTH responses in the brain. Alternatively, the

animals' immune system may have been over stimulated by constant use of tail lines (necessary for the injection of gadolinium) resulting in a low level inflammatory response at the site of the BCG deposit.

6.5.2 ADC Changes

In this study, a region of increased water diffusion, or ADC, was found surrounding a central core of decreased ADC. The area of the hyperintense region observed on ADC maps increased with time, until the lesion had passed the active inflammatory phase after which point, the area decreased again. Similarly, the area of reduced ADC appeared to increase substantially at the point of maximal inflammatory response which subsequently decreased. Furthermore, these changes in ADC were highly correlated.

Until recently, only three studies have been carried out investigating diffusion in EAE (Heide 1993), (Richards 1995), (Verhoye 1996), the most commonly used animal model of MS, and only one study has been carried out on a demyelinating MS-like lesion (Degaonkar 2002). In that study, similar findings of an area of reduced ADC within the demyelinating lesion, surrounded by a region of increased ADC were reported (Degaonkar 2002). In most diffusion studies carried out in MS patients increased water diffusion occurs in the lesions (Larsson 1992), (Christiansen 1993), (Horsfield 1996), (Tievsky 1999), (Droogan 1999), (Werring 2000), and a correlation has been found between the severity of clinical impairment and the ADC values of the white matter in MS patients (Verhoye 1996).

The work presented here, is in agreement with results from clinical studies where acute MS plaques have higher ADC's than chronic plaques (Christiansen 1993). It has been suggested that the increase in ADC is brought about by an increase in diffusion of water molecules in a plane orthogonal to fibre orientation (Christiansen 1993), (Heide 1993),

(Degaonkar 2002). In the current study, areas of increased ADC correlated significantly with areas of BBB breakdown and T_2 hyperintensity. These findings suggest that oedema resulting from BBB breakdown maybe the underlying cause of the increased ADC. However in both clinical (Werring 2000), and EAE studies (Heide 1993), the ADC of brain tissue has been shown to increase prior to gadolinium enhancement of the lesion. Similarly, occasionally in the current study an increased ADC was observed before BBB breakdown. At these time-points it is possible, therefore that increased ADC reflects other events such as demyelination, which alter the structure of the brain parenchyma, consequently giving rise to increased diffusion. However, demyelination in the DTH model is restricted to the hypercellular core, i.e. the hypointensity on ADC trace maps, and myelin loss is not apparent in the hyperintense ADC region. Thus, demyelination is unlikely to contribute to the increased ADC observed in the DTH lesion.

In this study, it was found that the total area of change on ADC trace maps correlated with both the area of BBB breakdown, and the total area of signal change on T_2-weighted images. Additionally in this study, ADC hyperintensity correlated with T_2 hyperintensity, which are both generally considered to reflect increased mobility of water protons, as would be expected in an oedematous region. Thus, these data strongly suggest that there is vasogenic oedema around the DTH lesion at the time of contrast enhancement.

Although most MS studies have demonstrated an increased ADC, the finding of a hypointense region on the ADC trace maps in the current work is in agreement with one clinical study in which areas of restricted diffusion were found (Iwasawa 1997). These regions were often found in lesions where there was no gadolinium enhancement. Similarly, in the current study, the decreased ADC was present even when there was no gadolinium enhancement. In Iwasawa's work, areas of decreased diffusion were also found at the edges of MS lesions where there are dense cellular borders, and it was

hypothesised that the hypercellularity caused decreased diffusion in those regions (Iwasawa 1997). In the DTH model, the lesion core is composed primarily of macrophages and T lymhocytes, and this region correlated spatially with decreased ADC. In addition, MHC class II expression was found to correlate both spatially and quantitatively with the ADC hypointense area. Since MHC class II is expressed predominately by cells in the hypercellular core, such as macrophages (Chapter 4), these findings provide further support for the hypothesis that a decreased ADC is brought about by the dense population of these cells.

Areas of hypointensity on both T_1- and T_2-weighted images did not correlate with the area of decreased ADC, this is probably because the spread on these data is relatively small, and consequently the data are grouped very closely together. However, spatially, these areas did coincide with each other. Interestingly, the hypointense regions on the different types of images correlated quantitatively with different histological parameters. The ADC hypointensity spatially correlated with MHC class II expression, whilst T_2 hypointensity quantitatively correlated with T & B lymphocytes and with reactive astrocytes. Spatially, the hypointensity on ADC maps, T_1- and T_2- weighted images correlated with loss of neurons, MHC class II expression, macrophage, and T & B lymphocyte recruitment. These observations suggest that many different factors are involved in ADC, T_1 and T_2 changes, and that there is a great deal of interaction between the different cell types in the inflammatory lesion.

The observation that no correlation was found between ADC changes and T_1 hypointensity, is also in agreement with clinical studies (Caramia 2002). It has been shown that the more hypointense a non-enhancing MS lesion is on T_1-weighted images, the greater the increased diffusion (Nusbaum 2000), which is in contrast to the work of

Tievsky et al. (Tievsky 1999). In the current study it was shown temporally, that when lesions were maximally hypointense on T_1-weighted images (Section 5.4.1), at the same time-point as maximal increased diffusion were observed.

A quantitative correlation was found between areas of ADC hypointensity and ADC hyperintensity, even though these areas were spatially distinct; the hyperintensity was found to surround the hypointense region. The close correlation between these parameters suggests that the factors causing both effects are tightly linked and progress with similar temporal characteristics. In fact, it is likely that the hyperintensity also occurs at the centre of the lesion, but that the presence of the hypointense region acts to mask the hyperintensity. When the total area of ADC change was considered, it was also found to correlate quantitatively with areas of reactive astrocytes, macrophage recruitment and MHC class II expression. However, none of the histological parameters were as widespread spatially as the ADC changes. This may reflect partial volume effects on the ADC trace maps, or a spread of the diffusion changes beyond the perimeter of the lesion. In that case, cytokines expressed by astrocytes, may be partly responsible for the more widespread changes in ADC. Alternatively, these findings may indicate a greater sensitivity of diffusion-weighted imaging to subtle changes at the lesion perimeter than T_2-weighted imaging or contrast enhancement.

6.5.3 Diffusion Anisotropy

In agreement with clinical MS studies (Droogan 1999), (Tievsky 1999), the DTH lesions exhibited a decreased anisotropy, which is likely to reflect loss of tissue structure. Similarly in EAE, a decreased diffusion anisotropy has been measured (Ahrens 1998). The area of reduced anisotropy was spatially co-incident with the areas of hypercellularity, and consequently with the areas of demyelination and neuronal loss, and

appeared to extend beyond the hypointense regions observed on T_1- and T_2-weighted images and also ADC trace maps. This decrease in anisotropy is related to loss of tissue structure brought about by increased tissue water and myelin loss within the DTH lesion.

In this study, anisotropy is measured using a rotationally variant method. It is a scalar standard deviation index that is proportional to the standard deviation of the 3 ADC's measured in the perpendicular directions x y and z, divided by their mean value (van Gelderen 1994). Although this method is known to underestimate the degree of diffusion anisotropy (Pierpaoli 1996), (Basser 1994), the consistent observation in this study that DTH lesions have decreased anisotropy is in agreement with clinical and EAE studies. Richards et al. (Richards 1995), investigated diffusion anisotropy in EAE-affected monkeys and discovered that chronic lesions have a preservation of anisotropy compared to acute EAE lesions. In the current study, there is similarly, a suggestion that anisotropy returned to normal once the acute inflammatory response had begun to resolve (days 19 to 31).

6.5.4 Magnetisation Transfer

In the current study, a decrease in MTR in the DTH lesion was found. This is in agreement with observations in the literature, that in MS a decrease in MTR in active lesions is reported, and this is generally considered to reflect demyelination. Similarly, EAE lesions have a reduced MTR (Gareau 2000),(Dousset 1992), and in accordance with the hypothesis that demyelination causes a reduced MTR, some animal studies have shown that a low MTR correlates with myelin loss and axonal destruction (Brochet 1999). However, other studies in EAE have suggested that a deceased MTR is more closely related to the inflammatory events accompanying demyelination, such as oedema (Gareau 2000). In the DTH animals showing a decreased MTR at the lesion site, there was also

extensive loss of myelin. However, myelin loss was restricted to the area of hypercellularity, whilst the MTR changes extended much further than this region. In some animals it was noted that the corpus callosum was almost completely absent from the injected hemisphere on the MTR maps. Upon histopathological investigation, it was found that although there was some myelin disruption, there was no loss of myelin in this region, thus it appears that the MTR changes observed in the DTH model, do not reflect demyelination *per se*, but other inflammatory events. This finding is in contradiction to the current view in MS, that demyelination is the underlying factor behind a reduced MTR.

As with ADC changes, MTR changes have been shown to precede lesion appearance (Filippi 1998). In agreement with this, in this study, the decrease in MTR was observed prior to gadolinium enhancement. An increased MTR has also been reported in EAE, and it was found that these values correlated with oedematous lesions (Dousset 1992). Although the DTH lesions appeared to be oedematous as suggested by the increased ADC and T_2-weighted image signal intensity (chapter 5), a concomitant increase in MTR was not observed.

6.5.5 Conclusions

In conclusion, the work described in this chapter has utilised more advanced MRI techniques that are commonly used in MS studies, to characterise different aspects of the ongoing pathology and lesion progression. The DTH lesion is contrast enhancing, a characteristic commonly found in acute MS lesions, and at the same time, increased diffusion of tissue water occurs around the lesion. The progressive breakdown and restoration of the BBB temporally correlates with increases in signal intensity on T_2-weighted images, and tissue ADC, which both subsequently decrease. All of these

changes appear to occur maximally between days 12 and 19. Decreased diffusion was observed at the lesion core, and this correlated spatially with macrophages, T & B lymphocytes, neuronal loss, and MHC class II expression, suggesting that these factors all play a role in the MRI visible changes. Contrast enhancement and T_2 hyperintensity was found to spatially correlate with reactive astrocytes, implying that astrocytes are important factors in the alteration of BBB permeability, thus affecting water diffusion and oedema. Decreased anisotropy and MTR were also observed at the lesion site. The decreased anisotropy appeared to coincide with areas of myelin loss, however, the reduction in MTR, was found to occur in spatially distinct regions from the hypercellular region, and, therefore myelin loss does not appear to be wholly responsible for the decreased MTR. Such correlations between diffusion changes, MTR and underlying histopathology have not been reported previously.

Chapter 7

Assessment Of Cerebral Blood Volume Changes

7.1 Introduction

The earliest report of flow (coherent motion) *in vitro* using MRI was published as early as 1951 by Suryan et al. cited by (Barbier 2001), although the earliest *in vivo* study was described by Le Bihan in 1985. In this early experiment, a comparison of random motion of blood flow through randomly oriented blood capillaries against Brownian motion was made. With some success, this technique used the principles of diffusion weighted MRI for the estimation of blood flow, which led to development of perfusion methods that are currently used in clinical practice. Perfusion weighted imaging utilises the effect of endogenous or exogenous tracers on the MR images to derive various haemodynamic parameters: cerebral blood volume (CBV), which may be defined as the fraction of the total tissue volume within a voxel occupied by blood, cerebral blood flow (CBF), defined as the volume of arterial blood delivered to the tissue per minute per tissue volume; and mean transit time (MTT), which corresponds to the average time it takes a tracer molecule to pass through the tissue (Luypaert 2001). These techniques are already important clinical tools in the diagnosis and treatment of patients with cerebrovascular disease, and other disorders such as Alzheimer's disease, however, to date, Multiple Sclerosis has received little attention in terms of cerebral perfusion.

Measurement of tissue perfusion depends on the ability to serially measure the concentration of a tracer agent in the organ of interest; these tracer agents may be exogenous, such as paramagnetic contrast agents (e.g. gadolinium), or endogenous agents

such as spin-labelled blood. There are two main methods currently used for perfusion imaging. The first is arterial spin labelling, which uses radiofrequency-labelled water in the blood as an endogenous, freely diffusible tracer. Perfusion is measured when subtraction of one image isolates the signal of the inflowing arterial blood in the slice of interest. The labelling has a very short half-life, resulting in low signal to noise on the images. Consequently, this technique is not ideal for monitoring changes in blood flow or perfusion, particularly small perturbations. The second major method currently used by clinicians, is dynamic susceptibility contrast imaging (also known as bolus tracking). With this method, regional cerebral perfusion is measured by assessing the first pass of a paramagnetic contrast, agent such as chelates of gadolinium (e.g. Gd-DTPA) through the tissue after a rapid intravenous injection. Large differences in the susceptibility between the capillaries containing the paramagnetic contrast agent and the surrounding tissues, result in strong field gradients in the neighbourhood of the vessel walls. As a consequence, direct signal dephasing occurs, and this can give contrast related to cerebral perfusion. A bolus of Gd-DTPA, administered as a short venous injection of a few sections duration, creates a dip in the NMR signal when it transits the brain as observed in Figure 7-1. Signal time-course data is converted to gadolinium tissue-concentration time-course information, using the relationship between T_2^* signal intensity and tracer tissue concentration (Rosen 1990). Determination of CBV is achieved by integration of the area under the gadolinium-concentration curve in Figure 7-1. CBF can be determined using the arterial input function from tissue concentration time data to determine the rate of clearance (MTT) through the capillary bed. The CBV can then be divided by the MTT to determine the CBF. However, obtaining reliable input function data, particularly in rats, is technically challenging and the majority of studies use this method to obtain CBV and MTT data only.

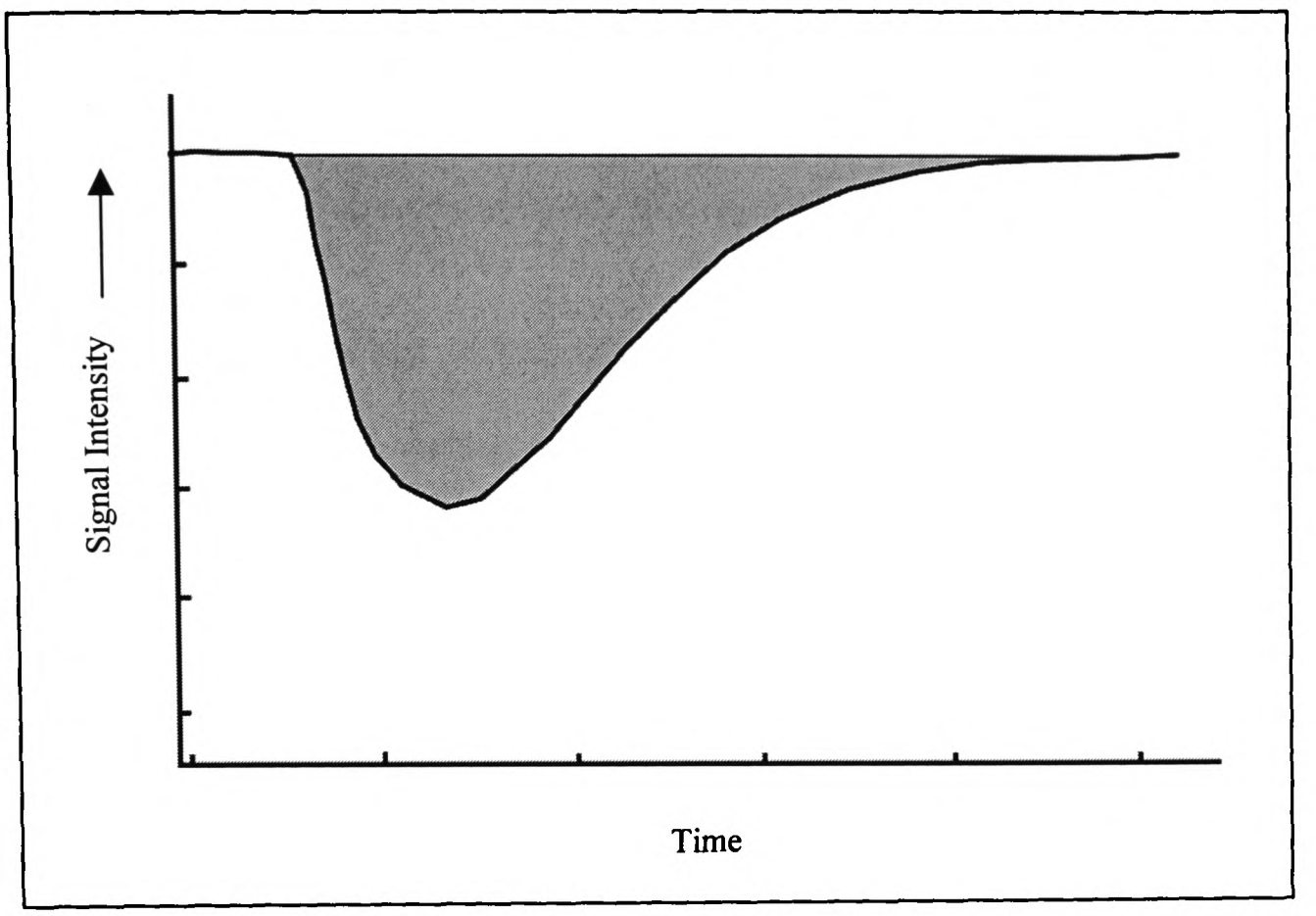


Figure 7-1: Illustration of the effect of the gadolinium bolus on the signal intensity as it passes through the tissue. The shaded area indicates the area from which the CBV is calculated.

At present, little published data exists on the subject of perfusion in MS patients. A reduction in rCBV in the MS lesion has been shown to occur at the time of contrast enhancement (Jensen 1995), (Petrella 1997). This reduction is thought to be brought about by oedema from resulting BBB breakdown and perivascular inflammation, which in itself causes vessel compression and reduced capillary resistance. It is also thought that axonal loss and reduction in neuronal activity results in reduction in metabolic rate, which in turn induces a reduction in lesion vascularity.

Other clinical perfusion and blood volume studies have used the non-MRI technique of Single Photon Emission Computed Tomography (SPECT). Similarly, with this method, MS patients have been found to have a reduced rCBF, which correlates with disability (Lycke 1993).

It has been hypothesised that an MS lesion results from localised hypoperfusion (Juurlink 1998). This hypothesis is based upon the observation that oxidative stress arising from

hypoperfusion in the brain causes oligodendrocyte damage. However, it has been shown that demyelination alone is insufficient to result in the formation of an inflammatory lesion (Juurlink 1998), and consequently this hypothesis is flawed.

To date, only one paper has shown, using MRI (and BBB permeability correction), that there is increased rCBV during the progression of an MS lesion. Haselhorst et al. (Haselhorst 2000) investigated perfusion in MS lesions, and found that enhancing lesions showed increased perfusion, which subsided with time. In addition, T_1 hypointense lesions were found have decreased perfusion.

In EAE, only one study has been published investigating perfusion. Increases in rCBF (measured using autoradiography), occurred at the time of BBB breakdown. The increases were hypothesised to be primarily due to increased glucose metabolism, resulting from increased inflammatory cell activation, causing a secondary increase in the blood flow (Juhler 1987).

The lack of MRI perfusion studies carried out in both MS and EAE, and the fact that much of the existing data is contradictory, suggests that further investigation is required to determine the relationship between cerebral haemodynamics and the development of an MS lesion. Neither clinical nor animal studies have investigated the underlying histopathological causes of rCBV changes. Therefore, in this study, an attempt will be made to investigate alterations in rCBV, and to correlate those changes with underlying histopathology.

7.2 Aims of this Chapter

The aim of this chapter was to investigate local cerebral haemodynamics in the form of regional cerebral blood volume (rCBV) by dynamic susceptibility contrast imaging in the

DTH model. Where changes occurred, correlations were made with alterations in vessel diameter using laminin expression, a component of the extracellular basement membrane and vessel endothelium, and with Cresyl Violet histology.

7.3 Materials and Methods

7.3.1 Surgery

As described previously in Chapter 3, heat-killed BCG was injected sterotaxically into the striatum of three-week-old male Lewis rats to initiate a DTH lesion. Surgery was performed under halothane-induced anaesthesia. Four weeks later, a peripheral challenge of TB in CFA was given into each of the hind limbs. In addition, three control groups were investigated, as summarised in Table 4-1. MRI was performed on all animals at the following time-points after peripheral challenge: 0 (n=15), 5 (n=13), 8 (n=9), 12 (n=9), 19 (n=8) and 31 (n=8) days. Temporary canuale were inserted into the tails of all animals in order to carry out bolus-tracking experiments at each time-point. Following MRI at specific time-points detailed above, the animals were transcardially perfusion-fixed and the brains removed for analysis.

7.3.2 MRI Techniques

Anatomical T_1- and T_2-weighted images were acquired (as described in Chapter 5) to determine lesion location, and to ensure the correct slice position at each time-point. The parameters used for the acquisition of these images are summarised in Table 5-2.

Cerebral blood volume maps were subsequently generated from a time-series of gradient echo images acquired with the parameters summarised in Table 7-1, during and following a bolus injection of a contrast agent and tracer kinetic analysis (Rosen 1990). A series of

40 FLASH (Frahm 1986) images were acquired at a rate of approximately 1 image per second. Following acquisition of 8 baseline images, a 100µl bolus of a standard Gd-DTPA based MRI contrast agent (Gadiodiamide, Omniscan, Nycomed Amersham, UK) was injected via a tail vein over a 4 second period.

Parameter	Value
Repetition time (TR)	20 msec
Echo time (TE)	10 msec
Field of view	3 x 2 cm^2
Slice Thickness	1 mm
Number of Averages	1
Number of Images	40
Total acquisition time	51 sec

Table 7-1: Summary of parameters used for the acquisition of FLASH (Frahm 1986) images for the creation of rCBV maps.

During MRI, anaesthesia was maintained with a mixture of 0.7-1.7% halothane in 70% N_2O/30% O_2, and physiological variables (core body temperature using a rectal probe, and heart-rate using a custom-built cardiac detector) were monitored throughout.

7.3.3 Perfusion and Fixation

At specific time-points during the DTH response, (0, 5, 8, 12, 19 and 31 days post-peripheral challenge) some animals were terminally anaesthetised and transcardially perfused with 0.9% NaCl solution as described in Section 3.4.2, to enable histology and immunohistochemistry to be carried out as described in Section 3.6.3. In addition, immunohistochemistry was also used to confirm the expression of laminin using an affinity purified polyclonal rabbit anti-laminin antibody (Sigma), which recognises all laminin isoforms. Frozen, serial sections (10µm thick) were cut from the paraformaldehyde-fixed tissue and mounted on gelatin-coated glass slides, which were then pre-treated with 0.04% pepsin in 0.1M HCl for 10 minutes at room temperature. Cresyl Violet histochemistry was used to evaluate the extent of dilated blood vessels

extending through the lesion. 50μm thick sections were taken to build up the lesion spatially. The Cresyl Violet also allowed assessment of general lesion composition.

7.3.4 Data Analysis

Maps of regional cerebral blood volume were created using standard tracer kinetic analysis of the time-series data sets (Rosen 1990). The rCBV maps were subsequently thresholded at a level that was equal to the mean signal intensity plus two standard deviations of the signal intensity of the non-injected hemisphere. This approach enabled areas of increased rCBV to be more easily visualised and quantitative analysis was performed on these thresholded rCBV maps. ROI's were drawn around the injected and non-injected hemispheres to obtain mean signal intensities and areas of brain with intensity identified using the thresholding method (i.e. more than 2 S.D's above the mean signal intensity of the contralateral hemisphere). The results are expressed as ratios of left/right (i.e. injected/non-injected) rCBV in order to assess hemispheric differences.

Cresyl Violet and laminin immunohistochemistry sections were examined under a light microscope to qualitatively evaluate the distribution of blood vessels and laminin expression in each lesion. Fields were selected to cover the whole of the hypercellular lesion, and dilated blood vessels were identified and traced using a camera lucida under the x6.3 objective. Drawings of the lesions were then scanned and stored as electronic jpeg images. The scanned drawings were then overlaid on to the MRI images using anatomical markers such as the corpus callosum and in some cases the ventricles to enable them to be scaled appropriately. In this manner, the spatial relationship between the dilated blood vessels and CBV changes could be determined.

7.3.5 Statistical Analysis

Differences in rCBV between controls and DTH animals at each time-point were tested by unpaired students t tests with welch correction, using Graphpad Instat as detailed in Table 3-4. Correlations between rCBV and other MRI parameters obtained from the previous chapters were determined using the Pearson r parametric test.

7.4 Results

DTH animals were imaged throughout the evolution of the DTH lesion (day 0, 5, 8, 12, 19 and 31) and were killed at selected time-points to correlate regional cerebral blood volume changes (rCBV) with developing histopathology. Control animals were studied at the same time-points.

7.4.1 Regional Cerebral Blood Volume (rCBV)

In DTH animals, injection of heat-killed BCG resulted in increases in rCBV in the injected hemisphere (Figure 7-2). Little, if any, increase was observed in the contralateral hemisphere. Visually, no substantial differences in rCBV were observed between the injected and contralateral hemisphere rCBV in control animals. The changes in rCBV were quantified as ratios of left hemispheric intensity to right hemispheric intensity on the thresholded CBV maps (Figure 7-4). Areas of increased rCBV that were identified from the thresholding method were also quantified (Figure 7-6,7), and again expressed as left/right hemispheric ratios. The rCBV appears elevated throughout much of the injected striatum relative to the contralateral hemisphere, but noticeably not within the enhanced region of interest. The areas of increased rCBV were spatially distinct from areas of BBB breakdown as shown in Figure 7-3, eliminating the possibility that the rCBV increases were artefactual arising from gadolinium leakage. Furthermore inspection of the bolus transit curves demonstrated that the signal decreased and subsequently returned to normal intensity with the expected profile observed in Figure 7-1. If gadolinium leakage were contributing significantly to the measured rCBV increases, it would be expected that the signal would remain depressed, but this was not the case.

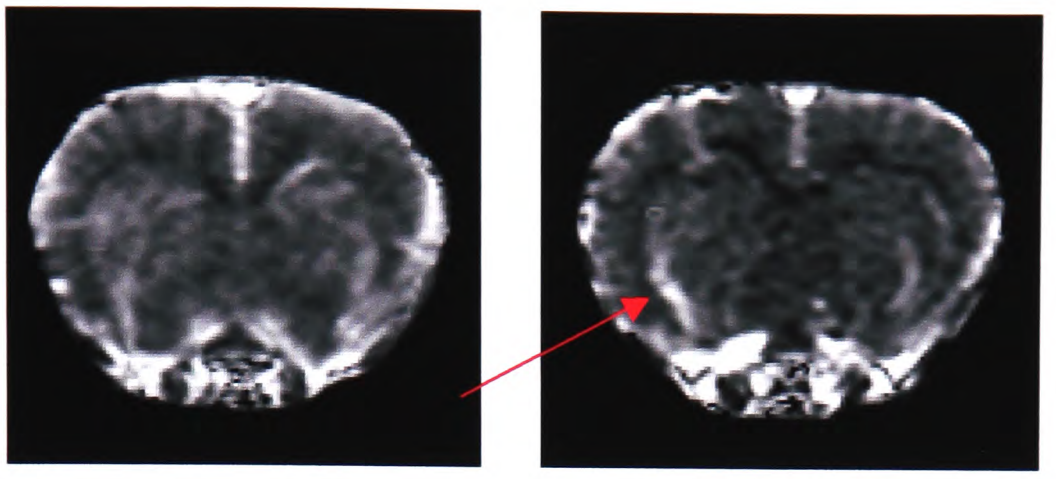


Figure 7-2: CBV map from DTH animals at days 0 and 8 showing increased rCBV in injected hemisphere at day 8. Asymmetry is apparent at the anterior striate artery, as shown by the arrow.

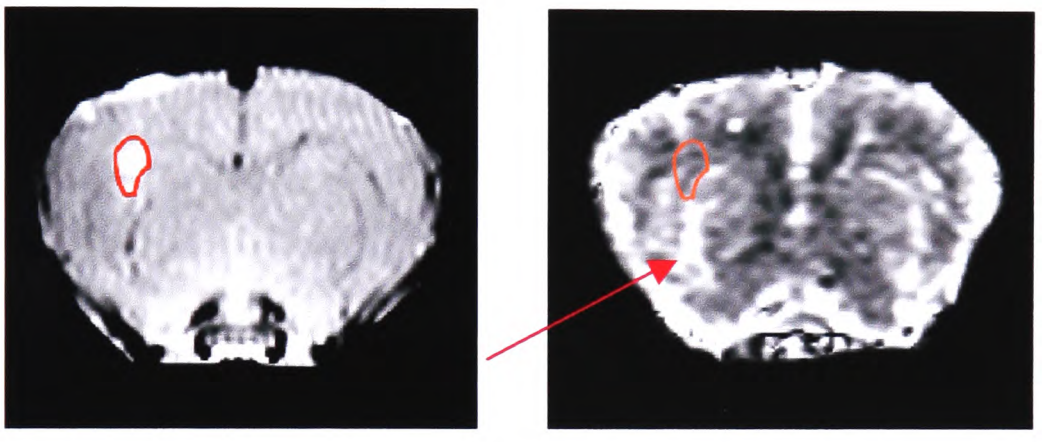


Figure 7-3: Post-contrast T_1-weighted image showing area of BBB breakdown, which does not overlap the area of increased rCBV in the same animal as indicated by the arrow.

7.4.2 Quantification from Thresholded Maps

CBV maps were thresholded as described in Section 7.3.4. This thresholding approach visually enhanced the changes in rCBV as can be seen in Figure 7-4. A significant change over time was observed in DTH animals (ANOVA $p<0.02$). No significant differences in rCBV were found between DTH and control groups at days 0 and 5 post-peripheral challenge. However, at day 8 clear increases were evident in DTH animals in the injected hemisphere. At this time-point the rCBV was greater in DTH animals than in any of the control groups (Figure 7-5) and was statistically significant to all control groups, as observed in Table 7-2 (unpaired t test DTH vs. NPC $p<0.001$; DTH vs. PB IC $p<0.05$; DTH vs. SAL PC $p<0.05$). Additionally, at day 12, a significant difference was found between DTH and PB IC controls, and at day 19 between DTH and SAL PC

controls. These statistical results are summarised in Table 7-2 and individual results are summarised in Appendix F.

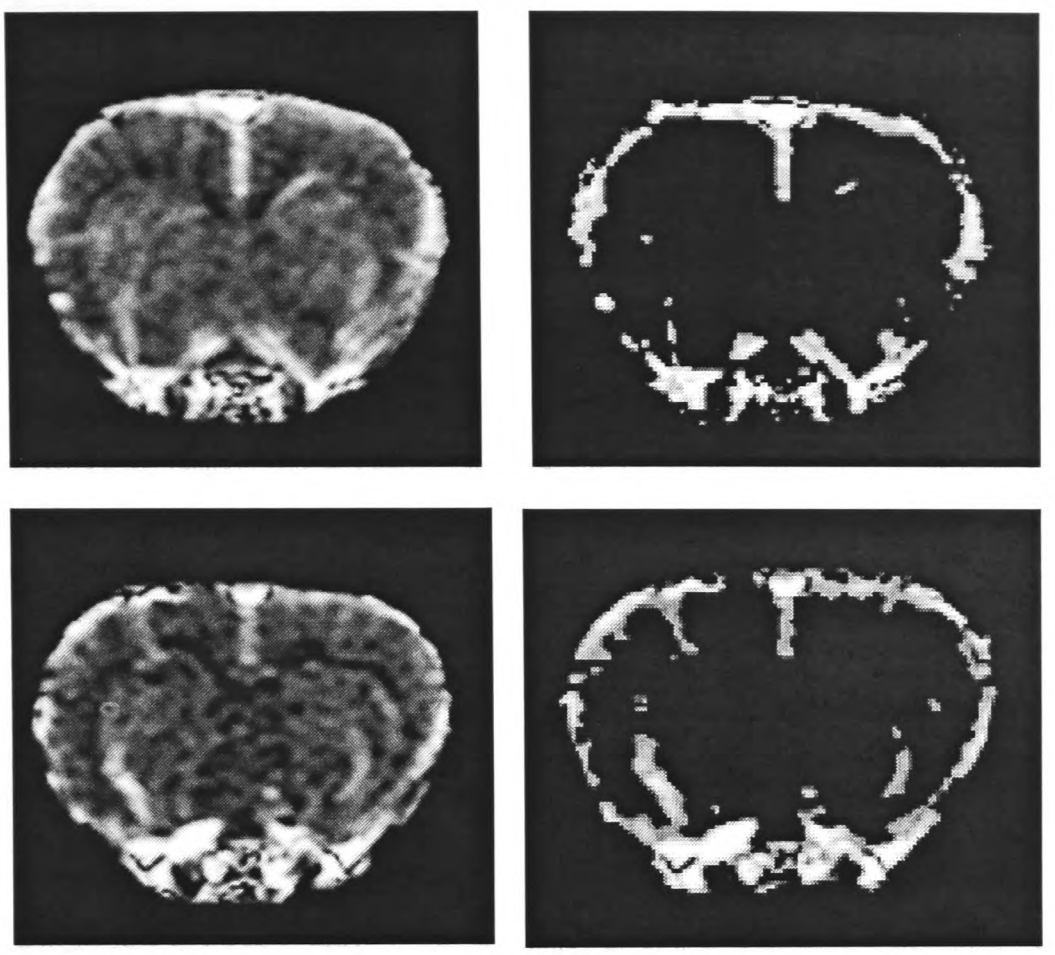


Figure 7-4: Unthresholded and thresholded CBV maps from DTH animals at day 0 and day 8 indicating increased rCBV in the injected (left) hemisphere.

rCBV						
Time-Point (Day)	**0**	**5**	**8**	**12**	**19**	**31**
NPC	/	$p<0.02$	$p<0.001$	$p<0.005$	$p<0.02$	$p<0.05$
SAL PC	/	/	$p<0.05$	/	$p<0.02$	/
PB IC	/	/	$p<0.05$	$p<0.02$	/	/

Table 7-2: Summary of unpaired t test results for between group comparisons of rCBV at each time-point, ('/' denotes difference is not significant, NPC, No peripheral challenge, SAL PC; Saline peripheral challenge, PB IC; Phosphate buffer intracerebral challenge).

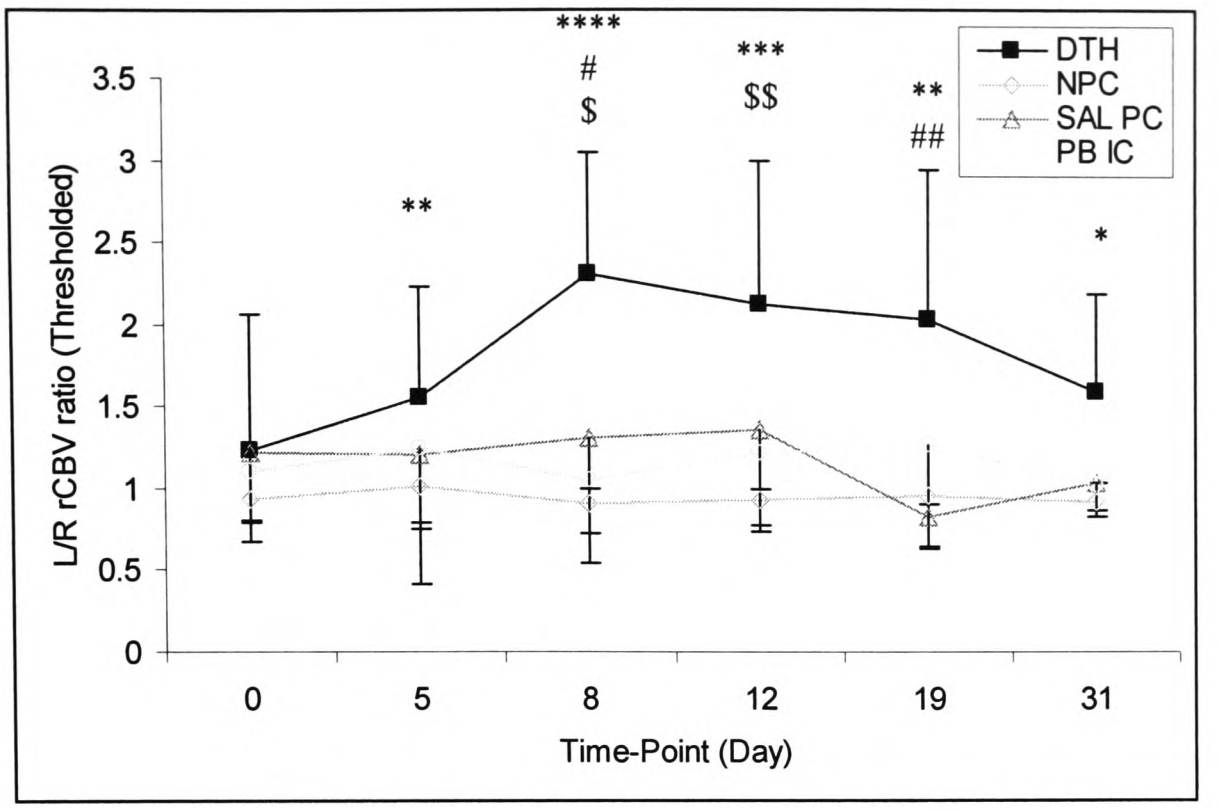


Figure 7-5: Graph to show left/right rCBV ratios obtained from CBV maps at time-points following peripheral challenge in DTH animals and control animals (NPC, No peripheral challenge, SAL PC; Saline peripheral challenge, PB IC; Phosphate buffer intracerebral challenge). Values are expressed as mean ± S.D. A significant difference was found in DTH animals over time (ANOVA $p<0.02$). Significant differences were found between DTH and control groups at days 5, 8, 12, 19 and 31 (unpaired t test ****$p<0.001$, ***$p<0.005$, **$p<0.02$, *$p<0.05$, ##$p<0.02$, #$p<0.05$, $$$p<0.02$, $$p<0.05$, where * versus NPC, # versus SAL PC and $ versus PB IC controls).

ROI's were drawn around the areas identified on thresholded CBV maps as increased rCBV (i.e. greater than 2 S.D's above the mean signal intensity of the non-injected (right) hemisphere). The temporal profile of the areas of increased rCBV in the injected hemisphere of DTH animals followed the same pattern as changes in left/right rCBV ratios observed on the thresholded maps (Figures 7-6, 7-7). At days 0 and 5, no significant differences between DTH and control groups were found, although in all cases there was a slightly greater CBV in the left hemisphere than the right. By day 8, a clear increase in the area of increased rCBV in the DTH animals was evident. However, although greater areas were observed in DTH animals than the three control groups, these areas were only significantly different from NPC controls (unpaired t test $p<0.02$), and PB IC controls ($p<0.02$). At day 12 the areas of elevated rCBV remained higher in DTH animals than in control groups, the difference between DTH and NPC controls was not quite significant ($p=0.0690$) and comparisons between DTH and other control groups were not significant. Areas that were greater than 2 S.D's above the mean signal intensity

in the non-injected hemisphere were minimal, and remained constant throughout the time-course (Figure 7-7). In the non-injected hemisphere, there were no significant differences between DTH and control animals. From day 12 to 31, areas of increased rCBV in DTH animals decreased. In general, areas of increased rCBV in controls remained constant throughout the time-course (Figures 7-6 & 7-7).

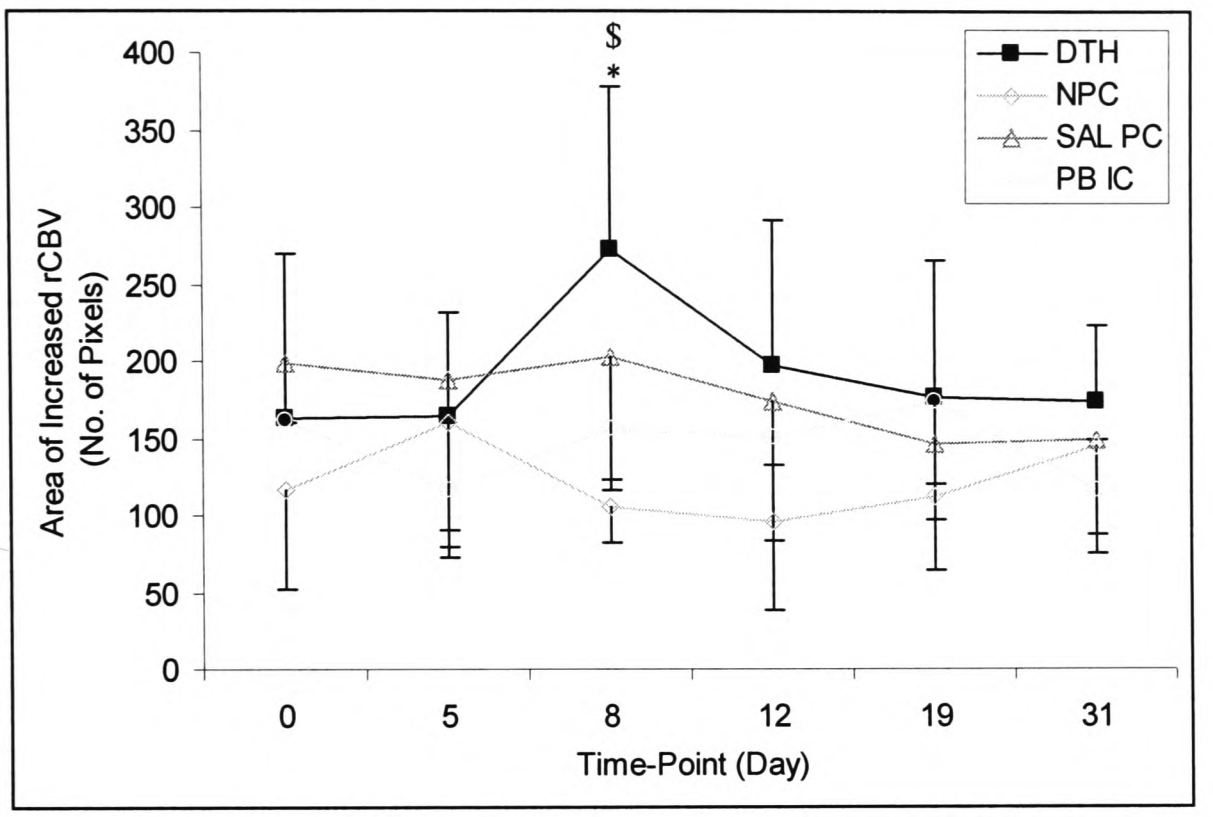


Figure 7-6: Graph to show area of increased rCBV in the injected hemisphere at time-points following peripheral challenge in DTH and control animals. (NPC, No peripheral challenge, SAL PC; Saline peripheral challenge, PB IC; Phosphate buffer intracerebral challenge). Values are expressed as mean ± S.D. (ANOVA $p=0.07$ for DTH group). *$p<0.002$ DTH v NPC, $$p<0.02$ DTH v PB IC.

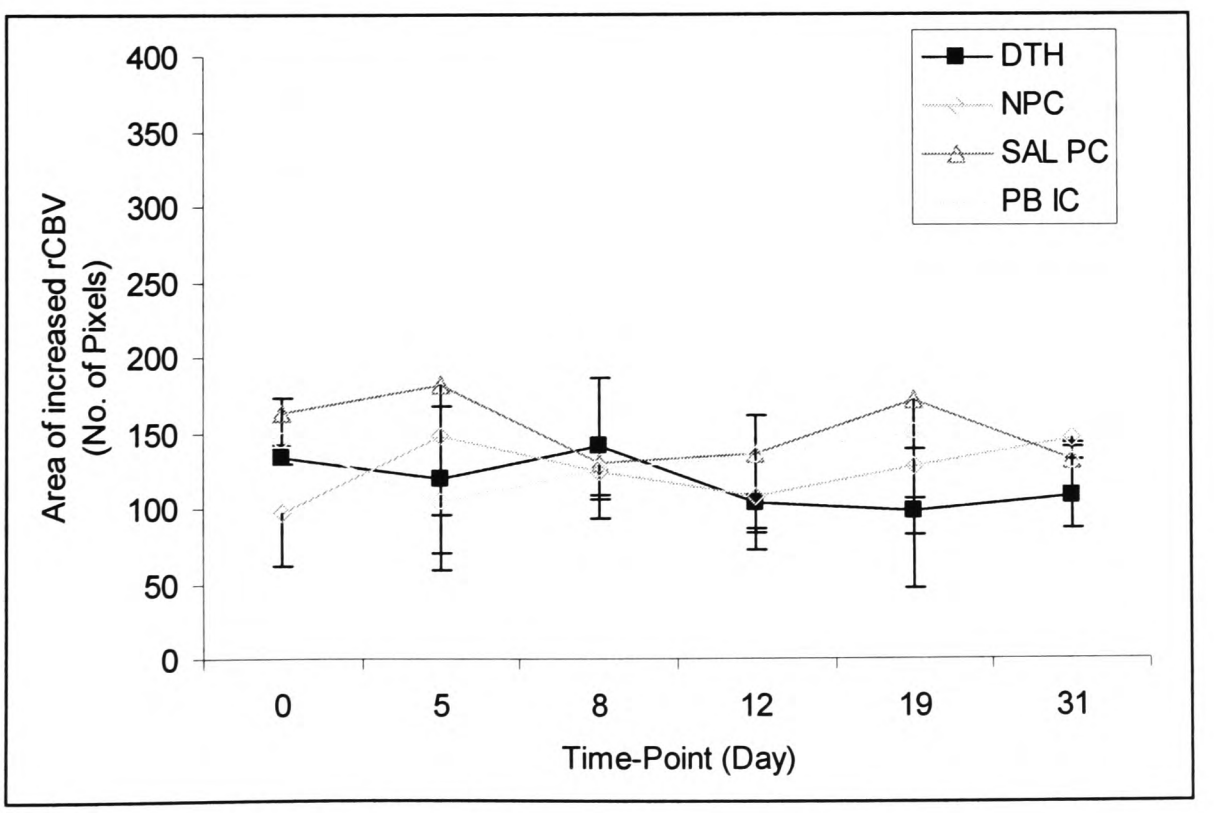


Figure 7-7: Graph to show area of increased rCBV in the contralateral hemisphere at time-points following peripheral challenge in DTH and control animals. (NPC, No peripheral challenge, SAL PC; Saline peripheral challenge, PB IC; Phosphate buffer intracerebral challenge). Values are expressed as mean ± S.D.

7.4.3 Laminin Expression

Laminin was consistently expressed throughout the brain parenchyma in all animals studied, in both ipsilateral and contralateral hemispheres (Figure 7-8). However, throughout the injected hemisphere, there was significant upregulation of laminin expression on vessels surrounding the hypercellular lesion. SAL PC controls had fewer laminin-positive vessels surrounding the lesion than DTH animals (Figure 7-9b). Another difference between SAL PC and DTH animals was that blood vessels at the interface of the hypercellular lesion with normal tissue appeared to express less laminin. In DTH animals, the lesion appeared to be defined by a rim of intensely positive stained laminin vessels. In contrast, in all control animals, the hypercellularity of the lesion appeared to be more diffuse, and laminin staining was more uniform around the lesion and throughout the injected hemisphere, rather than intensifying around the hypercellular lesion (see Figures 7-9 and 7-10). The number of vessels within the hypercellular area did not appear to differ from any controls. No differences were found between the contralateral and ipsilateral hemispheres in PB IC controls.

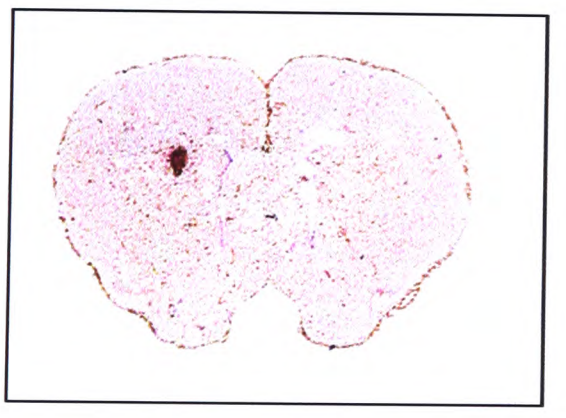


Figure 7-8: Histological section of the whole brain through the lesion site in a DTH animal at day 8, showing laminin expression throughout the brain and around the lesion site in the left hemisphere.

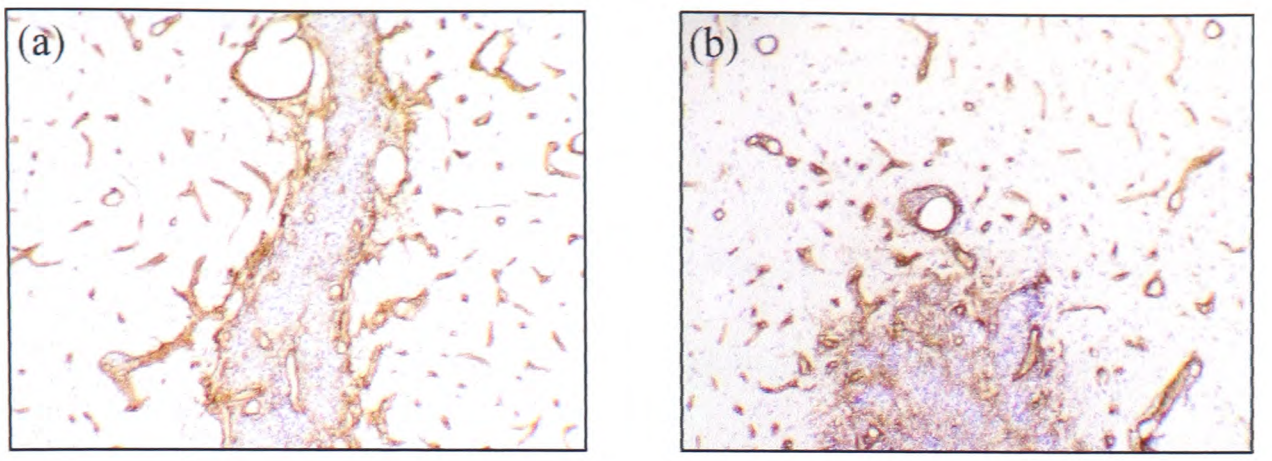


Figure 7-9: (a) Laminin expression (brown) on vessels in contact with the hypercellular lesion (purple) and also on vessels surrounding the lesion for some distance at day 8 in DTH animals (x4).

(b) Laminin expression was mainly upregulated on vessels in contact with the lesion in animals receiving a peripheral challenge of saline at day 8 (x4).

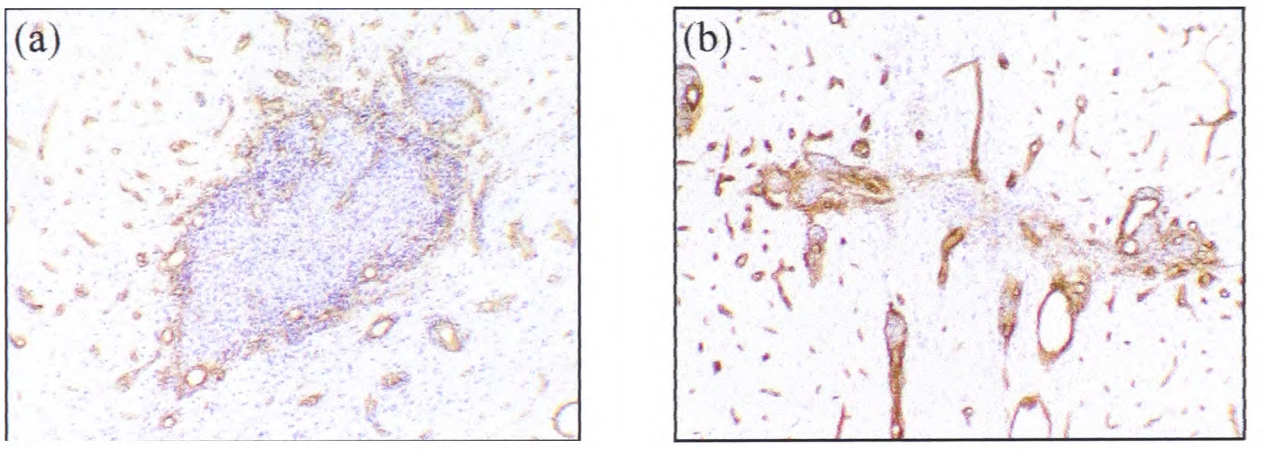


Figure 7-10: (a) Laminin expression (brown) on vessels at the interface of the hypercellular lesion (purple) and normal brain tissue appears to keep the lesion compact at day 12 in DTH animals (x4).

(b) Laminin expression around lesion in animals receiving peripheral challenge of saline also at day 12 indicating the less compact nature of the lesion (x4).

7.4.4 Cresyl Violet Blood Vessel Mapping

Large blood vessels were identified on various sections of Cresyl Violet histology throughout the lesion. In DTH animals, blood vessels throughout the injected hemisphere were considerably dilated, and could be mapped spatially on to the rCBV maps acquired at the same time-point (Figure 7-11). In the majority of cases, dilated blood vessels corresponded spatially to areas of increased rCBV visible on the thresholded maps.



Figure 7-11: Maximal increases in rCBV occur at day 8 in DTH animals, and dilated blood vessels (red) visible on Cresyl Violet stained sections can be spatially mapped onto areas of increased rCBV (white) on thresholded rCBV maps (see methods).

7.4.5 Correlations with other MRI Parameters

The parameters associated with rCBV increases (unthresholded and thresholded rCBV intensity, rCBV area) were investigated for correlations with other MRI parameters investigated in previous chapters. The full correlation graphs are given in Appendix F.2. No correlation was found between the rCBV increases (neither areas or intensities) and any of the MRI parameters investigated in previous chapters (Table 7-3).

MRI Parameter	Correlation
Area T_1 hypointensity	×
Area of T_2 hypointensity	×
Area of T_2 hyperintensity	×
Total area of T_2 signal change	×
Area of BBB breakdown	×
Area of ADC hypointensity	×
Area of ADC hyperintensity	×
Total area of ADC change	×

Table 7-3: Summary of correlation analysis between increases in rCBV and other MRI parameters obtained in previous chapters (T_1 and T_2 parameters from Chapter 5, BBB and ADC parameters from Chapter 6).

7.4.6 Correlations with other Histopathological Findings

No correlation was found between areas of increased rCBV and macrophage recruitment, T & B lymphocyte recruitment, MHC class II expression, or reactive astrocytes.

7.5 Discussion

In this chapter, it has been demonstrated that an increased regional cerebral blood volume (rCBV) occurs early in the progression of the DTH lesion. This increased rCBV intensity occurs maximally at day 8, preceding maximal changes in BBB permeability. After this time-point, the rCBV returns to levels observed in the naïve rat brain. The increased rCBV spatially correlated with dilated blood vessels, and a relationship was found between laminin expression and increased rCBV.

7.5.1 CBV changes

The rCBV findings presented in this chapter are in good agreement with those published recently regarding a clinical study of MS (Haselhorst 2000). An increase in rCBV was found in acute lesions, which subsequently decreased as the lesions became more gliotic. These increases were observed in enhancing lesions, and a correction was made to the CBV calculations for gadolinium leakage owing to BBB breakdown (Haselhorst 2000). It should be noted, however, that the increases observed in the current study *preceded* maximal contrast enhancement of the DTH lesion, which occurred at day 19 (see Chapter 6), a time-point which was much later than the time-point at which maximal rCBV changes occurred (day 8). If gadolinium leakage was the underlying cause of the increased rCBV, then maximal rCBV changes would have occurred at day 19, the time-point at which contrast enhancement was maximal. Furthermore, the increases in rCBV were found at a distance from the lesion *per se*, indicating that leakage of gadolinium from the lesion into the brain parenchyma did not give rise to the increased rCBV in the injected hemisphere. In addition, the current findings contrast with the Haselhort's clinical study where increased rCBV was found within the lesion itself (Haselhorst 2000).

Thus, two important novel findings emerge from this study, firstly that maximal rCBV increases precede significant contrast enhancement, and secondly that rCBV changes do not occur within the lesion itself, but around it, in normal appearing tissue.

Similar increases in rCBV have been found in other examples of widespread inflammation, such as HIV infection in the human brain (Tracey 1998). However, in the current work, maximal increases in rCBV occurred before significant contrast enhancement, which has not been previously reported. In addition, the current results agree with the sole animal study of rCBF in the EAE model of MS in the literature (Juhler 1986). However, once again the increased rCBF were detected within the EAE lesions, and at a time when contrast enhancement generally occurs (Namer 1992). It is unlikely, therefore, that those increases in rCBF occurred before contrast enhancement, although the authors hypothesise that the CBF changes could arise as an early event before the onset of clinical signs and histopathological changes. This highlights one of the limitations of the EAE model, in that until a lesion is gadolinium enhancing, the precise location of the lesion is unknown, as they can occur at any site in the brain. This feature makes it more difficult to investigate pre-lesional changes that may occur prior to enhancement.

Interestingly, in EAE, decreases in rCBF were also observed in the cortex (Juhler 1986). Here, in the DTH model, no evidence of a decreased rCBV was found at any site within the brain parenchyma. It was difficult to investigate the cortex in the injected hemisphere in this study, owing to the nature of the imaging sequence used. A heavily T_2* weighted gradient echo sequence was used, which is susceptible to artefacts arising from boundaries between air and tissue, such as that which occurs at the site of the burr hole in the animal's skull. The slice position throughout the MRI experiment was directly through this burr hole. As a consequence, a small region of signal loss was often

observed in the cortex underlying the burr hole on the T_2*-weighted images, thus precluding the rCBV measurements in that region. Development of a spin-echo sequence to measure CBV in these animals would allow investigation of cortical CBV.

Apart from the very small number of studies discussed above, the early rCBV results reported here are different to the majority of work published regarding blood volume and perfusion data in MS patients, where a reduced rCBV is reported (Jensen 1995), (Petrella 1997). Clinical studies are often only carried out after the observation of contrast-enhancing lesions, which define an MS lesion; therefore investigation of early blood flow and perfusion alterations prior to enhancement is difficult. The advantage of the DTH model, is that lesion progression can be followed from lesion induction through contrast-enhancement into the chronic stage, thus allowing investigation of MRI changes, such as perfusion, that may precede contrast-enhancement.

It has been shown that there is a positive correlation between reductions in rCBV and behaviour of lesions on T_2-weighted images during inflammatory processes occurring within the human brain (Blinkenberg 1999), (Hendrickse 2002), (unpublished observations from group colleagues). However, in this study, no significant correlations were found between increased rCBV and other MRI parameters. This may be because the areas of increased rCBV are spatially distinct from the changes that occurred on T_2-weighted images (Chapter 5) and ADC maps (Chapter 6). Furthermore, in this work only qualitative T_2-weighted images were acquired. Acquisition of T_2 maps in association with rCBF measurements might enable a more rigorous analysis of the relationship between rCBV changes and T_2 relaxation times.

Previously, intracerebral injection of the cytokine IL-1β has been shown to cause increased rCBV in the injected hemisphere (Blamire 2000). Further, in an unpublished

study, IL-1β has been found to be upregulated in the DTH lesion. In contrast to the study by Blamire et al., the DTH lesion lacks neutrophil recruitment, suggesting that IL-1β production within the lesion may, only in part, be responsible for the increased rCBV observed in this study.

7.5.2 Blood Vessel Dilation

Spatially, dilated blood vessels in the lesioned hemisphere correlated with areas of increased rCBV. In addition, laminin expression was upregulated throughout the injected hemisphere. Laminin is recognised by the β-integrins that are constitutively expressed on endothelial cells. Inflammatory cytokines such as IL-1β, induce changes in the levels and distribution of endothelial integrins (Sobel 1998). As mentioned above, unpublished data from the DTH model has shown that there is upregulation of specific cytokines in the DTH lesion, including IL-1β. Thus, it follows that one would expect to see an upregulation of laminin expression in and around the DTH lesion as a result of the effect of this cytokine on integrin expression. Although this is what was observed in this study, the major difference between DTH and SAL PC animals, was the less intense staining at the perimeter of the hypercellular lesion in the control animals. General expression of laminin around the lesion may have been brought about during the acute inflammatory response, causing laminin upregulation, affecting vessel structure without altering blood volume. The differences between intensity of staining at the edge of the hypercellular area may be brought about by greater inflammatory cell recruitment to the DTH lesion following peripheral challenge, and the continual cytokine expression. In contrast, lesions in control animals are likely to exhibit lower levels of cytokine expression, or to have stopped production entirely at the end of the acute inflammatory response that occurs after the initial intracerebral BCG injection.

Here, it was also qualitatively shown, that there is an increase in the number of blood vessels surrounding the DTH lesion, though quantification was difficult due to the variability in laminin staining. Immunohistochemistry was carried out at different times, and on tissue of different ages; these factors amongst others, affect antibody binding. In EAE, increases in rCBF were found to histologically correspond to areas of perivascular lymphocyte accumulation (Juhler 1986), and the results presented in this study disagree with these results. Here, it was found that dilated blood vessels could be spatially mapped to regions of increased CBV, rather than the areas of perivascular cell recruitment, which in this work is restricted to the hypercellular lesion.

7.5.3 Summary

In summary, this work has demonstrated that rCBV is increased during the progression of an MS-like lesion. The increases occur early in DTH lesion progression, and subsequently decrease as the permeability of the BBB increases and the lesion progresses. Such acute increases in rCBV have not been previously reported, either in MS or EAE. Dilated blood vessels in the injected hemisphere appear to map spatially to specific areas of increased rCBV. The results presented in this chapter suggest that monitoring regional changes in perfusion may be valuable in detecting early inflammatory events in the brain that are not associated with BBB breakdown. This approach may be particularly beneficial in the diagnosis and treatment of MS.

Chapter 8

Reactivation of the DTH Lesion

8.1 Introduction

8.1.1 Overview

Relapsing-remitting MS, which is the type of MS displayed by the majority of MS patients (85%), is characterised by the evolution of clinical symptoms over time, which may subsequently stabilise allowing the MS patient to recover. It has been postulated that numerous exogenous events, including infectious agents, are trigger factors for exacerbation and relapses of MS. The frequency of MS relapses widely varies, though on average it appears to be 0.8-1.0 relapses per annum. However, several decades may pass before a further relapse occurs, (for review see McDonald et al. (McDonald 1999)). The time-course of each relapse is characterised by worsening of clinical symptoms usually increasing from onset to reach a maximum after one or two weeks. After a few further weeks, the MS patient may recover and will continue to do so for a couple of months. Early in the progression of RR-MS full recovery from relapses generally occurs. Later on, however, as the residual neurological deficit accumulates, full recovery from relapses is less likely (McDonald 1999). A wide variety of pathophysiological events may underlie exacerbations or relapses, including demyelination, oedema, defects in synaptic transmission, and impairment of conduction (Buljevac 2002).

8.1.2 Clinical Studies of Exacerbation

In 1985, Sibley et al. published a prospective clinical study showing that minor infectious illnesses, presumably those that were viral, were potent triggers of MS relapses; i.e. the formation of new lesions were higher in the presence of viral infections of the respiratory or gastrointestinal tracts (Sibley 1985). In this landmark paper, it was also shown that urinary tract infections did not trigger relapses, although subsequently it has been shown that in 35% of MS patients, relapse of symptoms appeared to be triggered by a urinary tract bacterial infection (Rapp 1995). Later, another study was published, in which it was shown that treatment of MS patients with Interferon-γ (IFN-γ) precipitated exacerbations of MS (Panitch 1987). This finding led to the hypothesis that infectious agents were causing relapses via cytokine release, such as IFN-γ or Tumour necrosis factor-α (TNF-α). It was suggested that these cytokines were then acting on the immune system to enhance or induce an auto-reactive response to CNS antigens (Panitch 1987), by facilitating the entry of activated T cells into the CNS leading to exacerbation of the MS lesion.

To date, only two MRI studies have been carried out investigating the effect of peripheral infection in MS, in the first study it was shown that the volume of enhancing lesions was increased during viral respiratory infections (Edwards 1998). In the second, very recent, study investigating the relationship between infections and MS exacerbations, it was found that exacerbation caused worsening of clinical symptoms at the time of infection (Buljevac 2002). Furthermore, this study found that infection-related exacerbations were associated with a prolonged neurological deficit, but it was also found that there was no increase in the number of gadolinium enhancing lesions following infection.

8.1.3 The Infectious Hypothesis

Infectious agents are well known to rapidly expand the pool of immune cells that recognise the invading pathogen (Wucherpfennig 2001). An increase in the population of cells that recognise other antigens including those that react to self-proteins, e.g. MBP may be sufficient to cause disease. Persistent infection in the CNS is likely to provide an environment leading to activation of auto-reactive T cells, which contribute to the pathogenesis of chronic disease such as MS. If an infectious agent can persist and amplify the immune response, it can modify the expression of a T cell mediated autoimmune disease in an organ specific manner (Du 2002), such as in the CNS.

However, since the publication of the early papers by Sibley et al. and Panitch et al. discussed in the previous section, little firm evidence has been obtained to support the role of an infectious environmental trigger in MS relapses.

Some evidence for an environmental factor in MS has derived from studies of migrating populations, small epidemics and variation in prevalence with degrees of latitude. The prevalence of MS in northern Europe and the northernmost USA is greater than in southern Europe and southern USA (Elian 1993), (Elian 1990), (Gonzalez-Scorano 1999). Analysis of MS epidemics provides further support for the infectious hypothesis. In some islands, such as the Faroe Islands, MS was absent until World War II when cases began to rapidly develop with the introduction of British troops (Kurtzke 2001). This observation has led to the suggestion that MS may be triggered by a sexually transmitted infection (Hawkes 2002). Another supporting factor for the infectious hypothesis is elevated IgG levels in the cerebrospinal fluid of MS patients. High immunoglobulin G (IgG) levels are observed in CNS disorders of infectious origin, where they are directed towards the agent that caused the disease (Gilden 1999).

It has also been inferred that peptidoglycan, a component of bacterial cell membranes, is a mediator of sterile CNS inflammation in MS patients, in the apparent absence of bacteria. The mechanism is thought to result from T cell activation and local cytokine production. This finding suggests that this antigen may be a mediator of inflammation and exacerbation in the MS brain (Schrijver 2001).

8.1.4 Mechanisms behind Infection

Several possible mechanisms have been formulated to explain the theory behind the infectious hypothesis. One such mechanism is molecular mimicry, where cross-reactivity with myelin triggers MS, and epitope spreading in which tissue destruction results in presentation of previously sequestered self-antigens to auto-reactive T cells that are not specific for that organism (Schiffenbauer 1998), (Haring 2002). During molecular mimicry some T cells and antibodies that are elicited in response to antigens of the infectious agent also recognise relevant self-antigens in the CNS thereby initiating the destructive autoimmune process. This hypothesis has been shown in EAE (Lenz 2001), where a *Chlamydial pneumoniae* peptide (with homologous sequences with MBP) was able to induce EAE by the interaction of the homologous peptides with MHC class II gene products. Epitope spreading, has been shown to be important in the progression of myelin destruction in EAE and Theiler's Murine Encephalomyelitis virus (TMEV) (Miller 1997). Another potential mechanism behind the infectious hypothesis is that highly activated T cells responding to an unrelated infection, enter sites of chronic inflammation. Interactions between activated T cells, resident cells, and soluble mediators at the site of inflammation may result in bystander pathology (Haring 2002). Furthermore, infection may result in inflammation, leading to the secretion of a cascade of immunostimulatory cytokines, resulting in activation of diverse T cells populations, including those directed to auto-antigens (Birnbaum 1998). A further possibility is that

infections result from immune responses to families of endogenous proteins present in both the infectious organism and the host. The primary example of this would be heat shock proteins (HSP's) (Birnbaum 1998) since they are the immunodominant proteins of many bacteria. HSP's are expressed by microglia and oligodendrocytes at sites of inflammation, and have been shown to be present in the CNS of MS patients (for review see Birnbaum et al. (Birnbaum 1997)).

8.1.5 Animal Studies

A small number of studies carried out in EAE, have shown that bacterial enterotoxins can cause relapses of paralysis (Schiffenbauer 1993), (Brocke 1993). Injection of bacterial DNA into both TMEV and EAE models has been shown to exacerbate clinical symptoms (Tsunoda 1999). In contrast, EAE mice housed in specific pathogen free (SPF) surroundings suffer more severe relapses than those housed conventionally (Birnbaum 1998). It has been hypothesised that conventionally housed mice are frequently exposed to infectious agents, leading to a relative skewing of the immune response towards a Th2 phenotype, which is associated with milder and fewer relapses of EAE (Birnbaum 1998). In agreement with the cytokine-based hypothesis of MS relapse, administration of the cytokine IL-12 has been shown to exacerbate EAE and induce paralytic relapse when administered after recovery of clinical symptoms (Smith 1997). Furthermore, the clinical score of EAE in a mouse is worsened when infected with *Chlamydia pneumonia* (Du 2002), which is in accordance with clinical studies.

Despite clinical studies suggesting a link between infection and MS relapses, little experimental study has been undertaken to investigate the underlying neuropathology. Furthermore, the question still remains as to whether infections cause reactivation or enlargement of lesions, or cause development of new lesions, without exacerbating

neurological symptoms. Using MRI in association with an animal model, such as the DTH model, gives the unique ability to investigate the impact of a systemic inflammatory process on lesion evolution.

8.2 Aims of this Chapter

The aim of this Chapter was to determine the effect of a peripheral systemic inflammation, by bacterial lipopolysaccharide endotoxin on a DTH lesion once the primary inflammatory response has resolved. In order to reduce the time taken to initiate the DTH response, a modified spontaneous form of the DTH model was developed. In this model, a DTH-type lesion is induced at time of intracerebral BCG injection. Owing to these modifications, the acute inflammatory response was characterised using MRI to ensure it was consistent with the original DTH model and to determine when the lesion is largely resolved. In addition to T_1- and T_2-weighted imaging, diffusion-weighted, magnetisation transfer and perfusion imaging, T_1-, T_2- and T_2*- mapping was used to obtain quantitative measures on these parameters, since in earlier chapters, only qualitative data was acquired.

8.3 Methods

8.3.1 Experimental Model

A modified version of the previously described (Chapter 4) DTH model was used in this study. $5x10^5$ heat-killed BCG organisms in 1.5µl of 0.1M phosphate buffered saline were injected stereotaxically into the left striatum of three-week-old male Lewis rats (Charles River), weighing 100g. The BCG organisms were deposited at three sites; 0.5µl was injected at a depth of 4.0mm, 0.5µl at a depth of 3mm, and 0.5µl at a depth of 2mm. This modification resulted in a larger lesion spanning the striatum, which facilitated MRI investigation. In addition, 0.2µl of BCG organisms were deposited on the cortical surface of the brain to induce a spontaneous DTH response at the site of intraparenchymal BCG deposit. Injections were performed slowly over a period of 15 minutes to minimise damage caused by the injection *per se*. Surgery was performed under isoflurane-induced anaesthesia (0.8–1.5% isoflurane in 70% N_2O/30%O_2), and temperature was maintained throughout surgery via a homeothermic heating system (Harvard Apparatus Ltd, UK). Six weeks after the intracerebral injection, when the acute inflammatory response had mostly subsided, animals were anaesthetised with 1.5% isoflurane in 70% N_2O/30%O_2. 100µg of *E coli* endotoxin (LPS) in 1ml saline was injected intraperitoneally.

8.3.2 Experimental Groups

In addition to DTH animals injected with LPS, three groups of control animals were set up as detailed in Table 8.1; controls SAL PC received a peripheral challenge of sterile non-pyrogenic saline, controls NPC received no peripheral challenge. In addition, a group of naïve animals were imaged to determine the effect of age on MRI parameters; these animals received no intracerebral injection of BCG and no peripheral challenge.

SAL PC controls appeared to show some signs of exacerbation on post-contrast T_1-weighted images post-LPS challenge, albeit less than the LPS-challenged group. It was thought that repeated anaesthesia, and tail line insertion might have caused a low level of peripheral immune system activation in these animals. Post-mortem studies on animals that died due to unforeseen circumstances during the MRI protocol revealed congestion in the respiratory tract. If this was the scenario in the SAL PC control animals, repeated gaseous anaesthesia is likely to exacerbate this respiratory irritation, and act as natural peripheral inflammation, (instead of LPS). A further possibility is that repeated tail line insertion results in low level systemic activation of the inflammatory response, particularly during the very intensive imaging period occurring pre-challenge, six hours and 24 hours post-challenge. Consequently, in the NPC group, pre-challenge imaging was kept to a minimum to reduce the number of anaesthetic periods and tail line insertions. It was also thought that the saline peripheral challenge itself may have induced a low level of peripheral activation, and therefore this was omitted from the NPC controls. LPS and control animals were sacrificed for histology at 10 days post-challenge.

Experimental Group	Intracerebral Injection	Peripheral Challenge
LPS	BCG	LPS
Controls SAL PC	BCG	Saline
Controls NPC	BCG	n/a
Naïve	n/a	n/a

Table 8-1: Summary of different experimental groups used in this chapter.

8.3.3 Magnetic Resonance Imaging

Animals were anaesthetised with 2.5% isoflurane and were placed in a purpose-built head restraint system consisting of a bite bar and nose strap, integral to the MR coil, and then placed in the magnet. Anaesthesia was maintained in the magnet using 0.7-1.5%

isoflurane in 70% N_2O/30%O_2. The temperature of the animals was monitored using a rectal probe and maintained at 37°C using a circulating warm water system and heart rate was monitored throughout using a custom-built cardiac monitoring system.

Once the animals were in the magnet, a coronal scout image was acquired, using a fast spin-echo T_2-weighted sequence. From this scout, a horizontal image was positioned and acquired through the injection site 3.5mm below the surface of the brain. A single coronal slice centred on the injection site was selected for the full imaging protocol.

8.3.3.1 T_1- and T_2-weighted imaging

T_1- and T_2-weighted images were acquired using a spin-echo and fast spin-echo sequence respectively, using the parameters in Table 8-2. T_2-weighted images were acquired in both the transverse and coronal planes to aid positioning.

Parameter	T_1-weighted	T_2-weighted	
Slice Orientation	**Coronal**	**Transverse**	**Coronal**
Repetition time	0.5 sec	3.0 sec	3.0 sec
Echo time	0.013 sec	0.0375 sec	0.0375 sec
Field of view	3.5 x 3.5 cm^2	3.5 x 3.5 cm^2	3.5 x 3.5 cm^2
Slice Thickness	1 mm	2 mm	1 mm
Number of Averages	4	1	1
Total acquisition time	4 min 22 sec	1 min 15 sec	1 min 15 sec

Table 8-2: Summary of parameters used in the acquisition of T_1- and T_2-weighted images.

8.3.3.2 Quantitative T_1 and T_2, and T_2*-mapping

Quantitative T_1, T_2, and T_2*-mapping was carried out using the parameters in Table 8-3. T_1 maps were calculated from a series of images acquired using an inversion recovery sequence described in Chapter 3 with the inversion times summarised in Table 8-3. T_2 maps were calculated from a series of images acquired with a spin-echo sequence and

varying echo times (see Table 8-3). Standard Varian software was used to calculate the T_1 and T_2 relaxation times on a pixel-by-pixel basis. T_2* maps were created using in-house software (Dr Andrew Blamire) from images that were acquired using a gradient echo sequence and a range of echo times (see Table 8-3).

Parameter	T_1 map	T_2 map	T_2* map
Repetition time (TR)	5.025, 5.25, 5.5, 5.75, 7, 10 sec	3 sec	0.1 sec
Inversion Time	0.025, 0.25, 0.5, 0.75, 2, 5 sec	N/A	N/A
Echo time (TE)	0.015 sec	0.02, 0.04, 0.06 sec	0.008, 0.012, 0.016, 0.02, 0.026, 0.032 sec
Field of view	3.5 x 3.5 cm^2	3.5 x 3.5 cm^2	3.5 x 3.5 cm^2
Slice Thickness	1 mm	1 mm	1 mm
Number of Averages	1	1	1
Total acquisition time	12 min 34 sec	19 min 16 sec	1 min 16 sec

Table 8-3: Summary of parameters used in the acquisition of images for the creation of T_1, T_2 and T_2* maps.

8.3.3.3 Diffusion-weighted imaging

Diffusion-weighted images were acquired using a pulsed-gradient spin-echo sequence (Stejskal 1965), with three diffusion-weighting ("b") values (b is defined as $b = (\gamma G\delta)^2[\Delta - \delta/3]$, where G is the diffusion gradient strength, diffusion time (Δ) and the diffusion gradient duration (δ). Diffusion gradients were applied on all three axes sequentially, using the parameters in Table 8-4. Navigator echo correction was used to reduce motion artefacts (Ordidge 1994).

Parameter	Value
Gradient b Values	125, 500, 1000 $s.mm^{-2}$
Diffusion Gradient Duration (δ)	0.0125 sec
Diffusion gradient Separation (Δ)	0.0175 sec
Repetition time (TR)	2.0 sec
Echo time (TE)	0.0365 sec
Field of view	3.5 x 3.5 cm^2
Slice Thickness	1 mm
Number of Averages	1
Total acquisition time	12 min 51 sec

Table 8-4: Summary of parameters used in the acquisition of diffusion-weighted images for the creation of ADC trace maps.

8.3.3.4 Magnetisation Transfer (MT) imaging

MT maps were created from pairs of images acquired with and without magnetisation saturation, according to the equation (Mo-Ms)/Mo x 100%, (where Ms is the magnitude of signal when the saturation pulse is applied, and Mo is the magnitude of signal without the saturation pulse), (Dousset 1992). The parameters are listed in Table 8-5.

Parameter	Values
MT Pulse Length	32 msec
No of MT Pulses	12
Repetition time (TR)	1.5 sec
Echo time (TE)	0.013 sec
Field of view	3.5 x 3.5 cm^2
Slice Thickness	1 mm
Number of Averages	1
Total acquisition time	6 min 28 sec

Table 8-5: Summary of parameters used in the acquisition of magnetisation transfer data.

8.3.3.5 CBV Imaging

rCBV maps were generated from time-series images acquired during bolus injection of contrast agent and tracer kinetic analysis (Rosen 1990). A series of 40 FLASH images were acquired at a rate of approximately 1 image per 1.275 seconds. Following acquisition of 8 baseline images, a 100μl bolus of a gadolinium-based MRI contrast agent (Omniscan, Nycomed Amersham, UK) was injected via a tail vein over a 4 second period. Table 8-6 shows the parameters used for the acquisition of these images.

Parameter	Value
Repetition time (TR)	0.02 sec
Echo time (TE)	0.01 sec
Field of view	3 x 2.2 cm^2
Slice Thickness	1 mm
Number of Averages	1
Total acquisition time	51 sec

Table 8-6: Summary of parameters used for the acquisition of FLASH images for the creation of rCBV maps.

8.3.3.6 Imaging BBB Permeability

To assess BBB permeability, T_1-weighted images were acquired 10 minutes after the injection of a gadolinium-based contrast agent to identify areas of signal enhancement. The parameters used for acquisition of these T_1-weighted images are given in Table 8-3.

8.3.4 Experimental Protocol

MRI measurements were performed in each animal, at each time point in the following order: T_1-weighted, T_2-weighted, proton density and magnetisation transfer imaging, T_1-, T_2-, and T_2*-mapping, and diffusion-weighted imaging. Subsequently, rCBV data and post-contrast T_1-weighted images were acquired. Evaluation of all images acquired over the time course enabled determination of the temporal evolution of changes within the lesion. The total examination time was approximately 1 hour 45 minutes. MRI was performed on the day of intracerebral injection of BCG (day 0, n=7), and subsequently at days 1 (n=19), 5 (n=16), 19 (n=12) and 42 (n=16) post-intracerebral injection. LPS-challenge was given at day 42. Post-LPS challenge, MRI was performed at 6 (n=11), 24 (n=9) and 72 (n=5) hours. SAL PC control animals (n=4) were imaged at the same time-points as LPS-challenged animals, however, NPC control animals (n=3) were not imaged at day 19 to reduce the frequency of anaesthesia exposure and tail line insertion in an attempt to reduce the risk of peripheral infection.

8.3.5 Enzyme Linked Immunosorbent Assay (ELISA)

A separate group of animals were set up to investigate cytokine concentrations at times when CBV changes were maximal, (days 1 and 19 post-intracerebral injection). The concentrations of IL-1β and TNF-α in brain tissue were determined by ELISA. Tissue

samples were homogenised in phosphate buffer containing a cocktail of enzyme inhibitors and prepared for ELISA, as described in Section 3.4.3. The supernatants were assayed according to the IL-1β ELISA kit instructions (R&D), as given in Section 3.6.5.

8.3.6 Immunohistochemistry

10 days post-LPS challenge some animals were terminally anaesthetised and transcardially perfused with 0.9% NaCl solution, as described in Section 3.6.2, to enable histology and immunohistochemistry to be carried out, again as described in Section 3.6.3.

8.3.7 MRI Data Analysis

Apparent diffusion coefficient (ADC) maps were generated from diffusion-weighted images (Basser 1994). A crude measure of anisotropy was calculated as described in Section 6.3.4. Maps of rCBV were created and analysed as described previously in Section 7.3.4. ROI's were drawn around the injected and non-injected hemispheres to obtain mean signal intensities and areas of brain with increased signal intensity were identified using the thresholding method. Results were expressed as ratios of left/right in order to assess hemispheric differences. BBB permeability was assessed by comparing pre- and post-contrast T_1-weighted images; these images were clustered using cluster analysis, described in Section 3.8.2. Each cluster was then defined as a region of interest (ROI) and was superimposed onto the original T_1-weighted image to quantitatively investigate changes in BBB permeability. These changes were quantitated both in terms of intensity, and area of signal enhancement on the post-contrast T_1-weighted images. MTR maps were created on a pixel-by-pixel basis, as described in Section 6.3.4. ROI's were drawn around the lesion visible on MTR images, and the mean signal intensity of

these ROI's was quantified and compared with analogous ROI's in the contralateral hemisphere.

8.3.8 Statistical Analysis

Variations across time-points were assessed using ANOVA, and post-hoc tests were carried out using unpaired student t tests with Welch correction. Differences between controls and DTH animals at each time-point were tested by unpaired students t tests using Graphpad Instat (Table 3-4). Differences between injected and contralateral hemispheres in the same animal were tested using paired students t tests.

8.4 Results

The modified form of the DTH model used here, resulted in a noticeable lesion spanning a large area of the injected striatum and in most animals crossing the corpus callosum. MRI was performed at intervals after intracerebral injection of BCG and also following the administration of LPS peripherally. The results from these experiments are summarised in two sections; the spontaneous DTH inflammatory response resulting from the initial BCG injection, and the inflammatory response occurring post-LPS challenge.

8.5 Spontaneous DTH inflammatory Response

8.5.1 Cerebral Blood Volume

At the time of intracerebral injection, no changes in rCBV were observed. However, 1 day after the intracerebral injection of BCG into the parenchyma, up to an 8 fold increase in rCBV was observed throughout the injected hemisphere of all animals studied (Figures 8-1, 8-2). By 5 days, however, this increase in rCBV had reduced considerably, although remained elevated when compared to naïve animals. The same pattern was reflected in the areas of elevated rCBV identified by the thresholding method, described in section 8.3.7 (Figure 8-3). ANOVA demonstrated a significant ($p<0.0001$) change in both rCBV and the area of elevated rCBV with time.

Post-hoc unpaired t-tests revealed that at 24 hours post-intracerebral injection, the rCBV was significantly different from all other time-points (day 0 $p<0.02$, day 5 $p<0.005$, day 19 $p<0.001$, day 42 $p<0.001$). In addition, post-hoc unpaired t-tests also revealed that at 24 hours, the area of elevated rCBV was significantly different from all other time-points post-intracerebral injection (day 0 $p<0.05$, day 5 $p<0.005$, day 19 $p<0.001$, day 42 $p<0.001$). Although at day 19, the rCBV in the injected hemisphere appeared to still

elevated (Figure 8-1), no significant differences were found between other time-points. Individual results are summarised in Appendix G.1.

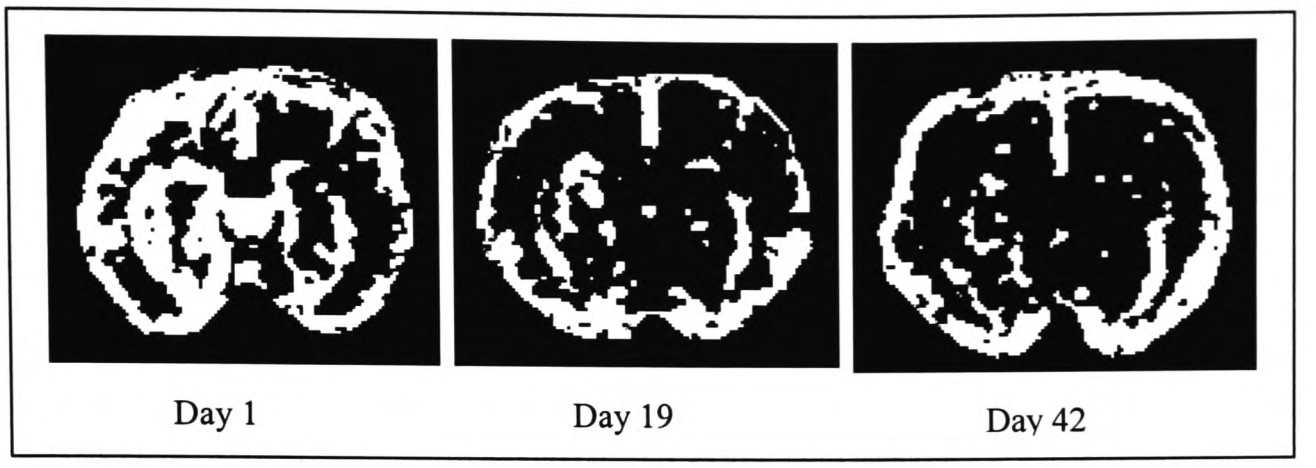


Figure 8-1: Thresholded CBV maps from 1, 19 and 42 days after intracerebral injection of BCG, showing up to 8 fold increases in rCBV 1 day after the intracerebral injection throughout the injected hemisphere.

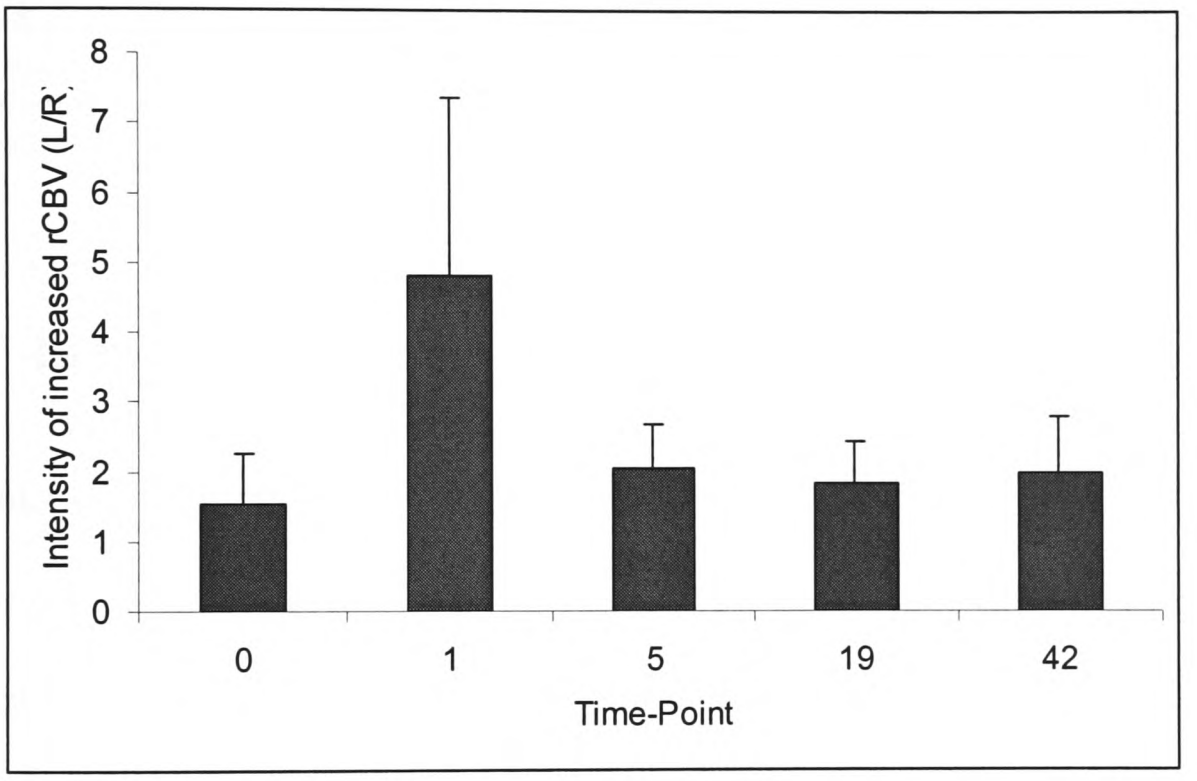


Figure 8-2: Graph to show the left/right hemispheric ratio of rCBV demonstrating large increases in rCBV 1 day after intracerebral injection of BCG. Measurements are taken from thresholded CBV maps and values are expressed as the mean ± S.D. Significant differences were found over time (ANOVA $p<0.0001$).

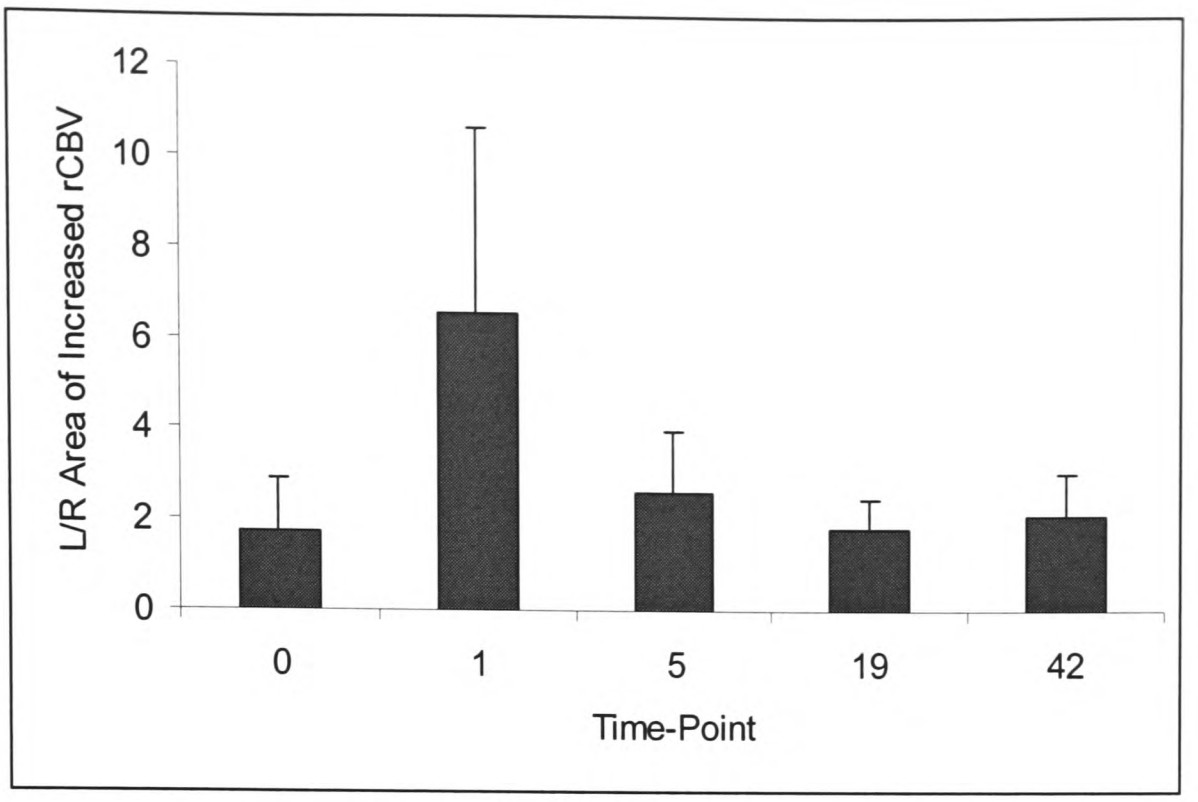


Figure 8-3: Graph to show the left/right hemispheric ratio of the areas of elevated rCBV again demonstrating the large increases in rCBV 1 day after intracerebral injection of BCG. Measurements are taken from thresholded CBV maps and values are expressed as the mean ± S.D. Significant differences were found over time (ANOVA $p<0.0001$).

8.5.2 ELISA

Previous studies published from this laboratory have shown that injection of the cytokine IL-1β, results in increased rCBV (Blamire 2000). In order to assess whether IL-1β was, at least in part, responsible for the increases in rCBV observed here, samples of cortex, striatum and injection site were analysed for the presence of IL-1β using ELISA, at days 1 and 19 after the intracerebral injection of BCG. IL-1β was readily detectable at 1 day after the injection of BCG into the brain parenchyma. Levels were far higher in the injected hemisphere, cortex and injection site than in the same regions in the contralateral hemisphere (Figure 8-4). A significant difference (paired t test $p<0.01$) was found between the left and right striatum at 1 day. The differences between the left and right cortices, and the left and right injection sites did not quite reach significance (paired t test $p=0.0930$ and $p=0.0805$ respectively). By day 19, levels of IL-1β had dropped to much lower levels.

Interestingly at day 19, the levels of IL-1β appeared to have increased throughout the contralateral hemisphere, although this only reached significance in the cortex compared to day 1 (paired t test $p<0.05$). The level of IL-1β was significantly (unpaired t test $p<0.01$) greater in the left striatum at 1 day than at 19 days, however the differences between day 1 and 19 in the left cortex did not quite reach significance ($p=0.0688$), and no difference was found between 1 day and 19 days in the injection site. Individual results are given in Appendix G.2.

The same samples were also analysed for the presence of TNF-α, and it was found that TNF-α was not present at levels that could be detected by ELISA at either days 1 or 19.

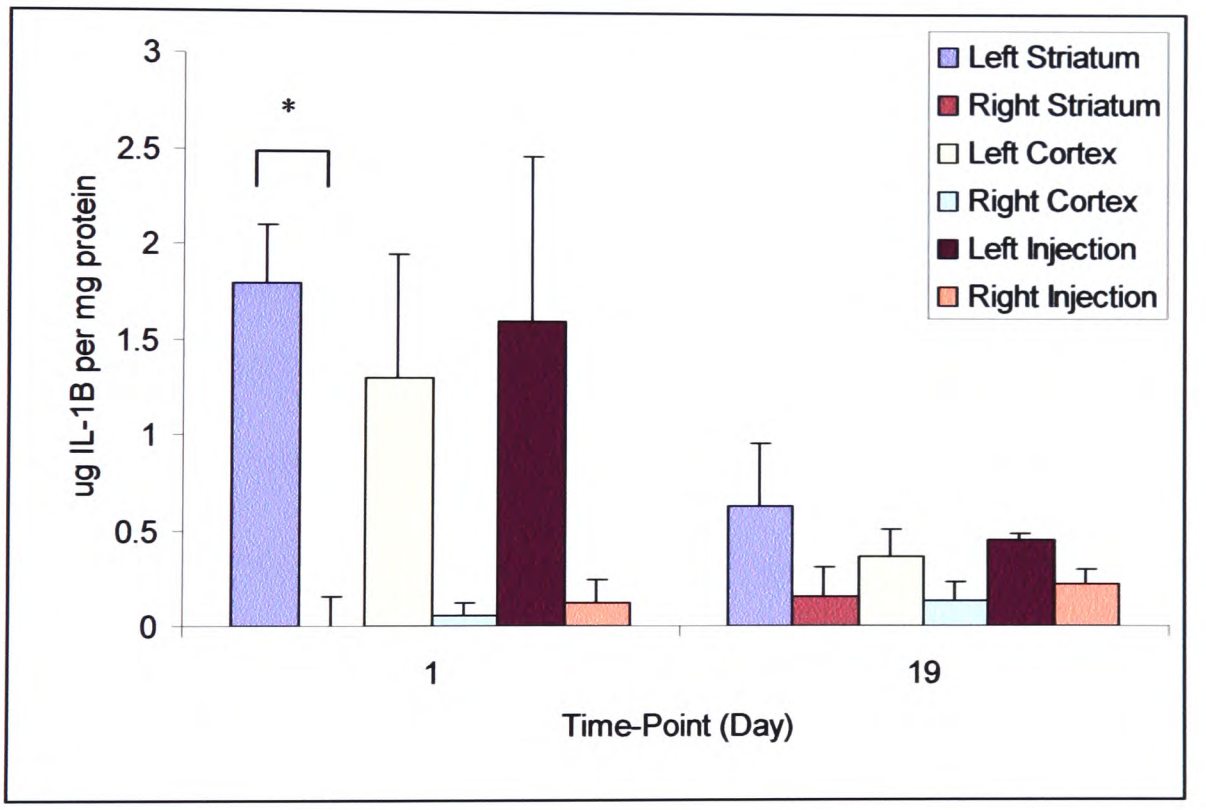


Figure 8-4: Concentration of IL-1β in the cortex, striatum and injection site 1 and 19 days after the intracerebral injection of BCG. Values are expressed as mean ± S.D. *$p<0.01$ paired t tests between injected and contralateral hemispheres.

8.5.3 Temporal Changes in T_1 Relaxation Time

8.5.3.1 Striatum

ROI's were chosen which covered the entire striatum, to obtain mean T_1 relaxation times at each time-point, since the hypointense and hyperintense regions present from day 0 (the day of intracerebral injection) at the lesion site, were difficult to separate (Figure 8-5). The T_1 relaxation time in the striatum of animals injected intracerebrally with BCG was initially longer than that observed in naïve animals (Figure 8-6), but ANOVA demonstrated a significant ($p<0.0001$) change in T_1 relaxation time over time in the injected striatum, since over time the region of increased T_1 resolved, resulting in an overall reduction in the T_1 relaxation time. A significant change over time was also observed in the contralateral hemisphere (ANOVA $p<0.005$), however, the reduction in T_1 of the injected striatum over time was more marked than that of the contralateral striatum. This is demonstrated by the observation that although the T_1 of the injected striatum appeared slightly longer than that of the contralateral striatum at 1 day, by days 19 and 42 it had become significantly shorter (paired t test $p<0.05$ and $p<0.02$ respectively). In contrast, T_1 measurements in naïve animals showed no significant differences over time and no left/right differences.

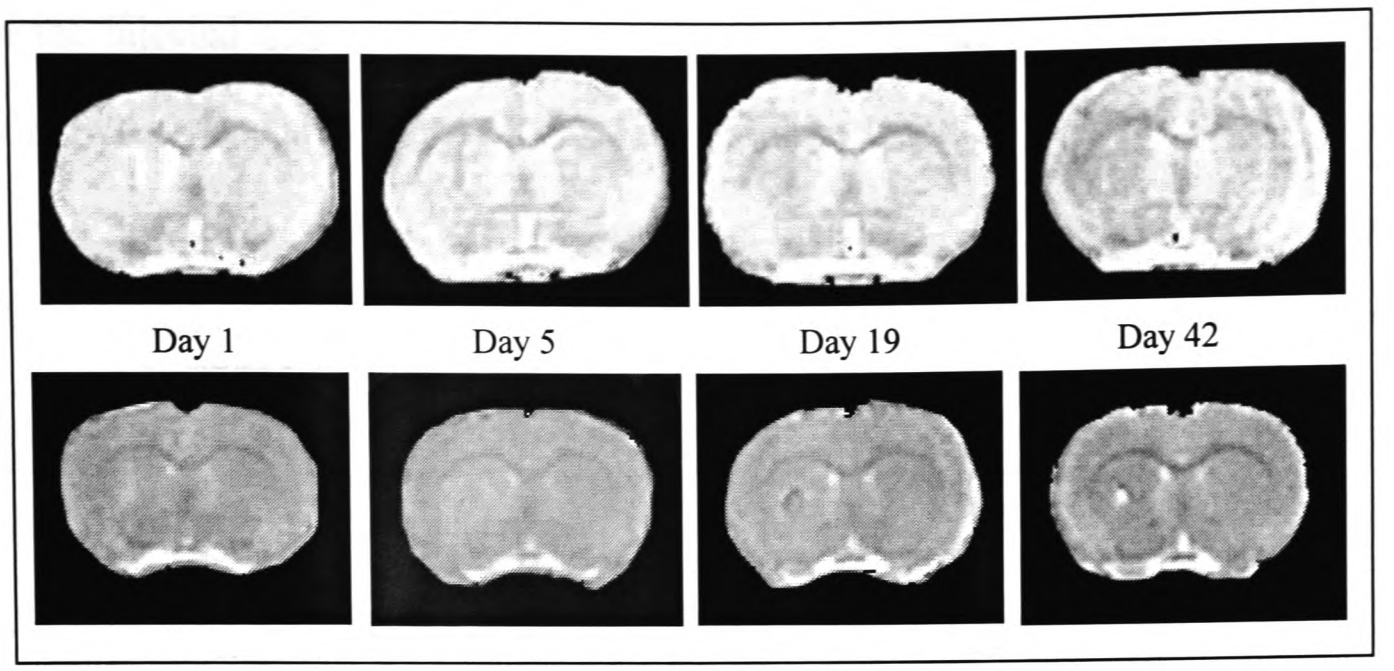


Figure 8-5: T_1 maps from two extremes of animal at days 1, 5, 19 and 42 following intracerebral injection of BCG, showing hypointense lesion site surrounded by hyperintense region at day 1 becoming less hypointense by day 42.

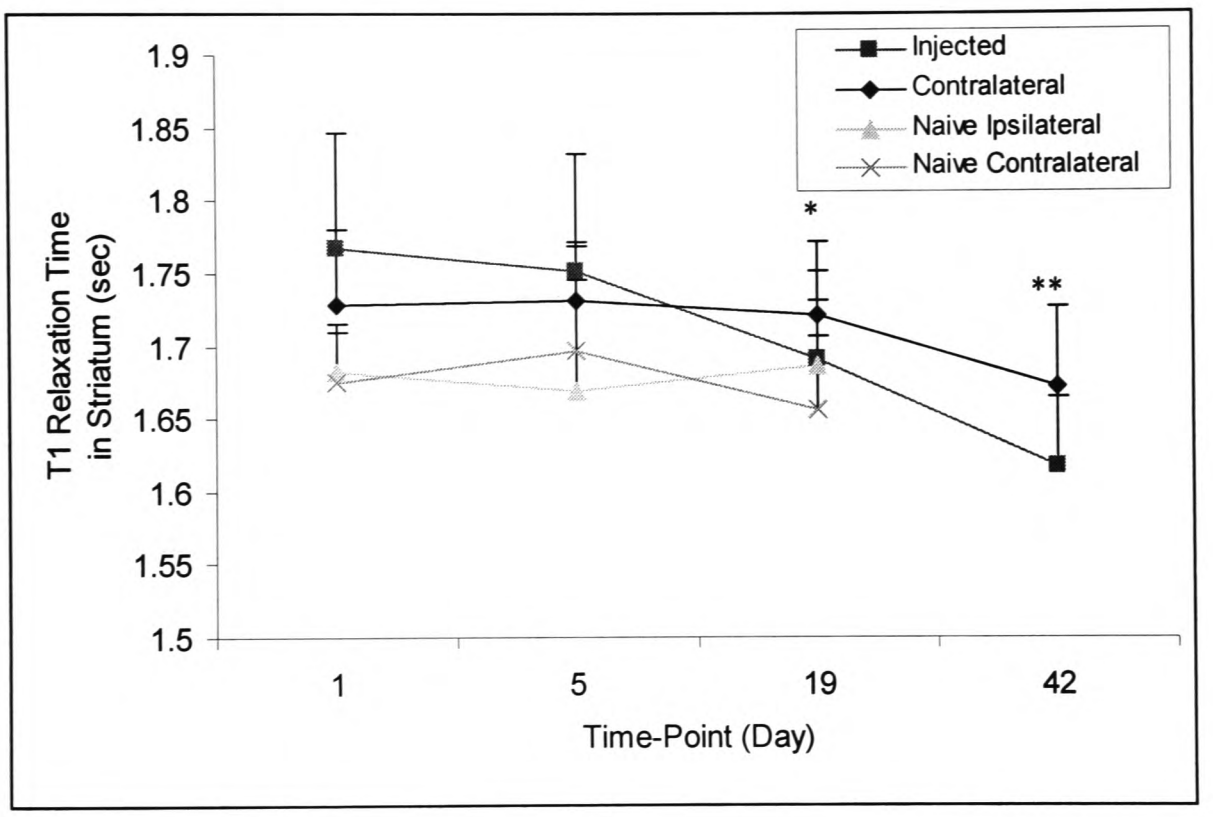


Figure 8-6: Graph to show T_1 relaxation time in the striatum after intracerebral injection of BCG. Naïve animals received no intracerebral injection. Values are expressed as the mean ± S.D. ANOVA demonstrated a significant ($p<0.0001$) change in the T_1 relaxation time over time in the injected striatum, and in the contralateral striatum ($p<0.005$). Significant differences were observed between injected and contralateral hemispheres at days 19 and 42 (paired t tests $^{**}p<0.02$, $^{*}p<0.05$ respectively).

8.5.3.2 Cortex

Compared to the striatum, the range over which the T_1 relaxation time changed in the cortex was much less. However, the T_1 relaxation time in both cortices was increased in all animals when compared to that of naïve animals throughout the acute inflammatory response (Figure 8-7). A significant (ANOVA $p<0.0001$) change in the T_1 relaxation

time in the injected cortex was found over time. At day 42, the relaxation time was significantly less (unpaired t test $p<0.001$) than at days 1, 5 and 19. In the contralateral cortex, ANOVA revealed that there was also a significant ($p<0.05$) change over time, and post-hoc unpaired t tests revealed that the T_1 relaxation time at day 42 was significantly less than at day 19 ($p<0.01$). No significant difference was found between the T_1 relaxation time between the injected and control hemispheres at any time-points before day 42. However, at day 42, the T_1 relaxation time in the injected cortex was significantly ($p<0.01$) less than that of the contralateral cortex. Once again, no change in T_1 relaxation with time was observed in naïve animals and no left/right differences were found.

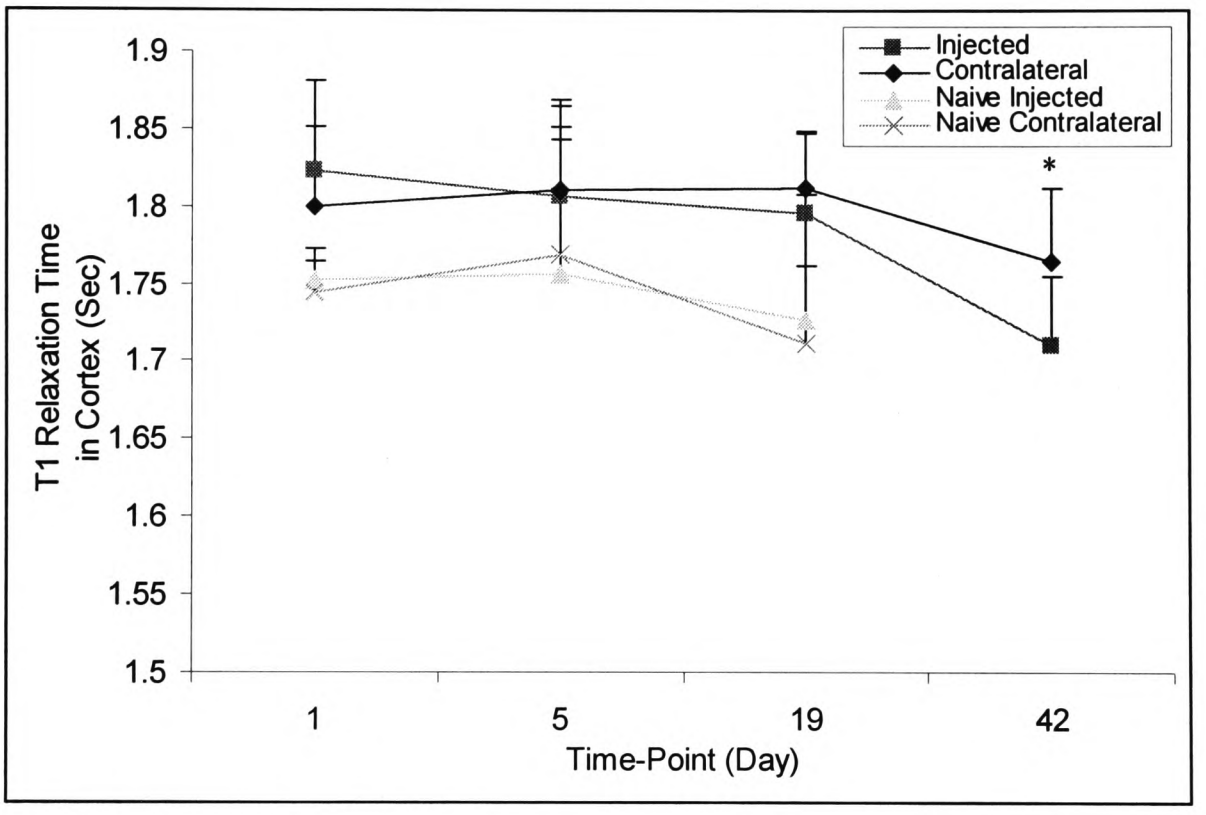


Figure 8-7: Graph to show T_1 relaxation times in injected and contralateral cortices after intracerebral injection of BCG. Naïve animals received no intracerebral injection. Values are expressed as the mean ± S.D. ANOVA demonstrated a significant decrease in the T_1 relaxation time over time in the injected cortex ($p<0.0001$), and in the contralateral cortex ($p<0.05$). A significant difference was observed between injected and contralateral cortices at day 42 (paired t test *$p<0.01$).

8.5.4 Temporal Changes in T_2 Relaxation Time

The lesion was visible as a hypointense region on both T_2-weighted images and T_2 maps. This region of reduced T_2 appeared to become less hypointense through the course of the acute period, but increased in spatial extent (Figure 8-8). Surrounding the hypointense

lesion was a hyperintense region that was maximal 1 day post-intracerebral injection (Figure 8-8), which had completely resolved by day 19.

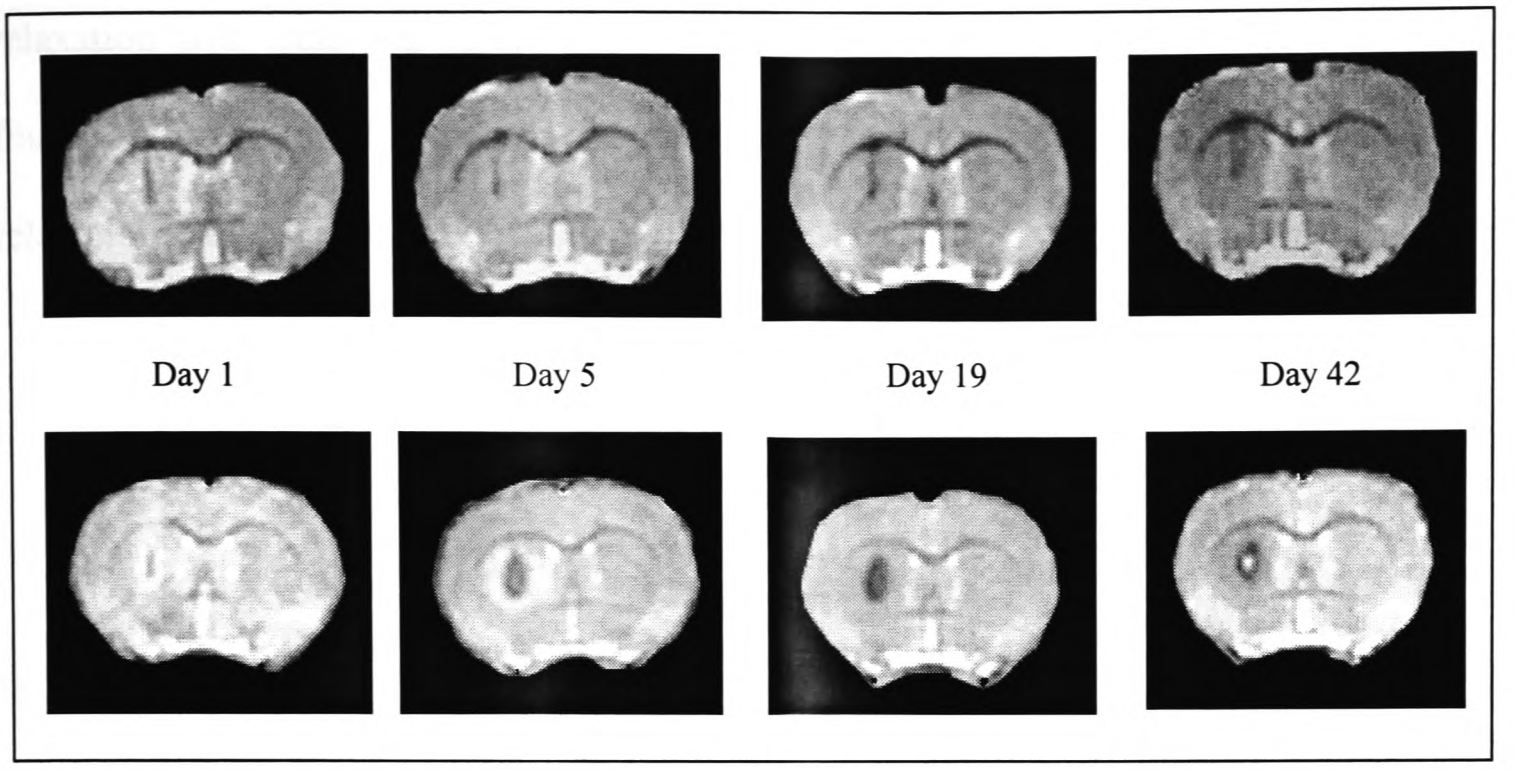


Figure 8-8: T_2 maps from two extremes of animal 1, 5, 19 and 42 days after intracerebral injection of BCG showing the hypointense lesion losing signal intensity with time. A hyperintense region was also observed surrounding the hypointense lesion core at day 5.

8.5.4.2 T_2 Relaxation Times in the Striatum

Despite the core region of decreased T_2 relaxation time, 1 day post-intracerebral injection of BCG, the T_2 relaxation time of the injected striatum was significantly increased compared to the contralateral striatum and notably longer than that of naïve animals (Figure 8-9). A significant (ANOVA $p<0.0001$) change in the T_2 relaxation time was found in the injected striatum over time. Post-hoc unpaired t tests comparisons revealed that the relaxation time at day 42 was significantly less than at day 1 and 5 ($p<0.001$), whilst at day 19, the relaxation time was significantly shorter than that at day 5 ($p<0.01$). In the contralateral striatum there was also a significant (ANOVA $p<0.001$) change over time, and post-hoc unpaired t tests revealed that the T_2 relaxation time at day 5 was significantly longer than the relaxation time at days 19 ($p<0.01$) and 42 ($p<0.001$) (Figure 8-9). Nevertheless, at each time-point, a significant difference was found between the injected and contralateral striatum (paired t tests day 1 $p<0.01$, day 5 $p<0.01$, day 19

$p<0.05$, and day 42, $p<0.0001$). Furthermore, by days 19 and 42, the T_2 relaxation time of the injected striatum was markedly shorter than that of naïve animals. No change in T_1 relaxation with time was observed in naïve animals and no left/right differences were found. No significant change in the area of the core hypointense region of reduced T_2 relaxation time was observed in any group (Appendix G.5).

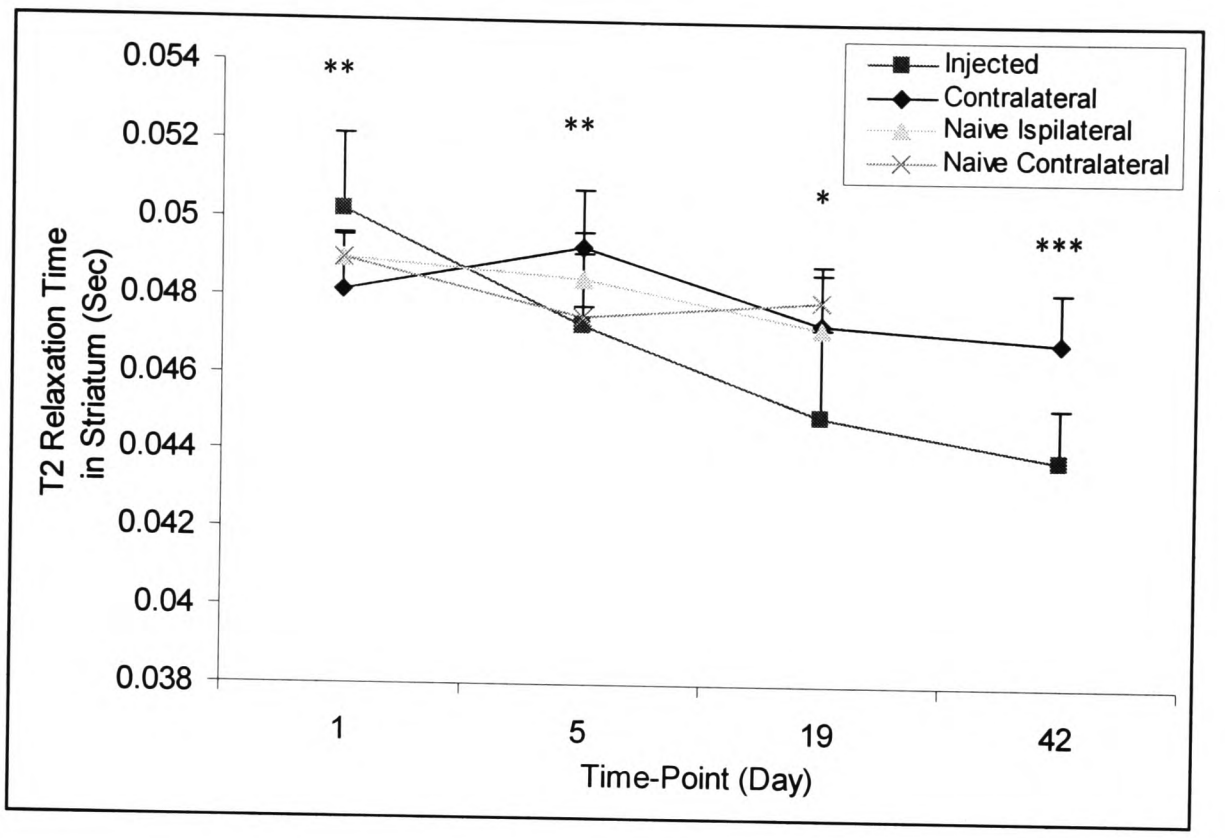


Figure 8-9: Graph to show T_2 relaxation time in injected and contralateral striata after intracerebral injection of BCG. Naïve animals received no intracerebral injection. Values are expressed as the mean ± S.D. A significant change in the T_2 relaxation time was found over time in the injected striatum (ANOVA $p<0.0001$), and in the contralateral striatum ($p<0.001$). Significant differences between the injected and contralateral hemispheres were observed at each time-point (paired t tests ***$p<0.001$, **$p<0.01$, *$p<0.05$).

8.5.5 T_2 Relaxation Times in the Lesion

When the hypointense lesion was drawn as an ROI, it was found that the T_2 relaxation time was shorter than that observed in the striatum of naïve animals (Table 8-7). A significant change in the relaxation time in the lesion was found over time (ANOVA $p<0.0001$). The T_2 relaxation time was significantly shorter at days 19 (unpaired test $p<0.001$) and 42 ($p<0.001$) than that at day 1 post-intracerebral challenge. The T_2 relaxation time at days 19 (unpaired t test $p<0.05$) and 42 ($p<0.01$) was also was significantly shorter than at day 5.

Time-Point (Day)	Striatal T_2 Relaxation Time (msec)	
	Lesion	Contralateral Striatum
1	44 ± 3 (11) *	48 ± 2 (11) *
5	41 ± 3 (16) ***	49 ± 2 (16) ***
19	37 ± 5 (12) **	47 ± 2 (12) **
42	37 ± 3 (16) ***	47 ± 1 (16) ***

Table 8-7: T_2 relaxation times in the lesion and analogous area in contralateral striatum after intracerebral injection of BCG obtained from T_2 maps. Values are expressed as the mean ± S.D for (n) animals. A significant (ANOVA $p<0.0001$) change in the T_2 relaxation time was found over time in the lesion, and contralateral hemisphere ($p<0.005$). Significant differences were observed between the injected and contralateral hemispheres at each time-point investigated (paired t tests *$p<0.02$, **$p<0.001$, ***$p<0.0001$).

8.5.5.2 T_2 Relaxation Times in the Cortex

As observed with the T_1 relaxation time, the range over which the T_2 relaxation time changed in the cortex was not as great as in the striatum. The T_2 relaxation times did not differ greatly from those observed in naive animals (Figure 8-10). Nevertheless, a significant (ANOVA $p<0.01$) change in the T_2 relaxation time in the injected cortex was found over time (Figure 8-10). Post-hoc unpaired t tests demonstrated that the relaxation time in the injected cortex at day 1 post-intracerebral injection was significantly higher than at day 5 (paired t test $p<0.005$) or 42 ($p<0.01$). A significant (ANOVA $p<0.005$) change over time was also found in the contralateral cortex, where the T_2 relaxation time was greater at day 5 than day 19 (unpaired t test $p<0.01$) or 42 ($p<0.01$). At day 5, the relaxation time in the contralateral cortex was significantly (paired t test $p<0.001$) higher than in the injected cortex. No significant differences were found between the injected and contralateral cortices at any other time-point.

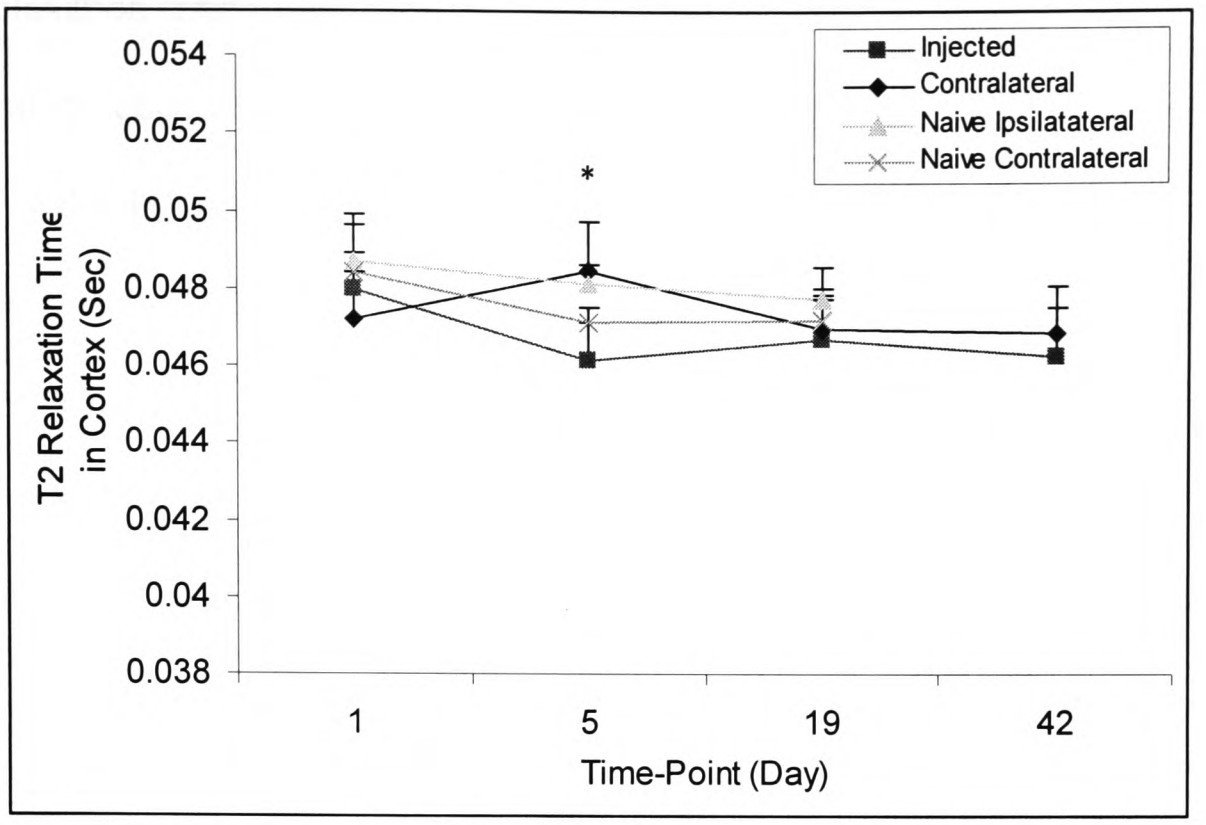


Figure 8-10: Graph to show T_2 relaxation times in the injected and contralateral cortices following intracerebral injection of BCG. Naïve animals received no intracerebral injection. Values are expressed as the mean ± S.D. A significant change in the T_2 relaxation time was found with time in the injected cortex (ANOVA $p<0.01$), and in the contralateral cortex ($p<0.005$). A significant difference was found between the injected and contralateral cortices at day 5 (paired t test $*p<0.001$).

8.5.6 Temporal Changes in T_2* Relaxation Time

The lesion exhibited a clear reduction in the T_2* relaxation time (Figure 8-11), and over time, the T_2* relaxation time of the lesion appeared to decrease further, becoming more visible as a hypointense region on T_2* maps. ROI's were chosen encompassing the entire striatum and also the lesion alone. Results were expressed in terms of L/R intensity ratios due to the dependence of T_2* relaxation time on local field gradients and shim gradients on a day-to-day basis.

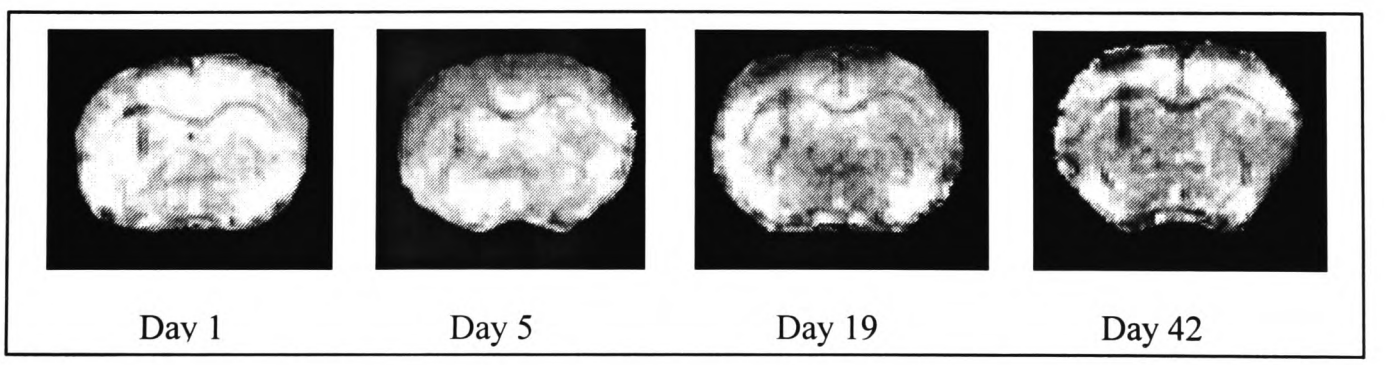


Figure 8-11: T_2* maps at 1, 5, 19 and 42 days following the intracerebral injection of BCG, showing a reduction in the T_2* relaxation time at the site of the lesion.

The T_2* relaxation time of the injected striatum significantly altered over time following intracerebral injection of BCG (ANOVA $p<0.005$) (Table 8-8). Post-hoc unpaired t tests revealed that the T_2* relaxation times at days 5, 19 and 42 were significantly shorter than at day 1 ($p<0.05$, $p<0.05$ and $p<0.01$ respectively). In addition, the relaxation time at day 42 was shorter than at day 19 ($p<0.05$). In terms of area, the lesion significantly increased in size during lesion progression (ANOVA $p<0.05$). Post-hoc unpaired t tests showed that the lesion was smaller in size at day 1 than at days 19 and 42 ($p<0.05$ and $p<0.02$ respectively).

Time-Point (Day)	Striatum T_2* Relaxation Time (L/R)	Area of Lesion on T_2* maps (No. of Pixels)
1	0.71 ± 0.16 (11)	51.7 ± 29.1 (11)
5	0.49 ± 0.21 (11)	63.6 ± 18.0 (11)
19	0.59 ± 0.10 (8)	79.3 ± 22.8 (8)
42	0.45 ± 0.15 (16)	81.6 ± 29.4 (16)

Table 8-8: T_2* relaxation times in the striatum following intracerebral injection of BCG. Values are expressed as the mean ± S.D for (n) animals. A significant change over time was observed in the T_2* relaxation time (ANOVA $p<0.005$) and also in the area of the lesion on T_2* maps (ANOVA $p<0.05$).

8.5.7 Magnetisation Transfer Ratio

ROI'S were chosen that covered the lesion and a corresponding region of size and location in the contralateral hemisphere on the magnetisation transfer ratio (MTR) maps (Figure 8-12). A significant (ANOVA $p<0.05$) change in the MTR was observed over time in the injected hemisphere, no significant change over time was observed in the contralateral hemisphere (Figure 8-13). Post-hoc paired t tests revealed that at day 42, the MTR was significantly less than at day 5 ($p<0.005$). The MTR of the lesion was significantly lower than the striatum of the contralateral hemisphere at each time-point (except day 0) after intracerebral injection of BCG (paired t tests; day 1, $p<0.01$, day 5, $p<0.0001$; day 19, $p<0.001$; and day 42, $p<0.001$).

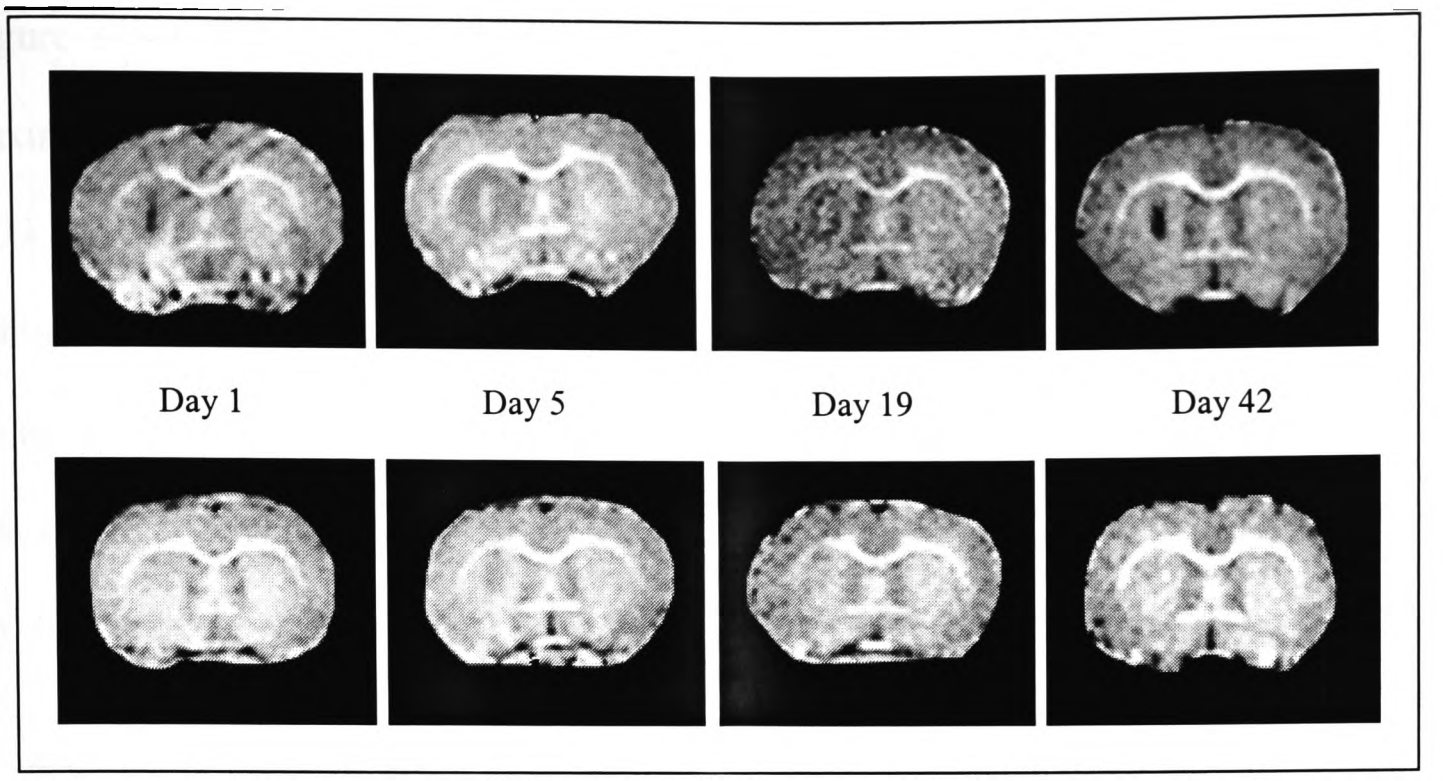


Figure 8-12: MTR maps from two extremes of animal obtained after intracerebral injection of BCG showing a central core of decreased MTR at day 1, becoming increased by day 5. Over time the MTR decreased further. In the majority of animals the MTR of the lesion was reduced at day 5, surrounded by a region of increased MTR, which decreased with time.

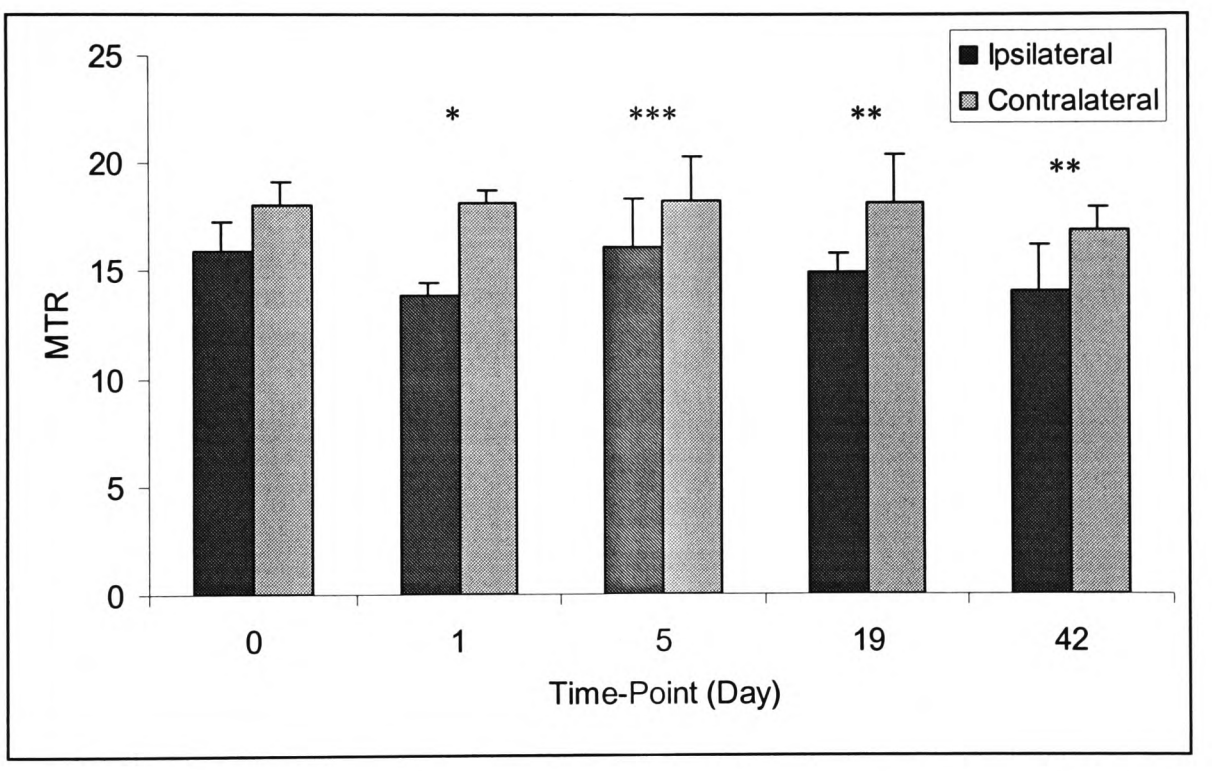


Figure 8-13: Graph to show MTR of the lesion and analogous ROI in the contralateral hemisphere after intracerebral injection of BCG. Values are expressed as the mean ± S.D. A significant (ANOVA $p<0.05$) change in the MTR was found over time in the injected hemisphere. Significant differences were found between injected and contralateral hemisphere at each time-point (paired t tests ***$p<0.0001$, **$p<0.001$, *$p<0.05$).

8.5.8 Temporal Changes in BBB Permeability

Detectable breakdown of the BBB was visible on post-contrast T_1-weighted images on the day of intracerebral BCG injection, which became more widespread by day 5. BBB breakdown persisted to some degree in all animals to day 19 and in some, to day 42

(Figure 8-14). ROI's were chosen that encompassed the areas of signal enhancement. Maximal enhancement in terms of signal intensity appeared to occur at the time of the BCG injection (Table 8-9). However, ANOVA revealed that there were no significant differences in the intensity of gadolinium enhancement over time ($p=0.081$). In terms of the area of BBB breakdown, this appeared to be maximal at day 5 (Figure 8-15). The area of enhancement changed significantly with time (ANOVA $p<0.0001$), such that at day 5, the area was significantly greater than that at 0 (unpaired t tests $p<0.01$), 1 ($p<0.001$), 19 ($p<0.05$) and 42 days post-intracerebral injection ($p<0.001$).

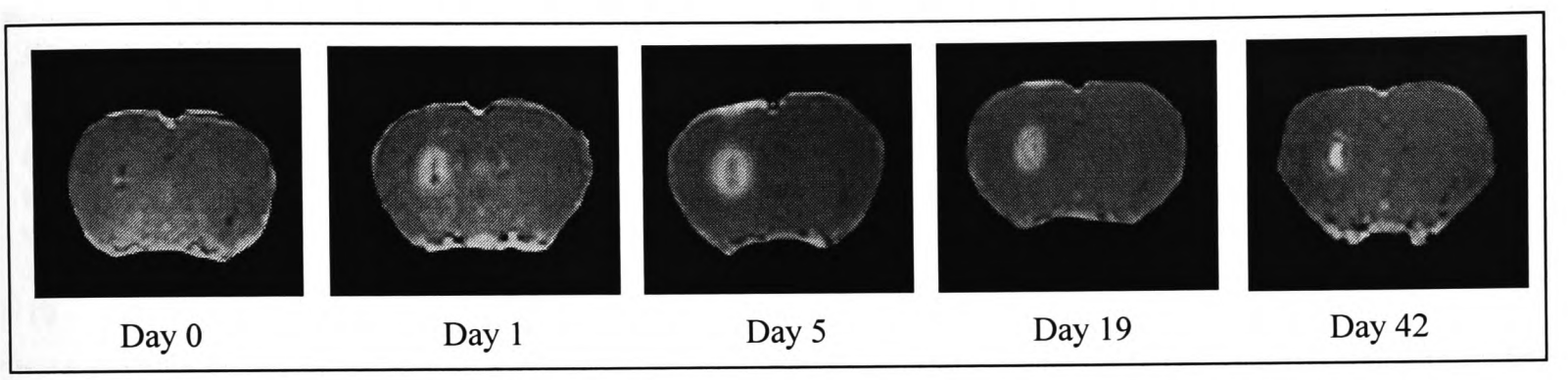


Figure 8-14: Post-contrast T_1-weighted images acquired throughout the acute inflammatory response following intracerebral injection of BCG, showing increased BBB permeability as indicated by signal enhancement. Spatially, maximal enhancement was observed at day 5 of the acute inflammatory response, and by day 42 the BBB permeability had mostly resolved.

Time-Point (Day)	Intensity of Gadolinium Enhancement (L/R)
0	1.47 ± 0.39 (4)
1	1.32 ± 0.17 (8)
5	1.40 ± 0.18 (15)
19	1.23 ± 0.17 (12)
42	1.20 ± 0.29 (14)

Table 8-9: Intensity ratio of signal enhancement on post-contrast T_1-weighted images acquired throughout the acute inflammatory response following intracerebral injection of BCG. Values are expressed as the mean ± S.D for (n) animals. No change over time was observed in the intensity of enhancement; however, a significant change in the area of enhancement was observed over time (ANOVA $p<0.0001$). The area of enhancement at day 5 was significantly greater than at every other time-point (unpaired t tests $p<0.0001$ when compared to day 42, $p<0.01$ when compared to day 0, $p<0.001$ when compared to day 1, $p<0.05$ when compared to day 19).

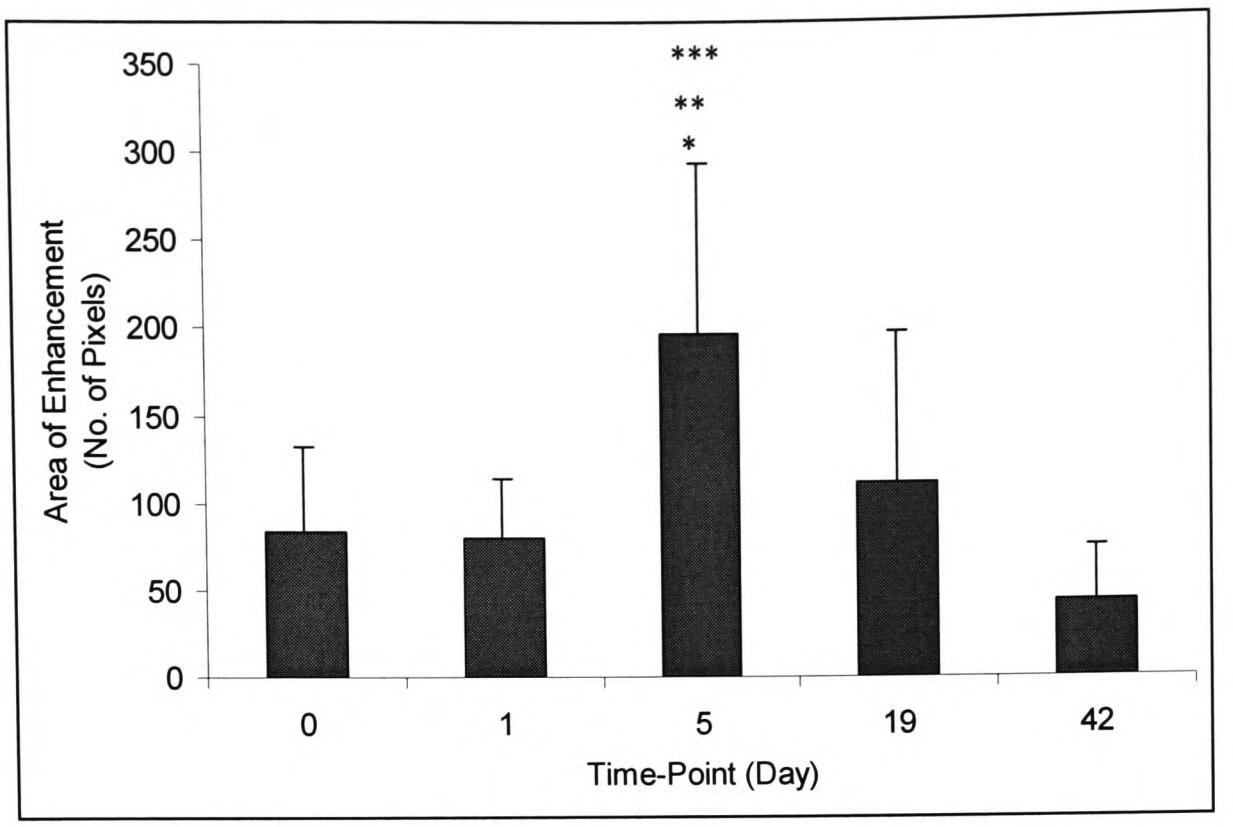


Figure 8-15: Graph to show area of BBB breakdown as identified by area of gadolinium enhancement observed on post-contrast T_1-weighted images acquired after intracerebral injection of BCG. Values are expressed as the mean ± S.D. A significant change over time was observed (ANOVA $p<0.0001$). Day 5 was significantly greater than every other time-point. Unpaired t tests ***$p<0.0001$ when compared to day 42, $p<0.01$ when compared to day 0, **$p<0.001$ when compared to day 1, *$p<0.05$ when compared to day 19.

8.5.9 Temporal Changes in ADC

Regions of decreased ADC were observed at the site of the BCG intracerebral injection on ADC trace maps from day 1 post-intracerebral injection. Surrounding this region was an area of increased ADC, which appeared to be maximally elevated between days 0 and 5 and subsequently returned to normal (Figure 8-16). A significant (ANOVA $p<0.005$) change in the ADC in the hyperintense region was also found over time (Figure 8-17). Post-hoc unpaired t tests revealed that the ADC in the injected hemisphere at day 0 was significantly greater than day 19 ($p<0.05$). In addition, the ADC in the injected hemisphere at day 1 was significantly greater than that at day 5 ($p<0.02$), 19 ($p<0.001$), or 42 ($p<0.005$). The hyperintensity observed at day 5 was also greater than that at day 1 ($p<0.02$), day 19 ($p<0.005$), and day 42 ($p<0.05$) post-intracerebral injection (Table 8-11).

During the early phase of lesion progression (from 0-5 days) the area of increased ADC, although spatially similar, tended to be somewhat larger than that of BBB breakdown (Table 8-10). Subsequently, the area of increased ADC reduced dramatically to become smaller than the region of BBB breakdown (days 19-42). ANOVA demonstrated that the area of increased ADC changed significantly ($p<0.005$) over time (Figure 8-18). Post-hoc unpaired t tests showed that at day 5, the area was significantly greater than at days 0, 19, and 42 post-intracerebral injection ($p<0.02$, $p<0.005$ and $p<0.005$ respectively) (Table 8-12). The core area of decreased ADC was difficult to quantify since in most animals the increase in ADC in surrounding regions dominated, and effectively cancelled out the reduction in ADC. Qualitatively the area of decreased ADC appeared to be maximal at day 5, after which time-point the ADC at the core of the lesion appeared to decrease with time. At day 42, in some animals, (5/11) the core of the lesion exhibited an increased ADC, surrounded by a mild decrease in ADC (see Figure 8-16).

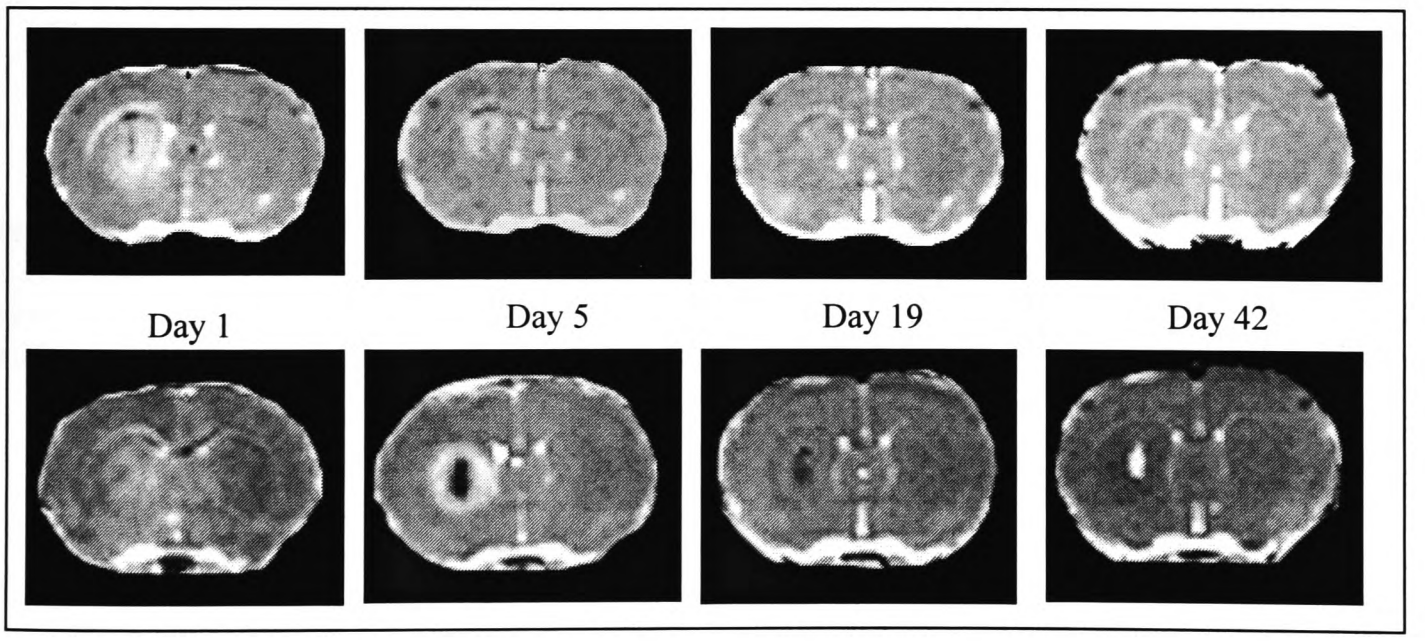


Figure 8-16: ADC maps in two animals acquired following intracerebral injection of BCG. At day 1, an area of decreased ADC was visible surrounded by an area of increased ADC. Both regions appeared to resolve over time, and in some animals an area of increased ADC was observed towards the end of the inflammatory response at the core of the lesion.

Time-Point (Day)	ADC (x 10^{-4} mm^2s^{-1}) Values in Region of Elevated ADC		Area of Increased ADC (No. of Pixels)
	ADC Hyperintensity	Contralateral	
0	8.1 ± 0.6 (4)*	6.8 ± 1.8 (4)*	133.5 ± 17.2 (4)
1	8.9 ± 3.5 (4)**	7.1 ± 2.5 (4)**	174.3 ± 63.5 (4)
5	8.4 ± 7.7 (9)***	6.8 ± 2.6 (9)***	303.9 ± 171.9 (9)
19	7.1 ± 2.5 (6)*	6.6 ± 3.2 (6)*	78.8 ± 50.5 (6)
42	7.3 ± 2.8 (3)	6.7 ± 1.9 (3)	34.7 ± 17.2 (3)

Table 8-10: ADC values in region of elevated ADC and areas of elevated ADC following intracerebral injection of BCG. Values are expressed as the mean ± S.D for (n) animals. A significant change in the ADC and area of elevated ADC was observed over time (ANOVA $p<0.005$ for ADC in hyperintense region, $p<0.005$ for area of increased ADC, paired t tests ***$p<0.0001$, **$p<0.001$, *$p<0.05$).

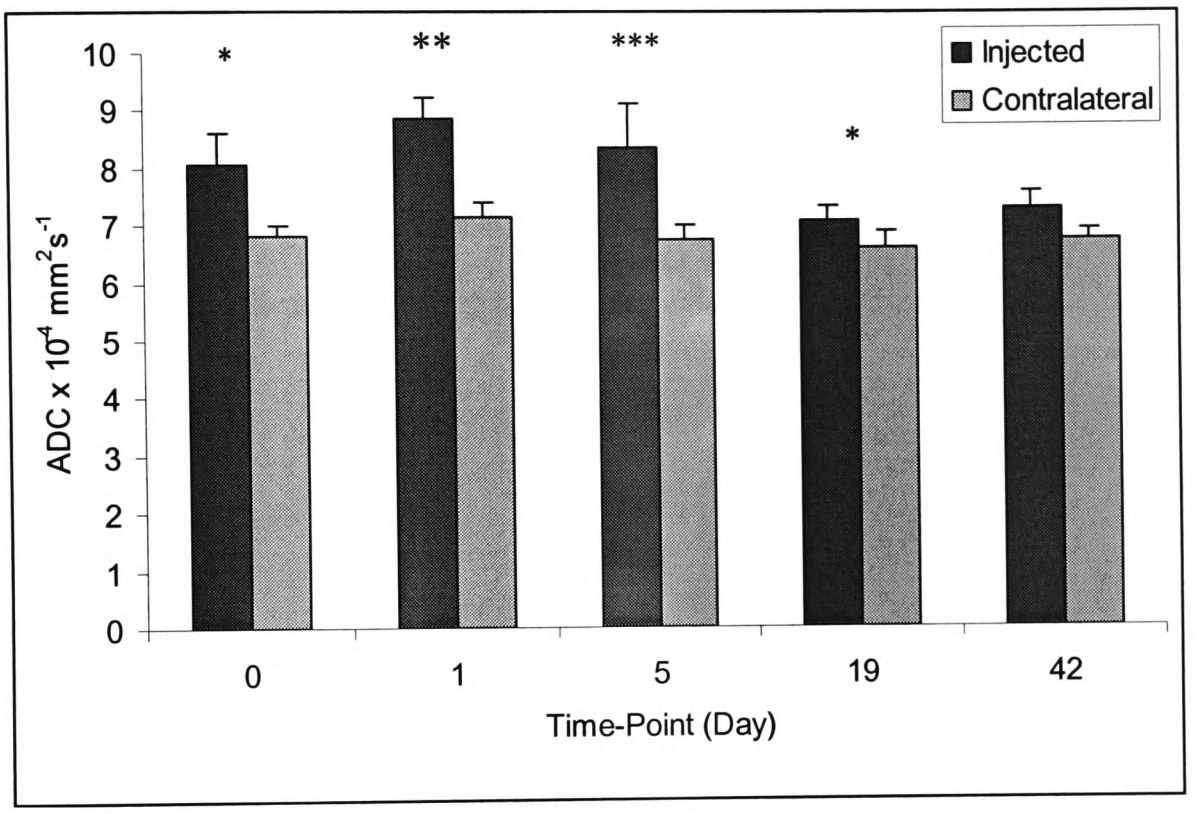


Figure 8-17: Graph to show ADC values in region of elevated ADC following intracerebral injection of BCG. Values are expressed as the mean ± S.D. A significant change over time was observed in the hyperintense region (ANOVA $p<0.005$), no significant change over time was observed in the contralateral striatum. Paired t tests ***$p<0.0001$, **$p<0.01$, *$p<0.05$.

ADC in Region of Elevated ADC					
Time-Point (Day)	0	1	5	19	42
0	-	/	/	$p<0.05$	$p=0.0829$
1	-	-	$p<0.02$	$p<0.001$	$p<0.005$
5	-	-	-	$p<0.005$	$p<0.05$
19	-	-	-	-	/
42	-	-	-	-	-

Table 8-11: Summary of unpaired t tests between different time-points for ADC in region of ADC hyperintensity ('/' denotes difference is not significant, values for comparisons that did not quite reach significance are also included).

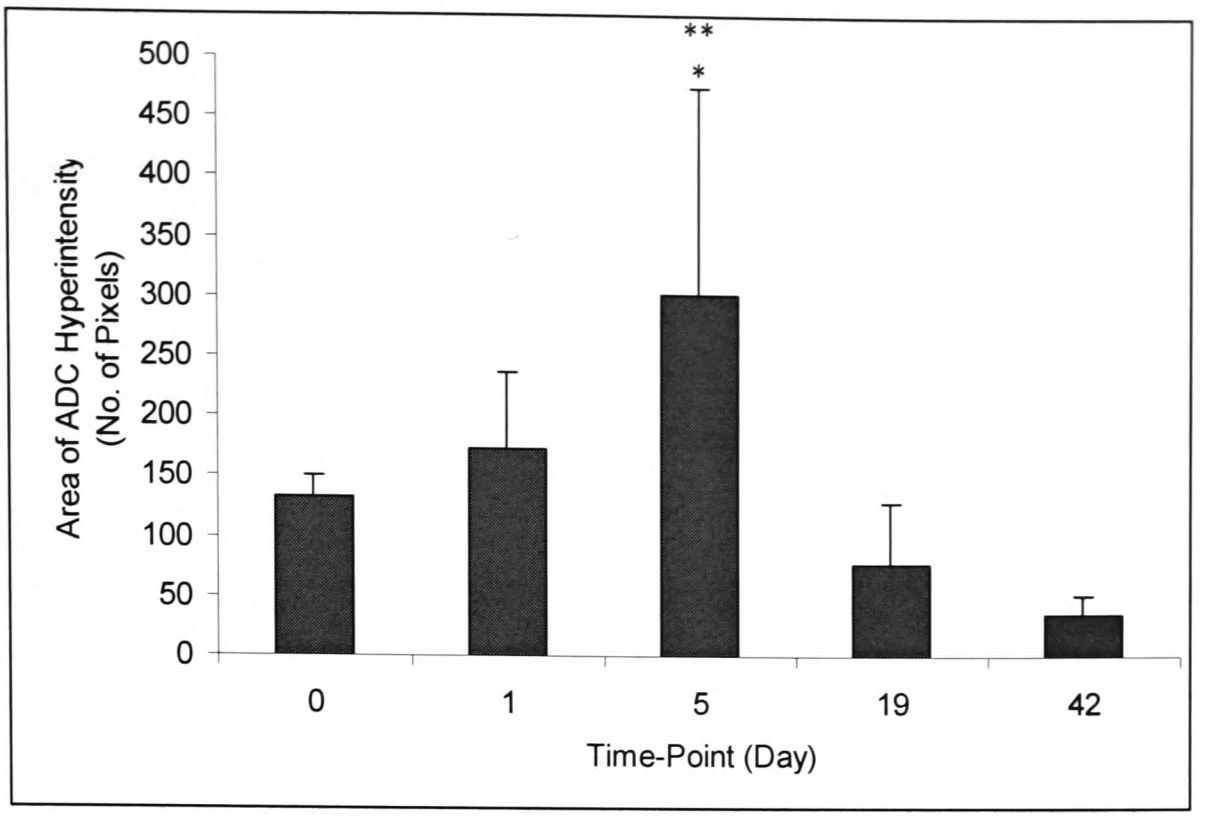


Figure 8-18: Graph to show the area of increased ADC following intracerebral injection of BCG. Values are expressed as the mean ± S.D. A significant change over time was observed (ANOVA $p<0.005$), unpaired t tests **$p<0.005$ when compared to days 19 and 42, *$p<0.02$ when compared to day 0.

Area of ADC Hyperintensity					
Time-Point (Day)	**0**	**1**	**5**	**19**	**42**
0	-	/	$p<0.02$	$p<0.005$	$p<0.005$
1	-	-	$p=0.0759$	$p<0.05$	$p<0.05$
5	-	-	-	$p<0.005$	$p<0.005$
19	-	-	-	-	/
42	-	-	-	-	-

Table 8-12: Summary of unpaired t tests between different time-points for area of ADC hyperintensity ('/' denotes difference is not significant, values for comparisons that did not quite reach significance are also included).

8.5.10 Temporal Changes in Diffusion Anisotropy

The lesion appears as a hypointense region on anisotropy maps (Figure 8-19), indicating a reduction in anisotropy. As the lesion progressed with time, diffusion anisotropy decreased. No changes were observed in the contralateral hemisphere.

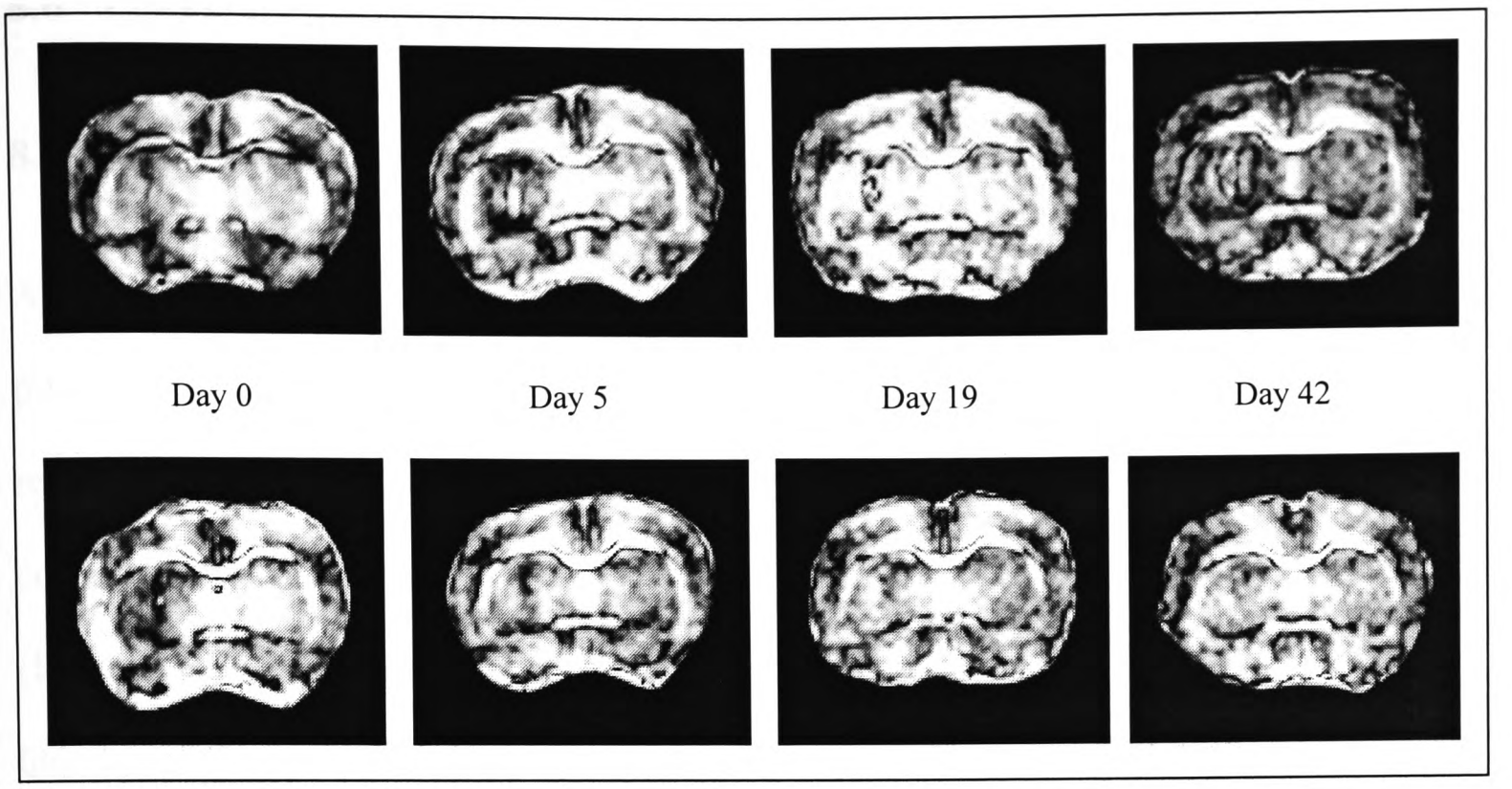


Figure 8-19: Diffusion anisotropy maps in two extremes of animal created from diffusion-weighted images in three orthogonal directions showing hypointense lesion with reduced anisotropy at day 0. The lesion becomes less anisotropic as the lesion becomes chronic.

8.6 POST-LPS Challenge

8.6.1 Behavioural effects of LPS administration

A few minutes after LPS-challenge, the rats became less active and there was obvious piloerection. The core body temperature of the rats was elevated, and the heart rate was reduced, as detected by heart rate monitoring during the MRI protocol. These signs were consistent with those previously reported in endotoxin induced sickness behaviour (Dantzer 2001). 24 hours after LPS injection, a small amount of discharge containing blood was observed around the nose and eyes, however by 72 hours these outward effects of the LPS injection appeared to have resolved.

8.6.2 Changes in rCBV Post-LPS Administration

Six hours post-LPS challenge, focal increases in rCBV were observed throughout the injected hemisphere (Table 8-13). Even in animals where the rCBV of the injected hemisphere was still elevated above normal at day 42 pre-LPS challenge, a marked increase in rCBV was observed post-LPS challenge (see Figure 8-20). These increases were not observed in any of the control animals (Table 8-13 and Figure 8-20). 24 hours post-LPS challenge, the rCBV still appeared to be raised in some animals (Figure 8-21). In the majority of animals, the rCBV of the injected hemisphere had decreased by 24 hours relative to that observed at 6 hours, although in a small number (3/9) it continued to rise. By 72 hours, the rCBV had returned to pre-challenge levels or below in most animals (7/9). No significant change over time was observed in any of the groups, probably because of different temporal profiles adding to natural biological variation.

Time-Point	Left/Right rCBV ratio		
	LPS	SAL PC	NPC
Day 42	1.69 ± 0.84 (9)	2.50 ± 0.55 (4)	2.22 ± 0.99 (2)
6 hrs	2.23 ± 0.93 (11)	2.12 ± 0.45 (4)	2.49 ± 1.66 (5)
24 hrs	1.71 ± 0.44 (9)	1.90 ± 0.43 (4)	1.55 ± 0.44 (3)
72 hrs	1.69 ± 0.45 (5)	2.30 ± 0.44 (4)	1.68 ± 0.50 (3)

Table 8-13: rCBV ratios pre-challenge (day 42) and post-LPS, saline (SAL PC) or no peripheral challenge (NPC) (6, 24 and 72 hours). Values are expressed as the mean ± S.D for (n) animals.

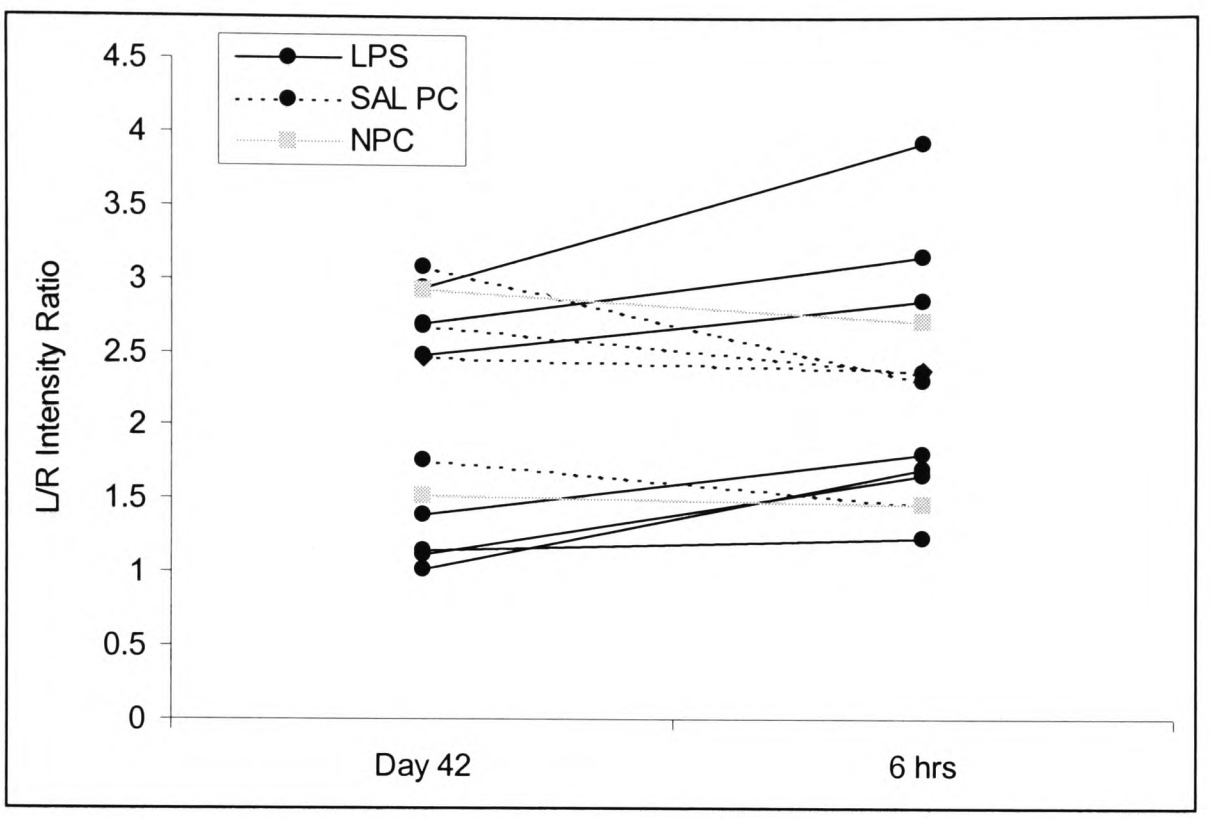


Figure 8-20: Graph to show increased rCBV six hours post-LPS. Values are expressed as the mean ± S.D. This increase was not observed in any of the control animals. Paired t test $p<0.005$ when compared to pre-challenge in LPS-challenged animals (day 42), $p<0.05$ in SAL PC animals, and no significant differences were found in NPC animals.

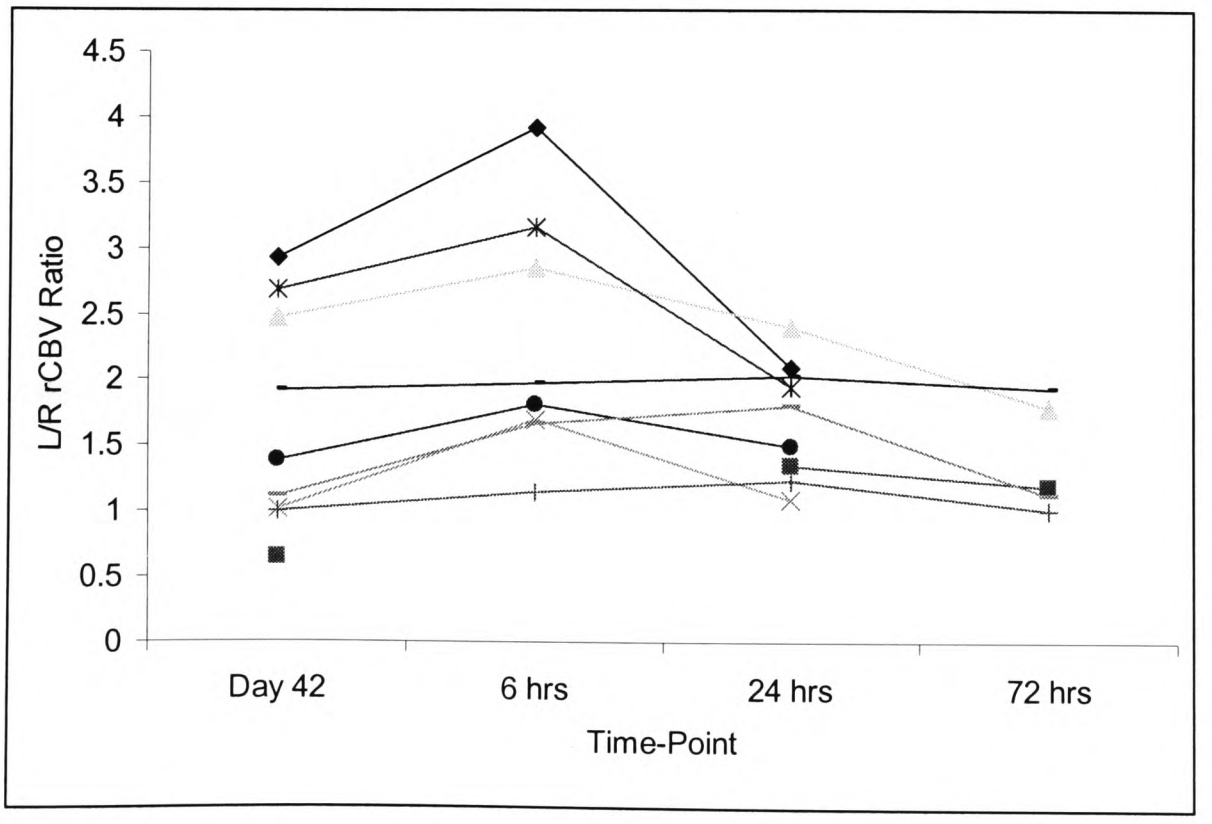


Figure 8-21: Graph to show temporal changes in rCBV in LPS-challenged animals post-LPS administration. Each line represents individual animal profiles.

8.6.3 Changes in T_1 Relaxation Time Post-LPS Challenge

8.6.3.1 Striatum

Peripheral challenge with LPS had the effect of significantly increasing the T_1 relaxation time in the striatum, in both the injected and contralateral hemispheres six hours post-challenge, which was visible on T_1 maps (Figure 8-22, 8-23). This increased T_1 relaxation time was not observed in either control group subjected to intracerebral BCG injection. The increase at 6 hours in LPS-challenged animals was significantly different from the T_1 relaxation time at 24 and 72 hours in the injected hemisphere and to 24 hours in the contralateral hemisphere (Table 8-14). In contrast, the T_1 relaxation times measured in the control animals appeared to either remain stable or decrease slightly over time (Figure 8-23). In the BCG-injected striatum, a significant difference in the T_1 relaxation time (using unpaired t tests) was found at 6 hours post-LPS challenge between LPS and NPC animals ($p<0.05$). In the contralateral hemisphere, a significant difference was found between LPS and NPC animals (unpaired t test $p<0.02$). After this time-point in LPS animals, the T_1 relaxation time in both the injected and contralateral striatum returned to pre-LPS values. In addition, a significant change in the T_1 relaxation time in the contralateral striatum of SAL PC animals was also found post-challenge (ANOVA $p<0.05$) (Table 8-15).

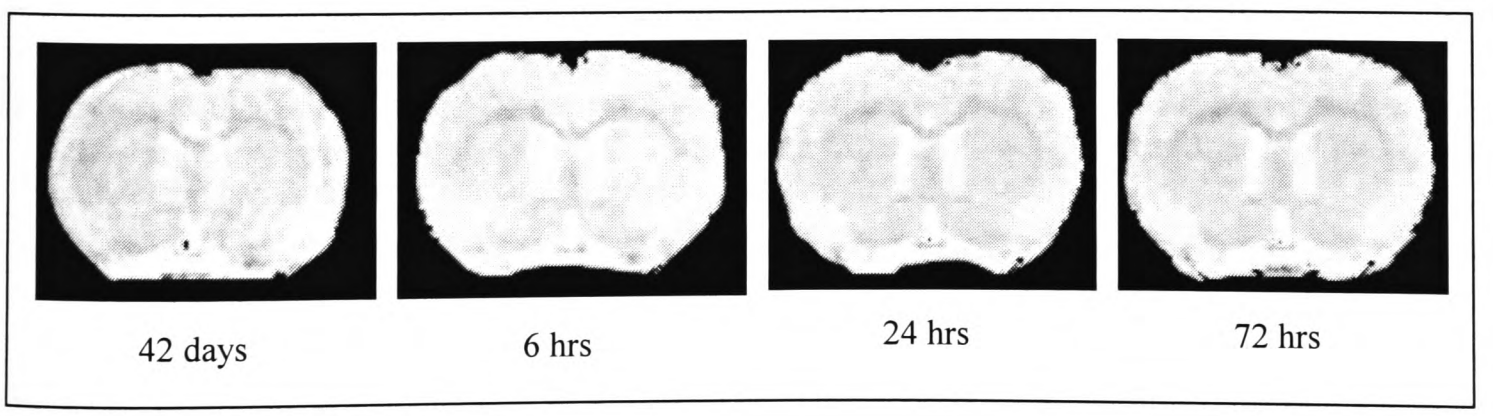
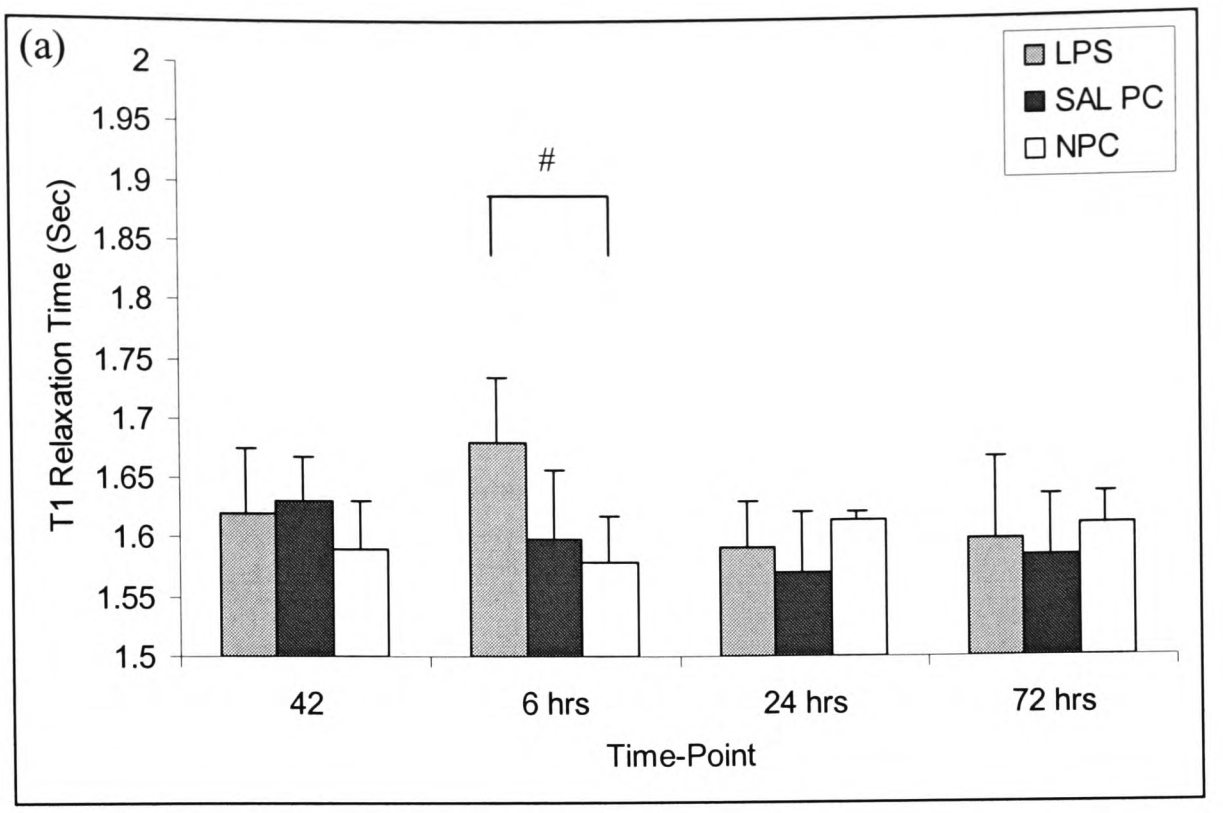


Figure 8-22: T_1 maps acquired pre-challenge (day 42) and 6, 24, and 72 hours post-LPS challenge showing increased T_1 in both hemispheres at 6 hours post-challenge.



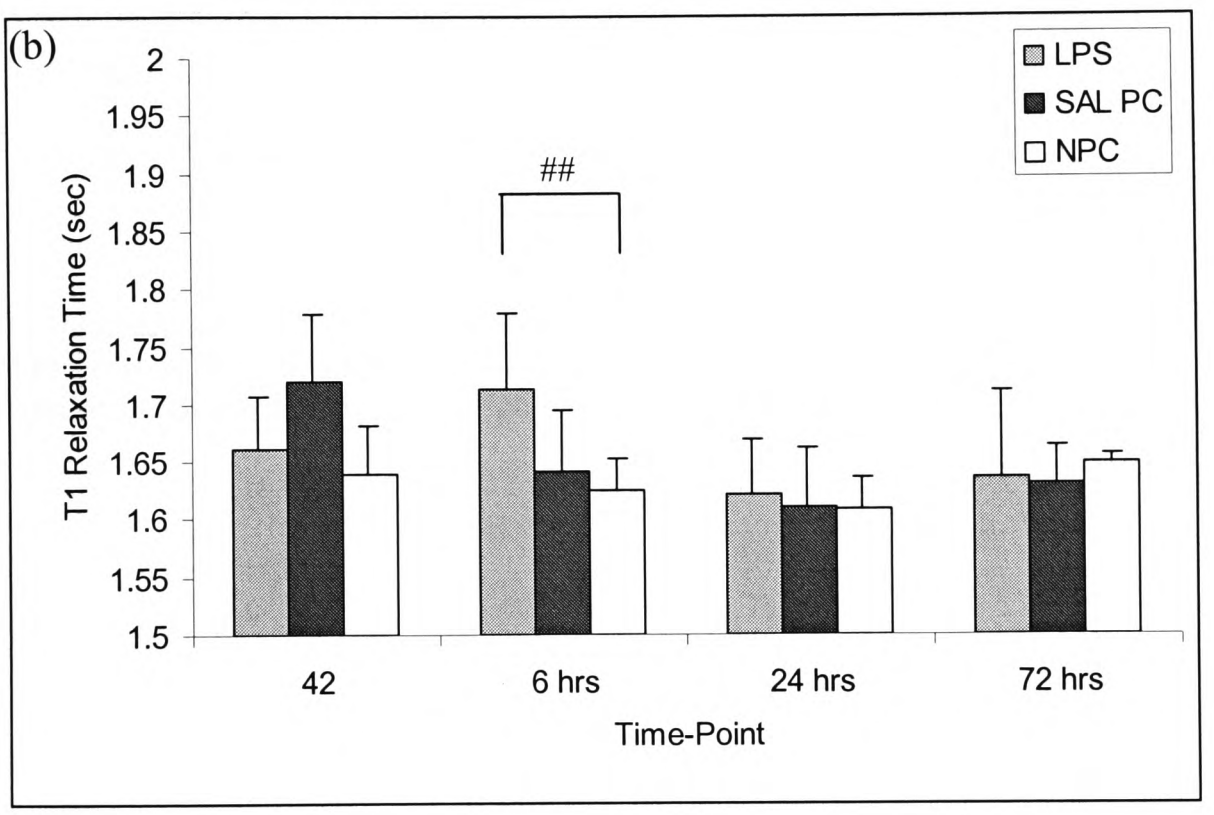


Figure 8-23: Graph to show T_1 relaxation times in (a) injected and (b) contralateral striata pre (day 42) and post-challenge (6, 24 and 72 hours) with LPS, saline (SAL PC) or no peripheral challenge (NPC). Values are expressed as the mean ± S.D. Significant differences were observed in both the injected and contralateral hemispheres at 6 hours (unpaired t tests ##$p<0.02$, #$p<0.05$).

	LPS Injected Striatum			
Time-Point	**Day 42**	**6 hrs**	**24 hrs**	**72 hrs**
Day 42	-	$p<0.05$	/	/
6 hrs	-	-	$p<0.005$	$p<0.05$
24 hrs	-	-	-	/
72 hrs	-	-	-	-

	LPS Contralateral Striatum			
Time-Point	**Day 42**	**6 hrs**	**24 hrs**	**72 hrs**
Day 42	-	$p=0.0690$	$p=0.0978$	/
6 hrs	-	-	$p<0.005$	$p=0.0679$
24 hrs	-	-	-	/
72 hrs	-	-	-	-

Table 8-14: Summary of unpaired t tests between different time points for T_1 relaxation time in injected and contralateral striata of LPS-challenged animals ('/' denotes difference is not significant, values for comparisons that did not quite reach significance are also included).

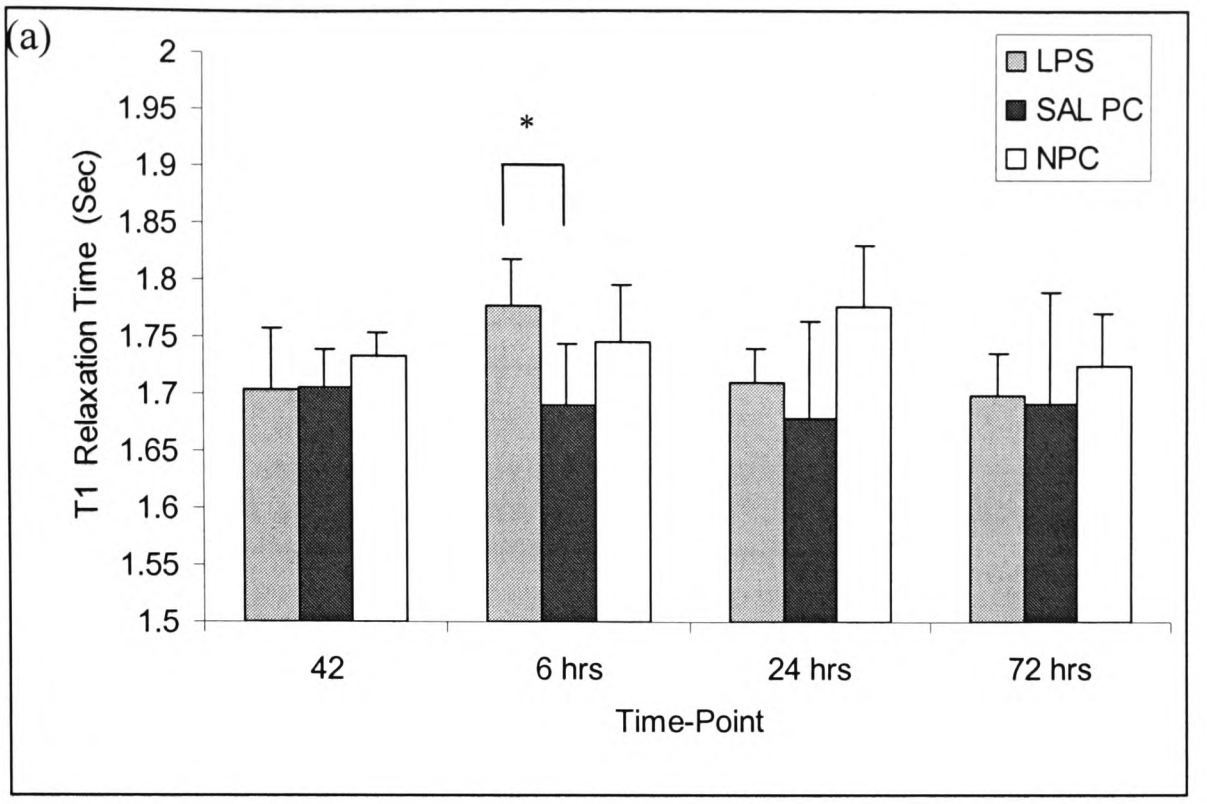
	SAL PC Contralateral Striatum			
Time-Point	**Day 42**	**6 hrs**	**24 hrs**	**72 hrs**
Day 42	-	$p=0.0984$	$p<0.05$	$p=0.0511$
6 hrs	-	-	/	/
24 hrs	-	-	-	/
72 hrs	-	-	-	-

Table 8-15: Summary of unpaired t tests between different time points for T_1 relaxation time in the contralateral striatum of SAL PC controls. No significant differences were found in the injected striatum ('/' denotes difference is not significant, values for comparisons that did not quite reach significance are also included).

8.6.4 Cortex

As for the striatum, the T_1 relaxation time appeared to increase considerably in both the injected and contralateral cortices 6 hours post-LPS challenge, a change that was not evident in either control group (Figure 8-24). The increase in the injected cortex in LPS-challenged animals at this time-point was significantly different to all other time-points (Table 8-16). In the contralateral cortex, the increase at 6 hours was significantly different to pre-challenge (unpaired t test $p<0.05$) and 24 hours post-LPS challenge ($p<0.005$) (Table 8-16). In the injected cortex, the increase in T_1 relaxation time at 6 hours in LPS animals was significantly (unpaired t test $p<0.05$) different from SAL PC

controls, although not from NPC controls. No significant differences were found between the injected or contralateral cortices at any of the time-points in any of the groups.



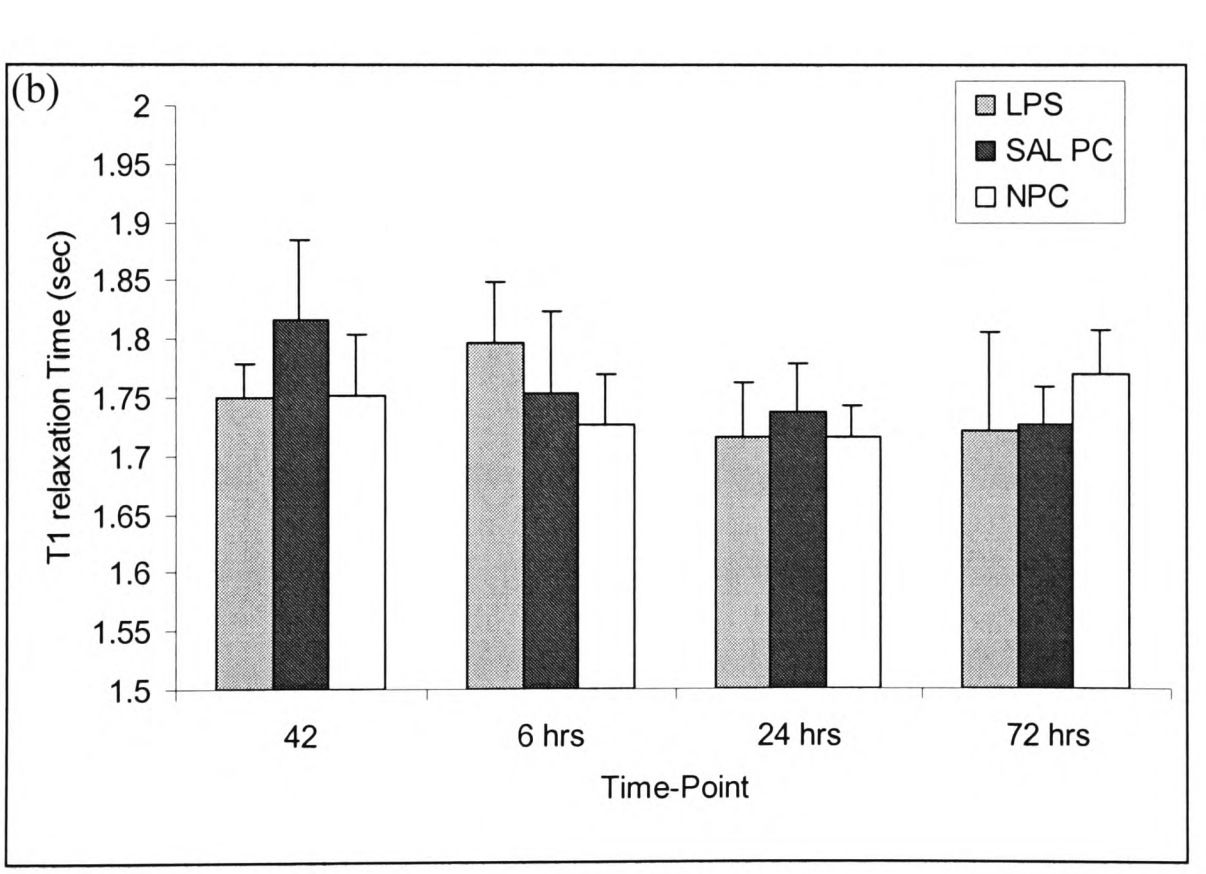


Figure 8-24: Graph to show T_1 relaxation times in (a) injected and (b) contralateral cortices pre (day 42) and post-challenge with LPS, saline (SAL PC) or no peripheral challenge (NPC) at 6, 24 and 72 hours. Values are expressed as the mean ± S.D. Significant differences were observed in the injected hemisphere 6 hours post-LPS challenge (unpaired t test *$p<0.05$).

	LPS Injected Cortex			
Time-Point	**Day 42**	**6 hrs**	**24 hrs**	**72 hrs**
Day 42	-	$p<0.005$	/	/
6 hrs	-	-	$p<0.005$	$p<0.005$
24 hrs	-	-	-	/
72 hrs	-	-	-	-

	LPS Contralateral Cortex			
Time-Point	**Day 42**	**6 hrs**	**24 hrs**	**72 hrs**
Day 42	-	$p<0.05$	$p=0.0809$	/
6 hrs	-	-	$p<0.005$	$p=0.0894$
24 hrs	-	-	-	/
72 hrs	-	-	-	-

Table 8-16: Summary of unpaired t-test results for T_1 relaxation time in injected and contralateral cortices of LPS-challenged animals between different time-points ('/' denotes difference is not significant, values for comparisons that did not quite reach significance are also included).

8.6.5 Changes in T_2 Relaxation Times post-LPS challenge

8.6.5.1 Striatum

Following LPS-challenge, no significant differences in the striatal T_2 relaxation time were found over time, either within or between any groups, or between groups at any time-point (Table 8-17). However, the T_2 relaxation time appeared to decrease progressively within the lesion itself as can be seen by the reduction in the hypointensity (Figure 8-25). Nevertheless, at each time-point post-LPS challenge, the T_2 relaxation time was significantly shorter in the injected striatum than in the contralateral (paired t test $p<0.001$ at each time point). In contrast, the T_2 relaxation time in SAL PC controls was significantly shorter in the injected striatum than in the contralateral striatum at 6 hours and 24 hours post-LPS challenge (paired t test $p<0.05$ in both cases). NPC controls only showed a significant difference between injected and contralateral hemispheres at 72 hours (paired t test $p<0.05$).

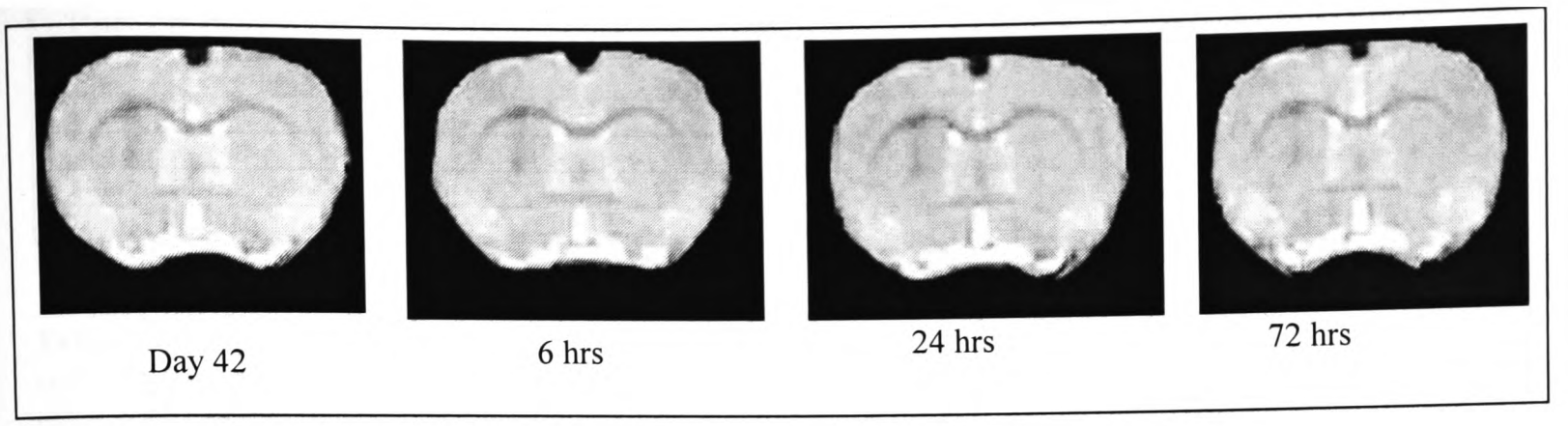


Figure 8-25: T_2 maps acquired pre-challenge (day 42), and 6, 24, and 72 hours post-LPS challenge.

Time-Point	Striatal T_2 Relaxation Time (msec)					
	LPS		SAL PC		NPC	
	Injected	Contralateral	Injected	Contralateral	Injected	Contralateral
Day 42	44 ± 1 (9)	47 ± 1 (9)	44 ± 2 (4)	47 ± 0.8 (4)	44 ± 0.9 (3)	48 ± 1 (3)
6 hrs	43 ± 0.6 (9)	46 ± 1 (9)	43 ± 2 (4)	47 ± 0.8 (4)	44 ± 0.7	45 ± 1 (3)
24 hrs	43 ± 1 (9)	46 ± 2 (9)	43 ± 1 (4)	46 ± 0.6 (4)	43 ± 1 (2)	45 ± 0.8 (2)
72 hrs	43 ± 2 (6)	45 ± 0.9 (6)	44 ± 2 (4)	45 ± 1 (4)	44 ± 1 (3)	46 ± 1 (3)

Table 8-17: T_2 relaxation time in both injected and contralateral striata pre-challenge (day 42), and 6, 24, and 72 hours post-LPS, saline (SAL PC) or no peripheral challenge (NPC). Values are expressed as the mean ± S.D for (n) animals.

8.6.5.2 Cortex

In the injected cortex, once again no significant changes in T_2 relaxation time over time were observed in any group, and no significant differences were found between the groups at any time-point (Table 8-18). Similarly, stable T_2 relaxation times were found in the contralateral cortex, although in SAL PC animals, the measured times at 72 hours post-LPS challenge were significantly (unpaired t test $p<0.05$) lower than at day 42 and at 6 hours post-LPS challenge (unpaired t test $p<0.02$). Although this decrease was significant, it was not a large change.

Time-Point	Cortex T_2 Relaxation Time (msec)					
	LPS		SAL PC		NPC	
	Ipsilateral	Contralateral	Ipsilateral	Contralateral	Ipsilateral	Contralateral
Day 42	46 ± 1 (9)	47 ± 1 (9)	47 ± 1 (4)	46 ± 0.4 (4)	46 ± 1 (3)	48 ± 2 (3)
6 hrs	45 ± 1 (9)	46 ± 1 (9)	45 ± 2 (4)	47 ± 0.3 (4)	47 ± 0.3 (3)	47 ± 0.7 (3)
24 hrs	45 ± 1 (9)	46 ± 2 (9)	45 ± 2 (4)	46 ± 0.9 (4)	46 ± 2 (3)	46 ± 0.7 (3)
72 hrs	46 ± 1 (6)	45 ± 1 (6)	47 ± 2 (4)	45 ± 0.7 (4)	46 ± 1 (3)	46 ± 0.5 (3)

Table 8-18: T_2 relaxation times in injected and contralateral cortices pre-challenge (day 42), and 6, 24, and 72 hours post-LPS, saline (SAL PC) or no peripheral challenge (NPC). Values are expressed as the mean ± S.D for (n) animals.

8.6.6 T_2* Striatum

The T_2* relaxation time in the injected hemisphere was consistently reduced in all animals post-challenge (Table 8-19). No significant changes in the T_2* relaxation time were found over time, either in LPS or control animals. In addition, the area of the lesion on T_2* maps did not significantly change over time (Table 8-20). However, at 24 hours post-LPS challenge, a significant difference was found in the area of the lesion on T_2* maps, between LPS and NPC controls.

Time-Point	Striatal T_2* Relaxation Time (L/R)		
	LPS	SAL PC	NPC
Day 42	0.78 ± 0.17	0.70 ± 0.18	0.82 ± 0.10
6 hrs	0.86 ± 0.20	0.78 ± 0.19	0.82 ± 0.12
24 hrs	0.76 ± 0.15	0.90 ± 0.06	0.70 ± 0.06
72 hrs	0.89 ± 0.19	0.82 ± 0.16	0.87 ± 0.11

Table 8-19: T_2* relaxation time of striatum pre-challenge (day 42), and 6, 24, and 72 hours post-LPS, saline (SAL PC) or no peripheral challenge (NPC). Values are expressed as the mean ± S.D. No significant differences were found between LPS-challenged and control animals in either hemisphere at any time-point.

Time-Point	Size of Lesion on T_2* maps (No. of Pixels)		
	LPS	SAL PC	NPC
Day 42	87.4 ± 28.9 (9)	82.5 ± 25.3 (4)	62.7 ± 38.2 (3)
6 hrs	98.2 ± 33.1 (9)	101 ±57.4 (4)	55.3 ± 34.9 (3)
24 hrs	100.9 ± 28.7 (9)*	79.25 ± 47.5 (4)	57 ± 18.5 (3)*
72 hrs	112.4 ± 38.8 (5)	109 ± 59.1 (4)	54 ± 38.1 (3)

Table 8-20: Area of lesion on T_2* maps pre-challenge (day 42), and 6, 24, and 72 hours post-LPS, saline (SAL PC) or no peripheral challenge (NPC). Values are expressed as the mean ± S.D for (n) animals. No significant changes were found over time in any group, and no significant differences were found between LPS-challenged and control animals at any time-point, (unpaired t test *$p<0.05$).

8.6.7 Magnetisation Transfer

Spatially, the area of reduced MTR appeared to alter over time in the LPS-challenged animals (Figures 8-26, 8-27), although, no significant change in intensity over time in any group was detected by ANOVA ($p=0.22$). However, by 72 hours post-LPS challenge the MTR appeared to decrease significantly from NPC animals (unpaired t test $p<0.005$). In contrast, in both groups of control animals, (SAL PC and NPC), the MTR appeared to increase over time; NPC animals showed a greater increase, but this did not quite reach significance (ANOVA $p=0.0502$). In those animals, the MTR at 72 hours post-LPS challenge was significantly (unpaired t test $p<0.01$) greater than pre-challenge values at day 42.

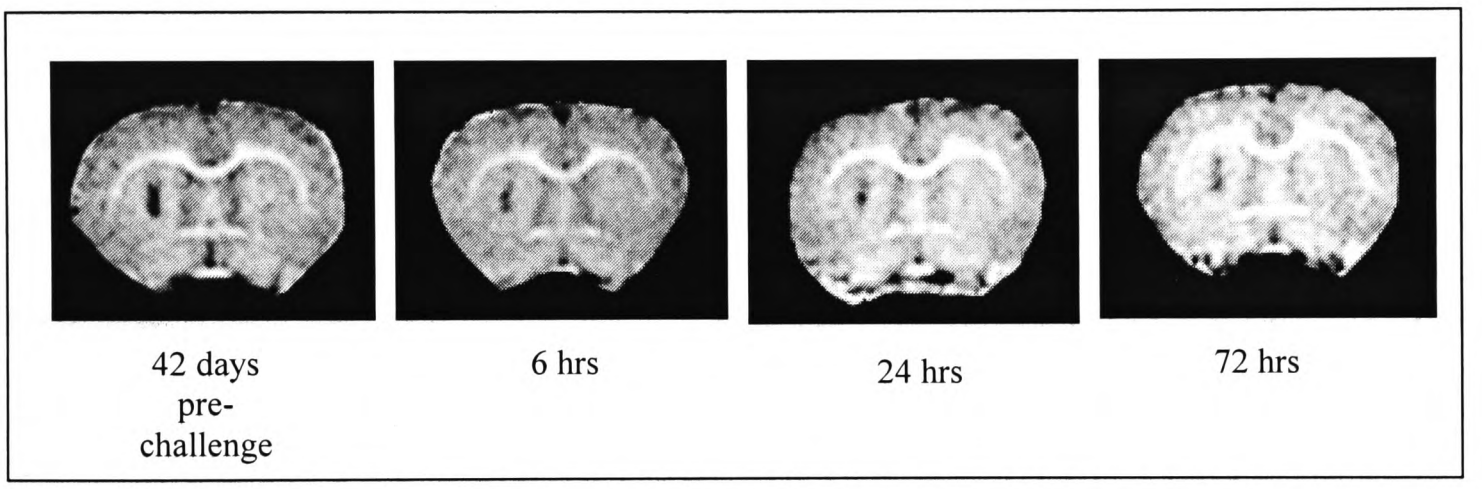


Figure 8-26: MTR maps obtained pre-challenge (day 42) and post-LPS challenge (6, 24 and 72 hours) showing reduced MTR of lesion.

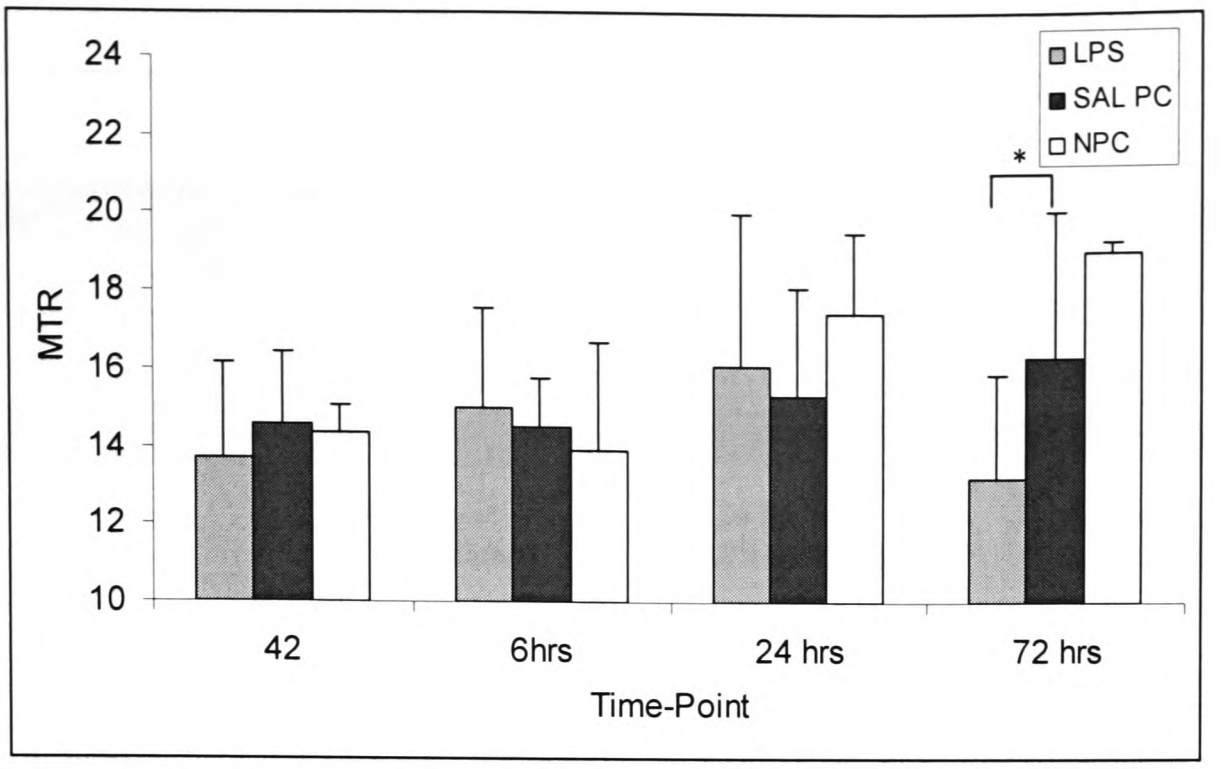


Figure 8-27: Graph to show MTR ratio of lesion pre-challenge (day 42) and post-challenge with LPS, saline (SAL PC) or no peripheral challenge (NPC) (6, 24 and 72 hours). Values are expressed as the mean ± S.D. Significant differences were found between LPS-challenged and NPC animals at 72 hours post-challenge (*$p<0.005$ unpaired t test).

8.6.8 Re-opening of the Blood-Brain Barrier

Increased permeability of the BBB was observed in 6/8 animals. An increase occurred in 4/8 animals 6 hours post-LPS challenge (Figure 8-28), and additionally, 2/8 animals showed delayed re-opening at 72 hours post challenge (Figure 8-29). However, in some SAL PC control animals, the BBB also appeared to re-open at 72 hours post-LPS challenge. NPC controls showed no change in BBB permeability at any these time-points.

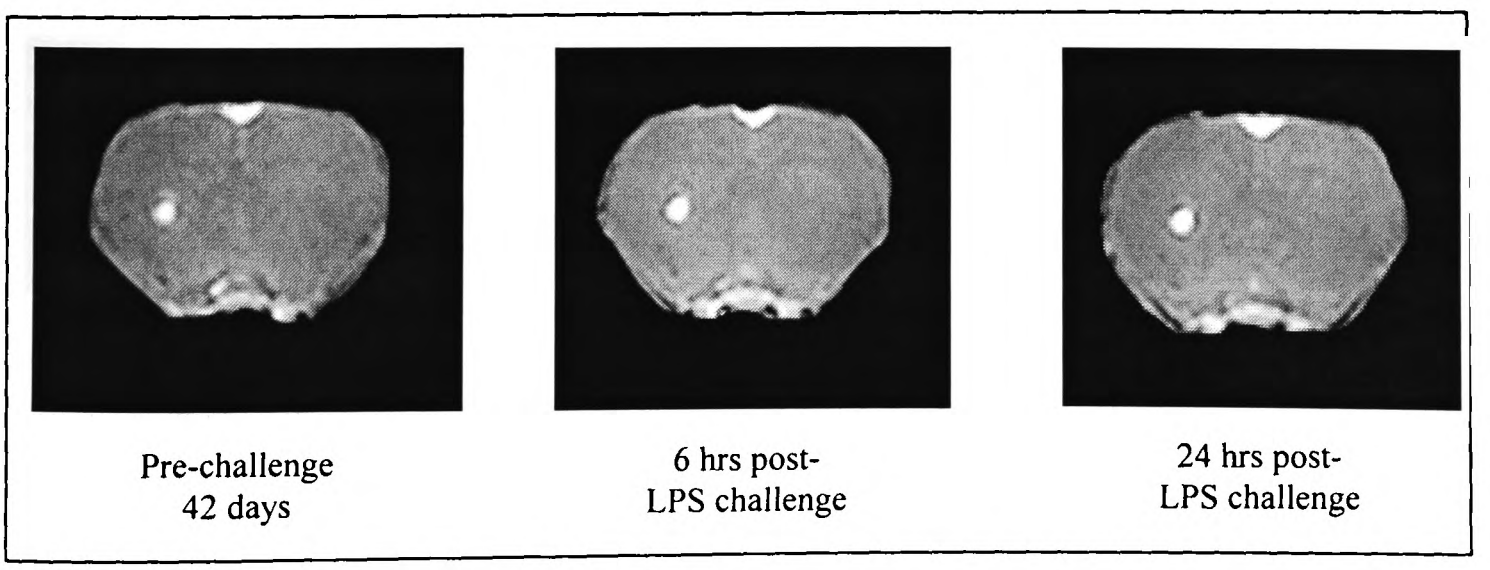


Figure 8-28: Post-contrast T_1-weighted images acquired pre-challenge (day 42) and post-LPS challenge at 6 and 24 hours, showing increased permeability of the BBB 6 hours post-challenge as indicated by gadolinium enhancement.

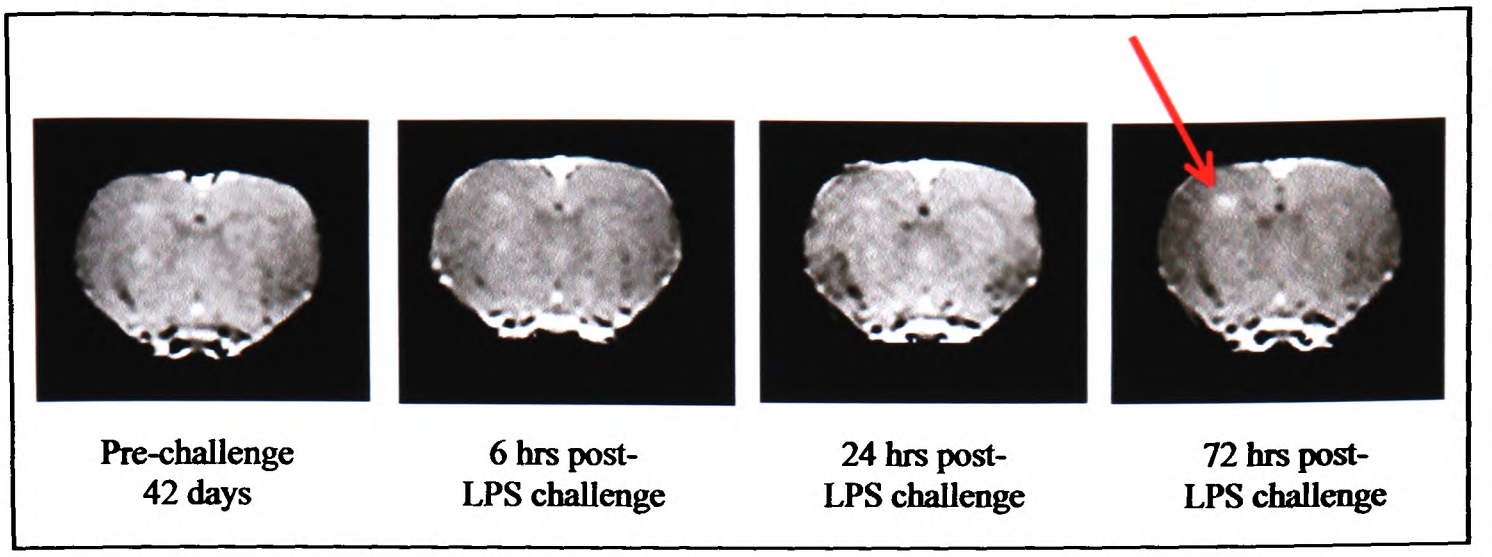


Figure 8-29: Post-contrast T_1-weighted images acquired pre-challenge (day 42) and post-LPS challenge at 6, 24 and 72 hours, indicate a delayed reopening (as indicated by arrow) of the BBB 72 hours post-challenge as indicated by gadolinium enhancement.

8.6.9 ADC Changes

Pre-challenge at 42 days, a region of decreased ADC was observed surrounding the lesion core. 6 hours post-LPS challenge this region appeared to resolve somewhat. However, by 24 hours, in some animals (5/9) a region of decreased ADC appeared that surrounded the lesion core and extended for some distance through the injected striatum and towards the ventral portion of the brain (Figure 8-30). In addition, 2/4 SAL PC controls and 1/3 NPC controls also showed this decrease.

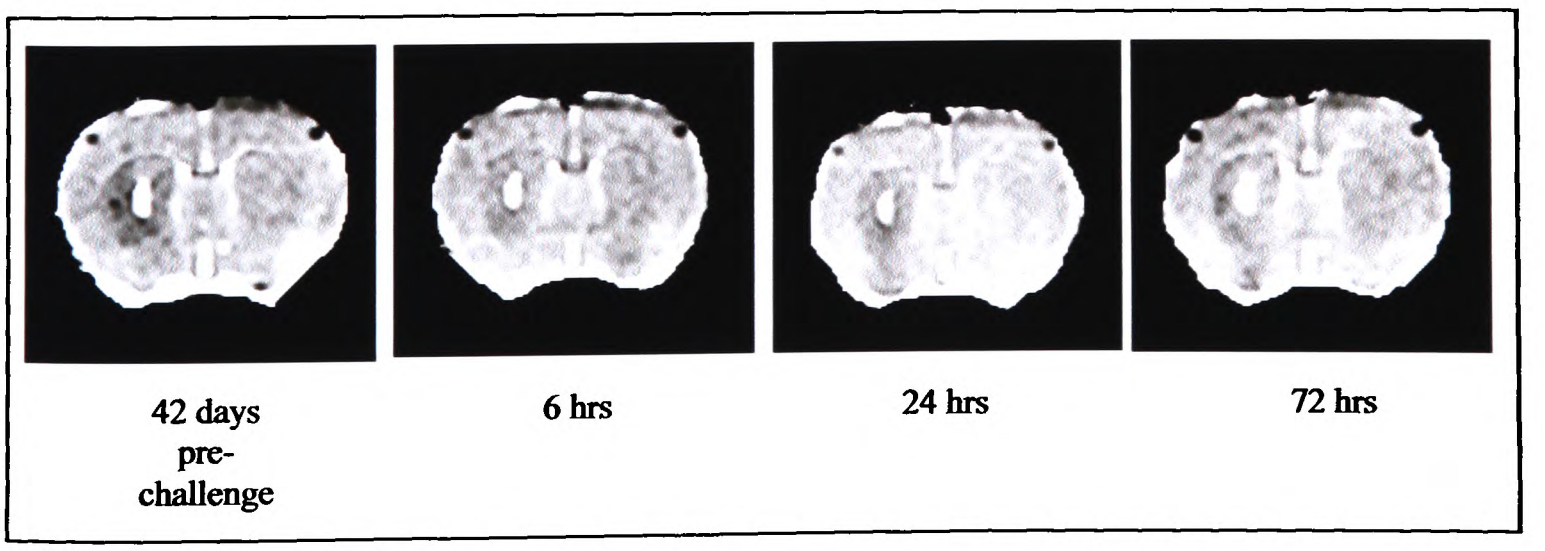


Figure 8-30: ADC maps acquired pre-LPS challenge (day 42), and 6, 24 and 72 hours post-challenge showing decreased diffusion surrounding the lesion core and extending down into the ventral brain at 24 hours.

8.6.10 Diffusion Anisotropy

Six hours post-LPS challenge, the lesion became more hypointense on anisotropy maps, indicating a decrease in anisotropy (as indicated by the arrow in Figure 8-31). This reduction in anisotropy progressed such that at 24 hours post-LPS challenge, the lesion appeared to be maximally hypointense.

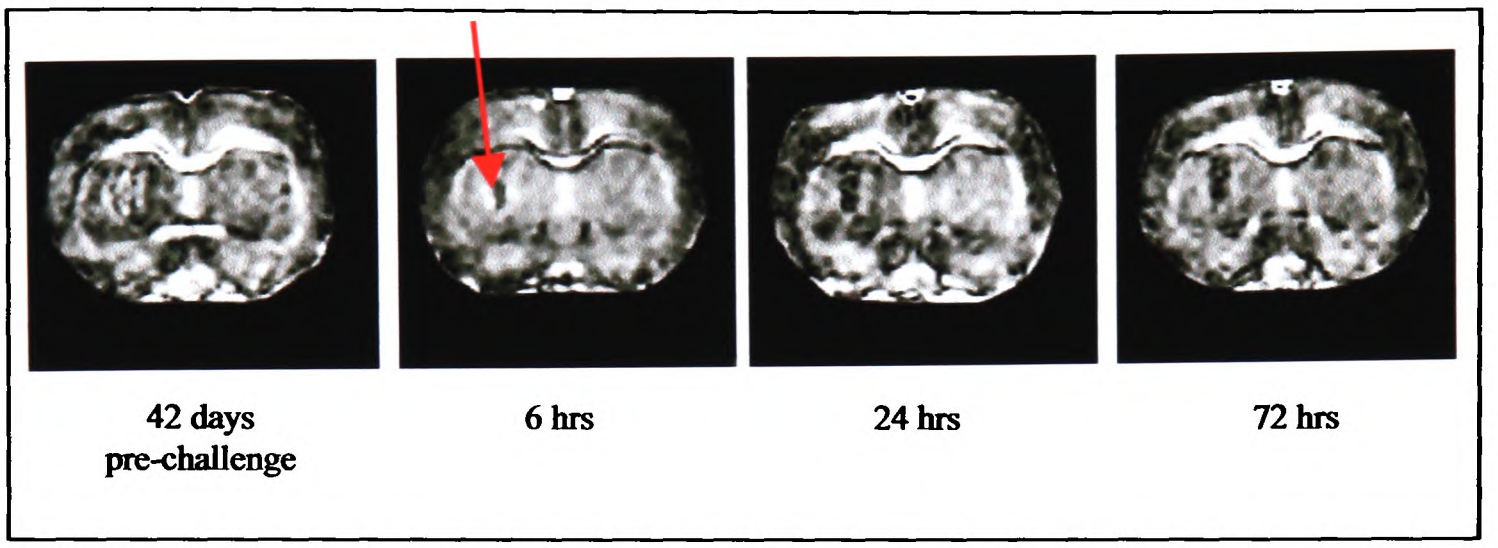


Figure 8-31: Diffusion anisotropy maps, acquired pre-challenge (day 42), and 6, 24, and 72 hours post-LPS, saline (SAL PC) or no peripheral challenge (NPC) showing hypointense lesion as indicated by the arrow.

8.6.11 Immunohistochemistry

10 days post-LPS challenge a large number of macrophages and a small number of neutrophils were present in the DTH lesion. Many of the cells in the hypercellular lesion expressed MHC class II (Figure 8-32a). In addition the perimeter of the lesion was surrounded by heavily activated reactive astrocytes with the astrocytic end feet touching the hypercellular lesion core (Figure 8-32b). The astrocytes appeared to be more aggressive than those observed in previous studies (Section 4.6.3). Reactive astrocytes were also found throughout the injected hemisphere, and notably some spreading down towards the ventral aspect of the brain. Loss of myelin was also observed (Figure 8-32c), and to a much greater extent to that reported in Section 4.6.2, probably owing to the more extensive nature of the lesion. Laminin staining was also carried out. Although laminin was expressed throughout the brain, marked up-regulation of laminin expression was

observed on vessels surrounding the lesion and throughout the injected hemisphere (Figure 8-33). In addition, there appeared to be an increase in the number of blood vessels surrounding the lesion.

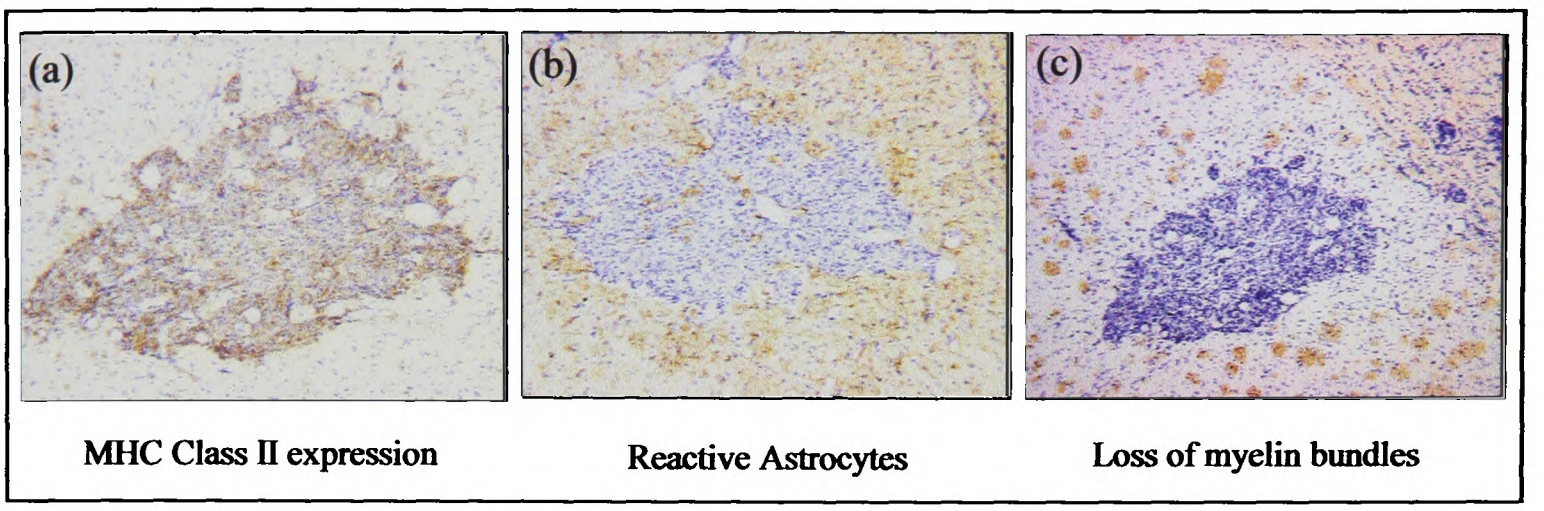


Figure 8-32: Immunohistochemical characteristics of the re-activated DTH lesion.
(a) Cells expressing MHC class II were stained brown were scattered across the purple hypercellular lesion.
(b) Reactive astrocytes, also stained brown surrounded the perimeter of the lesion.
(c) Loss of myelin bundles occurred throughout the lesion and in some cases across the corpus callosum.

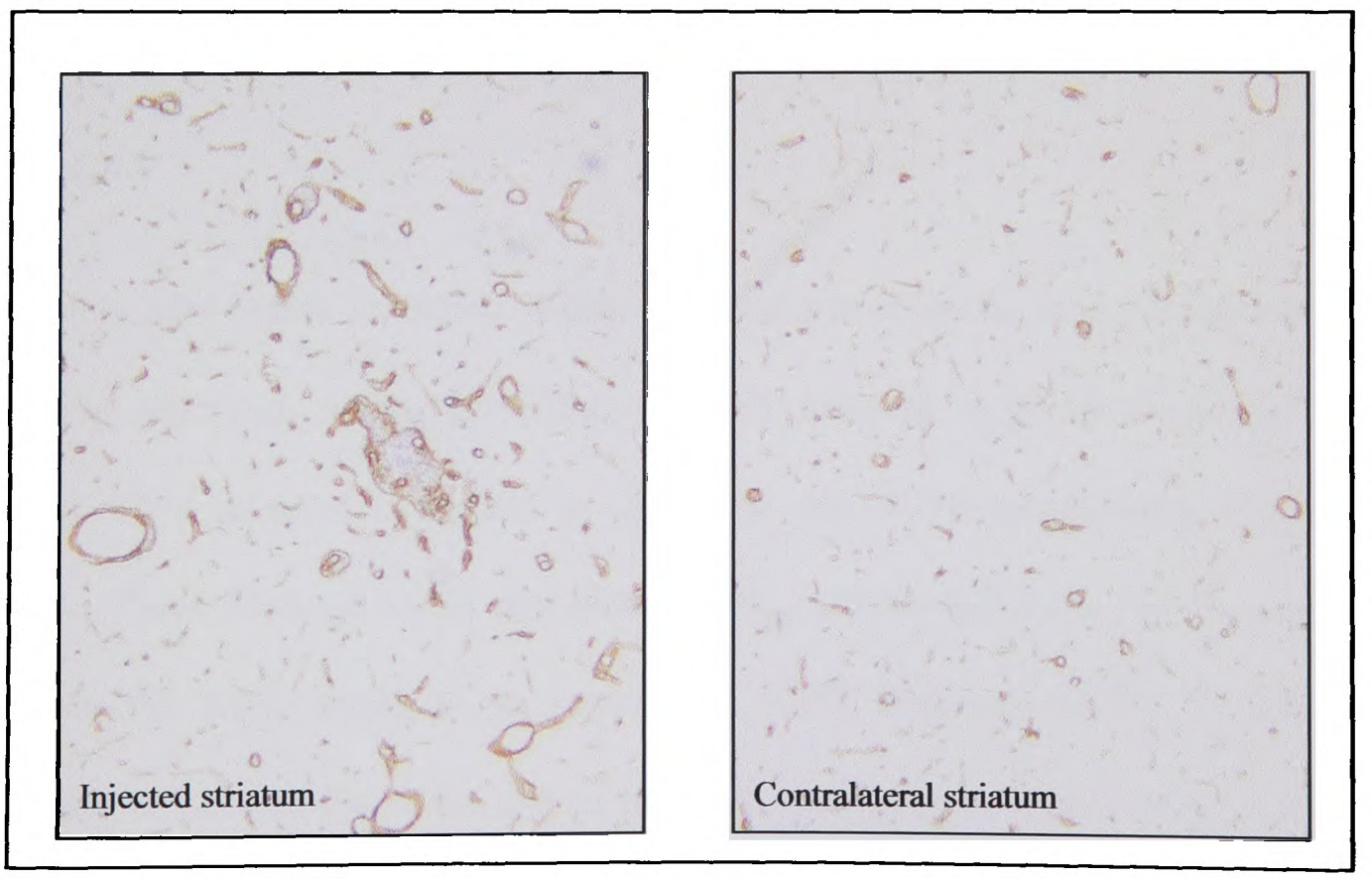


Figure 8-33: Expression of laminin on blood vessels surrounding the lesion and throughout the injected and contralateral striata. There appeared to be an increase in the number of blood vessels surrounding the lesion.

8.7 Discussion

8.7.1 Findings in this chapter

In this chapter it has been demonstrated for the first time that a peripheral challenge of *E coli* LPS endotoxin can re-activate a DTH lesion that was previously active. The primary effects of this exacerbation are, an acute increase in rCBV, and an increase in the T_1 relaxation time, followed by a delayed increase in BBB permeability. Additionally, changes in tissue water, MTR, and diffusion anisotropy were observed post-LPS challenge, although it is less clear whether these findings were specifically related to the LPS peripheral challenge. These findings, together with those pertaining to the acute evolution of the DTH lesion in this modified version of the DTH model will be discussed in detail below.

8.7.2 Acute Response

8.7.2.1 CBV

At 24 hours after lesion induction within the brain parenchyma, an acute increase in the rCBV was observed, which correlated with an increase in IL-1β production. The increased rCBV returned to normal levels by the end of the spontaneous inflammatory response. These findings are in accordance with previous studies in which injection of IL-1β into the brain results in an increase in rCBV (Blamire 2000). In that study, recruitment of neutrophils to the site of injection were also observed in agreement with other studies showing that IL-1β solely recruits neutrophils to the CNS (Blond 2002). Here, in the modified DTH lesion, neutrophils were also observed early in the DTH response, adding further support to the hypothesis that early rCBV changes are mediated

by IL-1β. These results also confirm and support the observations of increased rCBV prior to significant BBB permeability changes as previously described in Chapter 7. The findings here, that IL-1β is expressed widely in the striatum, suggest that the increases reported in earlier chapters study may be, at least in part, mediated by IL-1β. The use of antagonists or antibodies to block the action of IL-1β would yield information on the role of IL-1β in increasing rCBV.

8.7.2.2 T_1, T_2 and T_2* Relaxation Time

The T_1 relaxation time in both the brain striatum and cortex was increased acutely, followed by a subsequent decrease to below the levels observed in naïve animals, by the end of the acute inflammatory response. Similarly, this increase was observed in the T_2 relaxation time was also increased. In the striatum, changes in both T_1 and T_2 relaxation times were bi-directional. A core area of prolonged T_1 and shortened T_2 was apparent, which was surrounded by a region of shortened T_1 and prolonged T_2. The overall striatal values depend on which effect dominates at each time-point. The core region was present throughout the time-course, whereas the surrounding region of shortened T_1 and lengthened T_2 appeared to dominate during the early part of the inflammatory response (from days 0-5). The latter effects probably result from oedema and increased BBB permeability. The changes in the cortex occur remotely from the lesion, possibly brought about by the action of cytokines that may have the ability to diffuse (Blamire 2000), (Sibson 2002). In addition, a spin-echo sequence was used for acquiring the T_1 maps, therefore tissue oxygenation resulting from the increased rCBV would not have had an effect on the T_1 relaxation time.

Interestingly, an increased T_1 relaxation time was also observed in the contralateral hemisphere at the same time-point, suggesting that signals (either cytokine mediated, or via neuronal connectivity) from the injected hemisphere affect the contralateral hemisphere, possibly via the corpus callosum (Aboitiz 2003), (Maier 2003). However, the subsequent contralateral decrease was much less marked than any of the changes observed in the injected hemisphere. It has been suggested that the right hemisphere in mice (in this study, the contralateral hemisphere) controls the inductive influence of signals (coming from behaviour, endocrine and immune systems) emitted by the left (injected hemisphere) (Renoux 1988). The signals may be cytokine or neurochemical mediated, thus affecting neurons or inflammatory cells that may be present in either hemisphere. If this were the case then a contralateral increase in some immune functions and metabolic effects might be expected, which may in turn cause alterations in the T_1 relaxation time.

These investigations of quantitative T_1 and T_2 values confirm the results reported in Chapter 5, where a hypointense region was observed on T_1-weighted images. The consistent increase in T_1 relaxation time within the core of the lesion indicates that the observation on those images are not as a result of T_2 changes, but are a true alteration in the T_1 relaxation time. The results from this study that a decrease in T_1 and T_2 relaxation time occur after the initial increase, are in agreement with observations in EAE, where decreased T_1 and T_2 relaxation times are also reported (Karlik 1989).

Naïve animals, showed no alteration in either T_1 or T_2 relaxation time in the time allowed for the spontaneous DTH response. This suggests that the changes observed in DTH animals were not an age effect, but occur as a result of pathological processes occurring in and around the DTH lesion over time.

A decrease over time in the T_2* relaxation time was also observed within the lesion, after intracerebral injection of BCG. The T_2* relaxation time is affected by paramagnetic effects, such as deoxygenated blood and the presence of iron. In Chapter 5, it was hypothesised that macrophages that are present in the hypercellular lesion core may contain iron. The presence of these iron-rich macrophages in the lesion may underlie the decrease in the T_2* relaxation time in the lesion core.

8.7.2.3 Magnetisation Transfer, Diffusion-Weighting and Contrast Enhancement

Following intracerebral injection of BCG, the MTR of the lesion was reduced, possibly as a consequence of the extensive myelin loss within the lesion. In contrast to the DTH lesion described in Chapter 6, the modified DTH lesion was clearly visible as a region of reduced MTR. In this scenario, it is likely that the larger lesion caused greater cell recruitment and greater cytokine expression, thus adding to the effects of oedema and demyelination and resulting in a reduced MTR. Loss of the corpus callosum was observed on MTR images in Chapter 6, however in this study, this loss was not observed. This disparity is likely to be brought about by different lesion positions. In this study, the lesion was induced deeper in the striatum, making it unlikely that the lesion would oppose, and disrupt myelin bundles in the corpus callosum. A central core region of decreased ADC surrounded by a region of increased ADC was observed in all animals. The area of decreased ADC correlated spatially with the dense population of inflammatory cells at the lesion core. Thus, one hypothesis is that the dense core of cells results in a restriction of tissue water diffusion. Alternatively, a decreased ADC is associated with compromised energy metabolism, particularly in ischaemia (Rudin 2001). A further explanation may be a considerably elevated metabolic demand within the lesion core, owing to the greatly increased number of cells present. Recruited macrophages and

activated microglia will also be highly metabolically active at those time-points. Conversely, the increased ADC is likely to be due to the presence of oedema. In addition, a decrease in the diffusion anisotropy at the lesion core was observed, suggesting disruption of the order of myelinated axons, consistent with myelin and axonal loss. As with the previous study in Chapter 6, BBB breakdown occurred maximally at the same time as maximal changes in increased ADC, and increased T_2 signal intensity. This increase in BBB permeability resolved as time progressed, as did the increased ADC and T_2 relaxation time, indicating resolution of oedema. The decrease in MTR, ADC, T_1 and T_2, and diffusion anisotropy were all spatially coincident with each other (Figure 8-34 and 8-35). In addition, the region of increased ADC, increased MTR, T_1 and T_2, and broader region of decreased diffusion anisotropy were all spatially coincident with each other, as observed in Figure 8-34.

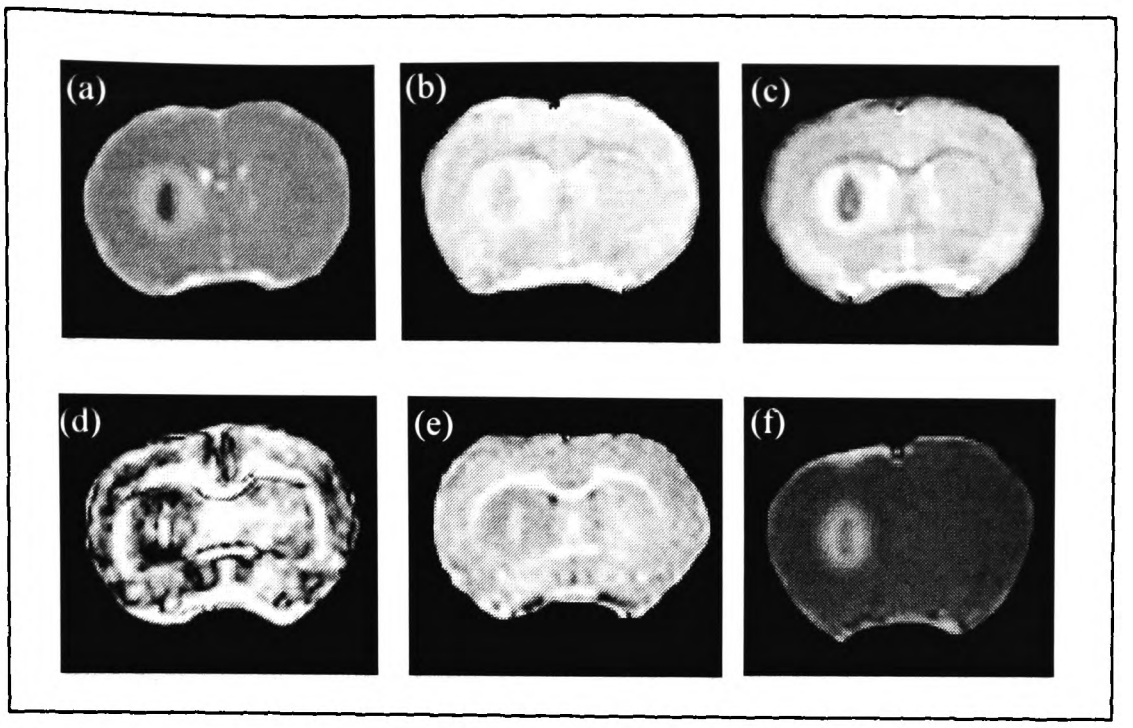
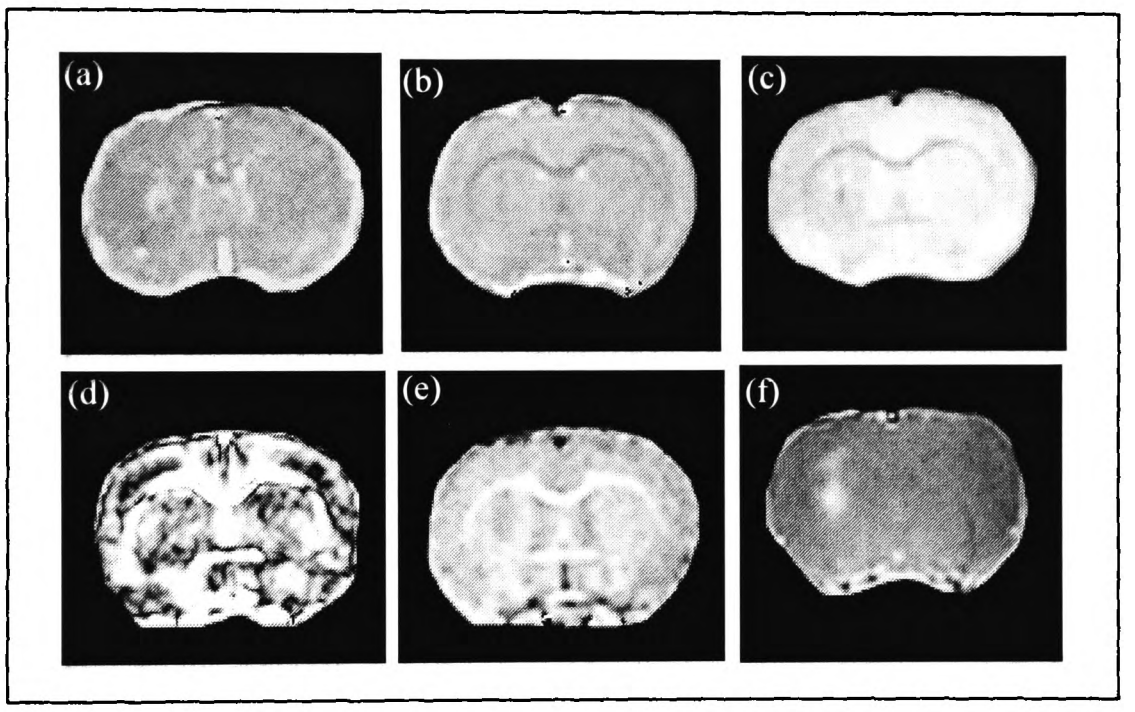


Figure 8-34: Areas of decreased ADC (a), T_1 (b), T_2 relaxation time (c), increased diffusion anisotropy (d) and MTR (e) all spatially coincide with each other. In addition, areas of increased ADC (a), T_1 (b) and T_2 relaxation time (c), decreased diffusion anisotropy (d), MTR (e) and BBB permeability (f), spatially correlate.



8.7.3 Post-LPS Inflammatory Response

Exposure to high levels of LPS, a component of the outer membrane of gram-negative bacteria often results in septic shock and death. Systemic LPS infection has also been reported to induce changes in osmolarity, oxygen consumption, fever, energy metabolism, multiple organ failure and different changes in the endocrine system, such as activation of the hypothalamic-pituitary adrenal axis (Lacroix 1998). Systemic LPS administration is a well accepted model of peripheral inflammation that activates the mononuclear phagocyte system and stimulates synthesis and release of cytokines, such as IL-1β, IL-6 and TNF-α,

into the circulation. The secretion of these cytokines by stimulated macrophages, neutrophils and lymphocytes is directly responsible for most of the effects of LPS in the brain (Lacroix 1998). LPS can act on the brain microvasculature leading to the transcriptional activation of pro-inflammatory genes, including those encoding the chemokines within CNS macrophages.

The qualitative observations from this study, that animals had reduced activity, and alterations in temperature regulation post-LPS challenge are in agreement with Combrinck et al. (Combrinck 2002), who showed that in a model of Prion disease, animals develop reductions in locomotor activity also. However, in that study, a hypothermic response, rather than hyperthermic was observed in animals 24 hours post-LPS challenge, but these differences may be due to difference disease models. The observations in the current study were only qualitative; further investigation of quantitative measurements of core body temperature in association with MRI changes might yield further information on the behavioural aspects of LPS effects.

8.7.3.1 rCBV changes

An increase in rCBV was observed 6-24 hours post-LPS challenge. This increase was not observed in any control animals, and this observation has not been previously reported. This result clearly demonstrates that a lesion within the CNS parenchyma can be exacerbated as a consequence of peripheral inflammation, in this case induced by LPS. The increased rCBV temporally coincides with the behavioural observations of increased temperature and reduced locomotor activity. Both the behavioural and increased rCBV results had resolved by 72 hours post-challenge. These increases may be brought about

by release of oxygen radicals, prostaglandin synthesis, nitric oxide synthase production and release of cytokines, since LPS is known to induce cytokines.

Induction of cytokine secretion by LPS occurs via a cascade of events. The LPS must first reach the bloodstream, where it binds to the LPS binding complex. This complex then binds to a CD14 receptor, which is expressed by monocytes and macrophages and therefore induces cytokine release. It has been previously shown that peripheral administration of LPS causes upregulation of CD14 receptor on cells of the vasculature of the rat brain (Lacroix 1998). Upregulation of CD14, and thus an increased cytokine release may be the mechanisms behind the elevated rCBV observed in this study. It has previously been shown that injection of IL-1β into the rat brain results in an increased rCBV (Blamire 2000). It was initially thought that induction of IL-1β expression by LPS might be the underlying mechanism behind the increased rCBV in this study. However, undetectable levels of IL-1β were found in the lesion 6 hours post-challenge. The presence of a small number of neutrophils in the lesion suggests that cytokine production may be occurring in levels that could not be detected. Alternatively, the changes in rCBV may be mediated by other mechanisms such as nitric oxide, a vasodilator produced by macrophages and microglia in response to inflammation (for review, see Willenborg et al. (Willenborg 1999)).

The acute increases in rCBV are likely to reflect increased metabolic demand, probably as a result of increasing recruitment of further inflammatory cells, especially neutrophils and macrophages. Metabolites may also be brought into the brain that are subsequently used by activated inflammatory cells, probably microglia.

8.7.3.2 T_1, T_2 and T_2* Relaxation time

At the same time as increased rCBV (6 hours post-LPS challenge), an acute increase in T_1 relaxation time was observed in both the striatum and cortex of LPS-challenged animals. This increase was observed in both the injected and contralateral hemispheres of LPS-challenged animals, but was not observed in control animals. The increase in T_1 was not associated with a concomitant increase in T_2 relaxation time, suggesting that mechanisms behind the increases post-challenge may be different to those behind the increases occurring after intracerebral injection of BCG. Similarly, no change in the T_2* relaxation time were observed post-challenge. Increases in T_1 without increases in T_2 have been observed in the spinal cord of EAE mice (Karlik 1986), this is observed when there is extensive cellular infiltration, (as was the case with the lesions in this study), and it is an established notion that T_1 relaxation time is increased in heavily gliotic lesions (Stewart 1984). Thus, it is possible that LPS administration causes increased astrocyte activation, resulting in increased gliosis of the lesion at six hours. The clearance of cytokines induced by LPS from the circulation would have the effect of reducing the activity of the reactive astrocytes in the DTH lesion resulting in a reduction of the T_1 relaxation time at later time-points.

An increased T_1 relaxation time was also observed in the contralateral hemisphere. As suggested in the previous section during the acute inflammatory response, this contralateral change adds further support to the idea that the two hemispheres of the brain can communicate. Thus, it is not clear if the effects of LPS on the injected hemisphere, or in the cortex are a direct exacerbation effect on the DTH lesion, which results in contralateral effects (as observed during the acute inflammatory response) or a global

effect of LPS on the brain. Further investigation of the relaxation rates in naïve animals challenged peripherally with LPS, would address this issue

8.7.3.3 Contrast Enhancement, Diffusion-Weighting and Magnetisation Transfer

BBB re-opening, which occurred in many animals after LPS-challenge may be brought about the action of cytokines. It has been shown that intracerebral injection of TNF-α results in BBB breakdown 24 hours after injection (Sibson 2002); IL-1β injection however, results in a more rapid re-opening of the BBB, that is dependent on neutrophils (Blamire 2000). Since LPS is known to cause the induction of IL-1β and TNF-α (Luheshi 1998), and the fact that neutrophils were present in small numbers post-challenge, both these cytokines and a host of other mediators may be responsible, at least in part, for facilitating BBB re-opening in this study. This re-opening of the BBB as a result of peripheral inflammation, as observed here, is in agreement with the clinical study by Edwards et al. (Edwards 1998) who showed some evidence indicating that increased BBB breakdown and inflammation occur during periods of infection. Both the results presented in this chapter and the work of Edwards et al. differ from the very recent clinical study of Buljevac et al. (Buljevac 2002), which showed that peripheral infection did not alter the number of enhancing lesions. In that study, MRI was performed after MS patients reported a clinical infection, but the average interval between identifying infection and the MRI scan was 7 days. As observed in the current study, the BBB permeability was increased 6 hours post-inflammation, suggesting that in the clinical situation, the MRI scan at 7 days post-infection is probably too late to identify enhancing lesions. In addition, in the current study, in some animals, BBB re-opening was observed at 6 hours, and in some animals at 72 hours. It is also likely that there is the same degree

of variability in the clinical situation, adding to the likelihood of missing the identification of enhancing lesions on MRI.

A decreased ADC was observed 24 hours post-challenge, however this did not appear to be restricted to the LPS-challenged animals, therefore this change in ADC may occur as a result of natural lesion progression. The decreased ADC occurred in the same regions as increased ADC during the acute DTH response. It is possible therefore, that oedema occurring in the acute inflammatory response may have locally restricted perfusion through capillary beds, resulting in reduced oxygenation of the brain tissue. Consequent metabolic compromise may underlie the subsequent decrease in ADC as has been observed in ischaemia (Rudin 2001). An alternative explanation, however, arises from the finding that reactive astrocytes were found to extend in many cases throughout the regions of decreased ADC. This phenomenon has also been observed in traumatic brain injury where large regions of reactive astrocytes coincide with areas of decreased ADC (Vorisek 2002). In contrast to the original DTH lesion, in Chapter 6, no correlation was found (Section 6.4.9) between the amount of astrogliosis and decreased ADC. It has been suggested that hypertrophy of astrocytic processes causes alterations in extracellular matrix components, resulting in additional diffusion barriers and thus a decrease in ADC.

Interestingly, a reduction in diffusion anisotropy in the core of the lesion occurred 24 hours after LPS-challenge. The reduced diffusion anisotropy at that time-point may be brought about by additional recruitment of inflammatory cells (aided by pro-inflammatory cytokine expression induced by LPS) to cause a densely populated region, with an organised tissue structure. This would have the effect of reducing diffusion anisotropy within that region. An acute reduction in MTR was observed also at the core of the lesion, 72 hours post-LPS injection. This observation has not been reported previously, and probably reflects further demyelination and inflammatory processes

occurring as a result of cytokine expression and additional inflammatory cell recruitment to the DTH lesion, rather than demyelination alone.

8.7.4 Summary

In conclusion, the MRI visible effects of the DTH lesion, as a model of chronic inflammation are exacerbated by a peripheral inflammation induced by LPS endotoxin. The primary effects of this exacerbation are an increase in rCBV with a concomitant increase in T_1 relaxation time, and re-opening of the BBB. Since the MRI-visible exacerbation occurred very soon after peripheral challenge, this has implications for the treatment of relapses in MS patients. Treatment for MS relapses might be more effective if given at the time, or as soon as possible after, the onset of a clinical infection, before the damaging metabolic effects, of the exacerbation occur, reducing the risk of long term neurological damage.

Chapter 9

Conclusions and Future Work

The bulk of study into Multiple Sclerosis has involved both clinical and experimental investigation using various animal models, such as EAE and TMEV. These models of MS have, to date, provided a great deal of information regarding the pathology and processes occurring as a result of chronic inflammation in the CNS, but much of the data available seem contradictory and there is still a lack of understanding of the pathology and mechanisms involved.

The development of the delayed type hypersensitivity (DTH) model as described in this thesis has shed a unique insight into the MRI-visible effects of the pathology occurring during a chronic demyelinating lesion, similar to those observed in MS patients and in EAE models.

9.1 Conclusions

The overall purpose of the work described in this thesis was to develop and characterise the DTH model using a range of MRI techniques, from those conventionally used such as T_1- and T_2-weighted imaging in association with contrast enhancement, to those techniques that provide more sensitive measures of disease processes, such as diffusion-weighted imaging, magnetisation transfer imaging and blood volume measurements.

The initial goal of this work was to correlate ongoing MRI changes with the underlying histopathological changes of the DTH lesion, with the additional aim of identifying MRI

markers of early disease activity. Peripheral infections are hypothesised to cause exacerbations of MS and the final aim of this thesis was to determine the effects of a peripheral challenge on the quiescent DTH lesion.

9.1.1 Evaluation of model

The first chapter in this thesis was concerned with development of the DTH model and evaluation of this as a valid model for MRI investigation of an MS-like lesion. The DTH model was modified to obtain a larger lesion without a spontaneous DTH inflammatory response. The lesion was characterised in terms of inflammatory cell recruitment, MHC class II expression, neuronal loss, areas of BCG antigen spread, and IgG permeability as a measure of BBB compromise. Although many of the results are previously published, the finding of neuronal loss within the DTH lesion is new. A further novel aspect of the current work is the demonstration of spatial mapping of the histological characteristics of the DTH lesion to each other. It was found the hypercellular core of the lesion consisted of macrophages and T & B cells, in which neuronal and myelin loss also occurred. Reactive astrocytes were found surrounding the lesion. Thus, this chapter successfully saw development of the DTH lesion for MRI investigation.

9.1.2 T_1- and T_2-weighted imaging

MRI characteristics of the DTH lesion were initially identified using conventional MRI techniques such as T_1- and T_2-weighted imaging, since these are used clinically for diagnosis and assessment of MS. It was found that the DTH lesion yielded similar MRI pathology to both the MS and EAE lesion, in that the DTH lesion was both hypointense on T_1-weighted images and hyperintense on T_2-weighted images. In addition, the DTH lesion appeared to have a hypointense core on T_2-weighted images. This latter finding is

new, and may be unique to the DTH model. However, another explanation is that the T_2 hyperintensities observed in MS patients may be so overt that they block out, or cancel the effects of any T_2 hypointensity. If this is the case, the DTH lesion may yield new insights into the events occurring within MS lesions that have not been detected previously. The DTH lesion appeared to progress in terms of spatial extent on both T_1- and T_2-weighted images, which is also in agreement with clinical studies of MS.

9.1.3 Contrast Enhancement, Diffusion and Magnetisation Transfer.

The contrast enhancement, diffusion-weighted and magnetisation transfer imaging characteristics of the DTH lesion were also investigated. Both diffusion-weighted and magnetisation transfer methods have been shown clinically to identify changes in MS patients prior to lesion appearance on T_1- and T_2-weighted images, so it was thought that these methods might provide more sensitive measures of pathology. It was found that the DTH lesion exhibited both decreases and increases in diffusion. The maximal increase in ADC occurred at the same time as maximal contrast enhancement and maximal T_2 hyperintensity, suggesting the presence of oedema as a consequence of BBB breakdown. The lesion core was found to have a loss of anisotropy and a decreased ADC, which is most likely to be brought about by the dense population of cells, however the decreased ADC did not correlate quantitatively with the T_1 and T_2 hypointensities. The contrast enhancement findings are in agreement with clinical and EAE studies in the literature as are the findings of increased diffusion and decreased anisotropy. However, the decrease in diffusion is less commonly observed. This again, may be an MRI characteristic specific to the DTH lesion, or it may be that large increases in diffusion mask the effects of a central core of decreased ADC in MS patients. Although similar findings have been reported previously in MS and animal models, temporal progression and evolution of

contrast enhancement and altered diffusion have not been shown. In addition, this study has demonstrated the spatial coincidence of different MRI parameters, for example, the T_2 hyperintensity was found to spatially map to areas of increased ADC and BBB permeability. Results of the magnetisation transfer imaging experiments described in this thesis indicate that there is a reduced MTR in the core of lesion that is coincident with myelin loss. Interestingly, however, there appears to be more widespread changes that affect the corpus callosum, which have not been previously observed and which occur in tissue that appears normal on conventional T_2-weighted images. It is unclear what the underlying mechanism behind these decreases in MTR are, since demyelination is currently believed to be the major factor for loss of MTR, but, in the DTH lesion, myelin loss occurred only within the hypercellular core. This suggests that structural changes in NAWM that gives rise to a decrease in MTR that is not associated with demyelination.

9.1.4 rCBV changes

Regional cerebral blood volume (rCBV) was also investigated and it was established that an increased rCBV is one of the earliest events to occur in the pathology of the DTH lesion. These changes preceded maximal BBB permeability changes, and maximal changes on other MRI images (increased ADC, T_2 hyperintensity). Areas of increased rCBV were observed in areas distant from the DTH lesion, and probably occur as a result of increased cytokine production (e.g. IL-1β) by macrophages and T cells recruited to the DTH lesion. Other studies in the literature regarding rCBV (all clinical) have shown a decreased rCBV at the lesion core, but these studies have all been carried out when the lesion was active, as defined by contrast-enhcancement. In contrast, in this investigation, early CBV changes were found, which were not associated with marked alterations in BBB permeability. Such observations have not been previously reported and suggest that

monitoring of regional changes in rCBV may be of particular value in detecting early inflammatory events in the MS patient prior to BBB breakdown.

9.1.5 MRI-Histology Correlations

Once the MRI features of the DTH lesion were established, each MRI change was correlated with the underlying histopathology. Recruitment of T & B lymphocytes and macrophages, expression of MHC class II, and reactive astrocytes were investigated. Various spatial correlations were found, which provide information regarding the pathology underlying the MRI changes. The areas of T_2 hyperintensities, contrast enhancement, increased ADC spatially correlated with the area of reactive astrocytes, and thus, it seems likely that reactive astrocytes play a role in breakdown of the BBB. In addition, the hypercellular lesion core, composed of numerous T cells, macrophages, and cells expressing MHC class II, was found to spatially map to the hypointense regions present on ADC maps, T_1- and T_2-weighted images. The lesion core also exhibited both loss of neurons and myelin suggesting that these too might be important in the pathology causing the appearance of the hypointense regions on T_1- and T_2-weighted images, and ADC trace maps. The increased rCBV appeared to be associated with an up-regulation of Laminin expression, which is associated with the vasculature of the brain. In addition, major blood vessels were dilated and these also mapped to the focal increases in rCBV. T_2 hypointense areas correlated with recruitment of macrophages and T & B lymphocytes, and reactive astrocytes. In terms of quantitative correlations, it was found that T_2 hyperintense areas correlated with both areas of reactive astrocytes and MHC class II expression. The area of contrast enhancement correlated with recruitment of T & B lymphocytes. Areas of both increased and decreased ADC quantitatively correlated with MHC class II expression, and in addition, the area of ADC hyperintensity correlated with macrophage recruitment. These quantitative correlations have not been previously

reported and suggest associations between the immunohistochemical markers and MRI changes rather than underlying causes.

9.1.6 LPS Reactivation of the Immune Response

Although infections have been implicated in reactivation of the immune response for decades, very little experimental evidence has been obtained to support this hypothesis. In Chapter 8, the effect of LPS administration on a quiescent CNS lesion, was investigated. The DTH lesion was modified further in this chapter, to make the lesion larger in spatial extent, and additional MRI techniques were used. Quantitative measurements of the T_1 and T_2 relaxation time, revealed initial increases in both parameters, in the core of DTH lesion, which subsequently decreased with time, supporting the results described in Chapter 5. In addition, it was demonstrated that the early rCBV changes (that preceded significant contrast enhancement) may, at least in part, be brought about by the production of IL-1β, as detected by ELISA. In the second part of this chapter, the DTH lesion, which was once immunologically active, was shown to be reactivated by a systemic infection with *E coli* LPS. This reactivation was primarily observed as an increase in rCBV, but also as an increase in the T_1 relaxation time and re-opening of the BBB. The increases in T_1 relaxation time, rCBV, and BBB permeability occurred very early after infection, (6 hours) post-LPS challenge, and subsequently resolved. In addition, a decreased ADC was observed, but it is unclear whether this is a result of natural lesion progression or occurs as a result of the peripheral challenge. These changes in a chronic demyelinating inflammatory lesion, as a consequence of a peripheral infection, have not been previously reported, and have significant implications for the treatment and management of MS patients. In addition, these results suggest that peripheral infection may be implicated in the reactivation of other CNS pathologies, such as stroke or traumatic brain injury.

9.2 Future Work

9.2.1 Investigation of Individual Cell Types

In this work, animals were imaged then sacrificed in order for immunohistochemistry to be carried out. To correlate immunohistochemistry and MRI changes, up to 8 different immunological characteristics were investigated in the same animal, requiring a vast number of tissue sections. In some cases, where the lesion may not have extended very far rostrocaudally, not all sections may have been cut from the centre of the lesion, resulting in an incomplete reconstruction of the DTH lesion. Future studies should focus on setting up separate groups of animals to study specific cell types in the DTH lesion based on the data reported here in order to fully investigate the spatial and quantitative correlations found in the current work. In addition, in these studies, the location of macrophages spatially correlated with decreased ADC and T_1 and T_2 hypointense regions. Similar experiments carried out in macrophage-depleted animals would yield vital information on the contribution of macrophages, both to the pathogenesis of the DTH lesion, and to the mechanisms behind the MRI changes.

9.2.2 Investigation of MTR Changes

In the original DTH lesion two distinct regions of decreased MTR, one within the lesion itself and one more remote in the corpus callosum, were observed on MTR maps. The corpus callosum exhibited a clear reduction in MTR during the inflammatory response, which requires further investigation, since this decrease occurred at a distance from the lesion site and was not associated with myelin loss. Furthermore, in the modified DTH lesion, in some animals, in addition to the decreased MTR observed in the lesion, a decreased MTR was observed surrounding it, suggesting different mechanisms behind

each of these reductions in MTR. Full quantification of magnetisation transfer, and the interaction of other MRI parameters, such as the T_1 relaxation time, may help to identify the different mechanisms and pathologies behind MTR changes. In addition, the application of other methodologies reported to be sensitive to myelin content, such as $T_1\rho$ (Mitchell 1997), may aid elucidation of this issue.

9.2.3 Mechanisms Behind Immune Response Reactivation

In chapter 8, immunohistochemistry was carried out on LPS-challenged animals much later than the MRI-observed exacerbation. At that time, no particular immunohistological characteristic correlated with reactivation of the DTH lesion. However, any histopathological processes that did occur as a result of exacerbation of the lesion may well have resolved by this time-point, thus leaving plenty of scope for further investigation. It is unclear whether the LPS exacerbation results in new activation of inflammatory cells already present in the lesion, or recruitment of new, additional cells to the lesion. Recruitment of specific cell types, such as T & B lymphocytes could be investigated using immunohistochemistry at the time of increased T_1 relaxation time, rCBV and BBB permeability (six hours), to address this issue. Although findings in this chapter suggest that IL-1β production may, at least in part, be responsible for the increased rCBV during the acute response, IL-1β could not be detected post-LPS challenge. It is possible that the increases in IL-1β are below the detection limit, however, blocking the action of IL-1β using antagonists or antibodies would yield more information on the role of IL-1β in the increased rCBV. Nitric oxide (NO) is a vasodilator and has been implicated in the pathogenesis of EAE and MS lesions; see Willenborg et al. for review (Willenborg 1999). It is quite possible therefore, that NO also has an important role in the pathogenesis of the DTH model, which warrants

investigation of NO and its effect on CBV. In LPS-challenged animals, a decreased ADC was observed surrounding the DTH lesion post-challenge. However, this decrease was also observed in some control animals, therefore, further investigation is required. Greater sample numbers might provide further information about whether the changes are due to reactivation of the DTH lesion, or as a result of natural lesion progression.

9.2.4 Magnetic Resonance Spectroscopy

Magnetic Resonance Spectroscopy (MRS) has also been widely used to study MS and EAE, in particular to study metabolites resulting from myelin breakdown (see Wolinsky 2002 for review). The initial DTH lesion used in this thesis was not consistently large enough to obtain a region of interest on which MRS could be successfully carried out in a reasonable time-frame. Using the modified DTH lesion, a proton spectroscopy investigation of brain metabolites, such as N-acetyl aspartate and choline in the lesion might yield information on neuronal loss and demyelination.

9.2.5 Pharmacological Inhibition and Novel Contrast Agents

Pharmacological agents have already been used in the inhibition of the DTH lesion by targeting MMPs (Matyszak 1996). The application of MRI to this model may help to determine what part MMPs play in the different MRI changes. The use of novel contrast agents, especially those linked to USPIO, would also be interesting to investigate the time-course and profile of specific cell recruitment, such as macrophages. Investigation of macrophage recruitment using USPIO has already been carried out in EAE animals, but serial imaging over long periods of time is difficult since lesions occur randomly throughout the brain. Since the DTH model has the advantage that the precise time of induction and location of the lesion is known, serial imaging can be carried out in the

same animal and correlation with histopathological processes is easier. Expression of adhesion molecules such as ICAM-1 or the selectins early in the progression of the DTH lesion when recruitment of inflammatory cells is maximal, has been investigated using MRI in EAE (Sipkins 2000). In other models of CNS inflammation, a contrast agent targeted to E-selectin has been used to identify early endothelial activation (Sibson 2002). Preliminary investigation of selectin expression early in DTH lesion progression, revealed no significant findings, either with the same contrast agent or with immunohistochemical techniques. However, it is possible that using the modified lesion, where changes are more overt, selectin expression would occur at a level that could be detected by MRI, or immunohistochemistry.

Thus, the results observed in the studies reported here might have important implications, not only in the experimental field, but also in the clinical setting. In the experimental and clinical setting, the MRI techniques described here, such as T_1- and T_2-weighted imaging, contrast enhanced T_1-weighted imaging, diffusion-weighted, perfusion and MTR imaging might be applied to studies of neuroprotective agents. In contrast, in the clinical setting, measurement of rCBV is likely to be important in assessing early changes prior to BBB compromise, as well having a considerable impact on the treatment and management of MS and other neuropathologies, such as stroke or head injury.

Appendix A

A.1 Abbreviations

ABC - Avidin Biotin peroxidase complex

ADC - Apparent Diffusion Coefficient

ANOVA-Analysis of Variance

APC - Antigen Presenting Cell

BBB - Blood Brain Barrier

BCG - Bacillus Calmette-Guerin

CBV - Cerebral blood volume

CFA - Complete Freund's adjuvant

CNS - Central Nervous System

DAB - Diaminobenzidine

DTH - Delayed Type Hypersensitivity

DWI - Diffusion Weighted Imaging

EAE - Experimental Allergic Encephalomyelitis

ELISA - Enzyme Linked Immunosorbent Assay

FID - Free Induction Decay

GFAP - Glial Fibrillary Acidic Protein

IgG - Immunoglobulin G

IL- - Interleukin

i.p. - intraperitoneal

LPS - Lipopolysaccharide

MBP - Myelin Basic Protein

MHC - Major Histocompatibility Complex

MOG - Myelin Oligodendrocyte Glycoprotein

MMP - Matrix Metalloproteinase

MRI - Magnetic Resonance Imaging

MS - Multiple Sclerosis

MT - Magnetisation Transfer

NAWM - Normal Appearing White Matter

NO - Nitric oxide

NPC- No peripheral Challenge

PB IC - Phosphate buffer Intracerebral challenge

PBS - Phosphate Buffered Saline

PLP - Paraformaldehyde Lysine Periodate

RF - Radiofrequency

$T_1\rho$ - T_1 rho relaxation time

TB - Tuberculosis

TE - Echo Time

TNF-α - Tumour Necrosis Factor

TMEV

TR - Repetition Time

SAL PC - Saline Peripheral Challenge

Appendix B

B.1 Acetylcholinesterase method

Stock solution: 10M Copper sulphate 25gm/litre, 1M sodium acetate 136gm/l, 1M acetic acid 57ml/l, N/5 acetic acid (diluted N/1)

Dissolve 100mg acetylcholine iodide in 4ml distilled water. Precipate with 7ml 10M copper sulphate, adding initial portion a drop at a time with shaking. Stand for 10mins, and then centrifuge at 2000rpm for 20 minutes. Pipette off 10ml of the supernatant and add 62mg glycine, store in a refrigerator overnight. Add 1M sodium acetate dropwise to give the desired pH (5.0 – 5.2). Make up to 50ml with distilled water. (200mls)

Sulphide solution: 1g sodium sulphide dissolved in 45 ml N/5 acetic acid. pH 5-6.

Method:

Thaw frozen sections, and wash in distilled water x2.

Incubating medium on overnight on the rotating table

Wash x2 in distilled water for 10-15 minutes

Sodium sulphide solution for 2 mins in fume hood.

Appendix C

Histological Characteristics

C.1 Macrophage and T & B Lymphocyte counts, GFAP and MHC Class II Expression in DTH animals

Time-Point (Day)	Rat No	No. of Macrophages	No. of T cells	GFAP Expression	MHC Class II Expression	IgG Score
0	17	/	196.42861	3.42	3.294182	1
	19	/	59.5238	27.34	6.226823	1
	20	/	178.5714	0.29	5.29984	1
	21	/	89.2857	16.89	/	/
	31	/	/	15.43	/	/
	35	95.2381	196.4286	/	1.87718	2
	22	/	/	21.20	/	/
	46	/	/	/	/	0
	47	95.2381	41.6667	25.81	1.788159	0
	48	/	59.5238	10.77	/	0
		95.2381 ± 0 (2)	106.69 ± 62.51 (7)	15.14 ± 9.85 (8)	3.70 ± 2.05 (5)	0.71 ± 0.76 (7)
5	5	436.5079	293.6508	30.07	3.206021	3
	6	557.5397	59.5238	32.54	4.253715	2
	7	575.3968	51.5873	35.19	4.833419	0
	55	142.8571	190.4762	42.48	0.265025	0
	36	553.5714	553.5714	47.48	7.796076	3
	37	/	/	/	/	0
	38	380.9524	297.6190	87.15	3.337181	1
	f	482.1429	214.2857	/	/	/
		447.0 ± 151.81 (7)	237.24 ± 171.10 (7)	45.82 ± 21.26 (6)	3.95 ± 2.46 (6)	1.50± 1.38 (7)
8	39	619.0476	/	26.82	9.367082	0
	40	630.9524	/	28.92	6.979821	0
	41	500.0000	/	90.82	0.956844	0
		583.33 ± 72.33 (3)	/	48.85 ± 36.36 (3)	5.77 ± 4.33 (3)	/
12	42	458.3333	476.1905	60.69	19.50552	0
	43	636.9048	773.8095	47.83	8.231265	1
	44	/	83.3333	92.01	1.880239	0
	45	660.7143	279.7619	33.73	12.17235	1
	z	666.6667	1172.62	/	/	2
	AA	/	/	/	/	0
	AB	/	452.3810	/	/	2
	G	440.4762	440.4762	/	/	/
	R	250.0000	309.5238	/	/	/
		518.85 ± 99.05 (6)	498.51 ± 336.40 (8)	58.49 ± 24.86 (4)	10.45 ± 7.38 (4)	0.86 ± 0.90 (7)
19	1	475.1984	47.6190	36.19	18.43295	2
	2	450.3968	345.2381	82.96	40.46666	3
	3	526.7857	59.5238	68.97	18.19075	1
	4	611.1111	87.3016	87.40	17.81374	0
	AC	/	/	/	/	1
	AD	/	/	/	/	2
	AE	/	/	/	/	3
		515.83 ± 166.13 (4)	134.92 ± 141.19 (4)	62.71 ± 24.01 (4)	23.72 ± 11.16 (4)	1.71 ± 1.11 (7)
31	12	281.7460	/	95.42	18.65689	2
	13	345.2381	107.1429	/	7.59744	3
	14	547.6190	/	33.49	20.40805	3
	15	142.8571	238.0952	/	22.93624	3
	16	744.0476	458.3333	49.72	20.98893	3
	AF	/	345.2381	25.18	/	3
	AG	/	138.8889	/	/	3
	AH	/	285.7143	41.88	/	3
	O	404.7619	/	/	/	/
	J	226.1905	/	/	/	/
	95	136.9048	/	/	/	/
		353.67 ± 223.47 (8)	262.23 ± 130.95 (6)	48.93 ± 27.45 (5)	18.12 ± 6.08 (5)	2.88 ± 0.35 (8)

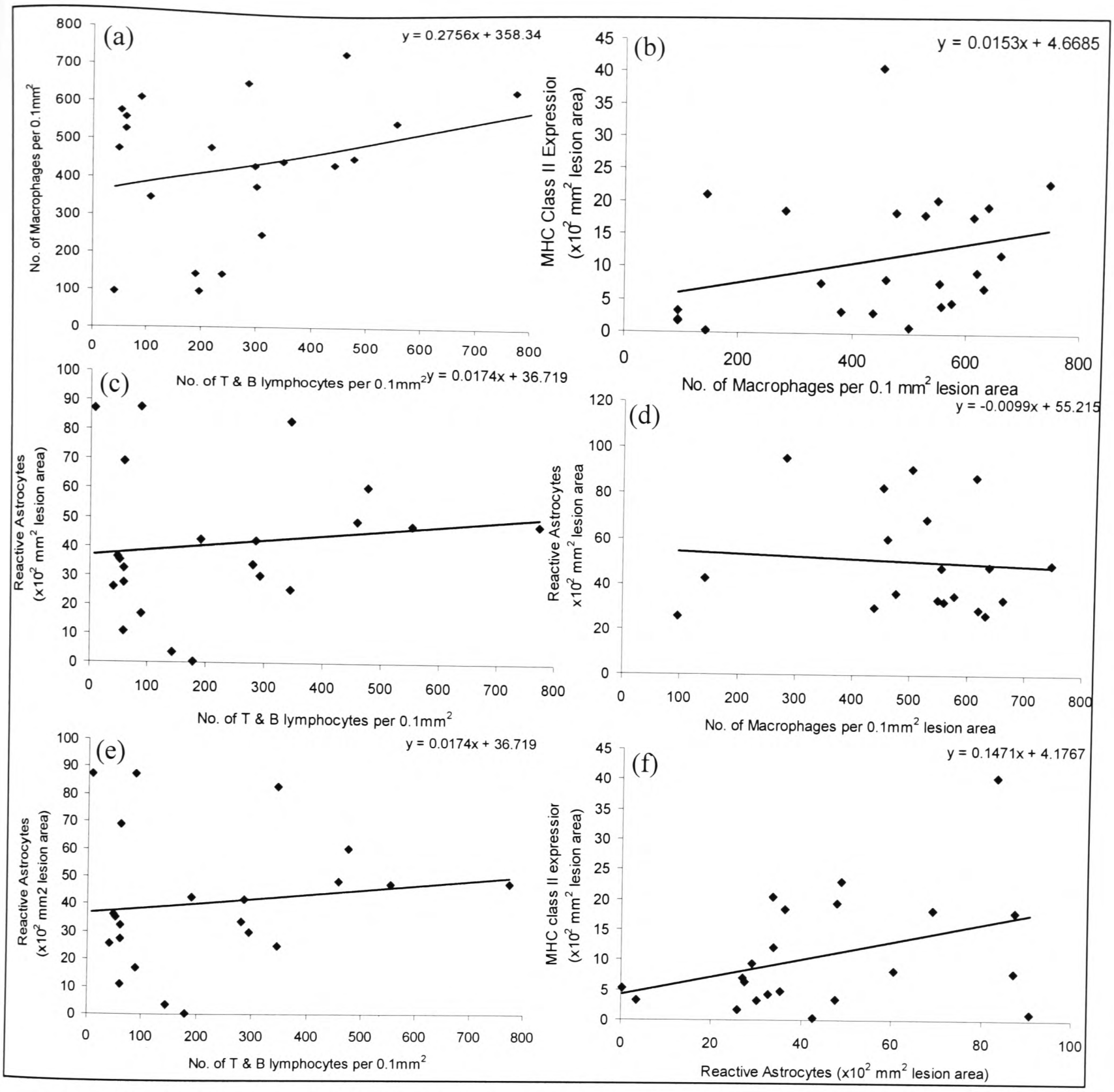
Table C-1: Macrophage and T & B lymphocyte cell counts, GFAP expression, MHC class II expression in DTH animals.

C.2 SAL PC

Time-Point (Day)	Rat No	No. of Macrophages	GFAP Expression	MHC Class II Expression
0	97	261.90 (1)	66.05	/
5	100	232.14	18.76	0.96377
	101	/	/	2.946603
	102	125	/	/
		178.57 ± 75.62 (2)		1.96 ± 1.40 (2)
8	103	309.52	29.39415	1.289383
	104	142.86	2.786174	0.407702
	105	/	/	0.613714
		226.19 ± 117.85 (2)	16.09 ± 18.81 (2)	0.77 ± 0.46 (3)
12	107	238.10	113.86	2.29993
	108	187.5	216.65	2.118205
	109	157.74	20.04025	1.921704
		194.44 ± 40.63 (3)	116.85 ± 98.34 (3)	2.11 ± 0.19 (3)
19	110	169.64 (1)	99.76022	/
	111	/	2.153216	4.157535
			50.96 ± 0.69 (2)	
31	113	166.67	/	2.273826
	115	202.38	21.74083	0.340347
		184.52 ± 25.25 (2)		1.31 ± 1.37 (2)

Table C-2: Macrophage cell counts, GFAP expression, MHC class II expression in SAL PC animals.

C.3 Correlation curves for Histological parameters



(a)-(f) Correlation curves for histological parameters; Areas of staining for MHC class II expression, reactive astrocytes, macrophages and T and B cell counts per lesion area staining.

Appendix D

T_1- and T_2-weighted imaging

D.1 T_1 and T_2-Hypointensities

D.1.1 DTH

Time-Point (Day)	Rat No.	Area of T_1 Hypointensity (No. of Pixels)	Intensity of T_1 Hypointensity (L/R)	Area of T_2 Hypointensity (No. of Pixels)	Intensity of T_2 Hypointensity (L/R)
0	1	62	0.976589	67	0.736735
	2	27	0.949928	70	0.81274
	3	60	0.979976	116	0.895591
	4	94	0.994627	78	0.94489
	47	21	0.910737	18	0.922899
	48	19	0.963269	26	0.890075
	17	26	0.662466	44	0.638419
	18	57	0.732974	56	0.531081
	19	55	0.851271	35	0.710306
	20	66	0.634348	42	0.785277
	33	/	/	64	0.916188
	35	53	0.875174	29	0.716222
	95	33	0.984588	44	0.911995
	96	33	0.929592	50	0.83913
		46.62 ± 22.1 (13)	0.88 ± 0.13 (13)	52.79 ± 25.4 (14)	0.80 ± 0.12 (14)
5	1	37	0.870586	115	0.764157
	3	27	0.920502	44	0.838641
	4	89	0.883739	36	0.834213
	36	50	0.903439	72	0.8887
	37	44	0.912348	51	0.953225
	38	23	0.944228	58	0.923477
	NA	20	0.937061	58	0.656815
	NB	/	/	62	0.722759
	NC	23	0.918812	50	0.773074
	ND	28	0.92866	57	0.883688
	55	48	0.867623	35	0.815869
	95	46	0.997272	50	0.859677
	96	28	0.953983	44	0.862097
		38.6 ± 19.2 (12)	0.92 ± 0.04 (12)	56.3 ± 24.4 (13)	0.83 ± 0.08 (13)
8	39	48	0.924299	82	0.945342
	40	63	0.923503	88	0.819177
	41	69	0.919936	72	0.857962
	NA	42	0.851819	38	0.77215
	NB	32	0.914877	39	0.53814
	NC	31	0.858351	30	0.678949
	ND	39	0.899756	62	0.625498
	95	21	0.973193	59	0.961279
	96	40	0.951842	56	0.878446
		42.8 ± 15.3 (9)	0.91 ± 0.04 (9)	58.4 ± 20.1 (9)	0.79 ± 0.15 (9)
12	42	18	0.967856	76	0.890871
	43	52	0.898367	70	0.811775
	45	24	0.91151	59	0.917314
	N	9	0.850975	35	0.96138
	O	21	0.98802	42	0.969593
	NA	33	0.877001	94	0.743235
	NB	30	0.876823	53	0.755642
	NC	27	0.901191	37	0.850447
	ND	22	0.85301	57	0.289079
	95	32	0.983605	50	0.962097
	96	20	0.905167	73	0.895277
		26.2 ± 11.0 (11)	0.91 ± 0.05 (11)	58.7 ± 18.2 (11)	0.82 ± 0.19 (11)
19	1	123	0.87316	94	0.735187
	2	73	0.853208	61	0.878238
	3	24	1.015517	79	0.929763
	4	93	0.874375	32	0.846992
	95	31	0.994665	93	0.973261
	96	27	0.93283	55	0.942124

Time-Point (Day)	Rat No.	Area of T_1 Hypointensity (No. of Pixels)	Intensity of T_1 Hypointensity (L/R)	Area of T_2 Hypointensity (No. of Pixels)	Intensity of T_2 Hypointensity (L/R)
		61.8 ± 41.1 (6)	0.92 ± 0.07 (6)	69.0 ± 24.2 (6)	0.88 ± 0.09 (6)
31	13	53	0.898253	77	0.883513
	14	50	0.855817	56	0.864496
	15	80	0.694167	44	0.688828
	16	31	0.735905	88	0.828234
	95	27	0.987905	51	0.96992
	96	33	0.933249	39	0.913319
	NA	39	0.85037	71	0.833206
	NB	33	0.908223	59	0.913474
	NC	24	0.847067	59	0.708037
	ND	32	0.882893	73	0.889083
		40.2 ± 16.8 (10)	0.86 ± 0.09 (10)	59.9 ± 15.8 (11)	0.85 ± 0.09 (11)

Table D-1: T_1 and T_2 hypointensities for DTH animals.

D.1.2 NPC

Time-Point (Day)	Rat No.	Area of T_1 Hypointensity (No. of Pixels)	Intensity of T_1 Hypointensity (L/R)	Area of T_2 Hypointensity (No. of Pixels)	Intensity of T_2 Hypointensity (L/R)
0	116	11	0.975832	54	0.864465
	117	30	0.996469	86	0.874331
	118	33	0.981377	95	0.766023
	119	24	0.999591	65	0.823337
		24.5 ± 9.8 (4)	0.99 ± 0.01 (4)	75.0 ± 18.8 (4)	0.83 ± 0.05 (4)
5	116	11	0.974228	51	0.964316
	117	27	0.979893	63	0.848035
	118	27	0.973634	33	0.745052
	119	18	0.963898	68	0.810187
	120	33	0.820474	79	0.744108
		23.2 ± 8.7 (5)	0.94 ± 0.07 (5)	54.5 ± 9.4 (5)	0.82 ± 0.09 (5)
8	116	8	0.9974	66	0.970407
	117	30	0.96098	58	0.815634
	119	29	0.985241	45	0.769767
	120	26	0.840152	49	0.757274
		23.2 ± 10.3 (4)	0.95 ± 0.07 (4)	54.5 ± 9.4 (4)	0.83 ± 0.10 (4)
12	116	9	0.970514	56	0.926585
	117	30	0.943663	48	1.067905
	120	28	0.796689	49	0.750386
		22.3 ± 11.6 (3)	0.90 ± 0.09 (3)	51.0 ± 4.4 (3)	0.91 ± 0.16 (3)
19	116	22	0.972208	48	0.966306
	117	26	0.955775	59	0.839092
	120	27	0.788527	43	0.739847
		25.0 ± 2.7 (3)	0.91 ± 0.10 (3)	50.0 ± 8.2 (3)	0.85 ± 0.11 (3)
31	116	13	0.984457	57	0.919536
	120	24	0.765945	28	0.695609
		18.5 ± 7.8 (2)	0.88 ± 0.15 (2)	42.5 ± 20.5 (2)	0.81 ± 0.16 (2)

Table D-2: T_1 and T_2 hypointensities for controls receiving no peripheral challenge (NPC).

D.1.3 SAL PC

Time-Point (Day)	Rat No.	Area of T_1 Hypointensity (No. of Pixels)	Intensity of T_1 Hypointensity (L/R)	Area of T_2 Hypointensity (No. of Pixels)	Intensity of T_2 Hypointensity (L/R)
0	97	15	0.982245	47	0.901643
	98	27	0.971194	53	0.834175
	99	/	/	28	0.562967
		21.0 ± 8.5 (2)	0.98 ± 0.01 (2)	42.7 ± 13.1 (3)	0.77 ± 0.18 (3)
5	100	26	0.950461	47	0.757672
	101	35	0.957566	49	0.919743
	102	0	1	18	0.927976
		20.3 ± 18.2 (3)	0.97 ± 0.03 (3)	38.0 ± 17.4 (3)	0.87 ± 0.10 (3)
8	103	/	/	39	0.786555
	104	36	0.9819	42	0.857815
	105	21	0.922507	26	0.89578
	106	27	0.949435	38	0.844027
		28.0 ± 7.0 (3)	0.95± 0.03 (3)	35.7 ± 8.5 (4)	0.85 ± 0.06 (4)
12	107	29	0.987999	20	0.945559
	108	18	0.958014	21	0.910344
	109	16	0.952681	26	0.91725
		26.5 ± 9.2 (3)	0.97 ± 0.02 (3)	26.3 ± 8.3 (3)	0.90 ± 0.04 (3)
19	110	20	0.987194	26	0.926854
	111	33	0.893157	36	0.806928
		26.5 ± 9.2 (2)	0.94 ± 0.07 (2)	31.0 ± 7.1 (2)	0.87 ± 0.08 (2)
31	113	28	0.974096	30	0.978451
	114	12	0.943449	23	0.93361
	115	35	0.929395	30	0.773002
		25.0 ± 11.8 (3)	0.95 ± 0.02 (3)	27.7 ± 4.0 (3)	0.90 ± 0.11 (3)

Table D-3: T_1 and T_2 hypointensities for controls receiving a peripheral challenge of saline (SAL PC).

D.2 Total T_2 Signal Change and T_2 Hyperintensities

D.2.1 DTH

Time-Point (Day)	Rat No.	Area of T_2 hyperintensity (No. of Pixels)	Intensity of T_2 hyperintensity (L/R)	Area of Total T_2 Signal change (No. of Pixels)	Intensity of Total T_2 Signal Change (L/R)
0	1	41	1.067178	71	0.688012769
	2	26	1.025356	108	0.862851438
	3	/	/	131	0.916712613
	4	69	1.080556	79	0.90824885
	33	35	1.039633	91	0.859756098
	35	21	1.043382	46	0.766578249
	17	28	1.069275	61	0.662722938
	19	33	1.052682	78	0.76301334
	20	26	1.123629	60	0.839089801
	47	19	1.044004	70	0.943027727
	48	36	1.027514	51	0.877025641
	95	26	1.009406	95	0.928925825
	96	19	1.010366	46	0.834848873
		32.09 ± 14.22 (11)	1.04 ± 0.02 (11)	75.9 ± 25.2 (13)	0.83 ± 0.09 (13)
5	1	53	1.015454	187	0.887947378
	3	24	1.003309	306	0.915300393
	4	/	/	260	0.874311665
	36	38	1.045387	218	0.981208747
	37	81	1.091435	120	1.040576706
	38	99	1.003071	147	0.963679544
	55	83	1.03422	134	0.928127608
	95	46	1.070209	89	0.966833757
	96	60	1.031494	100	0.891910392
	NA	60	1.024994	154	0.717091103
	NB	57	1.037601	112	0.922911873
	NC	15	1.001281	73	0.806663972
	ND	48	1.489099	60	1.335414634
		53.3 ± 24.2 (12)	1.07 ± 0.13 (12)	150.8 ± 73.8 (13)	0.94 ± 0.14 (13)
8	39	48	1.034311	209	0.950918725

Time-Point (Day)	Rat No.	Area of T_2 hyperintensity (No. of Pixels)	Intensity of T_2 hyperintensity (L/R)	Area of Total T_2 Signal change (No. of Pixels)	Intensity of Total T_2 Signal Change (L/R)
	40	36	1.007045	130	0.85676482
	41	90	1.023441	247	0.907923487
	NA	83	1.083662	56	0.989130435
	NB	/	/	154	0.723051038
	NC	26	1.040848	152	0.741015625
	ND	90	1.025786	163	0.807746751
	95	91	1.022769	110	0.969866854
	96	48	1.073846	73	0.852350315
		64.0 ± 27.2 (8)	1.04 ± 0.03 (8)	143.8 ± 60.7 (9)	0.87 ± 0.10 (9)
12	42	66	1.034374	151	0.918108843
	43	112	1.012341	261	0.917230329
	44	33	1.026329	58	0.930898204
	45	74	1.036446	296	0.960341174
	NA	38	1.000885	119	0.753522754
	NB	58	1.05899	107	0.768032314
	NC	80	1.055335	78	0.944575901
	ND	/	/	142	0.416100206
	N	69	1.059571	90	0.966653677
	O	206	1.136268	130	1.159192825
	95	50	1.03247	85	0.97454789
	96	33	1.03718	65	0.862398965
		74.5 ± 49.5 (11)	1.04 ± 0.04 (11)	131.8 ± 74.9 (12)	0.88 ± 0.18 (12)
19	1	63	1.009389	140	0.827993104
	2	176	1.044175	209	0.950918725
	3	151	1.012416	200	0.973843276
	4	31	1.008268	169	0.919581825
	N	78	1.011257	61	1.009956441
	O	183	1.201922	221	1.18766678
	95	66	1.016124	75	0.934031414
	96	59	1.040944	59	0.925695899
		100.9 ± 59.4 (8)	1.04 ± 0.07 (8)	141.8 ± 68.4 (8)	0.97 ± 0.10 (8)
31	13	0	1	155	0.855568393
	14	57	1.022269	112	0.885252396
	15	29	1.145687	93	0.785840708
	16	58	1.091883	147	0.883546975
	NA	/	/	107	0.857063024
	NB	49	1.129343	130	0.950848746
	NC	24	1.019642	96	0.736845978
	ND	28	1.160257	117	0.983223528
	O	88	1.029499	138	0.926100327
	95	33	1.0552	102	0.984508765
	96	14	1.016776	89	1.014028056
		38.0 ± 25.4 (10)	1.07 ± 0.06 (10)	116.9 ± 22.6 (11)	0.90 ± 0.09 (11)

Table D-4: Area of T_2 hyperintensity and total area of T_2 signal change for DTH animals.

D.2.2 NPC

Time-Point (Day)	Rat No.	Total Area of T_2 Signal Change (No. of Pixels)	Total Area of T_2 Signal Change (L/R)
0	116	43	0.889705
	117	56	0.8819
	118	75	0.751597
	119	68	0.798082
		60.5 ± 14.1 (4)	0.83 ± 0.07 (4)
5	116	58	0.968748
	117	70	0.864378
	118	176	1.002895
	119	60	0.794067
	120	52	0.756779
		83.2 ± 52.3 (5)	0.88 ± 0.11 (5)
8	116	53	0.965623
	117	55	0.841506
	119	54	0.807385
	120	43	0.826491
		51.25 ± 5.6 (4)	0.86 ± 0.07 (4)
12	116	46	0.927571
	117	55	0.808933
	120	46	0.734241
		49.0 ± 5.2 (3)	0.82 ± 0.10 (3)
19	116	42	0.966213
	117	63	0.854302
	120	51	0.746878
		52.0 ± 10.5 (3)	0.86 ± 0.11 (3)
31	116	42	0.957267
	120	82	0.812404
		62.0 ± 28.3 (2)	0.88 ± 0.10 (2)

Table D-5: Total area of T_2 signal change for controls receiving no peripheral challenge (NPC).

D.2.3 SAL PC

Time-Point (Day)	Rat No.	Total Area of T_2 Signal Change (No. of Pixels)	Total Area of T_2 Signal Change (L/R)
0	97	27	0.906854
	98	35	0.958204
		46.7 ± 27.4 (2)	0.82 ± 0.20 (2)
5	100	33	0.852836
	101	21	0.897881
	102	27	0.937081
		27.0 ± 6.0 (3)	0.90 ± 0.04 (3)
8	103	31	0.779644
	104	18	0.852568
	105	50	0.952068
	106	78	0.87111
		44.3 ± 26.1 (4)	0.86 ± 0.07 (4)
12	107	60	0.994036
	108	29	0.990302
	109	26	0.981179
		38.3 ± 18.8 (3)	1.00 ± 0.01 (3)
19	110	42	0.885872
	111	12	0.86569
		27.0 ± 21.2 (2)	0.88 ± 0.01 (2)
31	113	31	0.935025
	114	36	0.938284
	115	45	0.823629
		37.3 ± 7.1 (3)	0.90 ± 0.07 (3)

Table D-6: Total area of T_2 signal change for controls receiving a peripheral challenge of saline (SAL PC).

Appendix E

Contrast Enhancement, Diffusion and Magnetisation Transfer

E.1 Area and Intensity of BBB Breakdown

E.1.1 DTH

Time-Point (Day)	Rat No.	Area of BBB Breakdown (No. of Pixels)	Intensity (L/R)
0	1	0	1
	2	0	1
	3	0	1
	4	0	1
	17	0	1
	18	0	1
	19	0	1
	20	0	1
	47	0	1
	48	0	1
	95	0	1
	96	0	1
		0 ± 0 (12)	1 ± 0 (12)
5	36	109	1.113683
	37	88	1.07782
	38	55	1.016284
	1	89	1.044205
	3	101	1.052181
	4	63	1.007662
	55	113	1.19058
	80	34	1.021671
	81	50	1.049139
	95	41	1.035069
	96	58	1.078232
		72.8 ± 28.1 (11)	1.06 ± 0.05 (11)
8	39	51	1.003416
	40	113	1.010635
	41	67	1.017084
	NB	176	1.455103
	NC	97	1.12996
	ND	54	1.036494
	80	31	1.059492
	95	76	1.05736
	96	92	1.046284
		84.1 ± 42.9 (9)	1.09 ± 0.15 (9)
12	42	315	1.070221
	43	308	1.094109
	45	152	1.032043
	NA	57	1.048083
	NB	110	1.065804
	NC	145	1.136075
	ND	147	1.093514
	95	71	1.041568
	96	113	1.040549
	O	170	1.300975
		150.4 ± 60.5 (10)	1.00 ± 0.32 (10)
19	1	264	0.918541
	2	345	1.059397
	3	70	1.021977
	4	127	0.919329
	95	107	1.031821
	96	109	1.07652
	N	107	1.045968
	O	238	1.247327
		159.63 ± 74.8 (8)	1.05 ± 0.10 (8)

Time-Point (Day)	Rat No.	Area of BBB Breakdown (No. of Pixels)	Intensity (L/R)
31	13	11	1.009945
	14	0	1
	15	0	1
	16	0	1
	95	72	1.031567
	96	127	1.054616
		5.8 ± 9.3 (6)	1.02 ± 0.05 (6)

Table E-1: Area and intensity of gadolinium enhancement indicating BBB breakdown in DTH animals.

E.2 SAL PC

Time-Point (Day)	Rat No.	Area of BBB Breakdown (No. of Pixels)	Intensity (L/R)
0	97	0	1
	98	0	1
		0 ± 0 (2)	1 ± 0 (2)
5	100	19	1.005683
	102	27	1.114928
		23.0 ± 5.7 (2)	1.06 ± 0.08 (2)
8	103	44	1.173344
	104	37	1.179807
	106	57	1.140978
		46.0 ± 10.2 (3)	1.16 ± 0.02 (3)
12	107	15	1.094193
	108	23	1.059181
		19.0 ± 5.7 (2)	1.08 ± 0.02 (2)
19	110	81	1.067593
	111	15	1.029047
		48.0 ± 46.7 (2)	1.05 ± 0.03 (2)
31	113	0	1
	115	0	1
		0 ± 0 (2)	1.0 ± 0 (2)

Table E-2: Area and intensity of gadolinium enhancement indicating BBB breakdown in SAL PC animals.

E.3 NPC

Time-Point (Day)	Rat No.	Area of BBB Breakdown (No. of Pixels)	Intensity (L/R)
0	116	0	1
	120	0	1
		0 ± 0 (2)	1 ± 0 (2)
5	116	50	1.202498
	117	55	1.154087
	119	19	1.238463
	120	36	1.087273
		4.0.0 ± 16.2 (4)	1.17 ± 0.07 (4)
8	116	27	1.187752
	117	38	1.172424
	119	37	1.198707
	120	77	0.981043
		44.8 ± 22.1 (4)	1.13 ± 0.10 (4)
12	116	26	1.129874
	117	48	1.067905
		37.0 ± 15.6 (2)	1.10 ± 0.04 (2)
19	116	63	1.088337
	117	29	1.074114
	120	48	0.973155
		46.7 ± 17.0 (3)	1.05 ± 0.06 (3)
31	116	0	1
	120	0	1
		0 ± 0 (2)	1 ± 0 (2)

Table E-3: Area and intensity of gadolinium enhancement indicating BBB breakdown in SAL PC animals.

E.4 ADC Hypointensities and Hyperintensities

E.4.1 DTH

Time-Point (Day)	Rat No.	Area of ADC Hypointensity (No. of Pixels)	Intensity of ADC Hypointensity (L/R)	Area of ADC Hyperintensity (No. of Pixels)	Intensity of ADC Hyperintensity (L/R)
0	1	21	0.923191	36	1.059322
	2	23	0.827456	/	/
	3	24	0.943978	34	1.028226
	4	16	0.916558	21	1.096419
	35	34	0.87747	18	1.052126
	17	38	0.996918	54	1.077186
	19	48	0.939189	88	1.130919
	20	26	0.990937	41	1.155488
	47	14	0.997019	24	1.197657
	48	18	0.983333	19	1.039617
	95	21	0.921811	41	1.049485
	96	/	/	36	1.143177
		25.7 ± 10.3 (11)	0.94 ± 0.05 (11)	44.8 ± 26.2 (11)	1.12 ± 0.10 (11)
5	1	20	0.985975	81	1.143043
	2	/	/	72	1.089947
	3	9	0.906841	30	1.002693
	4	23	0.751043	/	/
	55	/	/	70	1.109739
	36	49	0.949315	160	1.137931
	37	33	0.982644	122	1.116848
	38	30	0.97861	124	1.173295
	95	16	0.932515	28	1.059858
	96	33	0.940206	76	1.118681
		26.6 ± 12.4 (8)	0.93 ± 0.08 (8)	84.8 ± 43.7 (9)	1.11 ± 0.05 (9)
8	39	15	0.865459	158	1.071724
	40	16	0.886515	55	1.071135
	41	14	0.888446	87	1.023192
	NA	18	0.920635	25	1.039275
	NC	/	/	146	1.339688
	ND	50	0.902711	42	1.01849
	95	28	0.942918	70	1.076433
	96	20	0.924152	46	1.016129
		23.0 ± 12.8 (7)	0.90 ± 0.08 (7)	78.6 ± 49.0 (8)	1.08 ± 0.03 (8)
12	42	30	0.982374	66	1.065704
	43	39	0.928607	160	1.095937
	45	57	0.909211	113	1.023203
	NB	29	0.949013	39	1.051482
	NC	47	0.766578	50	1.005979
	ND	54	0.846154	42	1.127962
	N	/	/	142	1.216443
	O	30	0.966897	122	1.375399
	95	12	0.97451	83	1.028777
	96	19	0.992016	43	1.076305
		35.2 ± 15.3 (9)	0.92 ± 0.07 (9)	86.0 ± 45.1 (10)	1.11 ± 0.04 (10)
19	1	42	0.922531	135	1.028717
	2	78	0.9368	251	1.116055
	3	23	0.95481	110	1.084304
	4	48	0.922526	88	1.108663
	N	/	/	162	1.329032
	O	63	0.966206	291	1.105512
	95	25	0.989733	49	1.049505
	96	/	/	65	1.041584
		46.5 ± 21.5 (6)	0.94 ± 0.02 (6)	143.9 ± 87.0 (8)	1.11 ± 0.04 (8)
31	13	20	0.937951	68	1.026087
	14	48	0.988571	158	1.119829
	15	35	0.786816	109	0.975309
	16	44	0.963585	220	1.08011
	NA	32	0.935331	32	1.425641
	NB	20	0.979299	52	1.19598
	NC	32	0.90301	57	1.098522
	O	22	0.91433	55	1.070492
	95	34	0.923711	47	1.133475
	96	24	0.945892	51	1.09407
		31.1 ± 9.8 (10)	0.92 ± 0.08 (10)	84.9 ± 60.2 (10)	1.12 ± 0.06 (10)

Table E-4: ADC hypointensities and hyperintensities for DTH animals.

E.4.2 NPC

Time-Point (Day)	Rat No.	Area of ADC Hypointensity (No. of Pixels)	Intensity of ADC Hypointensity (L/R)	Area of ADC Hyperintensity (No. of Pixels)	Intensity of ADC Hyperintensity (L/R)
0	116	25	0.985989	69	1.08329
	117	27	0.880163	27	1.127213
	118	29	0.88557	27	1.01336
	119	11	0.985444	63	1.178499
		23.0 ± 8.16 (4)	0.93 ± 0.06 (4)	46.5 ± 22.7 (4)	1.10 ± 0.07 (4)
5	116	20	0.976104	64	1.080893
	117	39	0.978066	28	1.085172
	119	46	0.993215	46	1.10844
	120	32	0.985154	15	1.296715
		34.25 ± 11.09 (4)	0.98 ± 0.01 (4)	38.3 ± 21.4 (4)	1.14 ± 0.10 (4)
8	117	25	0.941866	36	1.104682
	120	19	0.953488	15	1.297521
		22.0 ± 4.2 (2)	0.95 ± 0.01 (2)	25.5 ± 14.9 (2)	1.20 ± 0.14 (2)
12	116	11	0.916918	49	1.14
	117	21	0.887593	45	1.124818
	120	39	0.96814	30	1.109569
		23.7 ± 14.2 (3)	0.92 ± 0.04 (3)	41.3 ± 10.0 (3)	1.12 ± 0.02 (3)
19	116	26	0.982869	40	1.149538
	117	15	0.946146	41	1.143744
	120	20	0.903932	24	1.151441
		20.3 ± 5.5 (3)	0.94 ± 0.04 (3)	35.0 ± 9.5 (3)	1.15 ± 0.004 (3)
31	116	18	0.977552	36	1.119474
	120	18	0.942122	39	1.084977
		18.0 ± 0 (2)	0.96 ± 0.03 (2)	37.5 ± 2.1 (2)	1.10 ± 0.02 (2)

Table E-5: ADC hypointensities and hyperintensities for controls receiving no peripheral challenge (NPC).

E.4.3 SAL PC

Time-Point (Day)	Rat No.	Area of ADC Hypointensity (No. of Pixels)	Intensity of ADC Hypointensity (L/R)	Area of ADC Hyperintensity (No. of Pixels)	Intensity of ADC Hyperintensity (L/R)
0	97	24	0.923379	27	1.042
	98	15	0.905622	47	1.081673
		19.5 ± 6.4 (2)	0.91 ± 0.01 (2)	37.0 ± 14.1 (2)	1.06 ± 0.03 (2)
5	100	23	0.910675	32	1.101952
	101	16	0.967033	11	1.083512
	102	24	0.926641	25	1.10142
		20.0 ± 5.7 (3)	0.95 ± 0.03 (3)	22.7 ± 10.7 (3)	1.10 ± 0.01 (3)
8	103	36	0.989247	29	1.059701
	104	21	0.956159	45	1.108511
	105	32	0.940678	20	1.159389
		29.7 ± 7.8 (3)	0.96 ± 0.02 (3)	31.3 ± 12.7 (3)	1.11 ± 0.05 (3)
12	107	12	0.96063	23	1.049116
	108	18	0.942505	20	1.00578
	109	27	0.975238	21	1.128049
		19.0 ± 7.6 (3)	0.96 ± 0.02 (3)	21.3 ± 1.5 (3)	1.06 ± 0.06 (3)
19	110	29	0.992079	15	1.11306
	111	29	0.96788	31	1.109244
		29.0 ± 0 (2)	0.98 ± 0.02 (2)	23.0 ± 11.3 (2)	1.11 ± 0.003 (2)
31	113	18	0.957806	32	1.068687
	115	20	0.990347	41	1.211416
		19.0 ± 1.4 (2)	0.97 ± 0.02 (2)	36.5 ± 6.4 (2)	1.14 ± 0.10 (2)

Table E-6: ADC hypointensities and hyperintensities for controls receiving a peripheral challenge of saline (SAL PC).

E.5 Total Area of ADC Change

E.5.1 DTH

Time-Point (Day)	Rat No.	Area of Total ADC Change (No. of Pixels)	Intensity of Total ADC Change (L/R)
0	1	98	1.06911765
	2	40	0.88129032
	3	51	0.97463284
	4	50	1.04411765
	35	53	0.82569975
	17	83	1.0361991
	19	138	1.04160888
	47	87	1.12283237
	48	98	1.04135894
	20	55	1.14916286
	95	53	1.0021692
	96	57	1.11804009
		71.9 ± 29.0 (12)	1.03 ± 0.54 (12)
5	1	96	1.05278174
	2	78	1.03506311
	3	127	0.99908925
	4	92	0.67771883
	55	113	1.05306122
	36	214	1.11675824
	37	206	1.11388889
	38	223	1.14592275
	95	91	0.97077244
	96	122	1.11965812
		136.2 ± 56.1 (10)	1.03 ± 0.14 (10)
8	39	180	1.08391608
	40	224	1.01388889
	41	216	1.05352113
	NA	119	0.96651189
	NC	128	1.32347826
	ND	128	0.93206951
	95	76	1.08974359
	96	52	1.02868852
		140.4 ± 62.1 (8)	1.06 ± 0.12 (8)
12	42	185	1.04525112
	43	181	1.06951341
	45	218	0.98918919
	NB	88	1.02728732
	NC	66	0.91428571
	ND	69	0.91419657
	N	103	1.1910299
	O	223	1.23538231
	95	110	1.0593692
	96	108	1.01840491
		135.1 ± 60.5 (10)	1.00 ± 0.06 (10)
19	1	290	1.01895735
	2	306	1.07671107
	3	219	1.05328434
	4	109	1.04837929
	N	277	1.31414474
	O	359	1.07097792
	95	56	1.03976143
	96	66	1.08606557
		210.3 ± 117.7 (8)	1.09 ± 0.09 (8)
31	13	135	0.99558174
	14	148	1.08426966
	15	162	0.97687075
	16	175	1.06241331
	NA	124	1.17491749
	NB	69	1.14593698
	NC	108	1.06125828
	O	107	1.02100162
	95	86	1.09462366
	96	64	1.01402806
		117.8 ± 38.0 (10)	1.06 ± 0.06 (10)

Table E-7: Total ADC change for DTH animals.

E.5.2 NPC

Time-Point (Day)	Rat No.	Area of Total ADC Change (No. of Pixels)	Intensity of Total ADC Change (L/R)
0	116	38	1.053083
	117	32	1.094778
	118	82	1.010168
	119	75	1.156425
		56.8 ± 25.4 (4)	1.08 ± 0.06 (4)
5	116	69	0.95759
	117	77	1.007463
	119	64	0.966938
	120	63	1.11312
		68.3 ± 6.4 (4)	1.01 ± 0.07 (4)
8	117	41	1.072944
	120	45	1.135291
		43.0 ± 2.8 (2)	1.10 ± 0.04 (2)
12	116	49	1.149291
	117	37	1.16473
	120	45	1.133887
		43.7 ± 6.1 (3)	1.15 ± 0.02 (3)
19	116	58	1.164278
	117	36	1.148726
	120	18	1.134123
		37.3 ± 20.0 (3)	1.15 ± 0.02 (3)
31	116	56	1.085921
	120	49	1.009404
		52.5 ± 5.0 (2)	1.05 ± 0.05 (2)

Table E-8: Total ADC change for controls receiving no peripheral challenge (NPC).

E.5.3 SAL PC

Time-Point (Day)	Rat No.	Area of Total ADC Change (No. of Pixels)	Intensity of Total ADC Change (L/R)
0	97	23	0.96994
	98	33	1.016771
		28.0 ± 7.1 (2)	0.99 ± 0.03 (2)
5	100	31	1.072261
	101	48	1.060268
	102	30	0.988119
		36.3 ± 10.1 (3)	1.04 ± 0.05 (3)
8	103	18	1.073852
	104	27	1.054507
	105	48	1.019355
		31.0 ± 15.4 (3)	1.05 ± 0.03 (3)
12	107	52	1.003906
	108	41	0.989691
	109	35	1.190265
		42.7 ± 8.6 (3)	1.06 ± 0.11 (3)
19	110	30	1.136461
	111	33	1.104822
		31.5 ± 2.1 (2)	1.12 ± 0.02 (2)
31	113	57	0.93361
	115	65	1.130719
		61.0 ± 5.7 (2)	1.03 ± 0.14 (2)

Table E-9: Total ADC change for controls receiving a peripheral challenge of saline (SAL PC).

E.6 Diffusion Anisotropy

E.6.1 DTH

Time-Point (Day)	Rat No.	Diffusion Anisotropy		
		Injected	Contralateral	L/R
0	1	0.1025	0.09244	1.108827
	2	0.1018	0.1205	0.844813
	3	0.1096	0.1255	0.873307
	4	0.1032	0.1	1.032
	35	0.09167	0.1078	0.850371
	95	0.0874	0.1049	0.833174
	96	0.0955	0.1024	1.072251
	80	0.1137	0.1153	0.986123
	81	0.1117	0.1141	0.978966
		0.102 ± 0.009 (9)	0.109 ± 0.011 (9)	0.953 ± 0.106 (9)
5	1	0.1002	0.1166	0.859348
	2	0.09364	0.1018	0.919843
	3	0.1053	0.1149	0.916449
	4	0.1212	0.1379	0.878898
	36	0.106	0.1084	0.97786
	37	0.1069	0.1035	1.03285
	38	0.1187	0.116	1.023276
	95	0.1023	0.101	0.987292
	96	0.09528	0.09815	0.970759
	80	0.1156	0.1027	0.888408
		0.107 ± 0.009 (10)	0.110 ± 0.012 (10)	0.945 ± 0.061 (10)
8	NA	0.1083	0.1116	0.97043
	39	0.1179	0.1102	1.069873
	40	0.1059	0.1159	0.913719
	41	0.09576	0.1136	0.842958
	95	0.09557	0.1012	0.944368
	96	0.09821	0.1069	0.918709
		0.108 ± 0.013 (6)	0.109 ± 0.005 (6)	0.943 ± 0.075 (6)
12	42	0.1027	0.1137	0.903254
	43	0.1117	0.1119	0.998213
	44	0.1057	0.1063	0.994356
	45	0.1167	0.1174	0.994037
	NB	0.1126	0.1471	0.765466
	NC	0.1079	0.1643	0.656726
	ND	0.1118	0.1487	0.751849
	O	0.104	0.1195	0.870293
	95	0.1196	0.1228	0.973941
	96	0.09636	0.105	0.917714
	80	0.1162	0.1249	0.930344
		0.110 ± 0.007 (11)	0.126 ± 0.0193 (11)	0.887 ± 0.115 (11)
19	2	0.1147	0.1162	0.987091
	3	0.1076	0.1219	0.882691
	4	0.1037	0.1099	0.943585
	N	0.1077	0.1136	0.948063
	95	0.09374	0.09776	0.958879
	96	0.1017	0.1125	0.904
		0.110 ± 0.014 (6)	0.114 ± 0.008 (6)	0.938 ± 0.040 (6)
31	12	0.1139	0.1195	0.953138
	13	0.1192	0.1222	0.97545
	14	0.1163	0.1175	0.989787
	15	0.1367	0.13771	0.992666
	16	0.1099	0.108	1.017593
	95	0.1	0.1113	0.898473
	96	0.1014	0.104	0.975
		0.114 ± 0.012 (7)	0.117 ± 0.011 (7)	0.972 ± 0.038 (7)

Table E-10: Diffusion anisotropy for DTH animals.

E.6.2 NPC

Time-Point (Day)	Rat No.	Diffusion Anisotropy		
		Injected	Contralateral	L/R
0	116	0.0944	0.1118	0.844365
	117	0.1012	0.1173	0.862745
	118	0.09459	0.1035	0.913913
	119	0.101	0.1033	0.977735
		0.10 ± 0.004 (4)	0.11 ± 0.007 (4)	0.90 ± 0.06 (4)
5	116	0.1061	0.1081	0.981499
	117	0.1101	0.1343	0.819806
	118	0.09742	0.1016	0.958858
	120	0.1377	0.1436	0.958914
		0.11 ± 0.02 (4)	0.12 ± 0.02 (4)	0.93 ± 0.07 (4)
8	117	0.09431	0.1022	0.922798
	119	0.1004	0.1048	0.958015
	120	0.1044	0.108	0.966667
		0.10 ± 0.005 (3)	0.11 ± 0.002 (3)	0.95 ± 0.02 (3)
12	117	0.1212	0.1306	0.928025
	120	0.1097	0.1118	0.981216
		0.12 ± 0.008 (2)	0.12 ± 0.01 (2)	0.95 ± 0.04 (2)
19	116	0.1222	0.1163	1.050731
	117	0.1044	0.1078	0.96846
	120	0.09556	0.1129	0.846413
		0.11 ± 0.01 (3)	0.11 ± 0.004 (3)	0.96 ± 0.10 (3)
31	116	0.1077	0.1073	1.003728
	120	0.0989	0.09707	1.018852
		0.10 ± 0.01 (2)	0.10 ± 0.01 (2)	1.01 ± 0.01 (2)

Table E-11: Diffusion Anisotropy values for controls receiving no peripheral challenge (NPC).

E.6.3 SAL PC

Time-Point (Day)	Rat No.	Diffusion Anisotropy		
		Injected	Contralateral	L/R
0	97	0.1088	0.1301	0.83628
	98	0.09632	0.1095	0.879635
		0.10 ± 0.009 (2)	0.12 ± 0.01 (2)	0.86 ± 0.03 (2)
5	100	0.1042	0.1035	1.006763
	101	0.1058	0.1022	1.035225
	102	0.1097	0.1027	1.06816
		0.10 ± 0.003 (3)	0.10 ± 0.0007 (3)	1.04 ± 0.03 (3)
8	103	0.09368	0.1045	0.896459
	104	0.09149	0.09792	0.934334
	105	0.09683	0.1001	0.967333
		0.09 ± 0.003 (3)	0.10 ± 0.003 (3)	0.93 ± 0.04 (3)
12	107	0.09847	0.1132	0.869876
	108	0.1097	0.1044	1.050766
	109	0.1232	0.1396	0.882521
		0.11 ± 0.01 (3)	0.12 ± 0.02 (3)	0.93 ± 0.10 (3)
19	110	0.09988	0.1162	0.859552
	111	0.1211	0.1166	1.038593
		0.11 ± 0.02 (2)	0.12 ± 0.0003 (2)	0.95 ± 0.13 (2)
31	113	0.1067	0.1122	0.95098
	115	0.1193	0.122	0.977869
		0.11 ± 0.009 (2)	0.12 ± 0.007 (2)	0.96 ± 0.02 (2)

Table E-12: Diffusion anisotropy for controls receiving a peripheral challenge of saline (SAL PC).

E.6.4 PB IC

Time-Point (Day)	Rat No.	Diffusion Anisotropy		
		Injected	Contralateral	L/R
0	67	0.09881	0.123	0.803333
	68	0.09855	0.1111	0.887039
	69	0.1017	0.1032	0.985465
		0.10 ± 0.002 (3)	0.11 ± 0.01 (3)	0.89 ± 0.09 (3)
5	71	0.1142	0.1013	1.127345
	72	0.115	0.1107	1.038844
	73	0.1226	0.1243	0.986323
		0.12 ± 0.005 (3)	0.11 ± 0.012 (3)	1.05 ± 0.07 (3)
8	74	0.1211	0.1265	0.957312
	76	0.1221	0.1119	1.091153
		0.12 ± 0.001 (3)	0.12 ± 0.01 (2)	1.02 ± 0.09 (2)
12	77	0.1179	0.1248	0.944712
	79	0.112	0.1154	0.970537
		0.11 ± 0.004 (2)	0.12 ± 0.01 (2)	0.96 ± 0.02 (2)
19	82	0.114	0.1075	1.060465
	83	0.1032	0.09789	1.054245
	84	0.1193	0.1161	1.027562
		0.11 ± 0.01 (3)	0.11 ± 0.01 (3)	1.05 ± 0.02 (3)
31	85	0.1015	0.1059	0.958451
	86	0.1132	0.1264	0.89557
		0.11 ± 0.01 (2)	0.12 ± 0.01 (2)	0.93 ± 0.04 (2)

Table E-13: Diffusion anisotropy for controls receiving an intracerebral injection of phosphate buffered saline (PB IC).

E.7 MTR

E.7.1 DTH

Time-Point (Day)	Rat No.	MTR of Striatum			MTR of Corpus Callosum		
		Injected	Contralateral	L/R	Injected	Contralateral	L/R
0	1	20.84	23.02	0.9053	22.48	25.25	0.8902970
	2	21.32	22.2	0.96036	20.56	25.22	0.815226
	3	21.26	22.68	0.93739	23.46	24.11	0.9730402
	4	20.85	23.22	0.897933	23.25	25.65	0.9064327
	33	/	/	/	21.82	22.36	0.9758497
	35	/	/	/	23.34	24.92	0.8365971
	80	14.52	18.19	0.798241	23.03	22.84	1.0083187
	81	22.25	22.25	1	15.49	22.36	0.6927549
	95	16.24	17.62	0.92168	17.27	20.43	0.8453255
	96	/	/	/	15.33	20.25	0.757037
		21.86 ± 1.02 (7)	22.78 ± 0.45 (7)	0.93 ± 0.04 (7)	20.60 ± 3.31 (10)	23.34 ± 1.99 (10)	0.88 ± 0.10 (10)
5	1	18.36	20.3	0.904433	19.55	23.79	0.8217739
	2	18.93	24.89	0.760546	/	/	/
	3	17.36	18.64	0.93133	21.49	22.1	0.9723982
	4	19.75	23.11	0.854608	21.41	26.54	0.8067069
	36	19.51	17.65	1.105382	19.42	20.5	0.9473171
	37	/	/	/	20.96	20.98	0.9990467
	38	19.64	21.01	0.934793	22.06	22.35	0.9870246
	80	19.59	20.22	0.968843	19.15	26.05	0.7351248
	95	18.17	23.19	0.783527	19.73	23.64	0.8346024
	96	18.6	21.25	0.875294	21.19	22.15	0.9566591
		18.93 ± 0.93 (9)	21.74 ± 2.80 (9)	0.86 ± 0.11 (9)	20.55 ± 1.08 (9)	23.12 ± 2.09 (9)	0.90 ± 0.10 (9)
8	39	21.59	22.76	0.948594	23.87	28.34	0.8422724
	40	19.79	22.07	0.896692	22.15	24.29	0.9118979
	41	20.38	20.69	0.985017	22.33	25.08	0.8903509
	80	15.64	18.15	0.861708	19.52	21.81	0.8950023
	95	16.56	17.84	0.928251	19.59	21.59	0.9073645
	96	16.62	17.46	0.95189	18.35	21.58	0.8503244
		20.59 ± 0.92 (6)	21.84 ± 1.05 (6)	0.94 ± 0.04 (6)	20.97 ± 2.12 (6)	23.78 ± 2.69 (6)	0.88 ± 0.03 (6)
12	42	17.91	19.95	0.897744	20.06	23.94	0.8379282
	43	20.43	20.91	0.977044	22.37	25.49	0.8775991
	44	18.52	20.07	0.92277	20.97	23.38	0.8969204
	45	18.16	20.41	0.88976	21.51	22.89	0.9.97117
	95	14.39	18.39	0.78249	17.22	21.35	0.8065574
	96	16.7	17.44	0.957569	18.12	19.76	0.917004
		18.76 ± 1.14 (4)	20.34 ± 0.43 (4)	0.92 ± 0.04 (4)	20.04 ± 2.00 (6)	22.80 ± 2.01 (6)	0.88 ± 0.05 (6)
19	1	24.67	21.58	1.143188	23.93	26.64	0.8982733
	2	20.45	23.25	0.87957	21.06	27.51	0.7655398
	3	21.92	23.96	0.914858	21.94	27.62	0.7943519
	4	26.43	24.85	1.063581	27.86	28.68	0.9714086
	95	15.56	16.97	0.916912	18.19	19.31	0.941999
	96	15.18	14.52	1.045455	18.18	18.55	0.9800539
		23.37 ± 2.69 (6)	23.41 ± 1.3 (6)	1.00 ± 0.12 (6)	21.86 ± 3.69 (6)	24.72 ± 4.54 (6)	0.89 ± 0.09 (6)
31	12	20.67	20.16	1.025298	24.04	23.93	1.0045967
	13	19.54	17.07	1.144698	22.55	21.15	1.0661939
	14	/	/	/	20.52	23.3	0.8806867
	15	/	/	/	24.47	20.75	1.1792771
	16	19.43	17.1	1.136257	/	/	/
	95	15.45	17.42	0.886912	18.02	20.57	0.8760331
	96	14.75	15.96	0.924185	16.03	17.73	0.9041173
		19.88 ± 0.67 (5)	18.62 ± 2.18 (5)	1.10 ± 0.07 (5)	20.94 ± 3.39 (6)	21.24 ± 2.21 (6)	0.99 ± 0.12 (6)

Table E-14: MTR values for DTH animals

E.7.2 NPC

Time-Point (Day)	Rat No.	MTR of Striatum			MTR of Corpus Callosum		
		Injected	Contralateral	L/R	Injected	Contralateral	L/R
0	116	15.53	17.63	0.880885	17.7	20.17	0.8775409
	117	13.77	16.07	0.856876	15.5	18.22	0.8507135
	118	15.75	15.7	1.003185	17.37	17.78	0.9769404
	119	15.86	14.57	1.088538	19.1	17.56	1.876993
		15.23 ± 0.98 (4)	15.99 ± 1.26 (4)	0.96 ± 0.11 (4)	17.42 ± 1.48 (4)	18.43 ± 1.19 (4)	0.95 ± 0.11 (4)
5	116	17.79	15.04	1.182846	20.64	17.97	1.148581
	117	16.48	15.7	1.049682	18.01	18.08	0.9961283
	119	16.48	16.51	0.998183	19.25	18.29	1.0524877
	120	14.78	12.54	1.178628	15.05	16	0.940625
		16.38 ± 1.24 (4)	14.95 ± 1.71(4)	1.10 ± 0.09 (4)	18.24 ± 2.38 (4)	17.59 ± 1.06 (4)	1.03 ± 0.09 (4)
8	116	16.36	15.31	1.068583	19.42	17.53	1.1078152
	117	15.97	14.31	1.116003	18.71	17.42	1.0740528
	119	15.71	14.8	1.061486	18.98	16.67	1.1385723
	120	16.41	14.43	1.137214	16.85	16.94	0.9946871
		16.11 ± 0.33 (4)	14.71 ± 0.45 (4)	1.10 ± 0.04 (4)	18.49 ± 1.13 (4)	17.14 ± 0.40 (4)	1.08 ± 0.06 (4)
12	116	19.5	18.95	1.029024	21.85	22.76	0.9600176
	117	18.94	18.9	1.002116	20.32	22.93	0.8861753
	120	19.46	19.34	1.006205	21.18	22.76	0.9421708
		19.3 ± 0.31 (3)	18.18 ± 1.77 (3)	1.00 ± 0.02 (3)	21.12 ± 0.77 (3)	22.72 ± 0.23 (3)	0.93 ± 0.04 (3)
19	116	15.24	15.54	0.980695	17.84	18.05	0.9883657
	117	18.83	19.35	0.973127	20.62	23.19	0.8891764
	120	17.14	16.09	1.065258	19.13	18.56	1.0307112
		17.07 ± 1.80 (3)	17.17 ± 1.72 (3)	1.00 ± 0.05 (3)	19.20 ± 1.39 (3)	19.93 ± 2.83	0.97 ± 0.07 (3)
31	116	17.05	17.68	0.964367	20.34	23.2	0.8767241
	120	19.64	17.95	1.09415	20.7	20.94	0.9885387
		18.35 ±1.83 (2)	17.8 ± 0.19 (2)	1.03 ± 0.09 (2)	20.52 ± 0.25 (2)	22.07 ± 1.60 (2)	0.93 ± 0.08 (2)

Table E-15: MTR values for control animals receiving no peripheral challenge (NPC).

E.7.3 SAL PC

Time-Point (Day)	Rat No.	MTR of Striatum			MTR of corpus callosum		
		Injected	Contralateral	L/R	Injected	Contralateral	L/R
0	97	16.43	17.26	0.951912	19.4	19.53	0.99337436
	98	15.31	16.35	0.936391	19.75	19.52	1.0117828
		15.87 ± 0.79 (2)	16.81 ± 0.64 (2)	0.94 ± 0.01 (2)	19.58 ± 0.25 (2)	19.53 ± 0.01 (2)	1.00 ± 0.01 (2)
5	100	17.38	18.29	0.950246	22.73	26.61	1.051827
	101	19	19.94	0.952859	20.25	23	0.8804348
	102	17.55	18.61	0.943041	23.05	23.08	0.9987002
		17.98 ± 0.89 (3)	18.95 ± 0.88 (3)	0.95 ± 0.01 (3)	22.01 ± 1.53 (3)	1.53 ± 0.83 (3)	0.98 ± 0.09 (3)
8	103	16.45	17.73	0.927806	18.84	20.22	0.9317507
	104	14.91	17.67	0.843803	17.31	20.81	0.8318116
	105	18.15	19.1	0.950262	22.93	19.22	1.1930281
		16.50 ± 1.62 (3)	18.17 ± 0.81 (3)	0.91 ± 0.06 (3)	19.69 ± 2.906 (3)	20.08 ± 0.80 (3)	0.99 ± 0.19 (3)
12	106	14.73	16.05	0.917757	20.46	19.15	1.0684073
	109	14.72	15.74	0.935197	19.67	19.4	1.0139175
		14.73 ± 0.01 (2)	15.90 ± 0.22 (2)	0.93 ± 0.01 (2)	20.42 ± 0.76 (2)	18.60 ± 1.18 (2)	1.04 ± 0.04 (2)
19	110	13.17	14.1	0.934043	17.52	16.16	1.0841584
	111	14.29	16.27	0.878304	17.87	20.69	0.8637023
		13.73 ± 0.79 (2)	15.19 ± 1.53 (2)	0.91 ± 0.04 (2)	17.70 ± 0.25 (2)	18.43 ± 3.20 (2)	0.97 ± 0.16 (2)
31	113	14.07	15.11	0.931171	19.33	18.43	1.0488334

Table E-16: MTR values for control animals receiving a peripheral challenge of saline (SAL PC).

E.7.4 PB IC

Time-Point (Day)	Rat No.	MTR		
		Injected	Contralateral	L/R
0	68	20.25	20.88	0.969828
	69	18.62	18.04	1.032151
		22.54 ± 0.55 (2)	22.48 ± 1.42 (2)	1.00 ± 0.04 (2)
5	71	13.77	11.35	1.213216
	72	13.26	17.17	0.772277
	73	18.94	17.70	1.070056
		17.87 ± 3.31 (3)	18.52 ± 1.51 (3)	0.97 ± 0.18 (3)
8	74	15.25	18.96	0.804325
	75	18.96	15.57	1.217726
	76	12.88	14.13	0.911536
		17.38 ± 3.56 (3)	17.89 ± 2.83 (3)	0.99 ± 0.28 (3)
12	77	13.89	13.28	1.045934
	79	16.90	18.51	0.91302
		18.39 ± 0.89 (2)	19.73 ± 4.40 (2)	0.95 ± 0.17 (2)
19	82	16.29	16.89	0.964476
	84	20.81	16.45	1.265046
		19.95 ± 3.26 (3)	19.09 ± 2.14 (3)	1.06 ± 0.29 (2)
31	85	15.84	17.32	0.811303
	86	14.58	15.98	1.022971
		18.49 ± 2.19 (2)	20.24 ± 0.91 (2)	0.92 ± 0.15 (2)

Figure E-1: MTR values for control animals receiving an intracerebral injection of phosphate buffered saline (PB IC).

Appendix F

CBV data

F.1.1 DTH

Time-Point (Day)	Rat No.	CBV Area No. of Pixels		CBV L/R Ratio		
		LHS	RHS	Area	Intensity	Intensity Thresholded
0	1	164	84	1.951473	1.005278	1.493018
	2	135	157	0.859926	0.996039	0.594282
	3	140	107	1.309054	1.022807	1.10021
	4	39	52	0.750035	0.980053	0.733902
	46	102	152	0.671299	0.957567	0.783029
	47	110	184	0.597942	0.934402	0.513405
	48	158	174	0.90795	1.010255	0.863551
	17	459	115	3.991767	1.093113	3.583922
	19	52	119	0.437026	1.049623	0.806037
	20	159	127	1.252294	1.072031	1.202104
	35	63	139	0.453222	1.001641	0.829807
	95	184	148	0.791277	1.048579	0.949243
	96	313	170	1.841176	1.124619	2.528585
	80	133	205	0.648668	1.012838	0.861697
	81	227	130	1.620905	0.954916	1.685364
		162.5 ± 107.3 (15)	133.8 ± 40.1 (15)	1.36 ± 0.95 (15)	1.24 ± 0.83 (15)	1.24 ± 0.83 (15)
5	1	177	112	1.580624	1.036493	1.354794
	2	71	82	0.865897	1.015481	1.134013
	3	226	127	1.779817	1.086198	1.648814
	36	204	183	1.115002	1.091232	1.492611
	37	129	67	1.925878	1.008299	1.44787
	38	71	113	0.619394	0.986168	0.578168
	L	99	47	2.10722	1.014407	1.811422
	N	159	146	1.089041	0.981257	1.29326
	O	187	140	1.335714	0.996527	1.446881
	95	152	128	1.187144	1.080017	1.647245
	96	291	183	1.590164	1.117367	2.561992
	80	151	73	2.068493	0.954205	2.79646
	81	228	200	1.139789	1.008929	1.054
		165 ± 66.6 (13)	119.1 ± 48.2 (13)	1.42 ± 0.47 (13)	1.03 ± 0.05 (13)	1.56 ± 0.67 (13)
8	39	243	110	2.208471	1.096965	2.396526
	40	221	217	1.018456	1.080472	1.574336
	41	147	143	1.028004	0.984909	1.531783
	NA	237	176	1.346591	1.093677	1.965275
	NB	246	82	3	1.089002	2.208013
	NC	341	126	2.706349	1.092172	3.373536
	ND	475	151	3.145695	1.359885	3.018712
	95	168	123	1.365897	1.066703	1.551169
	96	375	194	2.529412	1.134253	3.200795
		272.6 ± 105.1 (9)	140.4 ± 45.2 (9)	2.04 ± 0.86 (9)	2.31 ± 0.73 (9)	2.31 ± 0.73 (9)
12	42	133	81	1.642086	1.0338	1.716965
	43	74	34	2.34113	1.052513	1.97407
	45	197	57	3.455544	1.034247	1.751372
	N	216	103	2.097087	0.968059	1.907127
	O	78	48	1.625	1.049529	1.194853
	NB	253	160	1.58125	1.086272	1.833905
	NC	292	103	2.834951	1.114452	4.051036
	ND	171	124	1.379032	1.042917	1.641246
	96	375	194	1.933183	1.094044	3.022274
	80	178	186	0.9569892	(0.713645)	(0.989958)
		197.9 ± 93.3 (10)	103.5 ± 56.8 (10)	1.99 ± 0.73 (10)	2.12 ± 0.87 (9)	2.12 ± 0.87 (9)
19	1	37	77	0.4807	1.013155	1.315856
	2	160	187	0.85553	0.979102	0.640145
	3	181	60	3.01699	0.980541	1.897618
	4	203	106	1.914835	0.997052	2.077941
	N	127	89	1.426966	0.952155	2.190686
	O	162	113	1.433628	1.013627	1.635202
	95	184	85	2.164706	0.86058	3.577534
	96	358	163	2.196319	1.139423	2.905149

Time-Point (Day)	Rat No.	CBV Area No. of Pixels		CBV L/R Ratio		
		LHS	RHS	Area	Intensity	Intensity Thresholded
		176.5 ± 89.5 (8)	96.9 ± 41.5 (8)	1.67 ± 0.81 (8)	0.99 ± 0.08 (8)	2.03 ± 0.91 (8)
31	12	114	113	1.009021	1.05099	1.072127
	13	144	118	1.220988	0.939522	1.110521
	15	241	104	2.317927	1.046011	1.447042
	16	133	120	1.10801	1.017957	1.12516
	N	199	88	2.261364	0.876686	1.860561
	O	238	135	1.762963	0.948177	2.002637
	95	132	163	0.809816	0.719914	1.310743
	96	191	38	5.026316	1.162542	2.795074
		174.0 ± 49.9 (8)	107.4 ± 34.9 (8)	1.94 ± 1.37 (8)	0.97 ± 0.13 (8)	1.59 ± 0.60 (8)

Table F-1: Individual values for CBV data in DTH animals, Area of increased rCBV, intensity of increased rCBV.

F.1.2 NPC

Time-Point (Day)	Rat No.	CBV Area (No. of Pixels)		L/R CBV		
		LHS	RHS	Area	Intensity	Thresholded Intensity
0	116	191	110	1.736364	1.106092	1.271523
	117	78	141	0.553191	0.992717	0.643224
	118	148	82	1.804878	1.038578	0.973451
	119	49	57	0.859649	0.985897	0.860977
		116.5 ± 64.8 (4)	97.5 ± 36.2 (4)	1.24 ± 0.63 (4)	1.03 ± 0.06 (4)	0.94 ± 0.26 (4)
5	116	258	230	1.121739	0.997124	1.309615
	117	91	62	1.467742	1.084262	1.041977
	119	193	222	0.869369	1.055967	0.928998
	120	98	80	1.225	1.007722	0.773312
		160.0 ± 80.2 (4)	148.5 ± 89.9 (4)	1.17 ± 0.25 (4)	1.04 ± 0.04 (4)	1.01 ± 0.23 (4)
8	116	132	111	1.189189	0.962721	0.919651
	117	81	130	0.62307	0.994877	0.809558
	119	94	108	0.87037	0.937647	0.739958
	120	113	146	0.773973	1.078936	1.148991
		105.0 ± 22.3 (4)	123.8 ± 17.8 (4)	0.86 ± 0.24 (4)	0.99 ± 0.06 (4)	0.90 ± 0.18 (4)
12	116	33	86	0.383721	0.961963	0.936919
	117	109	134	0.813433	1.012304	0.740549
	120	145	103	1.407767	1.13841	1.127606
		95.7 ± 57.2 (3)	107.7 ± 24.3 (3)	0.87 ± 0.51 (3)	1.04 ± 0.09 (3)	0.94 ± 0.19 (3)
19	116	95	82	1.158537	0.976204	1.011383
	117	120	171	0.701754	1.01719	0.96025
	120	123	127	0.968504	1.059616	0.909277
		112.7 ± 15.4 (3)	126.7 ± 45.0 (3)	0.94 ± 0.23 (3)	1.02± 0.04 (3)	0.96 ± 0.05 (3)
31	116	186	148	1.256757	0.986398	0.992431
	120	105	141	0.744681	1.08336	0.854502
		145.5 ± 57.3 (2)	144.5 ± 5.0 (2)	1.00 ± 0.36 (2)	1.03 ± 0.07 (2)	0.92 ± 0.10 (2)

Table F-2: Summary of areas of increased rCBV, intensity of thresholded rCBV maps, and intensity of unthresholded rCBV maps for control animals receiving no peripheral challenge (NPC).

F.1.3 SAL PC

Time-Point (Day)	Rat No.	CBV Area (No. of Pixels)		L/R CBV		
		LHS	RHS	Area	Intensity	Thresholded Intensity
0	97	173	179	0.96664	1.045501	0.921065
	98	223	148	1.50689	1.101295	1.516595
		198.0 ± 35.4 (2)	163.5 ± 21.9 (2)	1.24 ± 0.38 (2)	1.07 ± 0.04 (2)	1.22 ± 0.42 (2)
5	100	232	117	1.982576	1.09398	1.856876
	101	67	148	0.452805	1.003315	0.318007
	102	264	278	1.748168	1.068127	1.446058
		187.7 ± 115.3 (3)	181.0 ± 85.4 (3)	1.39 ± 0.82 (3)	1.06 ± 0.05 (3)	1.21 ± 0.80 (3)
8	103	152	115	1.321723	1.034229	1.486088
	104	154	120	1.283374	1.063689	0.952061
	105	304	154	1.973995	0.949839	1.508666
		203.3 ± 87.2 (3)	129.7 ± 21.2 (3)	1.53 ± 0.39 (3)	1.02 ± 0.06 (3)	1.31 ± 0.42 (3)
12	107	178	166	1.07193	1.031769	1.174586
	108	81	63	1.285252	0.937086	0.901869
	109	262	177	1.480049	1.046624	2.013496
		173.7 ± 90.6 (3)	135.3 ± 62.9 (3)	1.28 ± 0.20 (3)	1.01 ± 0.06 (3)	1.36 ± 0.58 (3)
19	110	128	216	0.592717	0.959367	0.700652
	111	164	125	1.31159	1.110998	0.955972
		146.0 ± 25.5 (2)	170.5 ± 64.4 (2)	0.95 ± 0.51 (2)	1.04 ± 0.11 (2)	0.83 ± 0.18 (2)
31	115	149	131	1.137298	1.042641	1.031111

Table F-3: Summary of areas of increased rCBV, intensity of thresholded rCBV maps, and intensity of unthresholded rCBV maps for control animals receiving a peripheral challenge of saline (SAL PC).

F.1.4 PB IC

Time-Point (Day)	Rat No.	CBV Area (No. of Pixels)		L/R CBV		
		LHS	RHS	Area	Intensity	Thresholded Intensity
0	67	161	156	1.032051	1.103113	1.31159
	69	162	134	1.208955	0.993646	0.88293
		161.5 ± 0.7 (2)	145.0 ± 15.6 (2)	1.12 ± 0.13 (2)	1.05 ± 0.08 (2)	1.10 ± 0.30 (2)
5	71	140	133	1.052632	1.051794	1.692344
	72	89	66	1.348485	0.971254	0.725642
	73	121	115	1.052174	1.053264	1.311805
		116.7 ± 25.8 (3)	104.7 ± 34.7 (3)	1.15 ± 0.17 (3)	1.03 ± 0.05 (3)	1.24 ± 0.49 (3)
8	74	120	88	1.363636	1.044308	1.254895
	75	166	140	1.185714	0.934164	1.406459
	76	184	147	1.251701	0.95416	0.47798
		156.7 ± 33.0 (3)	125.0 ± 32.2 (3)	1.18 ± 0.15 (3)	0.98 ± 0.06 (3)	1.05 ± 0.50 (3)
12	77	170	94	1.808511	0.973418	1.326542
	78	134	186	0.72043	0.967608	0.966154
	79	148	120	1.233333	1.075845	1.368708
		150.7 ± 18.2 (3)	133.3 ± 47.4 (3)	1.26 ± 0.54 (3)	1.01 ± 0.06 (3)	1.22 ± 0.22 (3)
19	82	151	120	1.258333	1.039724	0.90929
	83	77	64	1.203125	0.972898	0.897801
	84	293	265	1.10566	1.080607	1.63754
		173.7 ±109.8 (3)	149.7 ± 103.7 (3)	1.19 ± 0.08 (3)	1.03 ± 0.05 (3)	1.26 ± 0.42 (3)
31	85	88	99	0.888889	1.039422	0.914731
	86	146	164	0.906832	1.02441	1.143199
		117.0 ± 41.0 (2)	130.0 ± 43.8 (2)	0.90 ± 0.01 (2)	1.03 ± 0.01 (2)	1.03 ± 0.16 (2)

Table F-4: Summary of areas of increased rCBV, intensity of thresholded rCBV maps, and intensity of unthresholded rCBV maps for control animals receiving an intracerebral injection of phosphate buffered saline (PB IC).

F.2 Correlations with Histological Parameters

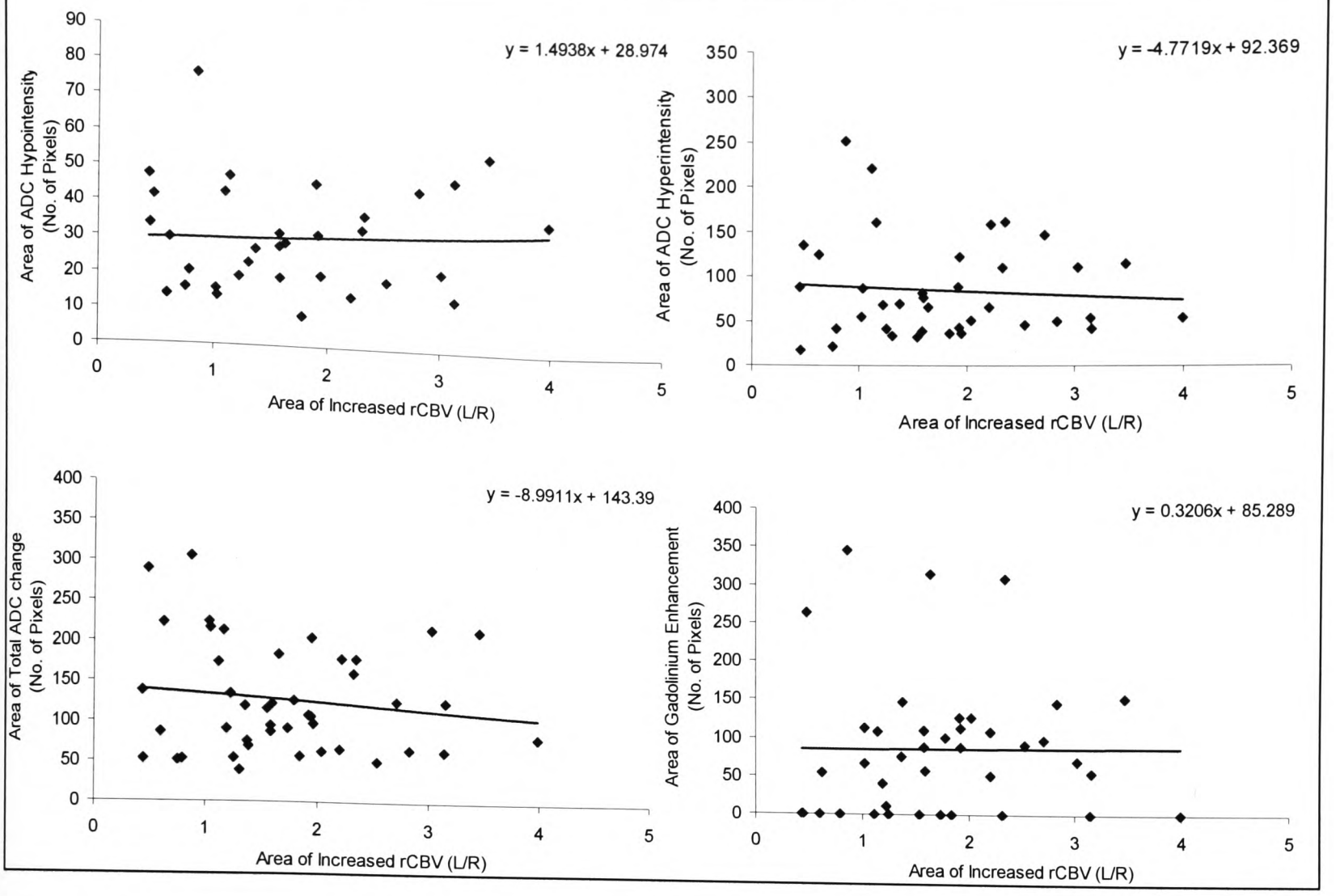


Figure F-1: Relationship between ADC change and rCBV increases

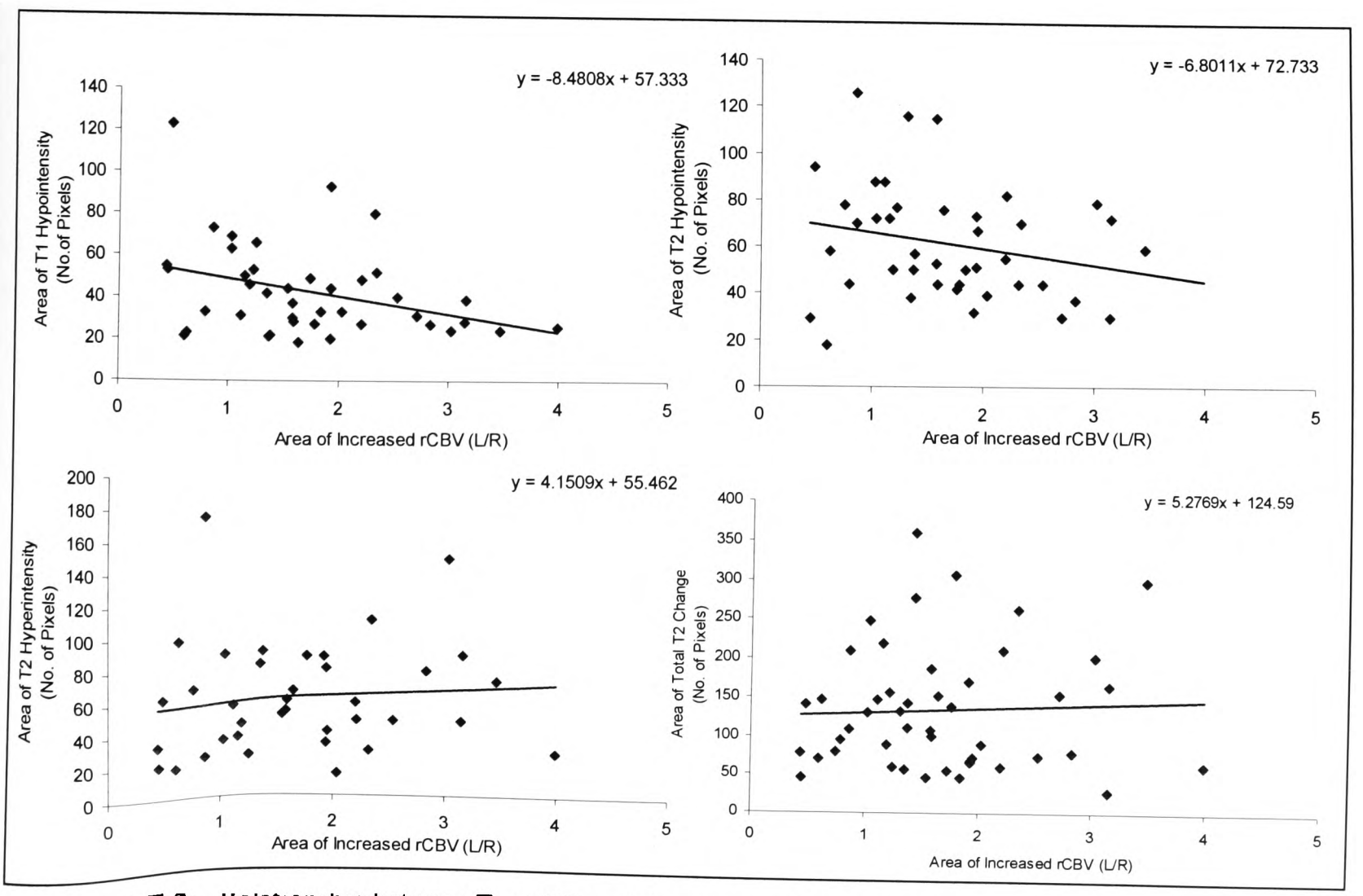


Figure F-2: Relationship between T_1 and T_2 weighted image changes and increased rCBV.

Appendix G

MRI Visible Exacerbation

G.1 CBV Changes

Time-Point (Day)	Rat No	CBV Area No. of Pixels		L/R CBV	
		LHS	RHS	Area	Intensity
0	122	62	147	0.349206	0.471795
	123	170	72	2.361111	1.758968
	125	247	83	2.975904	1.953028
	124	192	161	1.192547	1.984745
		167.75 ± 77.58 (4)	115.75 ± 44.76 (4)	1.7 ± 1.2 (4)	1.5 ± 0.7 (4)
1	122	435	107	3.8	3.823776
	123	729	114	6.394737	5.868089
	125	549	34	16.14706	6.653499
	137	472	150	3.146667	3.945869
	140	811	90	9.011111	7.782609
	142	323	43	7.511628	5.001976
	144	319	148	2.155405	2.980627
	145	452	132	3.424242	3.702509
	146	457	111	4.117117	3.79375
	138	459	60	7.65	3.305348
	139	663	81	8.185185	6.8681
	124	803	72	11.15494	8.597502
	141	407	103	3.951456	3.951456
	143	490	44	11.13636	11.13636
	147	805	62	12.98387	7.942257
	144b	356	67	5.313433	3.438647
	145b	231	136	1.698529	1.288341
	146b	122	32	3.8125	2.043861
	148b	271	117	2.316239	2.259809
		481.79 ± 201.21 (19)	89.63 ± 38.36 (19)	6.5 ± 4.1 (19)	4.8 ± 2.6 (19)
5	122	110	106	1.037736	1.259662
	123	233	116	2.008621	1.759136
	125	357	59	6.050847	2.924037
	126	286	80	3.575	3.160529
	137	152	109	1.394495	1.802433
	140	303	90	3.366667	2.008147
	142	282	143	1.972028	2.055144
	144	164	94	1.744681	1.743849
	145	183	58	3.155172	1.44292
	146	191	124	1.540323	1.278626
	138	287	93	3.086022	2.046215
	139	255	57	4.473684	3.046061
	124	337	137	2.459854	2.346276
	141	211	153	1.379085	1.495851
	143	102	54	1.888889	1.888889
	147	/	/	/	2.660742
		230.2 ± 79.26 (15)	98.2 ± 32.65 (15)	2.6 ± 1.4 (15)	2.0 ± 0.6 (16)
19	122	244	88	2.772727	1.666995
	125	307	131	2.343511	2.375672
	126	135	120	1.125	1.091801
	137	241	174	1.385057	1.770544
	140	287	228	1.258772	1.676455
	144	142	120	1.183333	1.056729
	145	284	174	1.632184	1.952459
	146	142	115	1.234783	1.293932
	138	329	132	2.492424	2.971174
	139	231	128	1.804688	2.497509
	124	220	78	2.820513	1.871
		232.91 ± 68.36 (11)	135.27 ± 42.51 (11)	1.8 ± 0.7 (11)	1.8 ± 0.6 (11)
42	122	114	148	0.77027	0.646061
	125	302	93	3.247312	2.932421
	126	283	122	2.319672	2.475472
	137	154	151	1.019868	1.013609
	140	331	107	3.093458	2.691929
	142	227	124	1.830645	1.396584

Time-Point (Day)	Rat No	CBV Area No. of Pixels		L/R CBV	
		LHS	RHS	Area	Intensity
	144	157	136	1.154412	1
	145	245	127	1.929134	1.931764
	146	157	164	0.957317	1.113116
	138	373	185	2.016216	2.679274
	139	333	129	2.581395	3.079526
	124	272	136	2	1.762454
	131	334	89	3.752809	2.459692
	141	248	163	1.521472	1.521472
	147	459	146	3.143836	2.924874
		265.93 ± 94.62 (15)	134.67 ± 26.36 (15)	2.1 ± 0.9 (15)	2.0 ± 0.8 (15)

Table G-1: Area of rCBV increases and L/R rCBV intensity ratio post LPS, saline or no peripheral challenge.

G.2 IL-1β ELISA results

G.2.1 24 hours

Sample	Rat No.	μg IL-1β/mg protein	
		Injected	Contralateral
Striatum	154	1.44	-0.15
	157	2.04	-0.03
	158	1.88	0.16
		1.79 ± 0.31 (3)	-0.01 ± 0.16 (3)
Cortex	154	1.62	0.06
	157	1.72	0.00
	158	0.55	0.12
		1.30 ± 0.65 (3)	0.06 ± 0.06 (3)
Injection Site	154	1.64	0.05
	157	2.44	0.26
	158	0.71	0.06
		1.60 ± 0.87 (3)	0.12 ± 0.12 (3)

Figure G-1: Concentration of IL-1β at 24 hours.

G.2.2 19 days

Sample	Rat No.	μg IL-1β/mg protein	
		Injected	Contralateral
Striatum	32	0.13	0.24
	33	0.86	0.04
	34	0.39	0.26
		0.63 ± 0.33 (3)	0.15 ± 0.16 (3)
Cortex	32	0.36	0.16
	33	0.26	0.06
	34	0.46	0.19
		0.36 ± 0.14 (3)	0.13 ± 0.10 (3)
Injection Site	32	0.68	0.72
	33	0.43	0.27
	34	0.48	0.16
		0.45 ± 0.03 (3)	0.22 ± 0.08 (3)

Figure G-2: Concentration of IL-1β at 19 days.

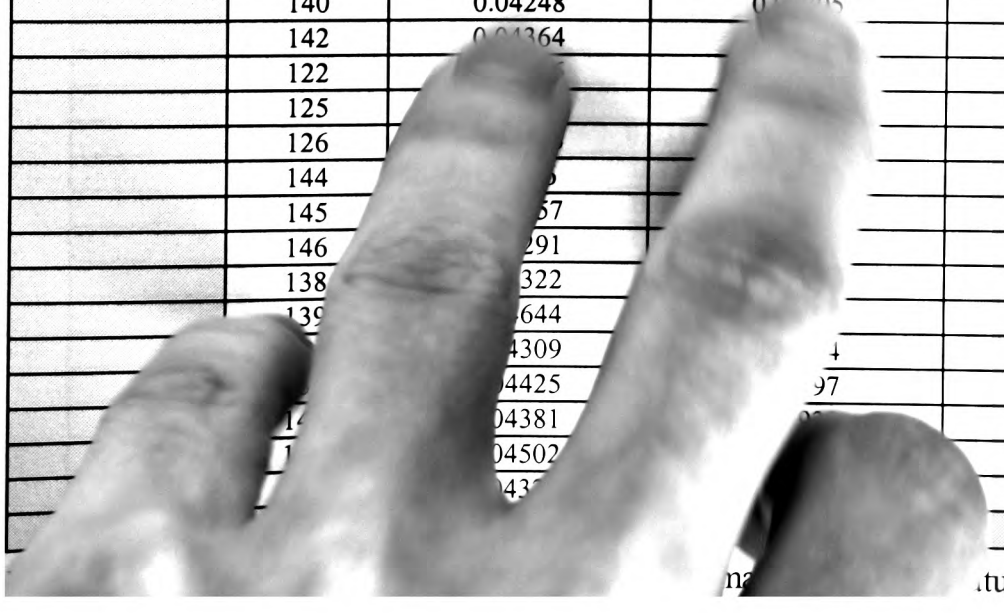
G.3 T_1 Relaxation Time

Time-Point (Day)	Rat No.	Striatum T_1 Relaxation Time (sec)		Cortex T_1 Relaxation Time (sec)	
		Injected	Contralateral	Injected	Contralateral
1	137	1.835	1.727	1.882	1.776
	140	1.802	1.693	1.903	1.753
	142	1.679	1.72	1.783	1.822
	138	1.899	1.78	1.918	1.785
	139	1.719	1.814	1.765	1.908
	141	1.721	1.689	1.786	1.803
	143	1.712	1.674	1.822	1.768
		1.77 ± 0.08 (7)	1.73 ± 0.05 (7)	1.82 ± 0.06 (7)	1.80 ± 0.05 (7)
5	137	1.695	1.73	1.759	1.874
	140	1.619	1.709	1.782	1.779
	142	1.735	1.75	1.911	1.84
	122	1.929	1.838	1.892	1.942
	123	1.855	1.752	1.828	1.845
	125	1.87	1.78	1.806	1.855
	126	1.84	1.693	1.828	1.734
	144	1.733	1.709	1.771	1.853
	145	1.73	1.712	1.787	1.755
	146	1.732	1.69	1.783	1.755
	138	1.726	1.691	1.788	1.71
	139	1.732	1.7	1.772	1.799
	124	1.718	1.749	1.824	1.807
	141	1.648	1.726	1.775	1.82
	143	1.722	1.736	1.836	1.814
	147	1.732	1.722	1.766	1.781
		1.75 ± 0.08 (16)	1.73 ± 0.04 (16)	1.81 ± 0.04 (16)	1.81 ± 0.06 (16)
19	137	1.67	1.696	1.827	1.81
	140	1.669	1.697	1.819	1.81
	142	1.641	1.719	1.794	1.792
	122	1.775	1.741	1.841	1.722
	125	1.68	1.74	1.758	1.818
	126	1.72	1.763	1.88	1.837
	144	1.692	1.735	1.805	1.844
	145	1.697	1.744	1.723	1.845
	146	1.672	1.752	1.725	1.843
	138	1.733	1.688	1.834	1.783
	139	1.713	1.716	1.828	1.832
	124	1.633	1.668	1.72	1.811
		1.69 ± 0.04 (12)	1.72 ± 0.03 (12)	1.80 ± 0.05 (12)	1.81 ± 0.04 (12)
42	137	1.623	1.692	1.75	1.734
	140	1.615	1.657	1.657	1.75
	142	1.571	1.72	1.696	1.726
	122	1.718	1.582	/	/
	125	1.681	1.7	1.728	1.752
	126	1.575	1.643	1.698	1.751
	144	1.547	1.645	1.811	1.803
	145	1.621	1.699	1.639	1.762
	146	1.633	1.606	1.697	1.772
	138	1.639	1.715	1.652	1.702
	139	1.635	1.68	1.727	1.805
	124	1.669	1.684	1.723	1.754
	131	1.58	1.803	1.668	1.89
	141	1.611	1.688	1.747	1.807
	143	1.617	1.606	1.742	1.704
	147	1.543	1.622	1.711	1.746
		1.62 ± 0.05 (16)	1.67 ± 0.05 (16)	1.71 ± 0.05 (15)	1.76 [illegible] (15)

Table G-2: T_1 relaxation times taken from T_1 maps in the striatum and cortex inflammatory response.

G.4 T_2 Relaxation Time

Time-Point (Day)	Rat No.	Striatum T_2 Relaxation Time (sec)		Cortex T_2 Relaxation Time (sec)	
		Injected	Contralateral	Injected	Contralateral
1	137	0.05034	0.05026	0.0475	0.04868
	140	0.049	0.0469	0.04817	0.04717
	142	0.0492	0.04856	0.0462	0.04845
	138	0.04753	0.04599	0.04573	0.04521
	139	0.04824	0.04962	0.04673	0.04868
	141	0.04983	0.04747	0.04853	0.0473
	143	0.05089	0.04546	0.04929	0.04615
	144	0.04904	0.04811	0.04588	0.04753
	145	0.0533	0.04863	0.05064	0.04721
	146	0.05152	0.04863	0.04877	0.04749
	147	0.05357	0.04724	0.05017	0.04548
		50 ± 2 (11)	48 ± 1 (11)	48 ± 2 (11)	47 ± 1 (11)
5	137	0.04545	0.04884	0.04537	0.04956
	140	0.04616	0.048	0.04716	0.04788
	142	0.04563	0.05155	0.04565	0.0502
	122	0.04969	0.04892	0.04565	0.04866
	123	0.04996	0.04965	0.04694	0.0494
	125	0.05105	0.04915	0.04676	0.04727
	126	0.04939	0.0524	/	/
	144	0.04564	0.04865	0.04399	0.04947
	145	0.04772	0.04827	0.04716	0.04727
	146	0.04685	0.04846	0.04661	0.04729
	138	0.04684	0.05193	0.04572	0.05072
	139	0.0476	0.04816	0.04606	0.0475
	124	0.04554	0.04993	0.04474	0.04889
	141	0.04512	0.04914	0.04645	0.04921
	143	0.0469	0.04794	0.04736	0.04745
	147	0.04697	0.04718	0.04704	0.04684
		47 ± 2 (16)	49 ± 2 (16)	46 ± 1 (15)	49 ± 1 (15)
19	137	0.0426	0.04861	0.04411	0.0499
	140	0.04517	0.04708	0.04633	0.0475
	142	0.04402	0.04761	0.04836	0.04724
	122	0.04077	0.04891	0.04626	0.04737
	125	0.04225	0.05027	0.04552	0.0487
	126	0.04466	0.0466	0.04543	0.0461
	144	0.04824	0.04481	0.04855	0.0446
	145	0.04572	0.04659	0.04762	0.04594
	146	0.04641	0.047	0.04754	0.04651
	138	0.04507	0.04854	0.04599	0.04875
	139	0.04758	0.04642	0.04766	0.04622
	124	0.047	0.04581	0.04733	0.04486
		45 ± 2 (12)	47 ± 2 (12)	47 ± 1 (12)	47 ± 2 (12)
42	137	0.0449	0.04527	0.04752	0.04649
	140	0.04248	0.04705	0.04508	0.04785
	142	0.04364		0.04736	0.04694
	122			0.04482	0.04755
	125			0.04803	0.04542
	126			0.04516	0.04731
	144			0.04647	0.04481
	145	57		0.04756	0.04688
	146	291		0.04427	0.04712
	138	322		0.04631	0.0463
	139	644		0.04785	0.04628
		4309		0.04475	0.047
		4425	97	0.0472	0.04629
	12	04381		0.04544	0.05036
	1	04502		0.04738	0.04646
		043		0.04534	0.0475
				46 ± 1 (16)	47 ± 1 (16)



...tum and cortex during the acute

G.5 T_2 Relaxation time in lesion

Time-Point (Day)	Rat No	Lesion T_2 Relaxation Time (sec)	Area of Lesion on T_2 maps (No. of Pixels)
1	137	0.04681	37
	140	0.04621	72
	142	0.03673	55
	138	0.04246	71
	139	0.0425	67
	141	0.04369	50
	143	0.04595	34
	144	0.04346	51
	145	0.05003	111
	146	0.04582	84
	147	0.04282	68
		44 ± 3 (11)	63.64 ± 21.96 (11)
5	137	0.04207	36
	140	0.040395	60
	142	0.03487	52
	122	0.03931	178
	123	0.04041	118
	125	0.04343	109
	126	0.039865	206
	144	0.04324	63
	145	0.04378	78
	146	0.04353	75
	138	0.04362	50
	139	0.04051	71
	124	0.04007	98
	141	0.04122	53
	143	0.04328	87
	147	0.03736	63
		41 ± 3 (16)	87.31 ± 46.70 (16)
19	137	0.03869	55
	140	0.0398	30
	142	0.03547	68
	122	0.02875	199
	125	0.0284	107
	126	0.032735	126
	144	0.0416	92
	145	0.04051	74
	146	0.03977	99
	138	0.03849	72
	139	0.042035	30
	124	0.03941	75
		37 ± 5 (12)	85.58 ± 45.76 (12)
42	137	0.03994	50
	140	0.03707	76
	142	0.03635	63
	122	0.03449	125
	125	0.03864	85
	126	0.031525	118
	144	0.03595	99
	145	0.03677	53
	146	0.03615	37
	138	0.037045	65
	139	0.04308	73
	124	0.033	29
	131	0.03052	61
	141	0.03723	67
	143	0.04092	60
	147	0.03603	85
		37 ± 3 (16)	71.63 ± 26.26 (16)

Table G-4: T_2 relaxation times in the lesion, and area of lesion taken from T_2 maps during the acute inflammatory response.

G.6 T_2* Relaxation Time

Time-Point (Day)	Rat No.	Lesion T_2* Relaxation Time (sec)	Area of Lesion on T_2* maps (No. of Pixels)	Striatum T_2* Relaxation Time (sec)		
				Injected	Contralateral	L/R
1	137	0.02029	17	0.03106	0.03266	0.95101
	140	0.02921	29	0.03469	0.03831	0.905508
	142	0.01785	83	0.02975	0.03985	0.74655
	138	0.02241	30	0.033321	0.03512	0.948776
	139	0.02694	39	0.0355	0.0451	0.78714
	141	0.02503	27	0.03469	0.04064	0.853593
	143	0.03026	24	0.0263	0.03185	0.825746
	147	0.02479	64	0.04075	0.04905	0.830785
	144	0.02556	94	0.03929	0.03798	1.034492
	145	0.03788	74	0.05075	0.04903	1.035081
	146	0.03489	88	0.04504	0.03734	1.206213
		0.027 ± 0.006 (11)	51.7 ± 29.1 (11)	0.036 ± 0.006 (11)	0.040 ± 0.006 (11)	0.92 ± 0.13 (11)
5	137	0.0198	80	0.03926	0.04382	0.895938
	140	0.01251	89	0.02851	0.04774	0.597193
	142	0.02003	82	0.03699	0.04871	0.759392
	144	0.03345	64	0.04142	0.04417	0.937741
	145	0.03106	49	0.04176	0.04721	0.884558
	146	0.03164	39	0.04961	0.05095	0.9737
	138	0.02682	48	0.04677	0.04566	1.02431
	139	0.01339	44	0.02749	0.04079	0.67394
	141	0.01525	61	0.03929	0.048	0.818542
	143	0.01591	86	0.04007	0.04152	0.965077
	147	0.03478	57	0.0455	0.04097	1.110569
		0.023 ± 0.009 (11)	63.6 ± 18.0 (11)	0.040 ± 0.003 (11)	0.045 ± 0.003 (11)	0.88 ± 0.15 (11)
19	137	0.02479	57	0.03132	0.04271	0.733318
	140	0.01681	59	0.02278	0.0301	0.756811
	142	0.02049	72	0.03838	0.04241	0.904975
	144	0.02824	94	0.04247	0.04266	0.995546
	145	0.02892	71	0.04088	0.03937	1.038354
	146	0.02076	121	0.0281	0.04751	0.591454
	138	0.01931	98	0.02283	0.0349	0.654155
	139	0.02199	62	0.02754	0.04047	0.680504
		0.023 ± 0.004 (8)	79.3 ± 22.8 (8)	0.032 ± 0.005 (8)	0.040 ± 0.005 (8)	0.79 ± 0.17 (8)
42	137	0.01991	58	0.02687	0.04726	0.568557
	140	0.0124	69	/	/	/
	142	0.0212	104	0.03348	0.05357	0.624977
	122	0.01556	102	0.03056	0.04028	0.758689
	125	0.01581	102	0.02774	0.04038	0.686974
	126	0.01834	58	0.03449	0.05014	0.687874
	144	0.01842	143	0.02409	0.02378	1.013036
	145	0.01845	59	0.02962	0.03555	0.833193
	146	0.02963	92	0.04021	0.03853	1.043602
	138	0.02739	92	0.03758	0.04117	0.912801
	139	0.01559	50	/	/	/
	124	0.02263	110	0.02906	0.04972	0.584473
	131	0.0236	78	0.03242	0.05329	0.608369
	141	0.01864	79	0.03723	0.04952	0.751817
	143	0.01585	19	0.04092	0.04563	0.896778
	147	0.024	90	/	/	/
		0.020 ± 0.005 (16)	81.6 ± 29.4 (16)	0.033 ± 0.008 (14)	0.044 ± 0.008 (14)	0.77 ± 0.16 (14)

Table G-5: T_2* relaxation times taken from T_2* maps for individual animals during the acute inflammatory response.

G.7 BBB Permeability

Time-Point (Day)	Rat No.	Area of BBB Breakdown (No. of Pixels)	Intensity of Breakdown (L/R)
0	122	25	1.115213
	123	73	1.37764
	124	144	2.035506
	125	91	1.364103
		83.25 ± 49.16 (4)	1.47 ± 0.39 (4)
1	122	123	1.431519
	123	124	1.577774
	124	68	1.455181
	125	72	1.438912
	144	48	1.112429
	145	31	1.143893
	146	77	1.223025
	147	94	1.207298
		79.63 ± 34.54 (8)	1.32 ± 0.17 (8)
5	122	64	1.641559
	124	311	1.446586
	125	386	1.758309
	126	376	1.382598
	137	103	1.243961
	138	203	1.340939
	139	173	1.203727
	140	147	1.265562
	141	131	1.396524
	142	204	1.40592
	143	102	1.206576
	144	242	1.770919
	145	189	1.354244
	146	209	1.282152
	147	120	1.282598
		197.33 ± 97.10 (15)	1.40 ± 0.18 (15)
19	122	305	1.586693
	124	160	1.395755
	125	195	1.477416
	126	189	1.205605
	137	57	1.077616
	138	107	1.237396
	139	71	1.141516
	140	59	1.17092
	144	98	1.115899
	145	0	1
	146	67	1.202934
	147	39	1.186426
		112.25 ± 85.28 (12)	1.23 ± 0.17 (12)
42	122	45	1.907696
	124	18	1.027596
	125	40	1.786295
	126	68	1.261983
	131	49	1.215053
	137	32	1.063484
	138	37	1.181878
	139	44	1.060406
	140	22	1.022049
	141	15	1.014428
	144	32	1.003665
	145	54	1.069575
	146	25	1.028961
	147	138	1.127474
		44.21 ± 30.70 (14)	1.20 ± 0.29 (14)

Table G-6: BBB permeability during the acute inflammatory response.

G.8 Diffusion Anisotropy

Time-Point (Day)	Rat No.	Injected Hemisphere	Contralateral Hemisphere
0	122	0.1141	0.1318
	123	0.09413	0.1072
	124	0.09249	0.09216
	125	0.0984	0.1153
		0.100 ± 0.010 (4)	0.112 ± 0.017 (4)
1	144	0.08326	0.1053
	145	0.09262	0.1173
	146	0.08556	0.104
	147	0.09566	0.1163
		0.089 ± 0.006 (4)	0.111 ± 0.007 (4)
5	122	0.08985	0.1073
	123	0.09722	0.1143
	125	0.0949	0.1121
	126	0.08848	0.09808
	137	0.1005	0.09757
	140	0.115	0.1041
	142	0.1075	0.09886
	144	0.084	0.09173
	145	0.1015	0.1067
	146	0.09466	0.1014
	124	0.1017	0.09554
	138	0.1009	0.09177
	139	0.1267	0.1063
	141	0.1017	0.103
	143	0.09444	0.1173
	147	0.09976	0.09677
		0.10 ± 0.01 (16)	0.103 ± 0.01 (16)
19	122	0.1043	0.1046
	125	0.1193	0.1119
	126	0.0925	0.09949
	137	0.09944	0.1058
	140	0.1005	0.09523
	142	0.09589	0.1031
	144	0.08788	0.09074
	145	0.09518	0.09926
	146	0.1038	0.1017
	138	0.09462	0.09483
	139	0.1042	0.105
	124	0.1033	0.09662
		0.100 ± 0.008 (12)	0.101 ± 0.006 (12)
42	122	0.1	0.1074
	125	0.09068	0.0962
	126	0.1147	0.1145
	137	0.09972	0.1032
	140	0.1031	0.1191
	142	0.09418	0.09071
	144	0.08666	0.09484
	145	0.09658	0.1088
	146	0.09338	0.1073
	124	0.09886	0.1115
	131	0.1074	0.1065
	138	0.1203	0.1066
	139	0.1046	0.1097
	141	0.09305	0.105
	143	0.1013	0.0996
	147	0.1027	0.1032
		0.100 ± 0.009 (16)	0.105 ± 0.007 (16)

Table G-7: Diffusion anisotropy values for the ipsilateral and contralateral hemispheres during the acute inflammatory response.

G.9 ADC and MTR Values

Time-Point (Day)	Rat No.	ADC in Hyperintensity	ADC in contralateral	Area of ADC Hyperintensity	MTR	
					Injected	Contralateral
0	122	0.000866	0.000682	114	13.85	17.66
	123	0.000735	0.000658	155	16.37	18.79
	124	0.000792	0.000699	128	17.07	19.11
	125	0.000832	0.00069	137	16.28	16.83
		8.1 ± 0.6 (4)	6.8 ± 1.8 (4)	133.5 ± 17.2 (4)	15.89 ± 1.41 (4)	17.86 ± 1.34 (4)
1	144	0.000922	0.000719	205	16.16	17.46
	145	0.000868	0.000747	89	16.28	17.05
	146	0.000851	0.000701	167	16.31	17.43
	147	0.000913	0.000689	236	15.36	18.23
		8.9 ± 3.5 (4)	7.1 ± 2.5 (4)	174.3 ± 63.5 (4)	13.91 ± 0.59 (4)	18.35 ± 0.59 (4)
5	122	0.000893	0.000711	500	16.19	19.31
	123	0.000893	0.000694	341	14.65	16.97
	125	0.000827	0.000681	443	/	/
	126	0.000848	0.000706	582	14.57	17.07
	137	/	/	/	19.57	21.03
	140	/	/	/	20.64	20.61
	142	/	/	/	13.45	16.06
	144	0.000811	0.000674	216	13.27	15.58
	145	0.000733	0.000653	100	15.65	17.59
	146	0.000767	0.000647	114	15.16	19.29
	124	0.00073	0.000641	211	16.48	19.16
	138	/	/	/	18.29	20.10
	139	/	/	/	18.07	18.96
	141	/	/	/	16.85	20.57
	143	/	/	/	17.42	18.38
	147	0.000764	0.000664	228	14.17	17.91
		8.4 ± 7.7 (9)	6.8 ± 2.6 (9)	303.9 ± 171.9 (9)	16.09 ± 2.28 (16)	18.19 ± 1.80 (16)
19	122	0.000685	0.000683	167	15.06	22.66
	123	0.000755	0.000683	107	/	/
	125	/	/	/	15.89	19.78
	126	/	/	/	15.62	19.15
	137	/	/	/	16.30	17.87
	140	/	/	/	15.73	15.65
	144	0.000708	0.000598	26	12.94	15.97
	145	0.000703	0.00066	60	15.40	17.03
	146	/	/	/	14.57	17.44
	138	/	/	/	14.43	18.33
	139	/	/	/	14.34	15.95
	124	0.00071	0.000665	53	14.00	21.54
	147	0.000688	0.00067	60	14.60	16.89
		7.1 ± 2.5 (6)	6.6 ± 3.2 (6)	78.8 ± 50.5 (6)	14.91 ± 0.94 (12)	18.11 ± 2.00 (12)
42	122	/	/	/	9.88	17.13
	123	/	/	/	/	/
	125	/	/	/	10.01	15.82
	126	/	/	/	12.62	17.66
	137	/	/	/	15.66	16.64
	140	/	/	/	13.81	15.70
	142	/	/	/	14.81	16.65
	144	0.00071	0.000654	32	15.46	17.00
	145	0.000722	0.000691	53	16.74	20.18
	146	/	/	/	14.33	17.19
	124	/	/	/	17.37	16.2
	131	/	/	/	11.51	16.38
	138	/	/	/	14.07	16.08
	139	/	/	/	15.98	17.19
	141	/	/	/	14.27	16.22
	143	/	/	/	13.71	16.95
	147	0.000763	0.000678	19	15.09	17.68
		7.3 ± 2.8 (3)	6.7 ± 1.9 (3)	34.7 ± 17.2 (3)	14.08 ± 2.17 (16)	16.74 ± 0.97 (16)

Table G-8: ADC and MTR values during the acute inflammatory response.

G.10 Post-LPS CBV Changes

Time-Point After Challenge	Rat No.	CBV area (No. of pixels)		CBV Area (L/R)	CBV Intensity (L/R)
		Injected	Contralateral		
6 hrs	125	450	141	3.191489	3.920101
	126	336	107	3.140187	2.844879
	137	233	173	1.346821	1.703384
	140	374	135	2.77037	3.157003
	142	223	136	1.639706	1.810983
	144	175	112	1.5625	1.141708
	145	299	152	1.967105	1.970399
	146	232	139	1.669065	1.669311
	132	262	99	2.646465	1.247642
	133	350	117	2.991453	3.328474
	134	202	111	1.81982	1.693614
		285.09 ± 84.29 (11)	129.27 ± 22.21 (11)	2.16 ± 0.75 (11)	2.23 ± 0.93 (11)
	138	160	114	1.403509	2.361111
	139	206	95	2.168421	2.302474
	124	218	158	1.379747	1.457036
	131	390	147	2.653061	2.37836
		243.5 ± 100.82 (4)	128.5 ± 29.13 (4)	1.90 ± 0.62 (4)	2.12 ± 0.45 (4)
	141	210	169	1.242604	1.458108
	143	145	106	1.367925	1.367925
	147	478	141	3.390071	2.714747
	135	499	20	24.95	5.297266
	136	259	77	3.363636	1.591233
		318.2 ± 160.81 (5)	102.6 ± 57.83 (5)	2.00 ± 1.21 (5)	2.49 ± 1.66 (5)
24hrs	122	147	105	1.4	1.339825
	125	234	130	1.8	2.088476
	126	152	29	5.241379	2.389444
	137	202	194	1.041237	1.0777
	140	211	105	2.009524	1.948545
	142	180	191	0.942408	1.484427
	144	96	60	1.6	1.236111
	145	367	248	1.479839	2.022137
	146	250	135	1.851852	1.794052
		204.33 ± 77.32 (9)	133 ± 68.95 (9)	1.93 ± 1.29 (9)	1.71 ± 0.44 (9)
	138	335	148	2.263514	2.372891
	139	259	148	1.75	1.663246
	124	244	192	1.270833	1.424155
	131	282	134	2.104478	2.138197
		280 ± 39.86 (4)	155.5 ± 25.21 (4)	1.85 ± 0.44 (4)	1.90 ± 0.43 (4)
	141	186	141	1.319149	1.319149
	143	190	149	1.275168	1.275168
	147	327	181	1.80663	2.061606
		234.33 ± 80.28 (3)	157 ± 21.17 (3)	1.47 ± 0.29 (3)	1.55 ± 0.44 (3)
72hrs	122	129	128	1.007813	1.178988
	126	379	81	4.679012	1.782995
	144	327	181	1.5	1.282119
	145	341	186	1.833333	2.242201
	146	335	193	1.735751	1.982245
		302.2 ± 98.86 (5)	153.8 ± 48.16 (5)	2.15 ± 1.45 (5)	1.69 ± 0.45 (5)
	138	292	124	2.815534	1.981567
	139	287	114	3.757895	2.840606
	124	304	120	2.533333	1.896154
	131	461	149	3.09396	2.48538
		336 ± 83.64 (4)	126.75 ± 15.39 (4)	3.05 ± 0.52 (4)	2.30 ± 0.44 (4)
	141	239	145	1.648276	1.156405
	143	178	119	1.495798	1.720286
	147	438	140	3.128571	2.162775
		285 ± 135.97 (3)	134.67 ± 13.80 (3)	1.57 ± 0.11 (3)	1.68 ± 0.50 (3)

Figure G-3: rCBV values in following LPS, saline (light grey), or no peripheral challenge (dark grey).

G.11 Post-LPS T_1 Relaxation Time

Time-Point After Challenge	Rat No.	Striatum T_1 Relaxation Time (sec)		Cortex T_1 Relaxation Time (sec)	
		Injected	Contralateral	Injected	Contralateral
6hrs	137	1.703	1.747	1.755	1.791
	140	1.696	1.745	1.826	1.844
	142	1.575	1.606	1.754	1.712
	122	1.74	1.719	1.763	1.782
	125	1.649	1.622	1.745	1.723
	126	1.622	1.749	1.723	1.851
	144	1.704	1.76	1.798	1.801
	145	1.72	1.795	1.798	1.849
	146	1.717	1.673	1.841	1.82
		1.68 ± 0.05 (9)	1.71 ± 0.06 (9)	1.77 ± 0.05 (9)	1.79 ± 0.06 (9)
	138	1.536	1.646	1.613	1.769
	139	1.573	1.635	1.698	1.752
	124	1.666	1.707	1.715	1.83
	131	1.623	1.576	1.735	1.66
		1.60 ± 0.07 (4)	1.64 ± 0.05 (4)	1.69 ± 0.05 (4)	1.75 ± 0.07 (4)
	141	1.602	1.64	1.733	1.751
	143	1.601	1.64	1.801	1.753
	147	1.535	1.592	1.705	1.677
		1.58 ± 0.04 (3)	1.62 ± 0.03 (3)	1.75 ± 0.05 (3)	1.73 ± 0.04 (3)
24hrs	137	1.559	1.656	1.662	1.741
	140	1.586	1.608	1.711	1.711
	142	1.593	1.621	1.682	1.758
	122	1.675	1.576	1.739	1.666
	125	1.563	1.693	1.693	1.763
	126	1.624	1.66	1.71	1.737
	144	1.56	1.53	1.721	1.665
	145	1.603	1.628	1.763	1.758
	146	1.562	1.618	1.715	1.645
		1.59 ± 0.04 (9)	1.62 ± 0.05 (9)	1.71 ± 0.03 (9)	1.72 ± 0.05 (9)
	138	1.532	1.62	1.618	1.707
	139	1.639	1.635	1.74	1.7662
	124	1.583	1.649	1.697	1.7778
	131	1.528	1.535	1.641	1.643
		1.57 ± 0.05 (4)	1.61 ± 0.05 (4)	1.68 ± 0.09 (4)	1.74 ± 0.04 (4)
	141	1.609	1.575	1.718	1.744
	143	1.624	1.624	1.788	1.687
	147	1.609	1.624	1.825	1.714
		1.61 ± 0.01 (3)	1.61 ± 0.03 (3)	1.78 ± 0.05 (3)	1.73 ± 0.03 (3)
72 hrs	122	1.691	1.728	1.746	1.835
	125	1.513	1.603	1.685	1.633
	126	1.577	1.711	1.638	1.796
	144	1.545	1.605	1.692	1.703
	145	1.605	1.638	1.713	1.732
	146	1.663	1.531	1.722	1.633
		1.60 ± 0.07 (6)	1.64 ± 0.07 (6)	1.70 ± 0.04 (6)	1.72 ± 0.08 (6)
	138	1.626	1.629	1.802	1.757
	139	1.616	1.676	1.739	1.741
	124	1.587	1.61	1.65	1.679
	131	1.513	1.605	1.578	1.726
		1.59 ± 0.05 (4)	1.63 ± 0.03 (4)	1.69 ± 0.10 (4)	1.73 ± 0.03 (4)
	141	1.604	1.657	1.725	1.784
	143	1.59	1.644	1.773	1.798
	147	1.641	1.645	1.681	1.725
		1.61 ± 0.03 (3)	1.65 ± 0.01 (3)	1.73 ± 0.05 (3)	1.73 ± 0.04 (3)

Table G-9: T_1 relaxation time following LPS, saline (light grey) or no peripheral challenge (dark grey).

G.12 Post-LPS T_2 Relaxation Time

Time-Point After Challenge	Rat No.	Striatum T_2 Relaxation Time (sec)		Cortex T_2 Relaxation Time (sec)	
		Injected	Contralateral	Injected	Contralateral
6hrs	137	0.04388	0.04756	0.04402	0.0472
	140	0.04364	0.04598	0.04552	0.04512
	142	0.04378	0.04683	0.04747	0.04665
	122	0.04312	0.04781	0.04549	0.04751
	125	0.04212	0.04516	0.04515	0.04464
	126	0.04342	0.04723	0.04452	0.04697
	144	0.04331	0.04504	0.04638	0.04521
	145	0.04346	0.04526	0.04543	0.04443
	146	0.04387	0.04439	0.04544	0.04427
		43.4 ± 0.55 (9)	46.14 ± 1.25 (9)	45.49 ± 1.00 (9)	45.78 ± 1.29 (9)
	138	0.04255	0.04556	0.0439	0.04656
	139	0.04687	0.04741	0.04788	0.04716
	124	0.04153	0.04649	0.04256	0.04702
	131	0.04253	0.04675	0.0457	0.04694
		0.043.37± 2.38 (4)	46.55 ± 0.77 (4)	45.01 ± 2.31 (4)	46.92 ± 0.26 (4)
	141	0.04491	0.04571	0.04677	0.04742
	143	0.04399	0.04638	0.04687	0.04618
	147	0.04349	0.04429	0.04626	0.04609
		0.044.13± 0.72 (3)	45.46 ± 1.07 (3)	46.63 ± 0.33 (3)	46.80 ± 0.74 (3)
24hrs	137	0.04115	0.0456	0.0456	0.04619
	140	0.04391	0.046	0.04613	0.04632
	142	0.04381	0.04563	0.04668	0.04606
	122	0.04246	0.04525	0.0461	0.04529
	125	0.04131	0.04271	0.0454	0.04314
	126	0.04276	0.04981	0.04342	0.04898
	144	0.0413	0.04515	0.04489	0.04615
	145	0.04332	0.04583	0.04534	0.04559
	146	0.04295	0.04556	0.04346	0.04569
		42.55 ± 1.08 (9)	45.73± 1.81 (9)	45.22 ± 1.14 (9)	45.93 ± 1.50 (9)
	138	0.04472	0.04565	0.04771	0.04555
	139	0.04259	0.04669	0.04487	0.04752
	124	0.04232	0.04667	0.04346	0.04673
	131	0.04234	0.04569	0.04499	0.04568
		42.99 ± 1.16 (4)	46.18 ± 0.58 (4)	452.58 ± 1.78 (4)	46.37 ± 0.93 (4)
	141	0.04165	0.04408	0.04448	0.04618
	147	0.04348	0.04519	0.0471	0.04521
		42.57 ± 1.29 (2)	44.64 ± 0.78 (2)	45.79 ± 1.85 (2)	45.70 ± 0.69 (2)
72 hrs	122	0.04282	0.04531	0.04694	0.04494
	125	0.04013	0.04207	0.04449	0.04339
	126	0.0427	0.04653	0.0447	0.04547
	144	0.04174	0.04424	0.04512	0.04532
	145	0.04449	0.04628	0.04694	0.046
	146	0.0439	0.04725	0.04523	0.04763
		42.63 ± 1.59 (6)	45.28 ± 1.88 (6)	45.57 ± 1.10 (6)	45.46 ± 1.38 (6)
	138	0.04629	0.04474	0.049	0.0444
	139	0.04529	0.04478	0.04785	0.04514
	124	0.0447	0.0435	0.04588	0.0447
	131	0.04132	0.04666	0.04458	0.04596
		44.40 ± 2.16 (40	44.92 ± 1.30 (4)	46.83 ± 1.98 (4)	45.05 ± 0.68 (4)
	141	0.04281	0.04485	0.04509	0.04607
	143	0.04386	0.04714	0.04485	0.04679
	147	0.04509	0.04699	0.04705	0.04711
		43.92 ± 1.14 (3)	46.33 ± 1.28 (3)	45.66 ± 1.21 (3)	46.43 ± 0.53 (3)

Table G-10: T_2 relaxation time following LPS, saline (light grey), or no peripheral challenge (dark grey).

G.13 Post-LPS T,* Relaxation Time

Time-Point After Challenge	Rat No.	Lesion T_2* Relaxation Time (sec)	Area of Lesion on T_2* maps (No. of Pixels)	Striatum T_2* Relaxation Time (sec)	
				Injected	Contralateral
6 hrs	122	0.01941	136	0.03773	0.04504
	125	0.01696	100	0.03474	0.04663
	126	0.017365	88	0.0392	0.05374
	137	0.0222	63	0.02958	0.04206
	140	0.02292	40	0.02463	0.02783
	142	0.02333	141	0.03172	0.05109
	144	0.0203	122	0.02026	0.01592
	145	0.02715	107	0.0354	0.03299
	146	0.022	87	0.03187	0.03643
		0.021 ± 0.003 (9)	98.22 ± 33.10 (9)	0.032 ± 0.006 (9)	0.039 ± 0.012 (9)
	138	0.01268	72	0.01275	0.0163
	139	0.02841	53	0.03926	0.0375
	124	0.02041	96	0.02948	0.04301
	131	0.01793	183	0.02404	0.03911
		0.020 ± 0.007 (4)	101 ± 57.43 (4)	0.026 ± 0.011 (4)	0.034 ± 0.012 (4)
	141	0.0156	46	0.02568	0.03605
	143	0.02702	26	0.0355	0.04418
	147	0.01408	94	0.02256	0.02392
		0.019 ± 0.007 (3)	55.33 ± 34.95 (3)	0.028 ± 0.007 (3)	0.035 ± 0.010 (3)
24 hrs	122	0.02247	117	0.04156	0.04408
	125	0.0148	80	0.02687	0.03229
	126	0.01893	127	0.02438	0.03501
	137	0.01438	56	0.02175	0.03843
	140	0.021535	63	0.02732	0.03764
	142	0.02249	115	0.03628	0.04039
	144	0.01725	123	0.01752	0.022593
	145	0.02259	133	0.03295	0.03658
	146	0.01783	94	0.02246	0.04454
		0.019 ± 0.003 (9)	100.89 ± 28.71 (9)	0.028 ± 0.008 (9)	0.037 ± 0.007 (9)
	138	0.024	60	0.03837	0.04475
	139	0.02795	30	0.04041	0.04282
	124	0.01982	85	0.03374	0.04756
	131	0.01876	142	0.02796	0.04331
		0.023 ± 0.004 (4)	79.25 ± 47.49 (4)	0.035 ± 0.006 (4)	0.0446 ± 0.002 (4)
	141	0.0215	78	0.03068	0.04657
	143	0.03304	50	0.04361	0.04467
	147	0.01463	43	0.0261	0.03447
		0.023 ± 0.009 (3)	57 ± 18.52 (3)	0.033 ± 0.009 (3)	0.042 ± 0.007 (3)
72 hrs	122	0.01831	179	0.03288	0.04864
	126	0.01662	102	0.03309	0.04902
	144	0.01554	100	0.02111	0.01903
	145	0.02499	104	0.0382	0.03859
	146	0.01763	77	0.02455	0.02607
		0.019 ± 0.004 (5)	112.4 ± 38.80 (5)	0.030 ± 0.007 (5)	0.036 ± 0.013 (5)
	138	0.01922	54	0.03271	0.03342
	139	0.02103	65	0.02663	0.03683
	124	0.019465	141	0.02227	0.02425
	131	0.01806	176	0.02335	0.03603
		0.019 ± 0.001 (4)	109 ± 59.09 (4)	0.026 ± 0.005 (4)	0.033 ± 0.006 (4)
	141	0.01937	31	0.02791	0.03284
	143	0.01975	33	0.02299	0.02976
	147	0.02361	98	0.03684	0.0373
		0.021 ± 0.002 (3)	54. 0 ± 38.11 (3)	0.029 ± 0.007 (3)	0.033 ± 0.004 (3)

Table G-11: T_2* relaxation time following LPS, saline (light grey), or no peripheral challenge (dark grey).

G.14 Post-LPS MTR

Time-Point After Challenge	Rat No.	Lesion MTR	
		Injected	Contralateral
6hrs	122	13.63	18.35
	125	11.00	18.54
	126	11.89	18.03
	137	16.95	16.70
	140	17.21	16.85
	142	14.48	16.91
	144	14.87	18.41
	145	18.56	19.45
	146	16.7	19.36
		15.03 ± 2.55 (9)	18.07 ± 1.04 (9)
	138	15.6	17.82
	139	15.48	14.59
	124	14.02	18.02
	131	13	17.35
		14.53 ± 1.24 (4)	16.95 ± 1.59 (4)
	141	15.14	16.2
	143	15.92	15.82
	147	10.74	11.14
		13.93 ± 2.79 (3)	14.39 ± 2.82 (3)
24 hrs	122	11.68	17.88
	125	9.83	18.44
	126	15.03	17.21
	137	17.66	18.83
	140	21.66	22.85
	142	19.81	21.79
	144	19.34	20.56
	145	15.5	16.09
	146	14.58	17.35
		16.12 ± 3.88 (9)	19 ± 2.26 (9)
	124	16.67	16.99
	131	12.08	17.16
	138	18.39	22.85
	139	14.14	17.16
		15.32 ± 2.78 (4)	18.54 ± 2.87 (4)
	141	16.45	18.34
	143	19.83	19.31
	147	16.15	17.66
		14.48 ± 2.04 (3)	18.44 ± 0.83 (3)
72 hrs	122	11.78	14.96
	125	9.012	18.76
	126	12.19	16.69
	144	15.09	17.52
	145	16.14	16.23
	146	14.94	17.97
		13.19 ± 2.68 (6)	17.02 ± 1.35 (6)
	124	13.13	16.9
	131	13.02	16.25
	138	19.74	21.56
	139	19.38	21.57
		16.32 ± 3.75 (4)	19.07 ± 2.89 (4)
	141	19.24	23.35
	143	18.89	21.13
		19.07 ± 0.25 (2)	22.24 ± 1.57 (2)

Table G-12: MTR values in the lesion following LPS, saline (light grey) or no peripheral challenge (dark grey).

G.15 Post-LPS Diffusion Anisotropy

Time-Point After Challenge	Rat No.	Diffusion Anisotropy		
		Injected	Contralateral	L/R
6 hrs	122	0.1448	0.1458	0.993141
	125	0.1076	0.1032	1.042636
	126	0.08851	0.109	0.812018
	137	0.09682	0.1284	0.75405
	140	0.1039	0.1187	0.875316
	142	0.1058	0.1009	1.048563
	144	0.09644	0.09882	0.975916
	145	0.07133	0.1006	0.709046
	146	0.1031	0.09687	1.064313
		0.102 ± 0.020 (9)	0.111 ± 0.023 (9)	0.919 ± 0.125 (9)
	124	0.1057	0.09959	1.061352
	131	0.1007	0.1048	0.960878
	139	0.1073	0.1134	0.946208
		0.105 ± 0.003 (3)	0.106 ± 0.007 (3)	0.989 ± 0.063 (3)
	141	0.112	0.1002	1.117764
	143	0.1008	0.1058	0.952741
	147	0.09934	0.1118	0.888551
		0.104 ± 0.008 (3)	0.106 ± 0.004 (3)	0.986 ± 0.117 (3)
24 hrs	122	0.09961	0.1146	0.869197
	125	0.096	0.1039	0.923965
	126	0.09536	0.1087	0.877277
	137	0.1001	0.1106	0.905063
	140	0.09294	0.128	0.726094
	142	0.1042	0.1175	0.886809
	144	0.1149	0.1152	0.997396
	145	0.09426	0.1026	0.918713
	146	0.1123	0.1295	0.867181
		0.101 ± 0.002 (9)	0.115 ± 0.005 (9)	0.886 ± 0.071 (9)
	124	0.1081	0.1059	1.020774
	131	0.1034	0.1087	0.951242
	138	0.09916	0.09817	1.010085
	139	0.1045	0.1044	1.000958
		0.104 ± 0.004 (4)	0.104 ± 0.004 (4)	0.996 ± 0.031 (4)
	141	0.1043	0.1028	1.014591
	143	0.09899	0.1064	0.930357
	147	0.1066	0.09737	1.094793
		0.103 ± 0.004 (3)	0.102 ± 0.003 (3)	1.013 ± 0.060 (3)
72 hrs	122	0.1092	0.1047	1.04298
	126	0.09617	0.1102	0.872686
	144	0.09742	0.09776	0.996522
	145	0.1129	0.1107	1.019874
	146	0.09363	0.09995	0.936768
		0.102 ± 0.009 (5)	0.105 ± 0.004 (5)	0.974 ± 0.120 (5)
	124	0.1008	0.115	0.876522
	131	0.0994	0.1176	0.845238
	138	0.1101	0.1047	1.051576
	139	0.1084	0.1068	1.014981
		0.105 ± 0.005 (4)	0.111 ± 0.006 (4)	0.947 ± 0.101 (4)
	141	0.09348	0.1108	0.843682
	143	0.1048	0.1094	0.957952
	147	0.1137	0.1004	1.13247
		0.104 ± 0.008 (3)	0.109 ± 0.001 (3)	0.978 ± 0.081 (3)

Table G-13: Anisotropy values following LPS, saline (light grey) or no peripheral challenge (dark grey).

G.16 Naïve T_1 and T_2 Relaxation Times

G.16.1 T_1 Relaxation Time

Time-Point (Day)	Rat No.	Cortex T_1 Relaxation Time (sec)		Striatum T_1 Relaxation Time (sec)	
		Injected	Contralateral	Injected	Contralateral
1	127	1.767	1.7210	1.704	1.6430
	128	1.748	1.7500	1.645	1.7000
	129	1.74	1.7820	1.699	1.7180
	70	1.755	1.7230	1.682	1.6370
		1.75 ± 0.01 (3)	1.74 ± 0.03 (3)	1.68 ± 0.03 (3)	1.67 ± 0.04 (3)
5	127	1.855	1.8460	1.726	1.7640
	128	1.788	1.7860	1.659	1.6650
	129	1.781	1.7750	1.727	1.7520
	70	1.601	1.668	1.563	1.6040
		1.76 ± 0.11 (3)	1.77 ± 0.07 (3)	1.67 ± 0.08 (3)	1.70 ± 0.08 (3)
8	70	1.657	1.7790	1.61	1.7120
12	127	1.675	1.606	1.657	1.658
	128	1.762	1.762	1.655	1.681
	129	1.753	1.763	1.677	1.679
		1.73 ± 0.05 (3)	1.71 ± 0.09 (3)	1.66 ± 0.01 (3)	1.67 ± 0.01 (3)
19	127	1.518	1.612	1.507	1.572
	128	1.766	1.823	1.704	1.788
	129	1.712	1.65	1.692	1.61
	70	1.703	1.662	1.664	1.571
		1.73 ± 0.03 (3)	1.72 ± 0.10 (3)	1.69 ± 0.02 (3)	1.66 ± 0.12 (3)
31	70	1.632	1.679	1.601	1.593

Table G-14: T_1 relaxation times in naïve animals.

G.16.2 T_2 Relaxation Time

Time-Point (Day)	Rat No.	Cortex T_2 Relaxation Time (sec)		Striatum T_2 Relaxation Time (sec)	
		Injected	Contralateral	Injected	Contralateral
1	127	0.04879	0.0469	0.04863	0.0486
	128	0.04842	0.0499	0.04964	0.0497
	129	0.04887	0.0485	0.04857	0.0486
		49 ± 0.2 (3)	48 ± 0.2 (3)	49 ± 0.6 (3)	49 ± 0.7 (3)
5	127	0.04866	0.0474	0.04983	0.0478
	128	0.04815	0.0467	0.04762	0.0475
	129	0.0476	0.0474	0.04794	0.0473
		48 ± 0.5 (3)	47 ± 0.4 (3)	48 ± 1 (3)	48 ± 0.3 (3)
12	127	0.04618	0.04692	0.04721	0.07834
	128	0.04842	0.04555	0.04932	0.04668
	129	0.04655	0.04464	0.04682	0.04684
		47.05 ± 1.20 (3)	45.70 ± 1.1 (3)	47.78 ± 1.3 (3)	57 ± 1.8 (3)
19	127	0.03835	0.03897	0.03988	0.04011
	128	0.04786	0.0476	0.04823	0.04732
	129	0.04769	0.04683	0.04624	0.04857
		48 ± 0.1 (3)	47 ± 0.5 (3)	47 ± 1 (3)	48 ± 0.9 (3)

Table G-15: T_2 relaxation times in naïve animals.

References

Aboitiz, F. M., J. (2003). "One hundred million years of interhemispheric communication: the history of the corpus callosum." Braz J Med Biol Res **36**: 409-20.

Barbier, E. Lamalle, L. Decorps, M. (2001). "Methodology of brain perfusion imaging." J Magn Reson Imaging **13**: 496-520.

Bakshi, R. B., RH. Bermel, RA. Caruthers, SD. Puli, SR. Tjoa, CW. Fabiano, AJ. Jacobs, L. (2002). "T2 hypointensity in the deep gray matter of patients with multiple sclerosis: a quantitative magnetic resonance imaging study." Arch Neurol **59**: 62-8.

Bakshi, R. D., J. Shaikh, ZA. Jacobs, L. (2001). "Gray matter T2 hypointensity is related to plaques and atrophy in the brains of multiple sclerosis patients." J Neurol Sci **185**: 19-26.

Barkhof, F. van Walderveen, M. (1999). "Characterization of tissue damage in multiple sclerosis by nuclear magnetic resonance." Philos Trans R Soc Lond B Biol Sci **354**: 1675-1686.

Barnes, D. Munro, PM. Youl, BD. Prineas, JW. McDonald, WI. (1991). "The longstanding MS lesion. A quantitative MRI and electron microscopic study." Brain **114**: 1271-80.

Barnes, D. McDonald, WI. Johnson, G. Tofts, PS. Landon, DN. (1987). "Quantitative nuclear magnetic resonance imaging: characterisation of experimental cerebral oedema." J Neurol Neurosurg Psychiatry **50**: 125-33.

Basser, P. Mattiello, J. LeBihan, D. (1994). "MR diffusion tensor spectroscopy and imaging." Biophys J **66**: 259-67.

Blamire, A. Anthony, DC. Rajagopalan, B. Sibson, NR. Perry, VH. Styles, P. (2000). "Interleukin-1beta - induced changes in blood-brain barrier permeability, apparent diffusion coefficient, and cerebral blood volume in the rat brain: A magnetic resonance study." J Neurosci **20**: 8153-9.

Birnbaum, G. Kotilinek, L. (1997). "Heat shock or stress proteins and their role as autoantigens in multiple sclerosis." Ann N Y Acad Sci **835**: 157-67.

Birnbaum, G. Kotilinek, L. Miller, SD. Raine, CS. Gao, YL. Lehmann, PV. Gupta, RS. (1998). "Heat shock proteins and experimental autoimmune encephalomyelitis. II: environmental infection and extra-neuraxial inflammation alter the course of chronic relapsing encephalomyelitis." J Neuroimmunol **90**: 149-61.

Bitsch, A. Kuhlmann, T. Stadelmann, C. Lassmann, H. Lucchinetti, C. Bruck, W. (2001). "A longitudinal MRI study of histopathologically defined hypointense multiple sclerosis lesions." Ann Neurol **49**(Jun;(6)): 793-6.

Blinkenberg, M. J., CV. Holm, S. Paulson, OB. Sorensen, PS. (1999). "A longitudinal study of cerebral glucose metabolism, MRI, and disability in patients with MS." Neurology **53**: 149-53.

Blond, D. Campbell, SJ. Butchart, AG. Perry, VH. Anthony, DC. (2002). "Differential induction of interleukin-1beta and tumour necrosis factor-alpha may account for specific patterns of leukocyte recruitment in the brain." Brain Res **958**: 89-99.

Brahic, M. (2002). "Theiler's virus infection of the mouse, or: of the importance of studying animal models." Virology **301**: 1-5.

Brochet, B. Douset, V. (1999). "Pathological correlates of magnetization transfer imaging abnormalities in animal models and humans with multiple sclerosis." Neurology **53**: S12-7.

Brocke, S. Gaur, A. Piercy, C. Gautam, A. Gijbels, K. Fathman, CG. Steinman, L. (1993). "Induction of relapsing paralysis in experimental autoimmune encephalomyelitis by bacterial superantigen." Nature **365**: 642-4.

Brosnan, C. Raine, CS. (1996). "Mechanisms of immune injury in multiple sclerosis." Brain Pathol **6**: 243-57.

Bruck, W. Bitsch, A. Kolenda, H. Bruck, Y. Stiefel, M. Lassmann, H. (1997). "Inflammatory central nervous system demyelination: correlation of magnetic resonance imaging findings with lesion pathology." Ann Neurol **42**: 783-93.

Bubis, J. Luse, SA. (1964). "An Electron microscopic study of experimental allergic encephalomyelitis in the rat,." Am J Path **44**: 299-317.

Buljevac, D. Flach, HZ. Hop, WC. Hijdra, D. Laman, JD. Savelkoul, HF. van Der Meche, FG. van Doorn, PA. Hintzen, RQ. (2002). "Prospective study on the relationship between infections and multiple sclerosis exacerbations." Brain **125**: 952-60.

Campi, A. Filippi, M. Comi, G. Scotti, G. Gerevini, S. Dousset, V. (1996). "Magnetisation transfer ratios of contrast-enhancing and nonenhancing lesions in multiple sclerosis." Neuroradiology **38**: 115-9.

Caramia, F. Pantano, P. Di Legge, S. Piattella, M. Lenzi, D. Paolillo, A. Nucciarelli, W. Lenzi, G. Bozzao, L. Pozzilli, C. (2002). "A longitudinal study of MR diffusion changes in normal appearing white matter of patients with early multiple sclerosis." Magn Reson Imaging **20**: 383-388.

Cercignani, M. Iannucci, G. Rocca, MA. Comi, G. Horsfield, MA. Filippi, M. (2000). "Pathologic damage in MS assessed by diffusion-weighted and magnetization transfer MRI." Neurology **54**: 1139-44.

Christiansen, P. Gideon, P. Thomsen, C. Stubgaard, M. Henriksen, O. Larsson, HB. (1993). "Increased water self-diffusion in chronic plaques and in apparently normal white matter in patients with multiple sclerosis." Acta Neurol Scand **87**: 195-9.

Combrinck, M. Perry, VH. Cunningham, C. (2002). "Peripheral infection evokes exaggerated sickness behaviour in pre-clinical murine prion disease." Neuroscience **112**: 7-11.

Cuzner, M. Hayes, GM. Newcombe, J. Woodroofe, MN. (1988). "The nature of inflammatory components during demyelination in multiple sclerosis." J Neuroimmunol **20**: 203-9.

Dantzer, R. (2001). "Cytokine-induced sickness behavior: mechanisms and implications." Ann N Y Acad Sci. **933**: 222-34.

Degaonkar, M. Jayasundar, R. Jagannathan, NR. (2002). "Sequential diffusion-weighted magnetic resonance imaging study of lysophosphatidyl choline-induced experimental demyelinating lesion: an animal model of multiple sclerosis." J Magn Reson Imaging **16**: 153-9.

Dijkstra, C. Dopp, EA. Joling, P. Kraal, G. (1985). "The heterogeneity of mononuclear phagocytes in lymphoid organs: distinct macrophage subpopulations in the rat recognized by monoclonal antibodies ED1, ED2 and ED3." Immunology **54**: 589-99.

Dousset, V. Grossman, RI. Ramer, KN. Schnall, MD. Young, LH. Gonzalez-Scarano, F. Lavi, E. Cohen, JA. (1992). "Experimental allergic encephalomyelitis and multiple sclerosis: lesion characterization with magnetization transfer imaging." Radiology **182**: 483-91.

Dousset, V. Ballarino, L. Delalande, C. Coussemacq, M. Canioni, P. Petry, KG. Caille, JM. (1999). "Comparison of ultrasmall particles of iron oxide (USPIO)-enhanced T_2-weighted, conventional T_2-weighted, and gadolinium-enhanced T_1-weighted MR images in rats with experimental autoimmune encephalomyelitis." AJNR Am J Neuroradiol **20**: 223-7.

Dousset, V. Delalande, C. Ballarino, L. Quesson, B. Seilhan, D. Coussemacq, M. Thiaudiere, E. Brochet, B. Canioni, P. Caille, JM. (1999). "In vivo macrophage activity imaging in the central nervous system detected by magnetic resonance." Magn Reson Med **41**: 329-33.

Dousset, V. Gomez, C. Petry, KG. Delalande, C. Caille, JM. (1999). "Dose and scanning delay using USPIO for central nervous system macrophage imaging." MAGMA **8**: 185-189.

Droogan, A. Clark, CA. Werring, DJ. Barker, GJ. McDonald, WI. Miller, DH. (1999). "Comparison of multiple sclerosis clinical subgroups using navigated spin echo diffusion-weighted imaging." Magn Reson Imaging **17**: 653-61.

Du, C. Yao, SY. Ljunggren-Rose, A. Sriram, S. (2002). "Chlamydia pneumoniae Infection of the Central Nervous System Worsens Experimental Allergic Encephalitis." J Exp Med **196**: 1639-44.

Duckers, H. Muller, HJ. Verhaagen, J. Nicolay, K. Gispen, WH. (1997). "Longitudinal in vivo magnetic resonance imaging studies in experimental allergic encephalomyelitis: effect of a neurotrophic treatment on cortical lesion development." Neuroscience **77**: 1163-73.

Edwards, S. Zvartau, M. Clarke, H. Irving, W. Blumhardt, LD. (1998). "Clinical relapses and disease activity on magnetic resonance imaging associated with viral upper respiratory tract infections in multiple sclerosis." J Neurol Neurosurg Psychiatry **64**: 736-41.

Elian, M. Dean, G. (1993). "Motor neuron disease and multiple sclerosis among immigrants to England from the Indian subcontinent, the Caribbean, and east and west Africa." J Neurol Neurosurg Psychiatry **56**: 454-7.

Elian, M. Nightingale, S. Dean, G. (1990). "Multiple sclerosis among United Kingdom-born children of immigrants from the Indian subcontinent, Africa and the West Indies." J Neurol Neurosurg Psychiatry **53**: 906-11.

Fazekas, F. Barkhof, F. Filippi, M. Grossman, RI. Li, DK. McDonald, WI. McFarland, HF. Paty, DW. Simon, JH. Wolinsky, JS. Miller, DH. (1999). "The contribution of magnetic resonance imaging to the diagnosis of multiple sclerosis." Neurology **53**: 448-56.

Frahm, J. Haase, A. Matthaei, D. (1986). "Rapid NMR imaging of dynamic processes using the FLASH technique." Magn Reson Med **3**: 321-7.

Filippi, M. (1999). "Magnetisation transfer imaging to monitor the evolution of individual multiple sclerois lesions." Neurology **53**: S18-S22.

Filippi, M. Rovaris, M. (2000). "Magnetisation transfer imaging in multiple sclerosis." J Neurovirol **6**: S115-20.

Filippi, M. Rocca, MA. Martino, G. Horsfield, MA. Comi, G. (1998). "Magnetization transfer changes in the normal appearing white matter precede the appearance of enhancing lesions in patients with multiple sclerosis." Ann Neurol **43**: 809-14.

Filippi, M. Dousset, V. McFarland, HF. Miller, DH. Grossman, RI. (2002). "Role of magnetic resonance imaging in the diagnosis and monitoring of multiple sclerosis: Consensus report of the White Matter Study Group." J Magn Reson Imaging **15**: 499-504.

Forge, J. Pedchenko, TV. LeVine, SM. (1998). "Iron deposits in the central nervous system of SJL mice with experimental allergic encephalomyelitis." Life Sci **63**: 2271-84.

Gareau, P. Rutt, BK. Karlik, SJ. Mitchell, R. (2000). "Magnetization transfer and multicomponent T_2 relaxation measurements with histopathologic correlation in an experimental model of MS." J Magn Reson Imaging **11**(6): 586-595.

Gass, A. Barker, GJ. Kidd, D. Thorpe, JW. MacManus, D. Brennan, A. Tofts, PS. Thompson, AJ. McDonald, WI. Miller DH. (1994). "Correlation of magnetization transfer ratio with clinical disability in multiple sclerosis." Ann Neurol **36**: 62-7.

Gehrmann, J. Banati, RB (1995). "The role of glial cells in immune responses in the brain." Molecular and Cellular Neurobiology(Immune Responses in the nervous system): 61-76.

Genain, C. Roberts, T. Davis, RL. Nguyen, MH. Uccelli, A. Faulds, D. Li, Y. Hedgpeth, J. Hauser, SL. (1995). "Prevention of autoimmune demyelination in non-human primates by a cAMP-specific phosphodiesterase inhibitor." Proc Natl Acad Sci U S A **92**: 3601-5.

Gijbels, K. Engelborghs, S. De Deyn, PP. (2000). "Experimental autoimmune encephalomyelitis: An animal model for multiple sclerosis." Neuroscience Research Communications **26**: 193-206.

Gilden, D. (1999). "Chlamydia: a role for multiple sclerosis or more confusion?" Ann Neurol **46**: 4-5.

Gold, R. Hartung, HP, Toyka, KV. (2000). "Animal models for autoimmune demyelinating disorders of the nervous system." Molecular Medicine Today **6**: 88-91.

Gonzalez-Scorano, F. Rima, B. (1999). "Infectious etiology in multiple sclerosis: the debate continues." Trends Microbiol **7**: 475-7.

Grossman, R. Lisak, RP. Macchi, PJ. Joseph, PM. (1987). "MR of acute experimental allergic encephalomyelitis." AJNR Am J Neuroradiol **8**: 1045-8.

Haring, J. Pewe, LL. Perlman, S. (2002). "Bystander CD8 T cell-mediated demyelination after viral infection of the central nervous system." J Immunol **169**: 1550-5.

Hart, B. Bauer, J. Muller, HJ. Melchers, B. Nicolay, K. Brok, H. Bontrop, RE. Lassmann, H. Massacesi, L. (1998). "Histopathological characterization of magnetic resonance imaging-detectable brain white matter lesions in a primate model of multiple sclerosis: a correlative study in the experimental autoimmune encephalomyelitis model in common marmosets (Callithrix jacchus)." Am J Pathol **153**: 649-63.

Haselhorst, R. Kappos, L. Bilecen, D. Scheffler, K. Mori, D. Radu, EW. Seelig, J. (2000). "Dynamic susceptibility contrast MR imaging of plaque development in multiple sclerosis: application of an extended blood-brain barrier leakage correction." J Magn Reson Imaging **11**: 495-505.

Hawkes, C. (2002). "Is multiple sclerosis a sexually transmitted infection?" J Neurol Neurosurg Psychiatry **73**: 439-43.

Hawkins, C. Mackenzie, F. Tofts, P. du Boulay, EP. McDonald, WI. (1991). "Patterns of blood-brain barrier breakdown in inflammatory demyelination." Brain **114**: 801-10.

Hawkins, C. Munro, PM. MacKenzie, F. Kesselring, J. Tofts, PS. du Boulay, EP. Landon, DN. McDonald, WI. (1990). "Duration and selectivity of blood-brain barrier breakdown in chronic relapsing experimental allergic encephalomyelitis studied by gadolinium-DTPA and protein markers." Brain **113**: 365-78.

Heide, A. Richards, TL. Alvord, EC Jr. Peterson, J. Rose, LM. (1993). "Diffusion imaging of experimental allergic encephalomyelitis." Magn Reson Med **29**: 478-84.

Hendrickse, J. Bisschops, RHC. van Osch, MJP. Bakker CJG. van der Grond, J. (2002). "Association Between Absolute T_2 Measurements Of Normal Appearing White Matter and Quantitive Cerebral Blood Flow." Proc ISMRM **10**.

Hickey, W. Kimura, H. (1988). "Perivascular microglial cells of the CNS are bone marrow-derived and present antigen in vivo." Science **239**: 290-2.

Hiehle, J. Jr. Grossman, RI. Ramer, KN. Gonzalez-Scarano, F. Cohen, JA. (1995). "Magnetization transfer effects in MR-detected multiple sclerosis lesions: comparison with gadolinium-enhanced spin-echo images and nonenhanced T_1-weighted images." AJNR Am J Neuroradiol **16**: 69-77.

Horsfield, M. Lai, M. Webb, SL. Barker, GJ. Tofts, PS. Turner, R. Rudge, P. Miller, DH. (1996). "Apparent diffusion coefficients in benign and secondary progressive multiple sclerosis by nuclear magnetic resonance." Magn Reson Med **36**: 393-400.

Iwasawa, T. Matoba, H. Ogi, A. Kurihara, H. Saito, K. Yoshida, T. Matsubara, S. Nozaki, A. (1997). "Diffusion-weighted imaging of the human optic nerve: a new approach to evaluate optic neuritis in multiple sclerosis." Magn Reson Med **38**: 484-91.

Jensen, C. Rostrup, E. Blinkenberg, M. Larsson, HBW. Henriksen O. (1995). "Relative Regional Cerebral Blood Volume in Multiple Sclerosis." Proc ISMRM: 1297.

Jordan, E. McFarland, HI. Lewis, BK. Tresser, N. Gates, MA. Johnson, M. Lenardo, M. Matis, LA. McFarland, HF. Frank, JA. (1999). "Serial MR imaging of experimental autoimmune encephalomyelitis induced by human white matter or by chimeric myelin-basic and proteolipid protein in the common marmoset." AJNR Am J Neuroradiol **20**: 965-76.

Juhler, M. (1987). "Simultaneous determination of regional cerebral blood flow, glucose metabolism, and pH in acute experimental allergic encephalomyelitis." J Cereb Blood Flow Metab **7**: 578-84.

Juhler, M. Paulson, OB. (1986). "Regional cerebral blood flow in acute experimental allergic encephalomyelitis." Brain Res **363**: 272-8.

Juurlink, B. (1998). "The multiple sclerosis lesion: initiated by a localized hypoperfusion in a central nervous system where mechanisms allowing leukocyte infiltration are readily upregulated?" Med Hypotheses **51**: 299-303.

Karlik, S. Strejan, G. Gilbert, JJ. Noseworthy, JH. (1986). "NMR studies in experimental allergic encephalomyelitis (EAE): normalization of T_1 and T_2 with parenchymal cellular infiltration." Neurology **36**: 1112-4.

Karlik, S. Gilbert, JJ. Wong, C. Vandervoort, MK. Noseworthy, JH. (1990). "NMR studies in experimental allergic encephalomyelitis: factors which contribute to T_1 and T_2 values." Magn Reson Med **14**: 1-11.

Karlik, S. Munoz, D. St Louis, J. Strejan, G. (1999). "Correlation between MRI and clinico-pathological manifestations in Lewis rats protected from experimental allergic encephalomyelitis by acylated synthetic peptide of myelin basic protein." Magn Reson Imaging **17**: 731-7.

Karlik, S. Wong, C. Gilbert, JJ. Noseworthy, JH. (1989). "NMR studies in the relapsing experimental allergic encephalomyelitis (EAE) model of multiple sclerosis in the strain 13 guinea pig." Magn Reson Imaging **7**: 463-73.

Katz, D. Taubenburger, JK. Cannella, B. McFarlin, DE. Raine, CS. McFarland, HF. (1993). "Correlation between magnetic resonance imaging findings and lesion development in chronic, active multiple sclerosis." Ann Neurol **34**: 661-9.

Keegan, B. Noseworthy, JH. (2002). "Multiple sclerosis." Annu Rev Med **53**: 285-302.

Kent, S. Karlik, SJ. Rice, GP. Horner, HC. (1995). "A monoclonal antibody to alpha 4-integrin reverses the MR-detectable signs of experimental allergic encephalomyelitis in the guinea pig." J Magn Reson Imaging **5**: 535-40.

Kermode, A. Thompson, AJ. Tofts, P. MacManus, DG. Kendall, BE. Kingsley, DP. Moseley, IF. Rudge, P. McDonald, WI. (1990). "Breakdown of the blood-brain barrier precedes symptoms and other MRI signs of new lesions in multiple sclerosis. Pathogenetic and clinical implications." Brain **113**: 1477-89.

Kornek, B. Storch, MK. Weissert, R. Wallstroem, E. Stefferl, A. Olsson, T. Linington, C. Schmidbauer, M. Lassmann, H. (2000). "Multiple sclerosis and chronic autoimmune encephalomyelitis: a comparative quantitative study of axonal injury in active, inactive, and remyelinated lesions." Am J Pathol **157**: 267-76.

Kuhlmann, T. Lingfeld, G. Bitsch, A. Schuchardt, J. Bruck, W. (2002). "Acute axonal damage in multiple sclerosis is most extensive in early disease stages and decreases over time." Brain **125**: 2202-12.

Kurtzke, J. Heltberg, A. (2001). "Multiple sclerosis in the Faroe Islands: an epitome." J Clin Epidemiol **54**: 1-22.

Lacroix, S. Feinstein, D. Rivest, S. (1998). "The bacterial endotoxin lipopolysaccharide has the ability to target the brain in upregulating its membrane CD14 receptor within specific cellular populations." Brain Pathol **8**: 625-40.

Larsson, H. Thomsen, C. Frederiksen, J. Stubgaard, M. Henriksen, O. (1992). "In vivo magnetic resonance diffusion measurement in the brain of patients with multiple sclerosis." Magn Reson Imaging(10(1)): 7-12.

Lassman, H. (1983). "Comparitive Neuropathology of Chroninc EAE and MS lesions."

Lenz, D. Lu, L. Conant, SB. Wolf, NA. Gerard, HC. Whittum-Hudson, JA. Hudson, AP. Swanborg, RH. (2001). "A Chlamydia pneumoniae-specific peptide induces experimental autoimmune encephalomyelitis in rats." J Immunol **167**: 1803-8.

LeVine, S. (1997). "Iron deposits in multiple sclerosis and Alzheimer's disease brains." Brain Res **760**: 298-303.

Loevner, L. Grossman, R., McGowan, JC. Ramer, KN. Cohen, JA. (1995). "Characterization of multiple sclerosis plaques with T_1-weighted MR and quantitative magnetization transfer." AJNR Am J Neuroradiol **16**: 1473-9.

Luheshi, G. (1998). "Cytokines and fever. Mechanisms and sites of action." Ann N Y Acad Sci **856**: 83-9.

Luypaert, R. Boujraf, S. Sourbron, S. Osteaux, M. (2001). "Diffusion and perfusion MRI: basic physics." Eur J Radiol **38**: 19-27.

Lycke, J. Wikkelso, C. Bergh, AC. Jacobsson, L. Andersen, O. (1993). "Regional cerebral blood flow in multiple sclerosis measured by single photon emission tomography with technetium-99m hexamethylpropyleneamine oxime." Eur Neurol **33**: 163-7.

Maier, S. (2003). "Bi-directional immune-brain communication: Implications for understanding stress, pain, and cognition." Brain Behav Immun. **17**: 69-85.

Mammi, S. Filippi, M. Martinelli, V. Campi, A. Colombo, B. Scotti, G. Canal, N. Comi, G. (1996). "Correlation between brain MRI lesion volume and disability in patients with multiple sclerosis." Acta Neurol Scand **94**: 93-6.

Mancardi, G. Hart, B. Roccatagliata, L. Brok, H. Giunti, D. Bontrop, R. Massacesi, L. Capello, E. Uccelli, A. (2001). "Demyelination and axonal damage in a non-human primate model of multiple sclerosis." J Neurol Sci **184**: 41-9.

Matyszak, M. Perry, VH. (1995). "Demyelination in the central nervous system following a delayed-type hypersensitivity response to bacillus Calmette-Guerin." Neuroscience **64**: 967-77.

Matyszak, M. Perry, VH. (1996). "A comparison of leucocyte responses to heat-killed bacillus Calmette-Guerin in different CNS compartments." Neuropathol Appl Neurobiol. **22**: 44-53.

Matyszak, M. Perry, VH. (1996). "Delayed-type hypersensitivity lesions in the central nervous system are prevented by inhibitors of matrix metalloproteinases." J-Neuroimmunol. **69**: 141-9.

Matyszak, M. Perry, VH. (1996). "The potential role of dendritic cells in immune-mediated inflammatory diseases in the central nervous system." Neuroscience **74**: 599-608.

Matyszak, M. Perry, VH. (1998). "Bacillus Calmette-Guerin sequestered in the brain parenchyma escapes immune recognition." J-Neuroimmunol. **82**: 73-80.

Matyszak, M. Townsend, MJ. Perry, VH. (1997). "Ultrastructural studies of an immune-mediated inflammatory response in the CNS parenchyma directed against a non-CNS antigen." Neuroscience **78**: 549-60.

McDonald, W. Ron, MA. (1999). "Multiple sclerosis: the disease and its manifestations." Philos Trans R Soc Lond B Biol Sci **354**: 1615-1622.

McLean, I. Nakane, PK. (1974). "Periodate-lysine-paraformaldehyde fixative. A new fixation for immunoelectron microscopy." J Histochem Cytochem **22**: 1077-83.

Miki, Y. Grossman, RI. Udupa, JK. van Buchem, MA. Wei, L. Phillips, MD. Patel, U. McGowan, JC. Kolson, DL. (1999). "Differences between relapsing-remitting and chronic progressive multiple sclerosis as determined with quantitative MR imaging." Radiology **210**: 769-74.

Miki, Y. Grossman, RI. Udupa, JK. Wei, L. Polansky, M. Mannon, LJ. Kolson, DL. (1999). "Relapsing-remitting multiple sclerosis: longitudinal analysis of MR images-lack of correlation between changes in T_2 lesion volume and clinical findings." Radiology **213**: 395-9.

Miller, D. Barkhof, F. Nauta, JJ. (1993). "Gadolinium enhancement increases the sensitivity of MRI in detecting disease activity in multiple sclerosis." Brain **116**: 1077-94.

Miller, D. (1994). "Magnetic resonance in monitoring the treatment of multiple sclerosis." Ann Neurol **36**: :S91-4.

Miller, D. Thompson, AJ. (1999). "Nuclear magnetic resonance monitoring of treatment and prediction of outcome in multiple sclerosis." Philos Trans R Soc Lond B Biol Sci **354**: 1687-1695.

Miller, S. Vanderlugt, CL. Begolka, WS. Pao, W. Yauch, RL. Neville, KL. Katz-Levy, Y. Carrizosa, A. Kim, BS. (1997). "Persistent infection with Theiler's virus leads to CNS autoimmunity via epitope spreading." Nat Med **3**: 1133-6.

Minagar, A. Shapshak, P. Fujimura, R. Ownby, R. Heyes, M. Eisdorfer, C. (2002). "The role of macrophage/microglia and astrocytes in the pathogenesis of three neurologic disorders: HIV-associated dementia, Alzheimer disease, and multiple sclerosis." J Neurol Sci **202**: 13-23.

Mitchell, JR. Jones, C. Karlik, SJ. Kennedy, K. Lee, DH. Rutt, B. Fenster, A. (1997). "MR multispectral analysis of multiple sclerosis lesions." J Magn Reson Imaging **7**: 499-511.

Morrissey, S. Stodal, H. Zettl, U. Simonis, C. Jung, S. Kiefer, R. Lassmann, H. Hartung, HP. Haase, A. Toyka, KV. (1996). "In vivo MRI and its histological correlates in acute adoptive transfer experimental allergic encephalomyelitis. Quantification of inflammation and oedema." Brain **119**: 239-48.

Morrissey, S. Deichmann, R. Syha, J. Simonis, C. Zettl, U. Archelos, JJ. Jung, S. Stodal, H. Lassmann, H. Toyka, KV. Haase, A. Hartung, HP. (1996). "Partial inhibition of AT-EAE by an antibody to ICAM-1: clinico-histological and MRI studies." J Neuroimmunol **69**: 85-93.

Namer, I. Steibel, J. Poulet, P. Armspach, JP. Mauss, Y. Chambron, J. (1992). "In vivo dynamic MR imaging of MBP-induced acute experimental allergic encephalomyelitis in Lewis rat." Magn Reson Med **24**: 325-34.

Namer, I. Steibel, J. Piddlesden, SJ. Mohr, M. Poulet, P. Chambron, J. (1994). "Magnetic resonance imaging of antibody-mediated demyelinating experimental allergic encephalomyelitis." J Neuroimmunol **54**: 41-50.

Namer, I. Steibel, J. Klinguer, C. Trifilieff, E. Mohr, M. Poulet, P. (1998). "Magnetic resonance imaging of PLP-induced experimental allergic encephalomyelitis in Lewis rats." J Neuroimmunol **92**: 22-8.

Namer, I. Steibel, J. Poulet, P. Armspach, JP. Mohr, M. Mauss, Y. Chambron, J. (1993). "Blood-brain barrier breakdown in MBP-specific T cell induced experimental allergic encephalomyelitis. A quantitative in vivo MRI study." Brain **116**: 147-59.

Nesbit, G. Forbes, GS. Scheithauer, BW. Okazaki, H. Rodriguez, M. (1991). "Multiple sclerosis: histopathologic and MR and/or CT correlation in 37 cases at biopsy and three cases at autopsy." Radiology **180**: 467-74.

Newman, T. Woolley, ST. Hughes, PM. Sibson, NR. Anthony, DC. Perry, VH. (2001). "T-cell- and macrophage-mediated axon damage in the absence of a CNS-specific immune response: involvement of metalloproteinases." Brain **124**: 2203-14.

Nijeholt, G. Bergers, E. Kamphorst, W. Bot, J. Nicolay, K. Castelijns, JA. van Waesberghe, JH. Ravid, R. Polman, CH. Barkhof, F. (2001). "Post-mortem high-resolution MRI of the spinal cord in multiple sclerosis: a correlative study with conventional MRI, histopathology and clinical phenotype." Brain **124**: 154-66.

Noseworthy, J. Lucchinetti, C. Rodriguez, M. Weinshenker, BG. (2000). "Multiple sclerosis." N Engl J Med **34**: 938-52.

Nusbaum, A. Lu, D. Tang, CY. Atlas, SW. (2000). "Quantitative diffusion measurements in focal multiple sclerosis lesions: correlations with appearance on TI-weighted MR images." AJR Am J Roentgenol **175**: 821-5.

Olson, J. Croxford, JL. Calenoff, MA. Dal Canto, MC. Miller, SD. (2001). "A virus-induced molecular mimicry model of multiple sclerosis." J Clin Invest **108**: 311-8.

Ordidge, R. Helpern, JA. Qing, ZX. Knight, RA. Nagesh, V. (1994). "Correction of motional artifacts in diffusion-weighted MR images using navigator echoes." Magn Reson Imaging **12**: 455-60.

Panitch, H. Hirsch, RL. Schindler, J. Johnson, KP. (1987). "Treatment of multiple sclerosis with gamma interferon: exacerbations associated with activation of the immune system." Neurology **37**: 1097-102.

Petrella, J. Grossman, RI. McGowan, JC. Campbell, G. Cohen, JA. (1996). "Multiple sclerosis lesions: relationship between MR enhancement pattern and magnetization transfer effect." AJNR Am J Neuroradiol **17**: 1041-9.

Petrella, J. Yang, Y. Richert., N. Lewis, B. Duyn, JH. McFarland, H. Franks, JA. (1997). "Dynamic Contrast MR measurements of relative cerebral blood volume in enhancing Multiple Sclerosis lesions: comparison to nonenhancing lesions and normal appearing white matter." Proc ISMRM: 646.

Pierpaoli, C. Basser, PJ. (1996). "Toward a quantitative assessment of diffusion anisotropy." Magn Reson Med **36**: 893-906.

Pike, G. De Stefano, N. Narayanan, S. Worsley, KJ. Pelletier, D. Francis, GS. Antel, JP. Arnold, DL. (2000). "Multiple sclerosis: magnetization transfer MR imaging of white matter before lesion appearance on T_2-weighted images." Radiology **215**: 824-30.

Prineas, J. Raine, CS. Wisniewski, H. (1969). "An ultrastructural study of experimental demyelination and remyelination. 3. Chronic experimental allergic encephalomyelitis in the central nervous system." Lab Invest **21**: 472-83.

Rapp, N. Gilroy, J. Lerner, AM. (1995). "Role of bacterial infection in exacerbation of multiple sclerosis." Am J Phys Med Rehabil **74**: 415-8.

Richards, T. Alvord, EC Jr. Peterson, J. Cosgrove, S. Petersen, R. Petersen, K. Heide, AC. Cluff, J. Rose, LM. (1995). "Experimental allergic encephalomyelitis in non-human primates: MRI and MRS may predict the type of brain damage." NMR Biomed **8**: 49-58.

Renoux, G. (1988). "The cortex regulates the immune system and the activities of a T-cell specific immunopotentiator." Int J Neurosci **39**: 177-87.

Rosen, B. Belliveau, JW. Vevea, JM. Brady, TJ. (1990). "Perfusion imaging with NMR contrast agents." Magn Reson Med **14**: 249-65.

Rovaris, M. Horsfield, MA. Filippi, M. (1999). "Correlations between magnetization transfer metrics and other magnetic resonance abnormalities in multiple sclerosis." Neurology **53**: S40-5.

Rovaris, M. Viti, B. Ciboddo, G. Gerevini, S. Capra, R. Iannucci, G. Comi, G. Filippi, M. (2000). "Brain involvement in systemic immune mediated diseases: magnetic resonance and magnetisation transfer imaging study." J Neurol Neurosurg Psychiatry. **68**: 170-7.

Rudin, M. Baumann, D. Ekatodramis, D. Stirnimann, R. McAllister, KH. Sauter, A. (2001). "MRI analysis of the changes in apparent water diffusion coefficient, T(2) relaxation time, and cerebral blood flow and volume in the temporal evolution of cerebral infarction following permanent middle cerebral artery occlusion in rats." Exp Neurol **169**: 56-63.

Schiffenbauer, J. Johnson, HM. Butfiloski, EJ. Wegrzyn, L. Soos, JM. (1993). "Staphylococcal enterotoxins can reactivate experimental allergic encephalomyelitis." Proc Natl Acad Sci U S A **90**: 8543-6.

Schiffenbauer, J. Soos, J. Johnson, H. (1998). "The possible role of bacterial superantigens in the pathogenesis of autoimmune disorders." Immunol Today **19**: 117-20.

Schreiber, K. Sorensen., PS. Koch-Henriksen, N. Wagner, A. Blinkenberg, M. Svarer, C. Petersen, HC. (2001). "Correlations of brain MRI parameters to disability in multiple sclerosis." Acta Neurol Scand **104**: 24-30.

Schrijver, I. van Meurs, M. Melief, MJ. Wim Ang, C. Buljevac, D. Ravid, R. Hazenberg, MP. Laman, JD. (2001). "Bacterial peptidoglycan and immune reactivity in the central nervous system in multiple sclerosis." Brain **124**: 1544-54.

Seeldrayers, P. Syha, J. Morrissey, SP. Stodal, H. Vass, K. Jung, S. Gneiting, T. Lassmann, H. Haase, A. Hartung, HP. et al (1993). "Magnetic resonance imaging investigation of blood-brain barrier damage in adoptive transfer experimental autoimmune encephalomyelitis." J Neuroimmunol **46**: 199-206.

Sibley, W. Bamford, CR. Clark, K. (1985). "Clinical viral infections and multiple sclerosis." Lancet **1:** 1313-5.

Sibson, N. Blamire, AM. Perry, VH. Gauldie, J. Styles, P. Anthony, DC. (2002). "TNF-alpha reduces cerebral blood volume and disrupts tissue homeostasis via an endothelin- and TNFR2-dependent pathway." Brain **125**: 2446-2459.

Sibson, N. Anthony, DC. Blamire, AM. Colet, JM. Muller, RN. Styles, P. (2002). "MRI detection of early endothelial activation in cytokine-induced CNS inflammation." Proc ISMRM **10**: 1236.

Sipkins, D. Gijbels, K. Tropper, FD. Bednarski, M. Li, KC. Steinman, L. (2000). "ICAM-1 expression in autoimmune encephalitis visualized using magnetic resonance imaging." J Neuroimmunol **104**: 1-9.

Smith, T. Hewson, AK. Kingsley, CI. Leonard, JP. Cuzner, ML. (1997). "Interleukin-12 induces relapse in experimental allergic encephalomyelitis in the Lewis rat." Am J Pathol **150**: 1909-17.

Sobel, R. Hinojoza, JR. Maeda, A. Chen, M. (1998). "Endothelial cell integrin laminin receptor expression in multiple sclerosis lesions." Am J Pathol **153**: 405-15.

Stejskal, E. Tanner, JE. (1965). "Spin diffusion measurements: spin echoes in the presence of a time-dependent field gradient." Journal of Chemical Physics **42**: 288-292.

Stewart, W. Alvord, EC. Hruby, S. Hall, LD. Paty, DW. (1985). "Early detection of experimental allergic encephalomyelitis by magnetic resonance imaging." Lancet **2**: 898.

Stewart, W. Alvord, EC Jr. Hruby, S. Hall, LD. Paty, DW. (1991). "Magnetic resonance imaging of experimental allergic encephalomyelitis in primates." Brain **114**: 1069-96.

Stewart, W. Hall, LD. Berry, K. Paty, DW. (1984). "Correlation between NMR scan and brain slice data in multiple sclerosis." Lancet **2**: 412.

Stohlman, S. Hinton, DR. (2001). "Viral induced demyelination." Brain Pathol **11**: 92-106.

Thompson, A. Miller, D. Youl, B. MacManus, D. Moore, S. Kingsley, D. Kendall, B. Feinstein, A. McDonald, WI. (1992). "Serial gadolinium-enhanced MRI in relapsing/remitting multiple sclerosis of varying disease duration." Neurology **42**: 60-3.

Tievsky, A. Ptak, T. Farkas, J. (1999). "Investigation of apparent diffusion coefficient and diffusion tensor anisotropy in acute and chronic multiple sclerosis lesions." AJNR Am J Neuroradiol **20**: 1491-9.

Tracey, I. Hamberg, LM. Guimaraes, AR. Hunter, G. Chang, I. Navia, BA. Gonzalez, RG. (1998). "Increased cerebral blood volume in HIV-positive patients detected by functional MRI." Neurology **50**: 1821-6.

Trapp, B. Bo, L. Mork, S. Chang, A. (1999). "Pathogenesis of tissue injury in MS lesions." J Neuroimmunol **98**: 49-56.

Truyen, L. van Waesberghe, JH. van Walderveen, MA. van Oosten, BW. Polman, CH. Hommes, OR. Ader, HJ. Barkhof, F. (1996). "Accumulation of hypointense lesions ("black holes") on T_1 spin-echo MRI correlates with disease progression in multiple sclerosis." Neurology **47**: 1469-76.

Tsunoda, I. Tolley, ND. Theil, DJ. Whitton, JL. Kobayashi, H. Fujinami, RS. (1999). "Exacerbation of viral and autoimmune animal models for multiple sclerosis by bacterial DNA." Brain Pathol **9**: 481-93.

Uhlenbrock, D. S., S. (1989). "The value of T1-weighted images in the differentiation between MS, white matter lesions, and subcortical arteriosclerotic encephalopathy (SAE)." Neuroradiology **31**: 203-12.

van Buchem, M. McGowan, JC. Kolson, DL. Polansky, M. Grossman, RI. (1996). "Quantitative volumetric magnetization transfer analysis in multiple sclerosis: estimation of macroscopic and microscopic disease burden." Magn Reson Med **36**: 632-6.

van Gelderen, P. de Vleeschouwer, MH. DesPres, D. Pekar, J. van Zijl, PC. Moonen, CT. (1994). "Water diffusion and acute stroke." Magn Reson Med **31**: 154-63.

van Waesberghe, J. Castelijns, JA. Scheltens, P. Truyen, L. Lycklana A Nijeholt, GJ. Hoogenraad, FG. Polman, CH. Valk, J. Barkhof, F. (1997). "Comparison of four potential MR parameters for severe tissue destruction in multiple sclerosis lesions." Magn Reson Imaging **15**: 155-62.

van Waesberghe, J. van Walderveen, MA. Castelijns, JA. Scheltens, P. Lycklama, a. Nijeholt, GJ. Polman, CH. Barkhof, F. (1998). "Patterns of lesion development in multiple sclerosis: longitudinal observations with T1-weighted spin-echo and magnetization transfer MR." AJNR Am J Neuroradiol **19**: 675-83.

van Waesberghe, J. Kamphorst, W. De Groot, CJ. van Walderveen, MA. Castelijns, JA. Ravid, R. Lycklama a Nijeholt, GJ. van der Valk, P. Polman, CH. Thompson, AJ. Barkhof, F. (1999). "Axonal loss in multiple sclerosis lesions: magnetic resonance imaging insights into substrates of disability." Ann Neurol **46**: 747-754.

van Walderveen, M. Barkhof, F. Hommes, OR. Polman, CH. Tobi, H. Frequin, ST. Valk, J. (1995). "Correlating MRI and clinical disease activity in multiple sclerosis: relevance of hypointense lesions on short-TR/short-TE (T1-weighted) spin-echo images." Neurology **45**: 1684-90.

van Walderveen, M. Scheltens, P. Kamphorst, W. Barkhof, F. David, R. Polman, CH. Valk, J. (1996). "Histopathologic correlate of hypointense lesions on T_1-weighted SE MR images in Multiple Sclerosis." Proc ISMRM **1**: 528.

van Walderveen, M. Scheltens, P. van Waesberghe, JHTM. Barkhof, F. Valk, J. Polman, CH. Kamphorst, W. (1997). "Hypointense lesions on T_1-weighted SE MR images correlate with axonal loss in Multiple Sclerosis." Proc ISMRM **1**: 75.

van Walderveen, M. Kamphorst, W. Scheltens, P. van Waesberghe, JH. Ravid, R. Valk, J. Polman, CH. Barkhof, F. (1998). "Histopathologic correlate of hypointense lesions on T_1-weighted spin-echo MRI in multiple sclerosis." Neurology **50**: 1282-8.

van Walderveen, M. Barkhof, F. Tas, MW. Polman, C. Frequin, ST. Hommes, OR. Thompson, AJ. Valk, J. (1998). "Patterns of brain magnetic resonance abnormalities on T_2-weighted spin echo images in clinical subgroups of multiple sclerosis: a large cross-sectional study." Eur Neurol **40**: 91-8.

Vavasour, I. Whittal, KP. MacKay, AL. Li, DK. Vorobeychik, G. Paty, DW. (1998). "A comparison between magnetization transfer ratios and myelin water percentages in normals and multiple sclerosis patients." Magn Reson Med **40**: 763-8.

Verhoye, M. Gravenmade, EJ. Raman, ER. Van Reempts, J. Van der Linden, A. (1996). "In vivo noninvasive determination of abnormal water diffusion in the rat brain studied in an animal model for multiple sclerosis by diffusion-weighted NMR imaging." Magn Reson Imaging **14**: 521-32.

Vorisek, I. Hajek, M. Tintera, J. Nicolay, K. Sykova, E. (2002). "Water ADC, extracellular space volume, and tortuosity in the rat cortex after traumatic injury." Magn Reson Med **48**: 994-1003.

Waddington, W. Blamire, AM. Rajagopalan, B. Styles, P. (1998). "An agglomerative hierarchical algorithm to define tissue types in images with no intervention." Proc ISMRM: 2069.

Wang, H. Matsui, M. Saida, T. (2002). "Immunological disturbances in the central nervous system linked to MRI findings in multiple sclerosis." J Neuroimmunol **125**: 149-54.

Werring, D. Brassat, D. Droogan, AG. Clark, CA. Symms, MR. Barker, GJ. MacManus, DG. Thompson, AJ. Miller, DH. (2000). "The pathogenesis of lesions and normal-appearing white matter changes in multiple sclerosis: A serial diffusion MRI study." Brain **123**: 1667-1676.

Willenborg, D. Staykova, MA. Cowden, WB. (1999). "Our shifting understanding of the role of nitric oxide in autoimmune encephalomyelitis: a review." J Neuroimmunol **100**: 21-35.

Wilson, M. Morgan, PS. Lin, X. Turner, BP. Blumhardt, LD. (2001). "Quantitative diffusion weighted magnetic resonance imaging, cerebral atrophy, and disability in multiple sclerosis." J Neurol Neurosurg Psychiatry **70**: 318-22.

Wisniewski, H. Bloom, BR. (1975). "Primary demyelination as a nonspecific consequence of a cell-mediated immune reaction." J Exp Med **141**: 346-59.

Wolff, S. Balaban, RS. (1989). "Magnetization transfer contrast (MTC) and tissue water proton relaxation in vivo." Magn Reson Med **10**: 135-44.

Wolinsky, J. Narayana, PA. (2002). "Magnetic resonance spectroscopy in multiple sclerosis: window into the diseased brain." Curr Opin Neurol **15**: 247-51.

Wucherpfennig, K. (2001). "Mechanisms for the induction of autoimmunity by infectious agents." J Clin Invest **108**: 1097-104.

Xu, S. Jordan, EK. Brocke, S. Bulte, JW. Quigley, L. Tresser, N. Ostuni, JL. Yang, Y. McFarland, HF. Frank, JA. (1998). "Study of relapsing remitting experimental allergic encephalomyelitis SJL mouse model using MION-46L enhanced in vivo MRI: early histopathological correlation." J Neurosci Res **52**: 549-558.

Young, I. Hall, AS. Pallis, CA. Legg, NJ. Bydder, GM. Steiner, RE. (1981). "Nuclear magnetic resonance imaging of the brain in multiple sclerosis." Lancet **2**: 1063-6.